

AN X-RAY CRYSTALLOGRAPHIC STUDY OF THE CRYSTAL STRUCTURES
OF FOUR TELLURIUM OXYSALT MINERALS: DUGGANITE, CHOLOALITE,
RODALQUILARITE, AND GRAEMITE

by

ANITA EVA LAM

B.Sc. Honours (Chemistry and Geological Sciences), The University of British Columbia, 1993

A THESIS SUBMITTED IN PARTIAL FULFILLMENT OF
THE REQUIREMENTS FOR THE DEGREE OF
MASTER OF SCIENCE

in

THE FACULTY OF GRADUATE STUDIES
(Department of Earth and Ocean Sciences)

We accept this thesis as conforming to the required standard

THE UNIVERSITY OF BRITISH COLUMBIA

August 1998

© Anita Eva Lam, 1998

In presenting this thesis in partial fulfilment of the requirements for an advanced degree at the University of British Columbia, I agree that the Library shall make it freely available for reference and study. I further agree that permission for extensive copying of this thesis for scholarly purposes may be granted by the head of my department or by his or her representatives. It is understood that copying or publication of this thesis for financial gain shall not be allowed without my written permission.

Department of Earth and Ocean Sciences

The University of British Columbia
Vancouver, Canada

Date August 31, 1998

ABSTRACT

The crystal structures of four tellurium oxysalt minerals, dugganite, choloalite, rodalquilarite, and graemite, were investigated with the use of single crystal X-ray crystallography.

The crystal structure of dugganite, ideally $\text{Pb}_3\text{Zn}_3\text{Te}^{6+}\text{As}_2\text{O}_{14}$, a 8.460(2), c 5.206(2) Å, V 322.6(2) Å³, space group $P321$, Z 1, has been solved by direct methods and Patterson techniques, and refined to an R index of 2.7% based on 636 unique reflections measured using $\text{MoK}\alpha$ radiation on an automated four-circle diffractometer. The structure consists of heteropolyhedral sheets of edge-sharing TeO_6 octahedra and PbO_8 snub disphenoids, oriented parallel to (001). The sheets are cross-linked by AsO_4 and ZnO_4 tetrahedra, which share corners to form an interlinked, two- and three-connected two-dimensional net parallel to (001). Cheremnykhite and kuksite are considered to be isostructural with dugganite, but with V and P respectively dominant at the As site.

The crystal structure of choloalite, ideally $\text{Cu}_3\text{Pb}_3\text{Te}^{4+}_6\text{O}_{18}(\text{Cl}, \text{H}_2\text{O})$, a 12.520(4) Å, V 1963(2) Å³, space group $P4_132$, Z 4, has been solved by direct methods and Patterson techniques, and refined to an R index of 5.2% based on 956 unique reflections measured using $\text{MoK}\alpha$ radiation on an automated four-circle diffractometer. The structure consists of distorted TeO_6 octahedra, $\text{Cu}\phi_5$ square pyramids (where $\phi = \text{Cl}$ and H_2O), $\text{Pb}(1)\text{O}_9$ triaugmented trigonal prisms, and $\text{Pb}(2)\text{O}_{12}$ icosahedra. The $\text{Pb}(1)\text{O}_9$ polyhedra polymerize to form a three-dimensional network, as do the $\text{Cu}\phi_5$ and $\text{Pb}(2)\text{O}_{12}$ polyhedra. The two networks fit together in three-dimensional space, leaving voids which are filled by the TeO_6 octahedra.

The crystal structure of rodalquilarite was originally solved, using photographic methods, to an R index of 9.2% by Dusausoy and Protas (1969). Rodalquilarite, ideally $\text{H}_3\text{Fe}_2(\text{TeO}_3)_4\text{Cl}$, a

9.021(1) b 5.1170(7), c 6.6539(8) Å, α 103.23(1)°, β 106.66(1)°, γ 78.07(1)°, V 283.15(6) Å³, space group $P\bar{1}$, Z 1 was redetermined and refined to an R index of 4.1% based on 1672 unique reflections measured using Mo $K\alpha$ radiation on an automated four-circle diffractometer. The structure consists of chains of FeO₆ octahedra parallel to the b -axis connected with tellurium polyhedra to form planes parallel to bc . These planes are held together by hydrogen and long (>3.0 Å) Te- ϕ (where ϕ = O or Cl) bonds.

A four-circle diffractometer equipped with synchrotron radiation was used to collect a data set for graemite, CuTeO₆·H₂O. Data yielded a 6.816, b 25.627, c 5.784, with all angles 90°. Structural models were refined to an R index of 6.9% in $Pmc2_1$ and to 7.7% in a reduced cell ($\frac{1}{2}a$) using $Pna2_1$. Neither of the models gave a satisfactory result although a substructure in $Pna2_1$ is proposed. Precession photographs show the presence of disorder in the structure. Further study, including upper level precession work and electron microprobe analysis, is required.

TABLE OF CONTENTS

ABSTRACT	ii
TABLE OF CONTENTS	iv
LIST OF TABLES.....	vii
LIST OF FIGURES	ix
PREFACE	xiv
ACKNOWLEDGEMENTS	xv
DEDICATION.....	xvi
1.0 INTRODUCTION	1
1.1 General Overview of Tellurium	1
1.1.1 <i>Discovery of tellurium</i>	1
1.1.2 <i>General chemistry of tellurium</i>	2
1.1.3 <i>Geochemistry and occurrence of tellurium</i>	3
1.1.4 <i>Uses of tellurium</i>	5
1.2 Tellurium Coordination and Structure in Minerals	5
1.2.1 <i>Tellurium (IV) coordination</i>	5
1.2.2 <i>Coordination of tellurium (VI)</i>	15
1.3 Known Tellurium Oxysalts and Structures	15
2.0 EXPERIMENTAL PROCEDURES.....	20
2.1 Crystal Selection and Preparation.....	20
2.2 Data Collection.....	21
2.2.1 <i>Single crystal X-ray diffraction using molybdenum X-radiation</i>	22
2.2.2 <i>Single crystal X-ray diffraction using synchrotron radiation</i>	23
2.3 Structure Solution and Refinement	24
2.3.1 <i>MISSYM</i>	25
2.3.2 <i>STRUCTURE TIDY</i>	25
2.4 Electron Microprobe Analysis.....	26
2.5 Infrared Analyses.....	27
2.6 Introduction to Bond Valence.....	27
3.0 DUGGANITE: CRYSTAL STRUCTURE AND REVISED FORMULA	29
3.1 Introduction	29
3.2 Experimental	31
3.3 Structure Solution and Refinement	33
3.4 Description of the Structure.....	39
3.4.1 <i>Tellurium coordination</i>	39
3.4.2 <i>Arsenic coordination</i>	39
3.4.3 <i>Lead coordination</i>	40

3.4.4 Zinc coordination.....	40
3.4.5 Structure connectivity	41
3.5 Discussion	51
3.6 Conclusions	52
4.0 CHOLOALITE: CRYSTAL STRUCTURE AND REVISED FORMULA	55
4.1 Introduction	55
4.2 Experimental	57
4.3 Structure Solution and Refinement	61
4.4 Description of the Structure.....	68
4.4.1 Te coordination.....	68
4.4.2 Copper coordination.....	69
4.4.3 Lead(1) coordination	71
4.4.4 Lead(2) coordination	71
4.4.5 Structure connectivity	73
4.5 Discussion	84
4.6 Conclusions	85
5.0 RODALQUILARITE, A REFINEMENT OF THE STRUCTURE.....	86
5.1 Introduction	86
5.2 Experimental	87
5.3 Structure Solution and Refinement	87
5.4 Description of the Structure Based on Earlier Work.....	97
5.4.1 Original structure description by Dusauroy and Protas (1969).....	97
5.4.2 Previous work done by Back (1990)	100
5.5 Description of the Refined Structure.....	102
5.5.1 Coordination of tellurium	102
5.5.2 Coordination of iron	103
5.5.2 Coordination of chlorine	103
5.5.3 Hydrogen-bonding	103
5.5.4 Structure connectivity.....	104
5.6 Conclusions About the Refinement of Rodalquilarite.....	116
6.0 GRAEMITE	117
6.1 Introduction	117
6.2 Experimental	118
6.3 Structure Solution and Refinement	119
6.3.1 Determination of possible space groups.....	119
6.3.2 Structure solution.....	126
6.4 Description of the Proposed Structure of Graemite.....	127
6.4.1 Description of the proposed substructure in $Pna2_1$	127
6.4.2 The proposed structure in $Pmc2_1$	128
6.5 Discussion	137
6.6 Conclusions	137

7.0 CONCLUSIONS	139
7.1 Dugganite, Choloalite, Rodalquilarite, and Graemite	139
7.2 A Comment on Experimental Procedures	141
7.3 Crystal Structure Analysis as a Means For Chemical Analysis of Crystals	144
8.0 CONSIDERATIONS FOR FUTURE RESEARCH	146
9.0 REFERENCES	149
APPENDIX A. COMMONLY USED SYMBOLS AND TERMS.....	155
APPENDIX B. CATEGORIZED TELLURIUM OXYSALT MINERALS	157
APPENDIX C. STRUCTURE FACTOR TABLES FOR DUGGANITE	162
APPENDIX D. STRUCTURE FACTOR TABLES FOR CHOLOALITE.....	167
APPENDIX E. STRUCTURE FACTOR TABLES FOR RODALQUILARITE	173
APPENDIX F. STRUCTURE FACTOR TABLES FOR GRAEMITE.....	183

LIST OF TABLES

	Page
1.1 Atomic radii of tellurium, selenium, and sulfur (Kudryavtsev, 1974).	4
1.2 Tellurium oxysalt minerals.	17-19
3.1 Chemical composition of dugganite.	32
3.2 Miscellaneous information: dugganite.	35
3.3 Atomic parameters for dugganite.	36
3.4 Selected interatomic distances (Å) and angles (°) for dugganite.	37
3.5 Bond-valence arrangement in dugganite.	38
3.6 Indexed powder diffraction patterns for dugganite.	53-54
4.1 Chemical composition of choloalite.	59
4.2 Miscellaneous information: choloalite.	63
4.3 Atomic parameters for choloalite.	64
4.4 Selected interatomic distances (Å) and angles (°) for choloalite.	65-66
4.5 Bond-valence arrangement in choloalite.	67
4.6 Bond lengths of twelve-coordinated lead icosahedra in different minerals.	72
5.1 Miscellaneous information: rodalquilarite.	89
5.2 Redetermined atomic parameters for rodalquilarite (based on the positions by Dusausoy & Protas, 1969).	90
5.3 Original atomic parameters from Dusausoy & Protas (1969).	91
5.4 Atomic parameters for rodalquilarite (based on <i>STRUCTURE TIDY</i> standardized positions).	92
5.5 Selected interatomic distances (Å) and angles (°) for rodalquilarite.	93-95
5.6 Bond-valence arrangement in rodalquilarite.	96
6.1 Atomic positions for the proposed graemite substructure solved in <i>Pna2₁</i> .	130
6.2 Atomic positions for the proposed graemite structure solved in <i>Pmc2₁</i> .	131

Appendix A

Commonly used terms and symbols.	156
----------------------------------	-----

Appendix B

B.1	Tellurite Minerals	158-159
B.2	Tellurate Minerals	160
B.3	Tellurium Oxysalt Minerals With Mixed Te^{4+} and Te^{6+} Valences	161

Appendix C

Observed and calculated structure factors for dugganite in $P321$.	163-166
---	---------

Appendix D

Observed and calculated structure factors for choloalite in $P4_132$.	168-172
--	---------

Appendix E

Observed and calculated structure factors for rodalquilarite in $P-1$.	174-182
---	---------

Appendix F

Observed and calculated structure factors for graemite in $Pna2_1$.	184-187
--	---------

LIST OF FIGURES

	Page
1.1 a) Three- and b) four-fold coordination of Te^{4+} (after Zemann 1969). Small circles: Te; large circles: O.	7
1.2 Coordination figure showing four oxygen atoms around Te^{4+} (after Zemann, 1971). Median distance of Te–Oa, Te–Ob, Te–Oc is 1.92 ± 0.08 Å; Te–Od varies from 2.08 to 2.98 Å.	7
1.3 The coordination of Te^{4+} as depicted by Lindqvist (1973). a) and b) show the idealized three- and four-fold coordinations including the lone electron pair.	9
1.4 Trigonal bipyramidal coordination showing in (a) the axial, a , and equatorial, e , positions (after Gillespie, 1972). Possible locations for the lone electron pair, E , are shown in (b) and (c) with the preferred orientation being (c).	12
1.5 Possible octahedral configurations of Te (IV) (after Brown 1974). The strength of the bond is correlated with the density of the line.	12
1.6 Back's (1990) depiction of Te^{4+} coordination. The lettering is consistent with Zemann (1971).	14
3.1 Coordination of the tellurium atom in dugganite.	43
3.2 Coordination of the arsenic atom in dugganite.	44
3.3 Coordination of the lead atom in dugganite.	45
3.4 Coordination of the zinc atom in dugganite.	46
3.5 The heteropolyhedral sheet in the dugganite structure, projected onto (001). The TeO_6 octahedra are indicated by a regular dot pattern, and the PbO_8 polyhedra by a random dot pattern.	47
3.6 The tetrahedral layer in the dugganite structure, projected onto (001). The AsO_4 tetrahedra are indicated with crosses and the ZnO_4 tetrahedra are ruled.	48

3.7	The dugganite structure projected onto (001). TeO_6 octahedra are shown with a regular dot pattern, AsO_4 tetrahedra with crosses, and ZnO_4 tetrahedra are ruled. The lead atoms are shown as spheres.	49
3.8	The dugganite structure projected onto (010). The shading is the same as in figure 3.7.	50
4.1	The infrared transmittance spectrum of choloalite. The absorption bands at 3260 cm^{-1} and 1590 cm^{-1} are indicative of water in the structure of choloalite.	60
4.2	Coordination of the tellurium atom in choloalite.	75
4.3	Coordination of the copper atom in choloalite.	76
4.4	Coordination of the lead (1) atom in choloalite.	77
4.5	Coordination of the lead (2) atom in choloalite.	78
4.6a	“Pinwheels” in the choloalite structure: (a) three $\text{Cu}\phi_5$ polyhedra; (b) four $\text{Pb}(1)\text{O}_9$ polyhedra.	79
4.6b	“Pinwheel” in the choloalite structure. Seven $\text{Pb}(2)\text{O}_{12}$ polyhedra linked by six $\text{Cu}\phi_5$ polyhedra.	80
4.7	Three-dimensional network of $\text{Pb}(1)\text{O}_9$ polyhedra. The Te atoms are shown as spheres. The positions of the 4_1 axes are evident.	81
4.8	Three-dimensional network of $\text{Cu}\phi_5$ and $\text{Pb}(2)\text{O}_{12}$ polyhedra. The Te atoms are shown as spheres.	82
4.9	Linkage of adjacent polyhedra to the TeO_6 octahedron. Bonds are shown for the central TeO_6 octahedron and those adjacent polyhedra linked to it by shared edges. Only the central cation is shown for those polyhedra that link by shared corners. The Te atoms are shown as spheres with NE to SW ruling and the Cu atoms are shown as spheres with NW to SE ruling. The $\text{Pb}(1)$ atoms are shown as spheres with a regular dot pattern, and the $\text{Pb}(2)$ atoms as spheres with a random dot pattern. The O atoms are shown as shadowed spheres and the Cl atoms as open, larger spheres.	83

5.1	Chains of FeO_6 octahedra in rodalquilarite projected onto the bc -plane (after Dusausoy and Protas, 1969).	98
5.2	Chains of FeO_6 octahedra in rodalquilarite projected onto the ab -plane (after Dusausoy and Protas, 1969).	99
5.3	Projection of the rodalquilarite structure onto the ac -plane showing the diverse bond types in the structure (after Dusausoy and Protas, 1969).	99
5.4	Eight-coordinated Te(1) and seven-coordinated Te(2) in rodalquilarite (after Back, 1990). The proposed sites of the electron lone pair are shown as the shaded areas.	101
5.5	Coordination of tellurium (1) in rodalquilarite. Solid bonds show the three short bonds on one side of the coordination polyhedron as found by Dusausoy and Protas (1969). Hollow bonds show the longer bonds not found in 1969.	105
5.6	Coordination of tellurium (2) in rodalquilarite. Shading of the bonds is the same as that in figure 5.5.	106
5.7	Coordination of the iron atom in rodalquilarite.	107
5.8	Coordination of the chlorine atom in rodalquilarite.	108
5.9	Hydrogen-bonding in rodalquilarite viewed down the b -axis. The hydrogen bonds are shown as dashed lines. The bonds found by Dusausoy and Protas (1969) are shown as solid bonds. Fe atoms are shown ruled, Te(1) atoms have a regular array of dots, Te(2) have a random array of dots, Cl atoms are shown as large open spheres, H atoms as small open spheres, and O atoms as shaded spheres.	109
5.10	Chains of edge-sharing iron octahedra parallel to the b -axis.	110
5.11	Te(1) and Fe polyhedra viewed down the a -axis. The Te polyhedra (regular dot pattern) are shown with bonds < 3.0 angstroms. The longer bonds of one tellurium atom are shown as dashed lines. Fe octahedra are shown ruled, Cl atoms as larger open spheres, O atoms as cross-hatched spheres, and H atoms as smaller open spheres. This figure shows Te(1) does not join the Fe octahedra in the c -direction. Notice the longer bonds to tellurium have a strong component in the a -direction.	111

5.12	Te(2) and Fe polyhedral sheet parallel to the <i>bc</i> -plane. The Te polyhedra (shown with dashes) are shown with bonds < 3.0 angstroms. The Fe octahedra are shown ruled and the Cl atoms are shown as open spheres. The axes are in the same orientation as figure 5.11.	112
5.13	Connectivity of rodalquilarite as viewed down the <i>c</i> -axis. The unit cell is shown with the <i>a</i> -axis roughly top to bottom and the <i>b</i> -axis left to right. The longer (hollow) bonds connect planes of Te/Fe polyhedra in the <i>a</i> -direction. The shading of bonds and atoms is the same as in figure 5.9.	113
5.14	Linkage of adjacent cations to Te(1) in rodalquilarite. The shading of atoms is the same as in figure 5.13. Hollow bonds indicate linking by corners while the solid bonds indicate linking by edges or faces.	114
5.15	Linkage of adjacent cations to Te(2) in rodalquilarite. The shading of atoms and bonds is the same as in figure 5.14.	115
6.1	Precession photograph of graemite showing <i>hk0</i> . Notice the streaking of reflections, along the <i>b</i> -axis, on odd <i>h</i> -levels.	122
6.2	Precession photograph of graemite showing <i>0kl</i> . All reflections are sharp.	123
6.3	Precession photograph of graemite showing <i>1kl</i> . All reflections are smeared along the <i>b</i> -axis.	124
6.4	Precession photograph of graemite showing <i>hk1</i> . Reflections are smeared on odd <i>h</i> -levels along the <i>b</i> -axis.	125
6.5	The <i>bc</i> -plane showing disorder in the proposed substructure of graemite in <i>Pna2₁</i> . Cu(1) atoms are shown as spheres with a regular pattern of dots, Cu(2) atoms as spheres with a random array of dots, Te(1) atoms as cross-hatched spheres, Te(2) atoms as spheres with NW to SE ruling, and Te(3) atoms with NE to SW ruling. Selected oxygen atoms are shown. O(1) and O(3) atoms are shown as shaded spheres and O(7) atoms are shown as open spheres. The proposed disorder is between the Te(2) and Te(3) atoms and between the O(1), O(3), and O(7) atoms.	132

- 6.6 The *ab*-plane of the proposed substructure of graemite in $Pna2_1$. Disorder is 133
not apparent in this orientation. The shading of cations is the same as that
in figure 6.5. All oxygens are shown. O(7) atoms are shown as open
spheres while the rest of the oxygens are shown as shaded spheres.
- 6.7 Disorder of Te(2) and Te(3) in the proposed graemite substructure in 134
 $Pna2_1$. Oxygen atoms bonded to either Te(2) or Te(3) are shown with
hollow bonds.
- 6.8 Connectivity of the proposed graemite substructure in $Pna2_1$ as viewed 135
down the *c*-axis. Hollow bonds show disorder between Te(2) and Te(3).
The shading of the atoms is consistent with figure 6.5.
- 6.9 Connectivity of the proposed graemite substructure in $Pna2_1$ as viewed 136
down the *a*-axis. The shading of bonds and atoms is the same as in figure
6.8.

PREFACE

Two papers based on the work from this thesis have been submitted to the Canadian Mineralogist. "THE CRYSTAL STRUCTURE OF DUGGANITE, $\text{Pb}_3\text{Zn}_3\text{Te}^{6+}\text{As}_2\text{O}_{14}$ " by Anita E. Lam, Lee A. Groat, and T. Scott Ercit has been accepted and is presently in press. It will appear in volume 3, pages unknown, 1998. The procedure leading to and including crystal structure solution and refinement was done by Anita Lam. Dr. L.A. Groat was the thesis supervisor and gave a guiding hand in all aspects of the work. Dr. T.S. Ercit performed the electron microprobe analysis and also provided guidance.

"THE CRYSTAL STRUCTURE AND REVISED FORMULA OF CHOLOALITE, $\text{Cu}_3\text{Pb}_3\text{Te}^{4+}_6\text{O}_{18}(\text{Cl},\text{H}_2\text{O})$ " by Anita E. Lam, Lee A. Groat, Joel D. Grice, T. Scott Ercit, and Elizabeth Moffatt has been submitted but has not yet been accepted. The procedure leading to and including crystal structure solution and refinement was done by Anita Lam. Dr. L.A. Groat was the thesis supervisor and gave a guiding hand in all aspects of the work. Dr. T.S. Ercit performed the electron microprobe analysis and he and Dr. J. Grice also provided guidance when it was required. Elizabeth Moffatt performed the infrared analysis.

ACKNOWLEDGEMENTS

A number of people have given me guidance, support, humour, and encouragement during the time it took to do this thesis. It has not been easy but it was worth it.

I thank Lee Groat for his guidance, help, encouragement, and especially his patience. He was always encouraging and supportive even when times were bleak. He is one of the nicest, most accommodating people I know. I also thank him for those Yukon adventures that I will never forget and will remember as some of the best times of my life.

The equipment and funding was provided by NSERC. The Canadian Museum of Nature provided many mineral samples. Thanks to Andy Roberts for providing the rodalquilarite and graemite crystal. Also, a thank you is extended to William Pinch for providing beautiful dugganite crystals.

I have the deepest heartfelt thank-you for Joel Grice, Scott Ercit, and Bob Gault from the Canadian Museum of Nature. Bob, as a kindred spirit and the receiver of many of my queens of spades. I probably learned the most about crystallography as an art and a science from Joel and Scott and it is difficult to express the magnitude of appreciation that I have for them.

During the course of this work, it was necessary to find a stress relief and I thank Bryon Cranston, Michelle Lamberson, Arne Toma, Lindsay Kelly, Dave Butler, and Sandy Stewart for introducing me to ice hockey.

I thank Mati Raudsepp and Jim Trotter for their advice as members of my advisory committee and Greg Dipple and Tad Ulrych as members of my examining committee. Thanks to H. Meyer and W. Morgenroth for collecting the graemite synchrotron data. I also thank Malcolm Back for the loan of his thesis, and Mark Cooper and Andy McDonald for their advice.

Thanks to Dave Dreisinger who gave me the opportunity to learn about hydrometallurgy.

I have made many friends since the start of my thesis and I would like to thank these special people: Shannon, Julie, Ben, Mike Lo, Mike F., Ed, Nathan, Jacqueline, Lawrence, Felix, Gerdia, Kevin, Jésus, Ellen, Nathalie, Elisabetta, Cari, Laurel, and Heike. Bé Wassink has been there for me through thick and thin and I am deeply grateful to him. I would also like to thank my parents, my great-aunt, my brothers Ray and Mike and my sister-in-law, Marina. A special thank-you goes to Pete(γπ) Daubeney for his love, humour, and support over the years.

Many people have helped me along the way in this venture and I apologize if I neglected to mention your name. All of you are in my heart and have helped to shape the person that I am.

Thank you.

DEDICATION

This work is dedicated to my parents, Wai Ying Lam and Chik Yuen Lam. It could not have been completed without their love and support. Thanks for working so hard for us and never giving me a rough time about what I was doing.

1.0 INTRODUCTION

This thesis examines the structures of one previously solved and three previously unsolved tellurium oxysalt minerals. A refinement of rodalquilarite (previously solved by Dusauroy and Protas 1969) and the structure solutions of dugganite and choloalite have been determined with the use of single crystal X-ray crystallography. A partial structure of graemite is proposed. This chapter will introduce tellurium as an element as well as the coordination of Te^{4+} and Te^{6+} in crystals.

1.1 General Overview of Tellurium

The history of the discovery of tellurium, its chemistry, occurrence, and some of its uses are discussed.

1.1.1 *Discovery of tellurium*

Tellurium, element 52 on the periodic table, was discovered by Austrian chemist Franz Joseph Mueller von Reichenstein in 1782. It was first encountered in the ores mined from the deposits of the Transylvania district. A different metal was extracted from a gold ore known then as *aurum album* (Heiserman, 1992) and specifically, from a mineral thought to be an alloy of bismuth and antimony which was referred to as white or grey gold. The unknown substance that was extracted was originally mistakenly identified as bismuth sulfide or antimony. Mueller von Reichenstein observed that the substance did not have the properties of antimony and concluded that it was an unknown metal that had an association with gold and he referred to it as

metallum problematicum or *aurum paradoxum* (Cooper, 1971). In 1784, Swedish chemist Torbern Bergman confirmed that the metal was not antimony. Mueller von Richenstein continued to work on the new metal and determined a number of its properties in 1785. Sixteen years after the initial speculation, Austrian chemist M. Klaproth confirmed the discovery with evidence that the metal had unique properties and gave Mueller von Richenstein full credit in a paper published in 1798. Klaproth named the element tellurium after the latin *tellus* meaning “earth”. In 1789, tellurium was also discovered independently by P. Kitaibel, a Hungarian student of natural sciences.

1.1.2 General chemistry of tellurium

Tellurium belongs to the group VIB family of elements along with oxygen, sulfur, selenium, and polonium. The elements of this group are known as “chalcogens” (derived from two Greek words “copper” and “born”) as they form minerals that are an important source of metals. Moving down the group VIB column on the periodic table, we see that the atomic radius increases, the electronegativity decreases, and the reducing properties of the negatively charged ion increase. With increasing atomic weight the elements become more metallic: oxygen and sulfur are insulators, selenium and tellurium are semi-conductors, and polonium is a conductor. Tellurium is classed as a metalloid (having both metallic and non-metallic properties) and is found on the periodic table sitting immediately to the right of the diagonal line that separates the metals and non-metals.

The electron configuration of this group can be summarized as ns^2np^4 , two electrons short of a full shell or noble gas configuration; the configuration for tellurium is $1s^22s^22p^63s^23p^63d^{10}4s^24p^64d^{10}5s^25p^4$ or $[Kr]4d^{10}5s^25p^4$. The common valence states of

tellurium are -2, 0, +4, and +6. In aqueous solution, Te^{4+} is the most stable of the states.

Notably, an oxidation state of +1 has also been demonstrated with the compound Te_2I_2 .

Compounds with Te^{2+} are unstable and the tellurium disproportionates to elemental Te and compounds of Te^{4+} . The different classes of tellurium-bearing minerals are: native elements and intermetallic compounds, tellurides, oxides, tellurites, and tellurates (Vlasov, 1966). In this thesis, the crystal structures of tellurite and tellurate minerals are studied.

1.1.3 Geochemistry and occurrence of tellurium

In nature, tellurium is closely associated with, and thus can be compared to, sulfur and selenium, two members of its family. Tellurium and selenium can be found in sulfide ores forming separate selenide and telluride minerals. Interestingly, selenium may substitute isomorphously for sulfur in sulfides because they are crystallochemically similar and have comparable sizes (Table 1.1). Tellurium, being larger in size, prefers to form independent telluride minerals often occurring as microsegregations in sulfide minerals. The most common form of tellurium in nature is that of tellurides. Sulfur, selenium, and tellurium are principal components of intrusive and extrusive magmas and of volcanic gases. Tellurium may be found in magmatic, pegmatitic, and hydrothermal deposits, especially if these are in close association with epithermal gold and silver deposits (Kroschwitz and Howe-Grant, 1997).

Table 1.1. Atomic radii of tellurium, selenium, and sulfur (Kudryavtsev, 1974).

Element	valence = 2- Atomic radius (Å)	valence = 4+ Atomic radius (Å)	valence = 6+ Atomic radius (Å)
Tellurium	2.22	0.89	0.56-0.61
Selenium	1.98	0.69	0.35
Sulfur	1.86	0.53	0.30-0.34

Tellurium is approximately the seventy-second most abundant element in the earth's crust with an abundance of 0.001 ppm compared with that of selenium at 0.05 ppm and sulfur at 340 ppm (Greenwood and Earnshaw, 1984.). Like selenium, tellurium mostly forms minerals with heavy metals and there are no naturally occurring light metal tellurides. The light metals prefer to combine ionically with oxygen and sulfur rather than with tellurium which has a prominent tendency towards covalent bonding (Vlasov, 1966). The elements that tellurium is known to form minerals with are: oxygen, sulfur, and the heavy elements of gold, silver, copper, mercury, nickel, iron, lead, bismuth, arsenic, and antimony.

Tellurium is known to have close associations with gold, lead, and to some extent, silver and bismuth. Showing a tendency to combine with gold, the main source of tellurium comes from gold telluride ores. Some of the more common tellurides are: hessite Ag_2Te , petzite Ag_3AuTe_2 , calaverite AuTe_2 , sylvanite $(\text{Au},\text{Ag})_2\text{Te}_4$, altaite PbTe , tetradymite $\text{Bi}_2\text{Te}_2\text{S}$, rickardite Cu_7Te_5 , and nagyagite $\text{Pb}_5\text{Au}(\text{Sb},\text{Bi})\text{Te}_2\text{S}_6$. Tellurium and selenium are widely disseminated without forming an ore and there are no reserves to speak of; large resources of tellurium and selenium are found in base metal sulfide deposits that are mined for copper, copper-nickel, copper-zinc, lead, silver, and gold. Weathering and oxidation of telluriferous minerals leads to the formation of rare tellurites and tellurates.

1.1.4 Uses of tellurium

Commercial tellurium is recovered from anode slimes of electrolytic copper refining. It can be added to copper and steels to improve machinability; to rubber to improve vulcanization, aging, mechanical properties, and heat and abrasion resistance; to cast iron to control the chill depth; as a colourant for ceramics and glasses; and can be used to form specialty glasses for infrared transmission.

1.2 Tellurium Coordination and Structure in Minerals

The coordination about Te^{4+} is complex, diverse, and difficult to describe, which has led to a long history of interpretation. Conversely, the coordination about Te^{6+} is relatively simple to describe. Over the years the understanding of Te^{4+} coordination has grown from relatively simple three- and four-coordinate geometries to more complex models involving up to eight or nine bonds, including some long, weakly bonding interactions. Selected historical descriptions of tellurium coordination are summarized here.

1.2.1 Tellurium (IV) coordination

Zemann (1968) noticed the varied coordination around Te^{4+} and attempted to categorize it as having either three- or four-coordination (Figure 1.1). Three-coordinated Te^{4+} results in a trigonal pyramid with $\text{Te}^{4+}\text{--O} \sim 1.95 \pm 0.05 \text{ \AA}$ and $\text{O--Te}^{4+}\text{--O}$ angles of $\sim 95^\circ$. Four-coordinated Te^{4+} exhibits a trigonal dipyramid with one corner of the equatorial plane unoccupied. Examining the bond angles in these two structures, he noticed that they deviated from the ideal

in both cases. He rationalized this effect as being the result of the lone pair of electrons occupying the free corner of the coordinate polyhedron (this is interpreted as the electron lone pair occupying the apex of the three-coordinated pyramid and occupying one corner of the equatorial triangle of the four-coordinated trigonal bipyramid.) Also suggested were intermediates between these two end-members which were described as having $(3 + 1)$ coordination. These coordination polyhedra can be linked to form groups, chains, sheets, and framework structures. Zemann (1968) wrote that the one-sided coordination causes the formation of relatively open structures as the closest oxygen on the side with the electron lone pair is often longer than the minimum distance of ~ 2.7 Å.

In 1971, Zemann published an additional paper on the stereochemistry of Te^{4+} with respect to oxygen coordination. It was revealed that the three nearest neighbours to tellurium have fairly constant bond lengths (ranging from 1.78 to 2.15 Å) and angles. He also noticed that the fourth bond length ranges from 2.08 to 2.98 Å and that its direction is markedly constant (Figure 1.2) if Te-O bonds ≥ 2.75 Å are excluded. Similarly, there is a directional component with additional oxygen atoms where Te-O distances of up to 3.0 Å occur; this is in addition to the shorter three or four Te-O bonds.

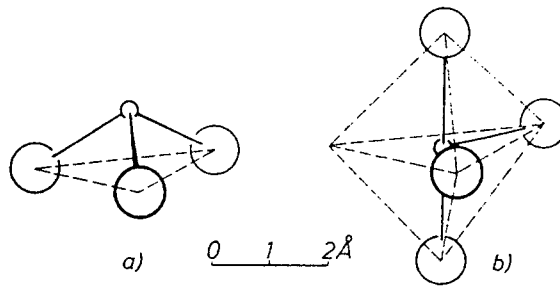


Figure 1.1. a) Three- and b) four-fold coordination of Te^{4+} (after Zemmann, 1969). Small circles: Te; large circles: O.

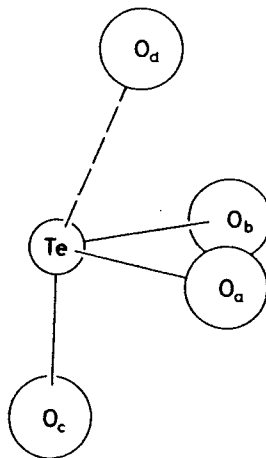


Figure 1.2. Coordination figure showing four oxygen atoms around Te^{4+} (after Zemmann, 1971). Median distance of Te– O_a , Te– O_b , Te– O_c is 1.92 ± 0.08 Å; Te– O_d varies from 2.08 to 2.98 Å.

For his dissertation, Lindqvist (1973) studied the coordinations of Te^{4+} and Te^{6+} . He found Te^{4+} to be either three- or four-coordinated forming pyramids and trigonal bipyramids (Figure 1.3). Many intermediates between these two forms were found as well. Occasionally, he found a fifth or sixth oxygen neighbour that interacted with tellurium. He reasoned that the inert pair of electrons requires a large space and thus limits the coordination of Te^{4+} to three or four strong bonds. The repulsions between the lone electron pair and the $\text{Te}-\text{O}$ bonds cause the polyhedra to distort away from its regular form. With regards to the directional component of the fifth and sixth oxygens as noted by Zemmann (1971), Lindqvist stated that “Merely the fact of specific orientations of oxygen atoms at distances ranging from ~ 2.2 to 3.0 \AA would suggest the presence of $\text{Te}^{4+}-\text{O}$ interactions, these being, of course, weaker than those corresponding to the short bonds (1.85 to about 2.10 \AA).” He suggested that $\text{Te}^{4+}-\text{O}$ distances less than 3.0 \AA should be considered as bonding distances.

Hanke (1973) suggested a simple way of determining whether tellurium is strongly affected by the fourth oxygen neighbour. If the strong $\text{Te}-\text{O}$ bond opposite to the fourth neighbour is longer than the other two strong bonds and if the angle is substantially larger than the other two bond angles, then tellurium should be considered four-coordinated.

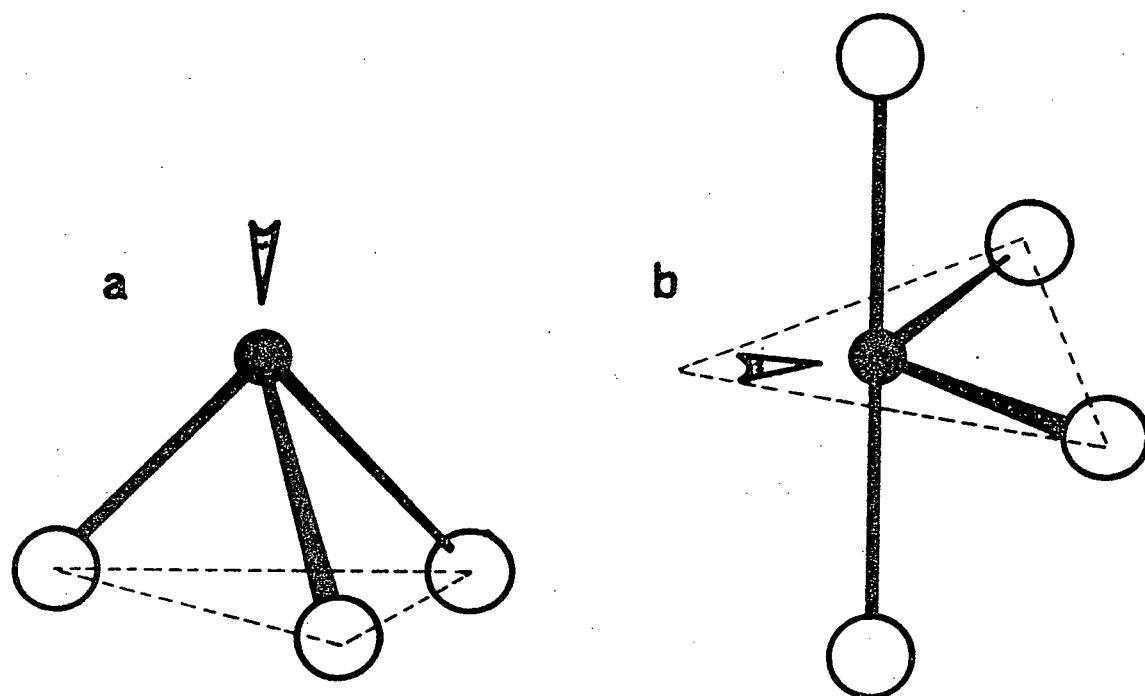


Figure 1.3. The coordination of Te^{4+} as depicted by Lindqvist (1973). a) and b) show the idealized three- and four-fold coordinations including the lone electron pair.

In describing the molecular geometry of the elements in the periodic table, Gillespie (1972) described various coordinations involving electron lone pairs. His work was based on the valence-shell electron-pair repulsion theory (VSEPR) and followed the rule “*The pairs of electrons in a valence shell adopt that arrangement which maximizes their distance apart, i.e., the electron pairs behave as if they repel each other.*” With regards to the tetrahedral AX_3E configuration (A = central atom, X = ligand, E = non-bonding or lone electron pair), Gillespie showed that the angles between the three ligands are less than that for an ideal tetrahedron (109.5°). This happens because the lone electron pair is larger and more spread out than the bonding pairs and so has more of a repulsive effect than if it were a bonding pair of electrons. This electron lone pair interaction with ligands is also seen in the trigonal bipyramidal AX_4E configuration with resulting bond angles that are smaller than the ideal angles of 90° (axial–equatorial), 120° (equatorial–equatorial), and 180° (axial–axial). In AX_4E , Gillespie (1972) also showed that while the lone electron pair may occupy either an axial or equatorial position (Figure 1.4) “non-bonding pairs will occupy the equatorial positions of a trigonal bipyramid arrangement because there is more room for them in these positions and because their interactions with neighbouring electron pairs are thereby minimized.” Both the AX_3E and AX_4E configurations have been used to describe the coordination around tellurium (IV).

Brown (1974) used the bond-valence method to study the irregular coordinations of the isoelectronic series: Sn(II), Sb(III), Te(IV), I(V), and Xe(VI). He described the cations as being at the center of octahedrons distorted by the lone pair of electrons. The distortion causes strong bonds to occur opposite weak bonds and intermediate bonds to be opposite each other. The lengthening of certain bonds results in five octahedrally-based configurations with three distinctive cases (Δ , \mathcal{C} , \mathcal{E}) and two intermediates (\mathcal{B} , \mathcal{D}) (Figure 1.5). Brown’s Δ configuration,

otherwise depicted as AX_4E (four-coordinated based on a trigonal bipyramid) has two strong, two intermediate, and two weak bonds. The \mathcal{C} configuration (AX_3E , three-coordinated, and based on a tetrahedron) has three strong and three weak bonds. The \mathcal{E} configuration (AX_5E , five-coordinated, and based on an octahedron) has one strong, one weak, and four intermediate bonds. The configurations \mathcal{B} and \mathcal{D} form intermediates between the others in a continuous series:

$$\mathcal{A} \leftrightarrow \mathcal{B} \leftrightarrow \mathcal{C} \leftrightarrow \mathcal{D} \leftrightarrow \mathcal{E}.$$

It was noticed that in almost all the cases, two to four longer bonds are situated proximal to the direction of the lone pair. Using bond-valence arguments and the ligand fluorine, Brown (1974) concluded, for configuration \mathcal{E} only, that “the weak bond is replaced by 3 or 4 weak bonds, but the 5 stronger bonds remain close to the octahedral configuration”. Although not explicitly stated by Brown himself, this is interpreted to mean that the coordinations about these cations can be up to nine-coordinated (5 stronger bonds and four weaker bonds arranged in the direction of the lone electron pair).

Galy *et al.* (1975) studied the effect of the electron lone pair on the stereochemistry of the oxides, fluorides, and oxyfluorides of: Ge(III), As(III), Se(IV), Br(V), Sn(II), Sb(III), Te(IV), I(V), Xe(VI), Tl(I), Pb(II), and Bi(III). For Te(IV), he found that the average Te–lone pair distance was 1.25 Å and that neither the electron lone pair nor the Te cation lay on the equatorial plane of the trigonal bipyramid. This distortion was thought to be caused by the repulsive interactions between the electron lone pair and the neighbouring oxygen atoms. With respect to figure 1.2, Te(IV) was found to be displaced towards Oc.

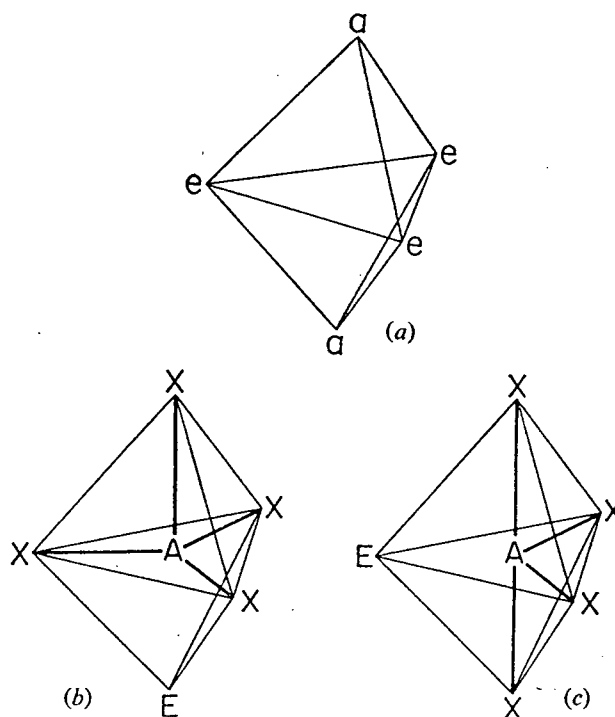


Figure 1.4. Trigonal bipyramidal coordination showing in (a) the axial, a , and equatorial, e , positions (after Gillespie, 1972). Possible locations for the lone electron pair, E , are shown in (b) and (c) with the preferred orientation being (c).

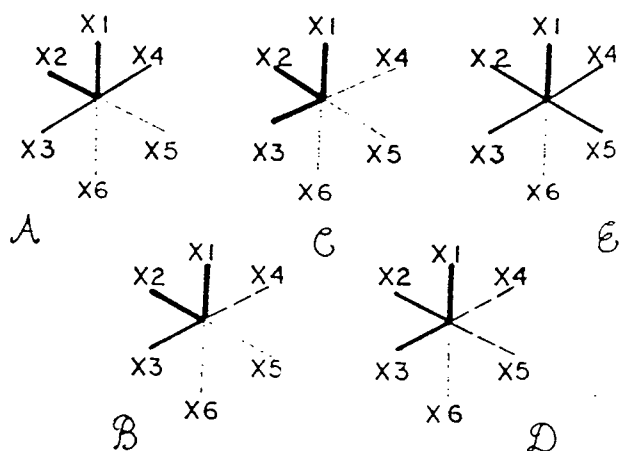


Figure 1.5. Possible octahedral configurations of Te^{4+} (after Brown, 1974). The strength of the bond is correlated with the density of the line.

In his study of tellurite minerals, Back (1990) used the bond-valence method to reveal the true tellurium coordinations of previously published structures. This was done because he noticed that many of the structures listed only the three or four shortest bonds (based on early interpretation of Te coordination) and neglected any of the intermediate or longer bonds. He found these intermediate and longer bonds to have important roles in holding some structures together. It was determined that tellurium could have a coordination anywhere from four to eight (Figure 1.6). It was also found that the longer bonds were directional although not as definite as the four shortest bonds. He summarize the coordination of tellurium as “distorted polyhedra with short bonds on one side and long bonds on the other side”. Noticing that all the tellurites studied were lone pair stereoactive, he tried to locate these electrons with geometric arguments. The lone pair interaction with the oxygens creates longer bond lengths and angles in certain directions with the lone pair almost certainly on the side of the polyhedron with larger bond lengths and angles.

Rossell (1992) reported the four tellurium atoms in $\text{Bi}_2\text{Te}_4\text{O}_{11}$ to be six-, seven-, and eight-coordinated but stated that “In reality, however, the coordination polyhedra of all four tellurium atoms of this structure can be considered as distorted octahedra, the distortion being largely the result of lone-pair repulsions.”

Over time, the coordination of Te^{4+} has been described in terms of an increasing number of bonds. It has been shown (Back, 1990) that, in some cases, the longer, weaker bonds are important in holding structures together and thus, they must be accepted as bonding interactions with Te^{4+} .

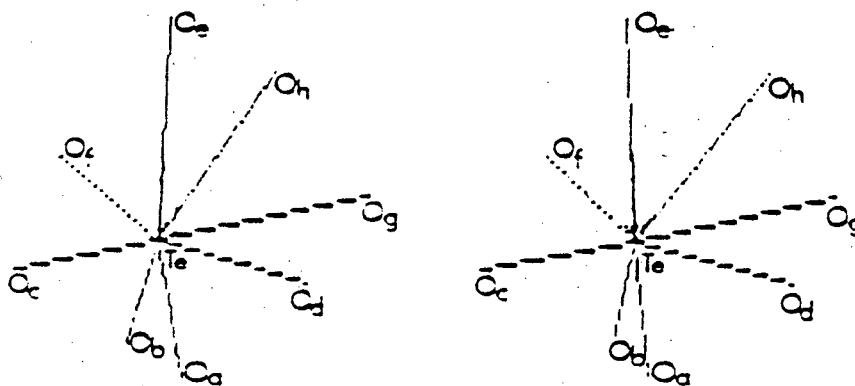


Figure 1.6. Back's (1990) depiction of Te^{4+} coordination. The lettering is consistent with Zemmann (1971).

1.2.2 Coordination of tellurium (VI)

Lindqvist (1973) found that Te^{6+} always tended to form octahedrons with oxygen and found no evidence that it forms other types of coordination polyhedra. The $\text{Te}^{6+}\text{--O}$ bond lengths varied between 1.85 to 2.05 Å with bond angles deviating by up to fifteen percent from the ideal octahedral values.

Te^{6+} is always six-coordinated and forms regular octahedrons. There is no difficulty with large distortions of bond lengths or angles as that found with Te^{4+} because there is no stereochemically active lone pair of electrons. The known tellurate mineral structures all report six-coordinated Te^{6+} octahedrons with the average bond lengths of $\text{Te}^{6+}\text{--O} \sim 1.93$ Å and the average $\text{O--Te}^{6+}\text{--O}$ bond angles $\sim 90^\circ$.

1.3 Known Tellurium Oxysalts and Structures

To date, there are sixty-seven known tellurium oxysalt minerals, of which thirty-six are tellurites, twenty-four are tellurates, and seven are Te-oxysalts with mixed Te^{4+} and Te^{6+} valences. The complete list of tellurium oxysalts, formulae, and structure references is found in Table 1.2. The categorized lists are located in Appendix B. Thirty-one of these minerals structures are known (including dugganite and choloalite), twenty-four are tellurites, six are tellurates, and one is a mixed valence structure. The majority of known structures are of tellurites, probably because tellurites are more common and thus more accessible than tellurates when searching for single crystals. Zemmann (1968) remarked that tellurium seemed to prefer the tetravalent state under the conditions for formation of natural tellurium oxysalts. This is

consistent with the fact that, in aqueous solution, Te^{4+} is the most stable valence state of tellurium.

It should be pointed out that in the course of this research, there was significant difficulty in obtaining crystals large enough for use with the single crystal X-ray diffractometer. Even though there was access to museum quality minerals (from the Pinch collection at the Canadian Museum of Nature) many of the crystals were found as crusts, powdery aggregates, or crystals that were obviously not singular. The difficulty in procuring single crystals is one of the factors limiting the structure solution rate of tellurium oxysalts minerals.

Table 1.2. Tellurium oxysalt minerals.

Name	Formula	Structure Reference
balyakinite	CuTeO_3	Lindqvist 1972
blakeite	$\text{Fe,TeO}_3(?)$	
burckhardtite	$\text{Pb}_2(\text{Fe,Mn})\text{Te}(\text{Si}_3\text{Al})\text{O}_{12}(\text{OH})_2 \cdot \text{H}_2\text{O}$	
carlfriesite	CaTe_3O_8	Effenberger <i>et al.</i> 1978
cesbronite	$\text{Cu}_5(\text{TeO}_3)_2(\text{OH})_6 \cdot 2\text{H}_2\text{O}$	
chekhovite	$\text{Bi}_2\text{Te}_4\text{O}_{11}$	Rossel <i>et al.</i> 1992
cheremnykhite	$\text{Pb}_3\text{Zn}_3\text{TeO}_6(\text{VO}_4)_2$	
chiluite	$\text{Bi}_6\text{Te}_2\text{Mo}_2\text{O}_{21}$	
choloalite	$\text{Pb}_3\text{Cu}_3\text{Te}^{4+}\text{O}_{18} \cdot (\text{Cl}, \text{H}_2\text{O})$	Lam <i>et al.</i> 1998
cliffordite	UTe_3O_9	Brandstätter 1981
cuzticite	$\text{Fe}_2\text{TeO}_6 \cdot 3\text{H}_2\text{O}$	
denningite	$(\text{Ca,Mn})(\text{Mn,Zn})\text{Te}_4\text{O}_{10}$	Walitzi 1964
dugganite	$\text{Pb}_3\text{Zn}_3\text{Te}^{6+}\text{As}_2\text{O}_{14}$	Lam <i>et al.</i> 1998
dunhamite	$\text{PbTeO}_3(?)$	
emmonsite	$\text{Fe}_2(\text{TeO}_3)_3 \cdot 2\text{H}_2\text{O}$	Pertlik 1972
eztlite	$\text{Pb}_2\text{Fe}_6\text{Te}_4\text{O}_{15}(\text{OH})_{10} \cdot 8\text{H}_2\text{O}$	
fairbankite	PbTeO_3	
ferrotellurite	$\text{FeTeO}_4(?)$	
frankhawthorneite	$(\text{Cu}^{2+})_4\text{Te}^{6+}\text{O}_4(\text{OH})_2$	Grice & Roberts 1995
girdite	$\text{H}_2\text{Pb}_3(\text{TeO}_3)(\text{TeO}_6)$	
graemite	$\text{CuTeO}_3 \cdot \text{H}_2\text{O}$	
jensenite	$(\text{Cu}^{2+})_3\text{Te}^{6+}\text{O}_6 \cdot 2\text{H}_2\text{O}$	Grice <i>et al.</i> 1996
juabite	$\text{Cu}_5(\text{TeO}_4)_2(\text{AsO}_4)_2 \cdot 3\text{H}_2\text{O}$	
keystoneite	$\text{H}_{0.8}\text{Mg}_{0.8}(\text{Ni,Fe,Mn})_2(\text{TeO}_3)_3 \cdot 5\text{H}_2\text{O}$	
khinite	$\text{Cu}_3\text{PbTeO}_4(\text{OH})_6$	
kinichilite	$\text{Mg}_{0.5}(\text{Mn}^{2+}, \text{Zn})\text{Fe}^{3+}(\text{TeO}_3)_3 \cdot 4.5\text{H}_2\text{O}$	Miletich 1995
kuksite	$\text{Pb}_3\text{Zn}_3\text{TeO}_6(\text{PO}_4)_2$	

Table 1.2 continued.

Name	Formula	Structure Reference
kuranakhite	PbMnTeO_6	
leisingite	$\text{Cu}(\text{Mg}, \text{Cu}, \text{Fe}, \text{Zn})_2\text{Te}^{6+}\text{O}_6 \cdot 6\text{H}_2\text{O}$	Margison <i>et al.</i> 1997
mackayite	$\text{FeTe}_2\text{O}_5(\text{OH})$	Pertlik and Gieren 1977
magnolite	Hg_2TeO_3	Grice 1989
mcalpineite	$\text{Cu}_3\text{TeO}_6 \cdot \text{H}_2\text{O}$	
moctezumite	$\text{Pb}(\text{UO}_2)(\text{TeO}_3)_2$	Swihart 1993
montanite	$(\text{BiO})_2\text{TeO}_4 \cdot 2\text{H}_2\text{O}$	
mroseite	$\text{CaTeO}_2(\text{CO}_3)$	Fischer <i>et al.</i> 1975
nabokoite	$\text{Cu}_7\text{TeO}_4(\text{SO}_4)_5 \cdot \text{KCl}$	Pertlik & Zemann 1988
oboyerite	$\text{H}_6\text{Pb}_6(\text{TeO}_3)_3(\text{TeO}_6)_2 \cdot 2\text{H}_2\text{O}$	
parakhinite	$(\text{Cu}^{2+})_3\text{PbTe}^{6+}\text{O}_6(\text{OH})_2$	Burns <i>et al.</i> 1995
paratellurite	$\alpha\text{-TeO}_2$	Thomas 1988
pingguite	$\text{Bi}_6\text{Te}_2\text{O}_{13}$	
plumbotellurite	$\alpha\text{-PbTeO}_3$	Mariolacos 1969
poughite	$\text{Fe}_2(\text{TeO}_3)_2(\text{SO}_4) \cdot 3\text{H}_2\text{O}$	Pertlik 1971
quetzalcoatlite	$\text{Cu}_4\text{Zn}_8(\text{TeO}_3)_3(\text{OH})_{18}$	
rajite	CuTe_2O_5	Hanke <i>et al.</i> 1973
rodalquilarite	$\text{H}_3\text{Fe}_2(\text{TeO}_3)_4\text{Cl}$	Dusauroy & Protas 1969
schieffelinite	$\text{Pb}(\text{Te}, \text{S})\text{O}_4 \cdot \text{H}_2\text{O}$	
schmitterite	$(\text{UO}_2)\text{TeO}_3$	Meunier & Galy 1973 Loopstra & Brandenberg 1978
smirnite	Bi_2TeO_5	
sonoraite	$\text{Fe}^{3+}\text{Te}^{4+}\text{O}_3(\text{OH}) \cdot \text{H}_2\text{O}$	Donnay <i>et al.</i> 1970
spiroffite	$(\text{Mn}, \text{Zn})_2\text{Te}_3\text{O}_8$	Cooper & Hawthorne 1996

Table 1.2 continued.

Name	Formula	Structure Reference
teineite	$\text{CuTeO}_3 \cdot 2\text{H}_2\text{O}$	Zemann & Zemann 1962 Effenberger 1977
tellurite	TeO_2	Beyer 1967
tlalocite	$\text{Cu}_{10}\text{Zn}_6\text{Te}_3\text{O}_{11}\text{Cl}(\text{OH})_{25} \cdot 27\text{H}_2\text{O}$	
tlapallite	$\text{H}_6(\text{Ca,Pb})_2(\text{Cu,Zn})_3\text{SO}_4(\text{TeO}_3)_4\text{TeO}_6$	
unnamed 604	$\text{Au}_4\text{Pb}_3\text{Te}_2\text{O}_{11}$	
unnamed 624	Au_2TeO_3	
unnamed 625	$\text{Au}_2\text{TeO}_6 \cdot 2\text{H}_2\text{O}$	
unnamed 626	$\text{Au}_2(\text{Bi,Te})\text{O}_3$	
unnamed 627	$(\text{Zn,Pb,Cu})_3\text{TeO}_6 \cdot 2\text{H}_2\text{O}$	
unnamed 628	$\text{Au}_6(\text{PbO}_3)_2\text{TeO}_4$	
unnamed 629	$\text{Au}_6\text{Pb}_2(\text{PbO}_3)_2(\text{TeO}_4)_3 \cdot 6\text{H}_2\text{O}$	
utahite	$\text{Cu}_5\text{Zn}_3(\text{TeO}_4)_4(\text{OH})_8 \cdot 7\text{H}_2\text{O}$	
winstanleyite	TiTe_3O_8	Meunier & Galy 1971
xocomecatlite	$\text{Cu}_3\text{TeO}_4(\text{OH})_4$	
yafsoanite	$(\text{Ca,Pb})_3\text{Zn}_3\text{Te}_2\text{O}_{12}$	Jarosch & Zemann 1989
yecoraite	$\text{Fe}_3\text{Bi}_5\text{O}_9(\text{TeO}_3)(\text{TeO}_4)_2 \cdot 9\text{H}_2\text{O}$	
zemannite	$(\text{H,Na})_2(\text{Zn,Fe})_2(\text{TeO}_3)_3 \cdot n\text{H}_2\text{O}$	Matzat 1968 Miletich 1995

2.0 EXPERIMENTAL PROCEDURES

This chapter will describe the experimental methods used to obtain single-crystal X-ray diffraction data. The general procedures are detailed in this chapter and deviations from these methods along with specific details are discussed in the individual chapter for each mineral.

2.1 Crystal Selection and Preparation

The first step in the procedure of single-crystal X-ray diffractometry is to choose an appropriate crystal for data collection. The crystal size is important with recommended maximum and minimum dimensions of 50 μm and 10 μm , respectively (Mark Cooper, personal communication, 1996). For this project, smaller crystals were desired because of the high absorption of X-rays that heavy elements such as tellurium and lead are known for; larger crystals absorb more X-rays and so the diffracted data may be inferior to the data collected with smaller crystals (Joel Grice, personal communication, 1995). It is highly desirable that the mineral selected be a true single crystal so that problems associated with twinning do not have to be dealt with. The job of structure solution and refinement is difficult enough without added problems that could have been prevented by the better selection of a crystal.

Rodalquilarite and graemite were provided as single crystals by Andrew Roberts of the Geological Survey of Canada. Dugganite and choloalite crystals were provided by the Canadian Museum of Nature (donated from the Pinch collection). The final data set for dugganite was collected on a crystal obtained directly from Mr. William Pinch of Rochester, New York, who generously provided beautifully formed octahedral crystals.

Single crystals of dugganite and choloalite were selected and the absence of twinning was confirmed by looking at the crystals under crossed polars of a polarizing microscope. Attempts to shape choloalite into a sphere were not successful as the crystals easily disintegrated in an air-driven, circular, abrasion grinder. The dugganite crystal used for data collection was not manually shaped because it was thought that its octahedral morphology would result in minimal problems with absorption and because earlier attempts at shaping dugganite crystals from the Canadian Museum of Nature were not successful due to disintegration of the crystals. Spherically-shaped crystals are highly desired for single-crystal X-ray crystallography because the absorption of X-rays is uniform. An absorption correction would still be required because it is unlikely that a perfect sphere could be generated, but the absorption correction would not be as influential on the final results.

Both the choloalite and dugganite crystals were mounted on glass fibres with the use of “five-minute” epoxy. The rodalquilarite and graemite crystals were provided mounted and no attempts were made to shape them for fear of losing the crystals. The dimensions and origins of the crystals used in this study are located in their respective chapters.

2.2 Data Collection

Two instruments were used for data collection: a Siemens *P3* automated four-circle diffractometer using molybdenum X-radiation (located at UBC) was used for all four minerals and the four-circle diffractometer at HASYLAB beam line D3 (Hamburg, Germany), using synchrotron radiation, was used to collect an additional data set for graemite.

2.2.1 Single crystal X-ray diffraction using molybdenum X-radiation

Each crystal was mounted on a Siemens P3 automated four-circle diffractometer equipped with a molybdenum-target X-ray tube (operating at 55 kV, 35 mA) and a precisely oriented graphite crystal monochromator mounted with equatorial geometry. The crystal was centered and the correct unit cell was selected from an array of real space vectors corresponding to potential unit cell axes. Least-squares refinement of these reflections, together with the orientation matrix relating the crystal axes to the diffractometer axes, produced the cell dimensions for each crystal. These dimensions were checked against the literature to be certain that the correct unit cell had been chosen.

Intensity data were collected in the θ - 2θ scan mode, using ninety-six steps with a scan range from $[2\theta (\text{MoK}\alpha_1) - 1.1^\circ]$ to $[2\theta (\text{MoK}\alpha_1) + 1.1^\circ]$ and a variable scan rate between 0.5 and 29.3°/min depending on the intensity of an initial one second count at the centre of the scan range. Backgrounds were measured for half the scan time at the beginning and end of each scan. The stability of the crystal alignment was monitored by collecting two standard reflections every twenty-five measurements.

Reflections uniformly distributed with regard to 2θ were measured at 5° intervals of ψ (the azimuthal angle corresponding to rotation of the crystal about its diffraction vector) from 0 to 355° , after the method of North *et al.* (1968). These data were used to calculate an absorption correction which was then applied to the entire data set. The data were also corrected for Lorentz, polarization, and background effects, averaged and reduced to structure factors.

Data and absorption collection statistics for each crystal and any deviations from this procedure is described in the individual chapter of each mineral.

2.2.2 Single crystal X-ray diffraction using synchrotron radiation

As previously mentioned, the final data collection for graemite was done using synchrotron light. This light is generated by accelerating electrons around a large circle at close to the speed of light. The electrons emit radiation in a continuous spectrum from 0.1 to 50,000 Å and this radiation is directed through beamlines to workstations. A monochromator is used to filter through the desired radiation.

Synchrotron radiation is a powerful light source and was used because of the perceived difficulties with the graemite crystal. The very small, tellurium-bearing crystal diffracted poorly and it was thought that with a more powerful light source, an improved data set could be obtained.

At 295 K, single crystal X-ray diffraction data of graemite were collected with the four-circle diffractometer at HASYLAB beam line F1. The wavelength used was 0.4959 Å. The collection was done by H. Meyer and W. Morgenroth. The lattice parameters of graemite are $a = 6.816$, $b = 25.627$, $c = 5.784$ Å, $\alpha = 90$, $\beta = 90$, $\gamma = 90^\circ$. A continuous scan mode was used with the ω axis rotated at a constant speed throughout the Bragg position. Scalers were recorded and cleared at fixed time intervals. After insertion of appropriate attenuator combinations, the scan speed was adjusted to record a maximum of 2500 counts, without exceeding measurement times of 0.1 to 1.0 s/step. A total of 3207 reflections (including test reflections) were recorded comprising four asymmetric units.

Data reduction included normalization to the primary beam intensity monitor and an on-line correction for the (measured) beam polarization, following the procedure of Kirfel and Eichhorn (1990). The data were corrected for absorption by approximating the shape of the

crystal with a polyhedron (eight faces). The unique data set ($R_{\text{int}} = 2.7\%$) comprised 3207 reflections.

2.3 Structure Solution and Refinement

The Siemens SHELXTL PC system of programs was used throughout this study. Scattering curves for neutral atoms together with anomalous dispersion coefficients were taken from Cromer and Mann (1968) and Cromer and Liberman (1970). Miscellaneous collection and refinement data are given in Tables 3.2, 4.2, and 5.1.

The procedure for the structure solution and refinement of each crystal was different and is detailed in each of their respective chapters. Generally, for structure solution, the heavy atoms of the mineral were located by using either Patterson or direct methods. This was followed by inputting the rest of the cations followed by the anions. Ultimately, the lowest R value was achieved with various steps including setting the cations and possibly anions anisotropic, restricting observed data to larger $\sigma(F)$ values, omitting individual reflections, using a weighting factor, and refining atoms versus a substituting element. Elements not found in the empirical formulas but possibly present by substitution were found suggested in the original chemical descriptions of the crystals. For choloalite and dugganite, these and other elements were searched for with the electron microprobe.

After structure solution and refinement, the program *MISSYM* (Le Page, 1987) was used in each case as a double-check to detect any missing symmetry that may have been present; none was ever found. Before the final refinements of the structures, the program *STRUCTURE TIDY* (Gelato and Parthé, 1987) was used to standardize the atomic positions according to the crystallographic conventions proposed by Parthé and Gelato (1984).

2.3.1 *MISSYM*

The computer program *MISSYM* (Le Page 1987) was used, after structure refinement, to detect any symmetry elements that may have been overlooked in dugganite, choloalite, and rodalquilarite. Citing incidents of crystal structures published in subgroups of the correct space groups (reviewed by Marsh and Herbstein, 1983; Baur and Tillmanns, 1986), this program was developed to serve as a double-check against such errors in the future. Le Page (1987) recommended that *MISSYM* be routinely used on structural data about to be published.

Using the atomic positions, the program is able to detect overlooked symmetry and quasi-symmetry. Inaccurate data or disorder of atoms may lead to incorrect results. *MISSYM* uses default errors of 1° (for the obliquity of metric symmetry elements) and 0.25 \AA (for atomic positions); this serves to create a range that safeguards against slightly inaccurate data but it may also create problems by causing the detection of extra symmetry elements in a correct structure. The program is not able to prove the presence of symmetry elements nor is it able to discriminate symmetry from quasi-symmetry and so, it is up to the user to examine the experimental data to confirm the reality of these symmetry elements.

2.3.2 *STRUCTURE TIDY*

Another program, *STRUCTURE TIDY* (Gelato and Parthé, 1987), was used on the refined structural parameters of dugganite, choloalite, and rodalquilarite. The program was written to help standardize the way in which crystal structures are reported, according to an earlier set of rules proposed by Parthé and Gelato (1984). By reviewing atomic coordinates, this standardization of crystal structures enables the recognition of similar structures.

The input consists of a space group symbol, unit cell parameters, and atomic positions which the program uses to output a reordered list (based on Wyckoff letters) of standardized atomic positions in a standard space group setting. The origin and orientation of the structure is chosen as the setting with the minimum standardization parameter, Γ . Where:

$$\Gamma = \sum_{i=1}^N (x_i^2 + y_i^2 + z_i^2)^{1/2}$$

N = number of representative atoms in the asymmetric unit

x, y, z = atomic coordinates

The standardization of slightly deformed structures or structures without well-defined atomic coordinates may give different results from isotypic structures. If so, it is suggested by Gelato and Parthé (1987) that all the possible settings be reviewed in an attempt to match the isotypic structures. Parthé and Gelato (1984) are careful to say that “standardized description should never replace any other description chosen to demonstrate a particular relationship to other structures, but should be given as an additional description”.

The work presented in this thesis is not fully standardized according to Parthé and Gelato (1984). The atomic coordinates have been changed in agreement to the program but the listing of atoms remains in the conventional way of cations first followed by anions.

2.4 Electron Microprobe Analysis

Electron microprobe analyses for choloalite and dugganite were obtained using a JEOL 733 electron microprobe with Tracor Northern 5500 and 5600 automation. Dr. T. Scott Ercit of the Canadian Museum of Nature performed both analyses using the wavelength-dispersion

mode. The operating conditions were as follows: voltage 15 kV, beam current 20 nA, and beam diameter 5 μm . Data were reduced using a PAP routine (program XMAZNT by C. Davidson, CSIRO). The analyses are given in Table 3.1 for dugganite and Table 4.1 for choloalite.

2.5 Infrared Analyses

Choloalite and dugganite crystals were sent to Elizabeth Moffatt at the Canadian Conservation Institute for infrared analyses. The results for dugganite were inconclusive. Experimental details and results for choloalite are given in chapter four.

2.6 Introduction to Bond Valence

After the final phase of structure refinement and electron microprobe analyses, the results for each crystal were subjected to bond-valence analysis. The strength of a bond can be quantified in terms of valence units (*v.u.*). The summation of the bond valences for all bonds to a central atom should result in a number equal to that atom's valence. This is expressed mathematically as:

$$\sum_j v_{ij} = V_i$$

where: v_{ij} = valence of bond between atoms i and j

V_i = valence of atom i

Values from Brown (1981) and Brese and O'Keeffe (1991) were used to generate bond-valence tables for each crystal. The results were then examined for deviations away from the formal valence of each atom. The equation used from Brown (1981) is:

$$s = (R / R_o)^{-N}$$

where: s = bond valence

R = observed bond length

R_o = bond length constant

N = slope of the correlation curve (given).

The equation used from Brese and O'Keeffe (1991) was based on Brown and Altermatt (1985) and is:

$$v_{ij} = \exp[(R_{ij} - d_{ij}) / b]$$

where: v_{ij} = bond valence between atoms i and j

R_{ij} = bond-valence parameter given in Brese and O'Keeffe (1991)

d_{ij} = observed bond length

b = universal constant, 0.37 Å (Brown and Altermatt, 1985).

The values from Brown (1981) presented an occasional problem as the paper does not contain constants for Te-Cl bonds.

3.0 DUGGANITE: CRYSTAL STRUCTURE AND REVISED FORMULA

3.1 Introduction

Dugganite was first described by Williams (1978) from three mine dumps in the Tombstone District, Cochise County, Arizona. The type material was discovered at the Emerald mine dump, occurring as "spherules of water-green hexagonal prisms abundant in a sugary, vuggy quartz matrix". Numerous crystals of dugganite were discovered at this locality, associated with parakhinite and other Te-oxysalt minerals. At the Old Guard mine dump, crystals of khinite are replaced on the outside by a druse of minute dugganite crystals. Other minerals found at this site include chloroargyrite, chrysocolla, quetzalcoatlite, and tenorite. At both the Emerald mine and Old Guard mine dumps, dugganite crystals were found associated with bromargyrite, chlorargyrite, and numerous unidentified Te-oxysalt minerals in quartz or manganese oxide gangue material. At the dump of the Joe Shaft mine, dugganite was found with other Te-oxysalt minerals, cerussite, emmonsite, and rodalquilarite.

Using Weissenberg and rotation photographs, Williams (1978) showed that dugganite is hexagonal, "perhaps" $P6/mmm$. Cell dimensions were refined from powder data: a 8.472(5), c 5.208(5) Å. The average chemical composition (obtained using spectroscopic techniques) was found to be PbO 55.3, CuO 1.2, ZnO 17.6, As₂O₅ 10.4, TeO₃ 14.0, H₂O (by the Penfield method) 1.5, total 100.0 wt %. Trace amounts of CO₂, Mo, Ag, and Cd also were detected. Additional (partial) analyses showed some substitution of Te for As. The chemical formula suggested by Williams (1978) was $Pb_3Zn_3(TeO_6)_x(AsO_4)_{2-x}(OH)_{6-3x}$, with x in the range 0.94 to 1.33; the generally accepted formula for dugganite is $Pb_3(Zn,Cu^{2+})_3(Te^{6+}O_6)(AsO_5)(OH)_3$.

A mineral resembling dugganite was also described by Kim *et al.* (1988) as a product of supergene oxidation in the Kuranakh deposit (central Aldan, Yakutia, Russia), where it is associated with calcite, cinnabar, gold, orpiment, altaite, clausthalite, descloizite, kuranakhite, naumannite, tiemannite, and yafsoanite. Single-crystal X-ray studies showed that the mineral is orthorhombic, with space group *Cmmm*, *C222*, *C2mm*, *Cm2m*, or *Cmm2*. Cell dimensions were refined from powder data: *a* 8.57(3), *b* 14.84(5), *c* 5.21(3) Å. The authors noted that X-ray data from “normal” dugganite can also be indexed on this cell. The average chemical composition (based on seven electron microprobe analyses) was found to be (in wt. %) PbO 51.47, ZnO 18.82, SiO₂ 0.96, P₂O₅ 0.70, V₂O₅ 3.61, As₂O₅ 12.16, Sb₂O₅ 0.07, TeO₃ 12.61, total 100.40. Note that this is *not* the average composition abstracted in *Am. Mineral.* 76, 1440, [1991]; that one was based on earlier analyses obtained using different standards and a non-standard data reduction routine. Recalculation on the basis of six Pb plus Zn atoms gave the formula Pb₃Zn₃Te(As,V,Si)₂(O,OH)₁₄. Other analogues of this mineral that contain V + Si >> As, or with significant substitution of P for As, were reported but not studied in detail by Kim *et al.* (1988).

Kim *et al.* (1990) described cheremnykhite and kuksite, two new minerals associated with dugganite in the Kuranakh deposit. The formulae, determined from electron microprobe analyses, were Pb₃Zn₃TeO₆(VO₄)₂ for cheremnykhite and Pb₃Zn₃TeO₆(PO₄)₂ for kuksite. X-ray diffraction studies showed that both minerals are orthorhombic (*Cmmm*, *C222*, *C2mm*, *Cm2m*, or *Cmm2*), with cell dimensions similar to those previously determined for dugganite from the same deposit (Kim *et al.* 1988). Their conclusion was that cheremnykhite, kuksite, and dugganite, are isostructural.

Dugganite has also been described from the Centennial Eureka mine dump in Juab County, Tintic District, Utah, where it occurs with other secondary Cu-, Te-oxysalt minerals (Marty *et al.* 1993).

3.2 Experimental

General details of the experimental methods used are found in Chapter two. The crystal used in this study is from the 400-foot level of the Empire mine, near Tombstone, Arizona. Fifty reflections with 2θ 7.83 to 45.69° were centered and from this the unit cell was derived. One sphere of reflections (3746 measurements, exclusive of standards) was collected from 3 to 60° 2θ . Eighteen of the reflections were rejected because of asymmetric backgrounds. Fourteen strong reflections were used for the absorption scan and the data (994 measurements) was used to calculate an absorption correction. The merging R index for the ψ -scan data set decreased from 8.5% before the absorption correction to 3.2% after the correction. Minimum and maximum transmissions were 0.030 and 0.068 respectively for the absorption-corrected data set. Of the 636 unique reflections, 558 were classed as observed [$I \geq 3\sigma(I)$].

Electron microprobe data for Si, P, Ca, As, and Te were collected for twenty-five seconds; data for all other elements were collected for fifty seconds. The standards used were almandine (AlK α), zircon (SiK α), Pb₇Ti(PO₄)₆ (PK α), CaTa₄O₁₁ (CaK α), VP₂O₇ (VK α), cuprite (CuK α), willemite (ZnK α), mimetite (AsL α), TeO₂ (TeL α), and crocoite (PbM α). The elements Mg, Fe, Co, and Ni were sought but not detected. The analytical results are given in Table 3.1 together with those from Williams (1978) and Kim *et al.* (1988).

Table 3.1. Chemical composition of dugganite.

		Williams (1978)*	Kim et al.(1988) [†]	This study [‡]
CaO	wt. %	negligible	–	0.24
PbO		55.3	51.47	53.13
CuO		1.2	0.00	1.06
ZnO		17.6	18.82	17.25
Al ₂ O ₃		–	–	0.07
SiO ₂		–	0.96	1.06
P ₂ O ₅		–	0.70	4.90
V ₂ O ₅		–	3.61	0.03
As ₂ O ₅		10.4	12.16	8.28
Sb ₂ O ₅		–	0.07	–
TeO ₃		14.0	12.61	13.48
H ₂ O		1.5	–	–
TOTAL		100.0	100.40	99.50
Ca ²⁺		negligible	–	0.06
Pb ²⁺		3.43	2.94	3.04
Cu ²⁺		0.21	0.00	0.17
Zn ²⁺		3.00	2.95	2.71
Al ³⁺		–	–	0.02
Si ⁴⁺		–	0.20	0.23
P ⁵⁺		–	0.13	0.88
V ⁵⁺		–	0.51	0.00
As ⁵⁺		1.25	1.35	0.92
Sb ⁵⁺		–	0.01	–
Te ⁶⁺		1.11	0.92	0.98
H ⁺		2.31	–	–
O ²⁻		14.25	14.02	13.90

Note: Oxides are expressed in weight percent; analyses are normalized on nine cations per formula unit. *Average of four AAS analyses for Pb, Cu, Zn, and three visible spectroscopy analyses for Te. As (two analyses) by UV spectroscopy. Trace Cd, Ag, Mo CO₂. Water by the Penfield method. [†]Average of seven electron microprobe analyses.

[‡]Average of six electron microprobe analyses.

3.3 Structure Solution and Refinement

Structure solution for dugganite was attempted with the recommended space group of *P6/mmm* but all trials failed to provide a good solution. Attempts with the space group *P3* were promising but the final results were never satisfactory. To save time, it was decided to solve for the atomic positions in *P1* (refined to an *R* index of 7.8% for an isotropic displacement model) and input those positions into *MISSYM* (Le Page 1987) to see which symmetry elements were present; this would hopefully lead to the correct space group. Using all atoms, *MISSYM* showed that a three-fold and three two-fold axes were missing which would give *P321* and *P312* as possible space groups. Interestingly, inputting only cation positions resulted in symmetry elements that correspond to the originally described *P6/mmm* space group. Both *P321* and *P312* space groups were used to try to solve the structure and *P321* gave a very good model whereas *P312* was never satisfactory. The assignment of phases to a set of normalized structure factors gave a mean value $|E^2 - 1|$ of 0.65, implying a non-centrosymmetric space group which agrees with the symmetry of the *P321* space group but not with the centrosymmetric *P6/mmm* space group. Both direct methods and Patterson techniques were used to solve the structure.

The structure was refined in *P321* to an *R* index of 4.7% for an isotropic displacement model. Conversion to anisotropic displacement factors for all of the atoms in the structure resulted in convergence at *R* and *wR* indices of 2.7 and 2.9%, respectively (3.9 and 10.4% for all 636 data). Addition of an isotropic extinction correction did not improve the results. The program *MISSYM* (Le Page 1987) was used to search for additional symmetry elements; none were indicated. The program *STRUCTURE TIDY* was used to standardize the positions according to crystallographic conventions and gave the final atomic positions.

Miscellaneous experimental information is given in Table 3.2. Positional coordinates and anisotropic and equivalent isotropic displacement factors are given in Table 3.3. Interatomic distances and angles are given in Table 3.4, and a bond-valence analysis in Table 3.5. Structure factors are listed in Appendix C.

Table 3.2. Miscellaneous information: dugganite.

a (Å)	8.460(2)	Rad/mono	MoK α /graphite
c	5.206(2)	Total reflections	3746
V (Å ³)	322.6(2)	Unique reflections	636
Space group	$P321$	R_{int} (%)	9.8
Z	1	$[I \geq 3 \sigma(I)]$	558
Crystal size (mm)	$0.1 \times 0.08 \times 0.05$	R (observed) %	2.7
μ (MoK α , mm ⁻¹)	49.89	R_w (observed) %	2.9
$R = \sum F_o - F_c / \sum F_o$			
$wR = \left[\sum (w \cdot F_o - F_c)^2 / \sum w \cdot F_o^2 \right]^{0.5}, w = 1$			

Table 3.3. Atomic parameters for dugganite.

Site	x	y	z	U_{11}^*	U_{22}	U_{33}	U_{12}	U_{13}	U_{23}	U_{eq}
Te	0	0	0	305(6)	305(6)	158(7)	153(3)	0	0	256(5)
As	1/3	2/3	0.5294(6)	237(11)	237(11)	369(18)	119(5)	0	0	281(9)
Pb	0.59472(9)	0	0	359(3)	380(4)	303(3)	190(2)	10(1)	20(3)	345(2)
Zn	0.2466(2)	0	1/2	343(8)	286(9)	248(9)	143(5)	-7(4)	-14(8)	299(7)
O(1)	0.122(1)	0.212(1)	0.217(2)	325(43)	363(48)	247(35)	109(38)	43(32)	-50(31)	339(35)
O(2)	0.467(2)	0.200(2)	0.339(2)	502(64)	671(77)	398(59)	48(62)	178(49)	-77(53)	632(56)
O(3)	1/3	2/3	0.239(4)	407(59)	407(59)	668(123)	203(30)	0	0	494(57)

* U_{ij} and U values are listed x 10^4

Table 3.4. Selected interatomic distances (Å) and angles (°) for dugganite.

Te-O(1)	× 6	<u>1.925(8)</u>	O(1)b-Pb-O(1)i		65.9(3)
<Te-O>		1.925	O(1)b-Pb-O(2)b	× 2	72.8(4)
			O(1)b-Pb-O(2)j	× 2	133.0(4)
As-O(2)a	× 3	1.64(1)	O(1)b-Pb-O(2)i	× 2	85.4(3)
-O(3)		<u>1.51(2)</u>	O(1)b-Pb-O(3)c	× 2	78.2(2)
<As-O>		1.61	O(1)b-Pb-O(3)f	× 2	132.5(2)
			O(1)i-Pb-O(2)j	× 2	113.4(3)
Pb-O(1)b	× 2	2.40(1)	O(2)-Pb-O(2)b	× 2	53.5(5)
-O(2)	× 2	3.00(1)	O(2)-Pb-O(2)j		100.0(5)
-O(2)b	× 2	2.70(1)	O(2)-Pb-O(3)c	× 2	89.0(4)
-O(3)c	× 2	<u>2.86(1)</u>	O(2)-Pb-O(3)f	× 2	70.0(4)
<Pb(1)-O>		2.74	O(2)b-Pb-O(3)c	× 2	113.4(5)
			O(2)b-Pb-O(3)f	× 2	<u>74.3(5)</u>
Zn-O(1)d	× 2	1.91(1)	<O-Pb-O>		91.5
-O(2)	× 2	<u>1.97(2)</u>			
<Zn-O>		1.94	O(1)d-Zn-O(1)a		129.8(4)
			O(1)d-Zn-O(2)	× 2	103.8(5)
O(1)-Te-O(1)e	× 6	89.2(3)	O(1)d-Zn-O(2)k	× 2	101.5(4)
O(1)-Te-O(1)f	× 3	85.5(5)	O(2)-Zn-O(2)k		<u>117.8(8)</u>
O(1)-Te-O(1)g	× 3	<u>96.8(5)</u>	<O-Zn-O>		109.7
<O-Te-O>		90.2			
O(2)a-As-O(3)	× 3	114.7(4)			
O(2)a-As-O(2)h	× 3	<u>103.8(5)</u>			
<O-As-O>		109.3			

Note: <M-φ> denotes the mean metal-ligand distance (Å). Equivalent positions: a = y, x, $\bar{z} - 1$; b = $\bar{y} + 1$, x - y, z; c = x, y - 1, z; d = $\bar{x} + y$, \bar{x} , z; e = \bar{y} , x - y, z; f = y, x, \bar{z} ; g = \bar{x} , $\bar{x} + y$, \bar{z} ; h = x - y, $\bar{y} + 1$, $\bar{z} + 1$; i = $\bar{x} + 1$, $\bar{x} + y$, \bar{z} ; j = x - y, \bar{y} , \bar{z} ; k = x - y, \bar{y} , $\bar{z} + 1$.

Table 3.5. Bond-valence* arrangement in dugganite.

	Te	As [†]	Pb	Zn	Total
O(1)	0.98(2) × 6 ↓		0.46(1) × 2 ↓	0.58(2) × 2 ↓	2.02
O(2)		1.18(3) × 3 ↓	0.092(5) × 2 ↓ × 1 → 0.202(6) × 2 ↓ × 1 →	0.48(3) × 2 ↓	1.95
O(3)		1.67(9)	0.134(4) × 2 ↓ × 3 →		2.07
Total	5.88	5.2	1.78	2.12	

*Calculated from the curves of Brese and O'Keeffe (1991). [†]Calculated assuming 54% As and 46%P.

3.4 Description of the Structure

There are four distinct cation sites in the dugganite structure. The coordinations of tellurium, arsenic, lead, and zinc are discussed followed by a description of the connectivity of the structure.

3.4.1 Tellurium coordination

The atom at the *Te* site, special position $1a$ (0,0,0), is coordinated by six O atoms forming a slightly distorted octahedron (Figure 3.1). The Te–O distances are 1.925 Å, and the O–Te–O angles range from 85.5 to 96.8° (mean 90.2°). The Te–O distances are similar to those previously described for lesingite (1.922 Å; Margison *et al.* 1997), jensenite (1.936 Å; Grice *et al.* 1996), frankhawthorneite (1.939 Å; Grice and Roberts 1995), parakhinite (1.92 Å; Burns *et al.* 1995), yafsoanite (1.929 Å; Jarosch and Zemann 1989), and carlfriesite (1.933 Å; Effenberger *et al.* 1978). The variance in the octahedron angle is 18.45, the mean octahedral quadratic elongation (Robinson *et al.* 1971) is 1.0053, and the polyhedral volume is 9.43 Å³. The electron-microprobe analyses, refined site-occupancy, and bond-valence analysis confirm that the site is completely occupied by Te⁶⁺.

3.4.2 Arsenic coordination

The atom at the *As* site, special position $2d$ ($1/3, 2/3, z$), is coordinated by four O atoms forming a distorted tetrahedron (Figure 3.2). The As–O distances are 1.64 Å ($\times 3$) and 1.51 Å (mean 1.61 Å), and the O–As–O angles are 103.8° and 114.7° (mean 109.3°). The variance in

the tetrahedron angle is 35.93, the mean tetrahedron quadratic elongation is 1.0080, and the polyhedron volume is 2.11 Å³. The average electron microprobe analysis indicates that the As site is occupied by As⁵⁺ (45%), P⁵⁺ (43%), Si⁴⁺ (11%), and Al³⁺ (1%). Refinement of the site occupancy for As and P shows 54(2)% As, 46(2)% P. The mean bond valence (Brese and O'Keeffe 1991) obtained using these proportions is 5.2 valence units (*v.u.*). The bond valence obtained using proportions from the average electron microprobe analysis is 5.0 *v.u.*, and the values for the coordinating O(2) and O(3) atoms are 1.91 and 2.02 *v.u.*, respectively.

3.4.3 Lead coordination

The atom at the *Pb* site, at special position 3*e* (*x*,0,0), is coordinated by eight O atoms forming a distorted snub disphenoid (Johnson 1965) (Figure 3.3). The Pb–O distances range from 2.40 to 3.00 Å (mean 2.74 Å) and the O–Pb–O angles vary from 65.9° to 133.0° (mean 91.5°). The polyhedral volume is 34.40 Å³. The Pb site is almost completely occupied by Pb²⁺, although the electron microprobe results suggest a small amount of substitution (2%) by Ca²⁺. Pb²⁺ is commonly lone-pair stereoactive, which typically results in a very asymmetrical (one-sided) coordination, with the lone pair of electrons positioned on the opposite side of the atom to the coordinating anions. However, the coordination of Pb²⁺ in dugganite is relatively symmetrical, and the difference-Fourier maps show no evidence of a lone pair of electrons.

3.4.4 Zinc coordination

The atom at the *Zn* site, special position 3*f* (*x*,0,1/2), is coordinated by four O atoms forming a distorted tetrahedron (Figure 3.4). The Zn–O distances range from 1.91 to 1.97 Å

(mean 1.94 Å); these are similar to the $^{[4]}\text{Zn-O}$ length (1.97 Å) calculated using ionic radii from Shannon (1976). The O–Zn–O angles range from 101.5 to 129.8° (mean 109.7°). There are two additional O(1) atoms at distances of 2.90 Å; it is unlikely that they form bonds with the atom at the Zn position. The tetrahedral angle variance is 135.30, the mean tetrahedral quadratic elongation is 1.0363, and the polyhedral volume is 3.55 Å³. The Zn site is almost completely occupied by Zn²⁺. The average electron microprobe results suggests a minor amount (6%) of substitution by Cu²⁺, although Cu²⁺ does not commonly occur in tetrahedral coordination (Eby and Hawthorne 1993).

3.4.5 Structure connectivity

The TeO₆ octahedra and PbO₈ polyhedra share edges to form a heteropolyhedral sheet parallel to (001) (Figure 3.5). Each TeO₆ octahedron shares three edges, each with a different PbO₈ polyhedron; the lengths of the shared edges are 2.61 Å. As expected, this is shorter than the unshared edges of the octahedron (2.70 Å × 6 and 2.88 Å × 3). Each PbO₈ polyhedron shares one edge with a TeO₆ octahedron, one edge with an AsO₄ tetrahedron (length 2.58 Å), and four edges with four other PbO₈ polyhedra. The length of the latter edges is 3.36 Å, which is shorter than the mean (3.87 Å) of the twelve unshared edges (3.04, 3.34, 3.47, 4.10, 4.59, 4.65 Å, all × 2).

The AsO₄ and ZnO₄ tetrahedra share corners to form an interlinked, two- and three-connected two-dimensional net parallel to (001) (Figure 3.6). The two AsO₄ tetrahedra in each unit cell point in opposite directions, with apical O(3) atoms oriented ± z. The three basal O(2) atoms are shared with different ZnO₄ tetrahedra. Each ZnO₄ tetrahedron shares two corners with AsO₄ tetrahedra. The rather complex Schläfli symbol (O'Keeffe and Hyde 1980) for the

resulting net is $(12^2.12^3)_6$. It is interesting to note that if the TeO_6 octahedra are considered as part of the net, the resultant Schläfli symbol is the much more conventional 6^3 (Figure 3.7).

The heteropolyhedral sheets of PbO_8 and TeO_6 are linked by AsO_4 and ZnO_4 tetrahedra (Figure 3.8). Each AsO_4 tetrahedron shares an apical O(3) atom with three PbO_8 polyhedra, and three basal As–O(2) edges (2.58 Å) with three PbO_8 polyhedra in a different sheet. The AsO_4 and TeO_6 polyhedra have no anions in common and thus are not directly joined. Each ZnO_4 tetrahedron shares two corners with two TeO_6 octahedra in different sheets, and four corners with six different PbO_8 polyhedra. The sheets of heteropolyhedral and layers of tetrahedra alternate along c to form the three-dimensional structure.

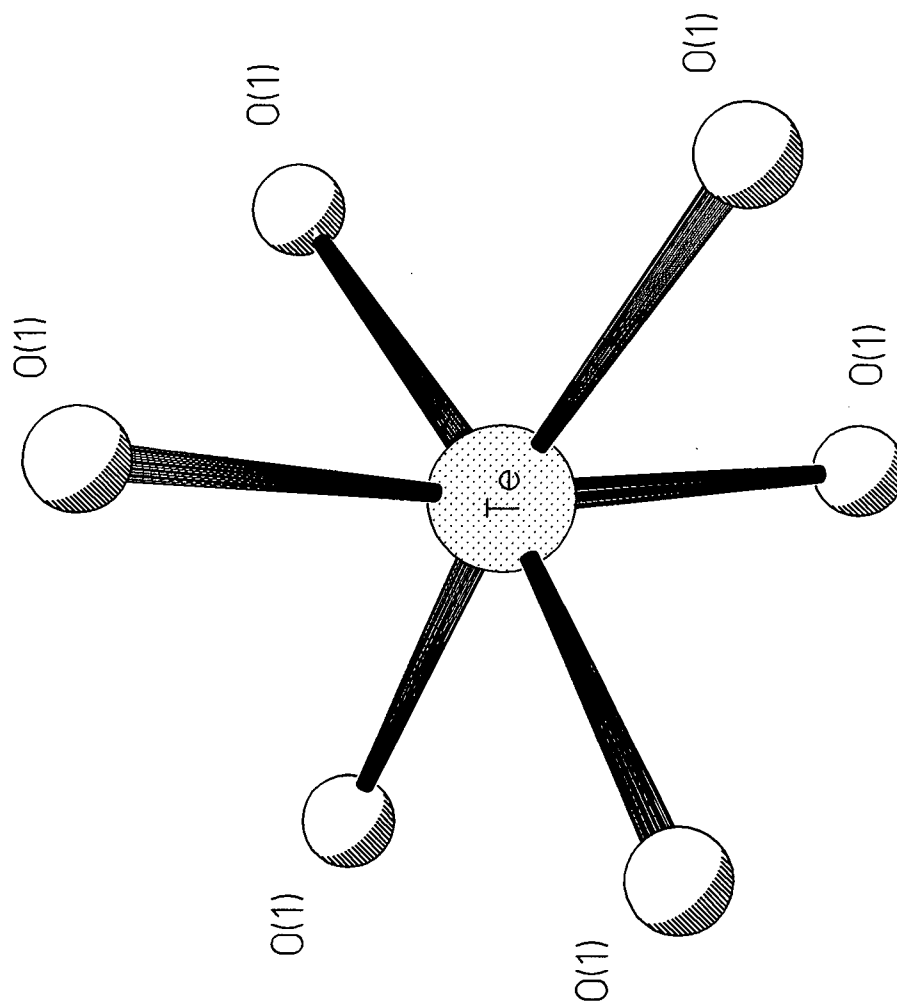


Figure 3.1 Coordination of the tellurium atom in dugganite.

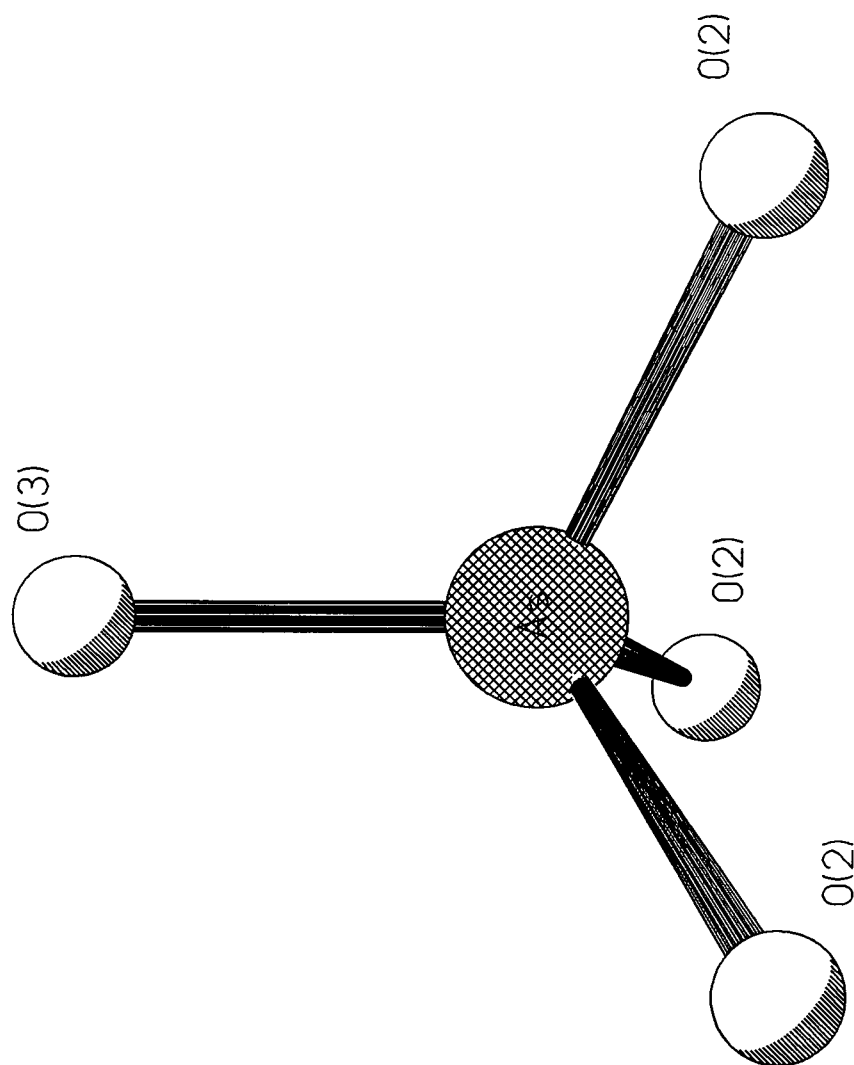


Figure 3.2. Coordination of the arsenic atom in dugganite.

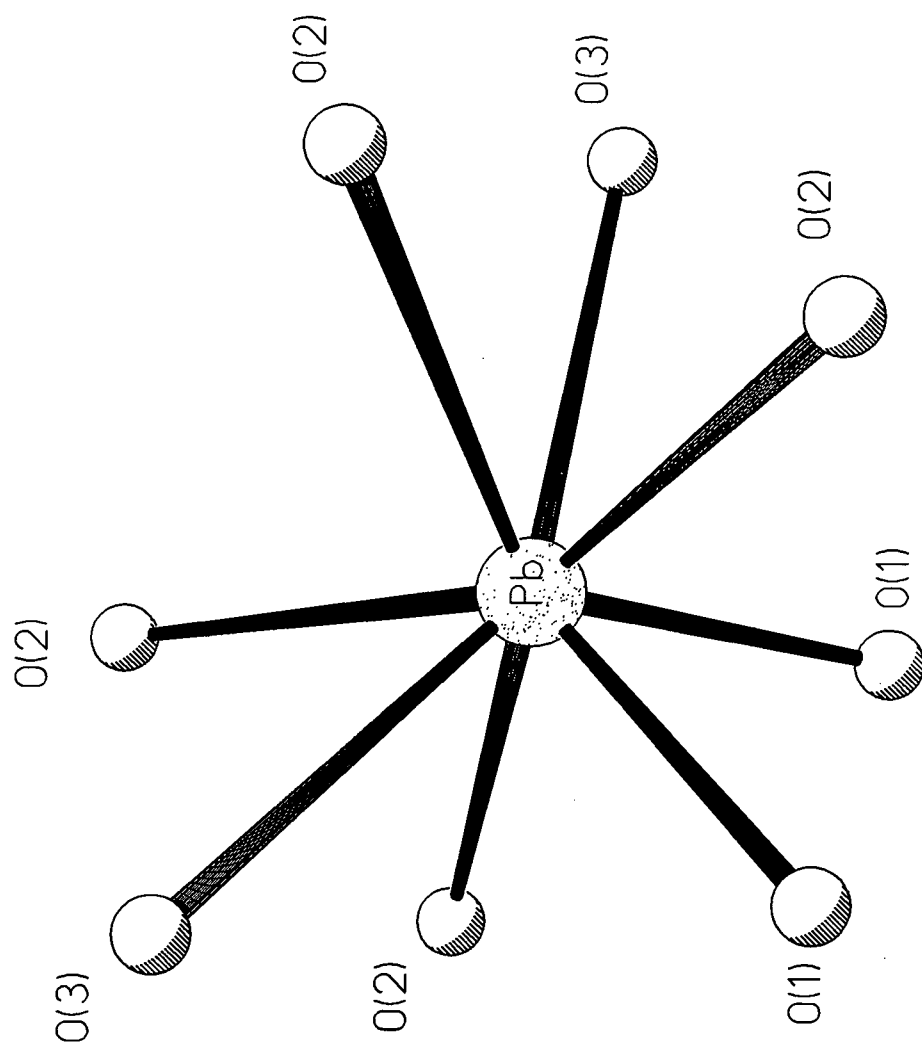


Figure 3.3. Coordination of the lead atom in dugganite.

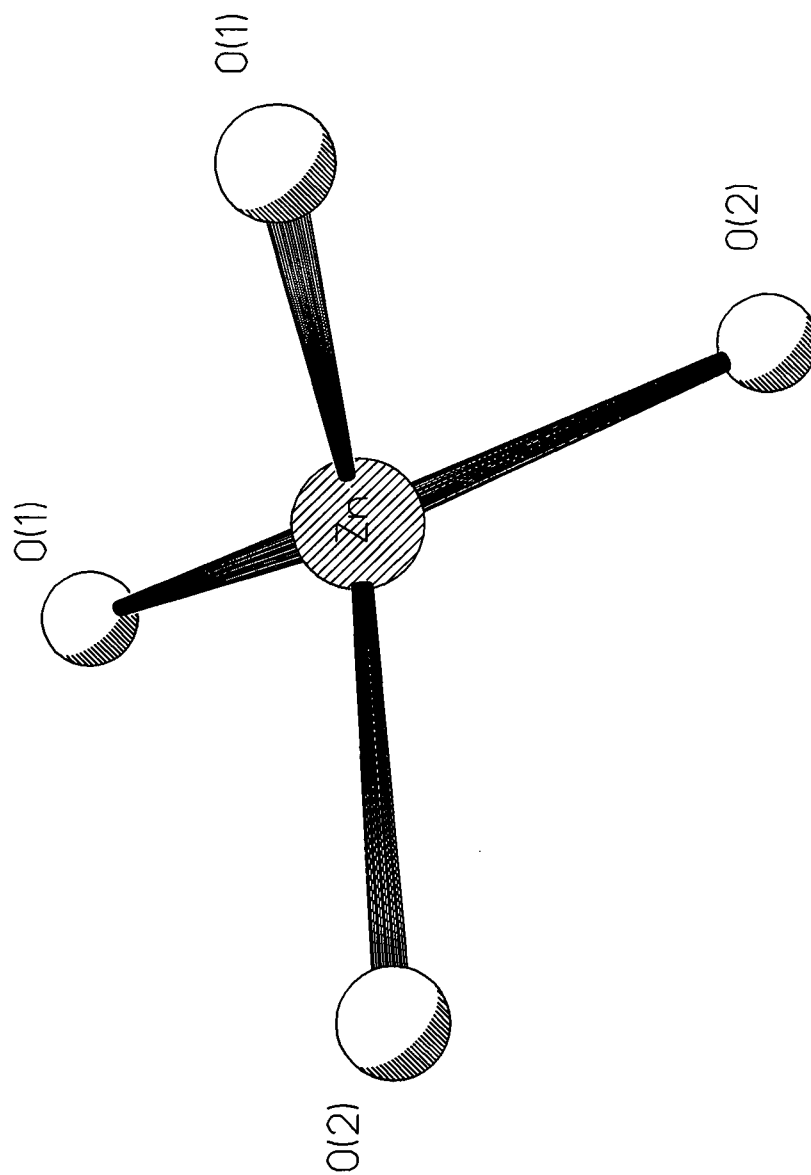


Figure 3.4. Coordination of the zinc atom in dugganite.

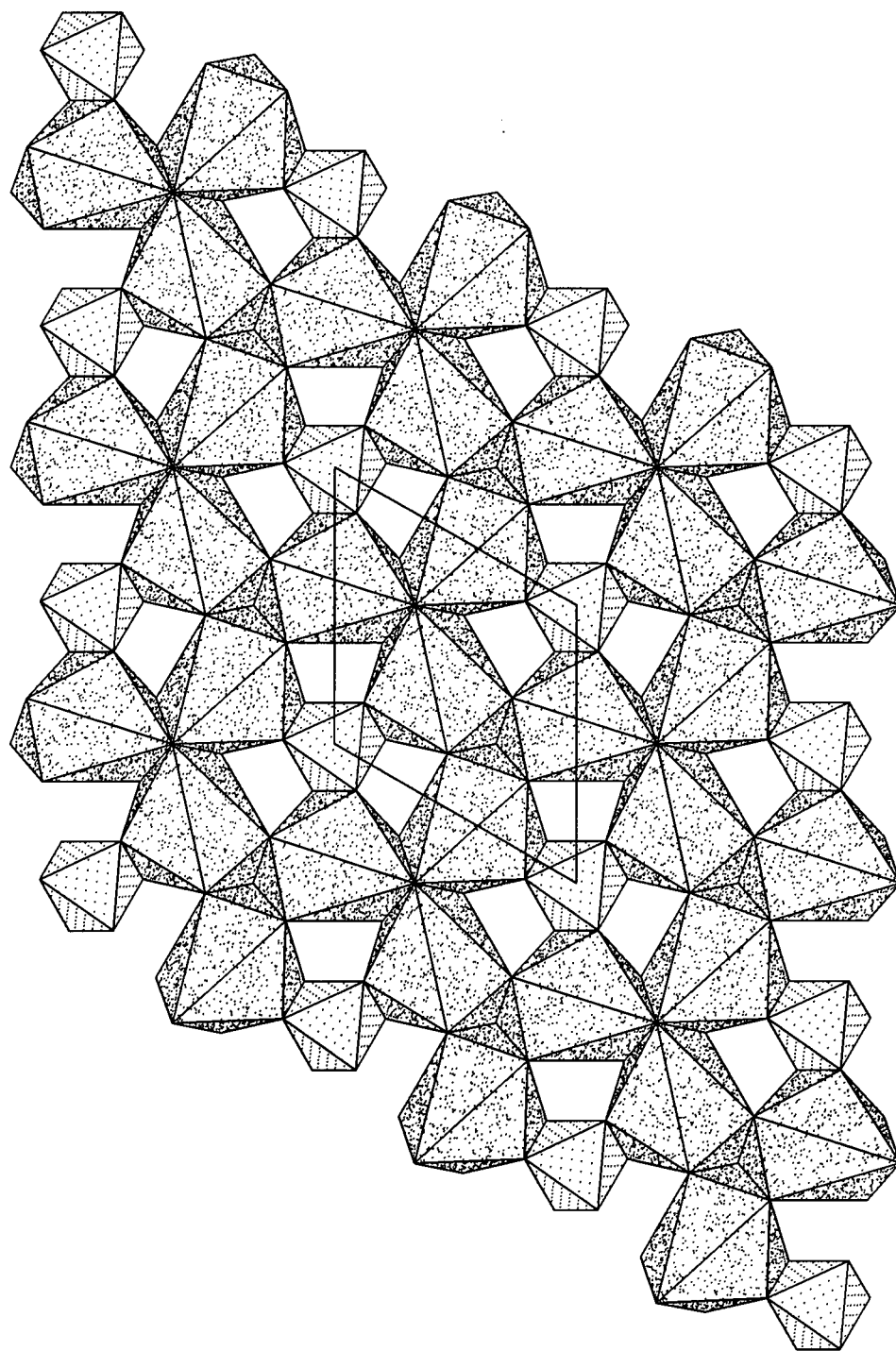


Figure 3.5. The heteropolyhedral sheet in the dugganite structure, projected onto (001). The TeO_6 octahedra are indicated by a regular dot pattern, and the PbO_8 polyhedra by a random dot pattern.

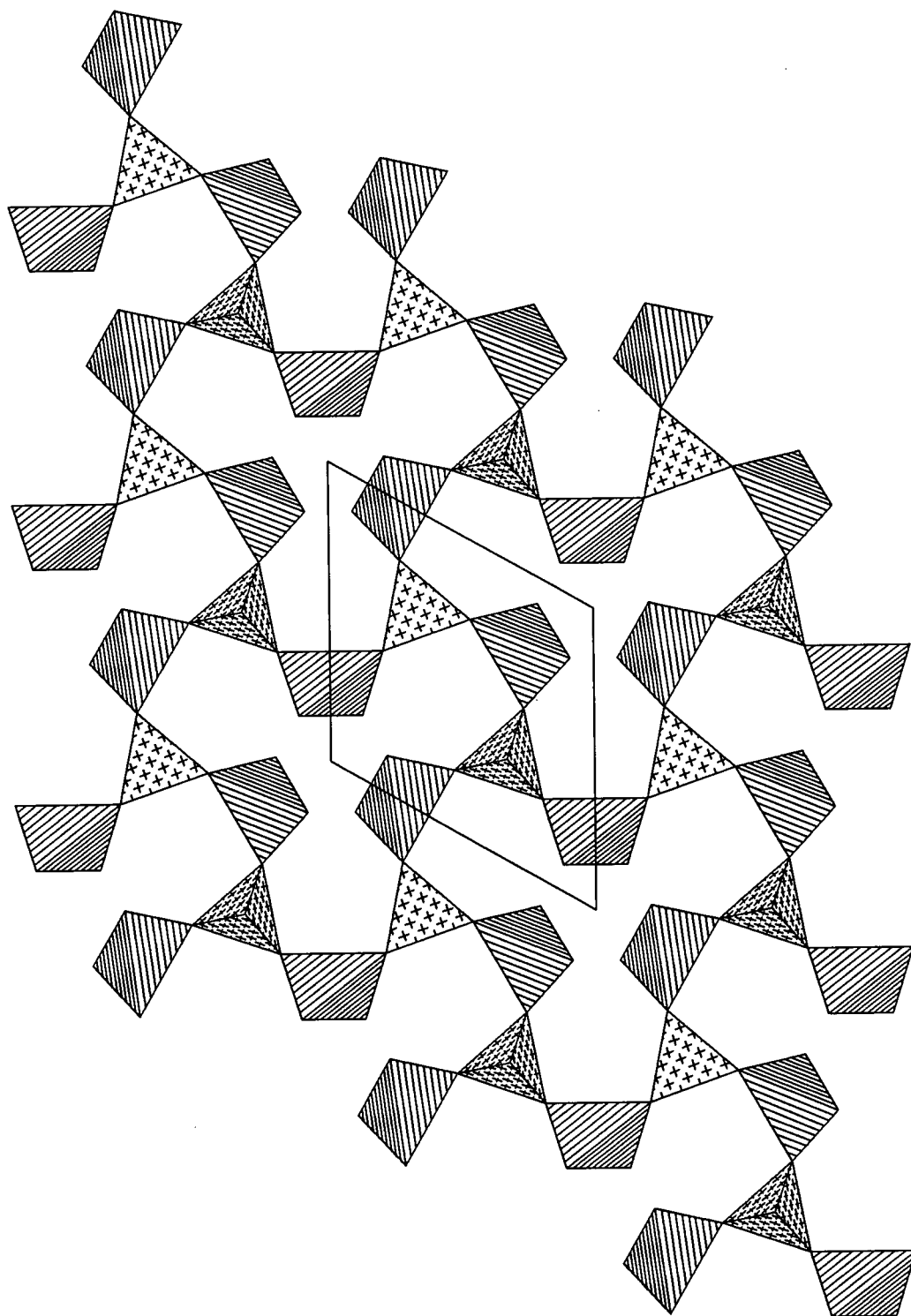


Figure 3.6. The tetrahedral layer in the dugganite structure, projected onto (001). The AsO_4 tetrahedra are indicated with crosses and the ZnO_4 tetrahedra are ruled.

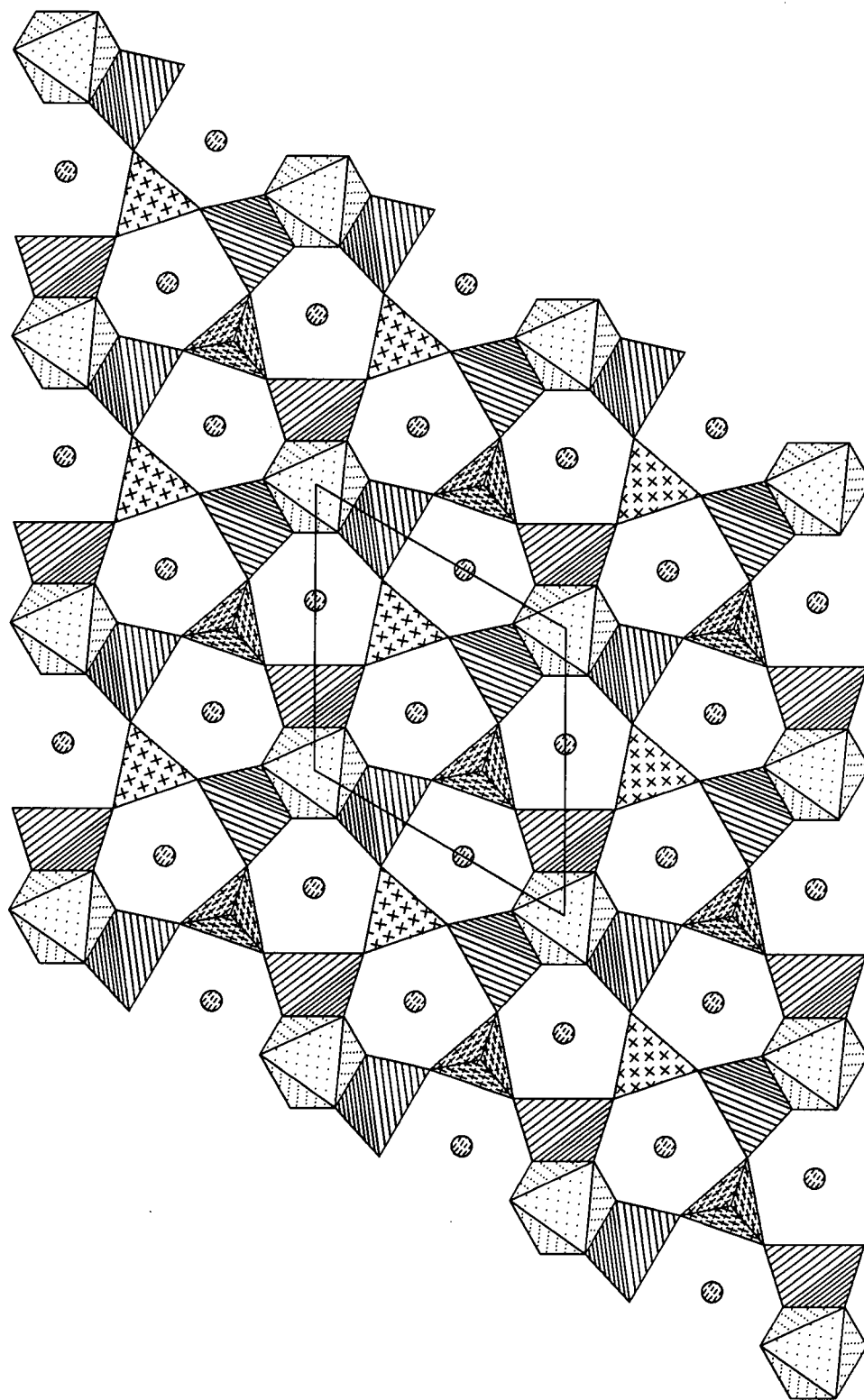


Figure 3.7. The dugganite structure projected onto (001). TeO_6 octahedra are shown with a regular dot pattern, AsO_4 tetrahedra with crosses, and ZnO_4 tetrahedra are ruled. The lead atoms are shown as spheres.

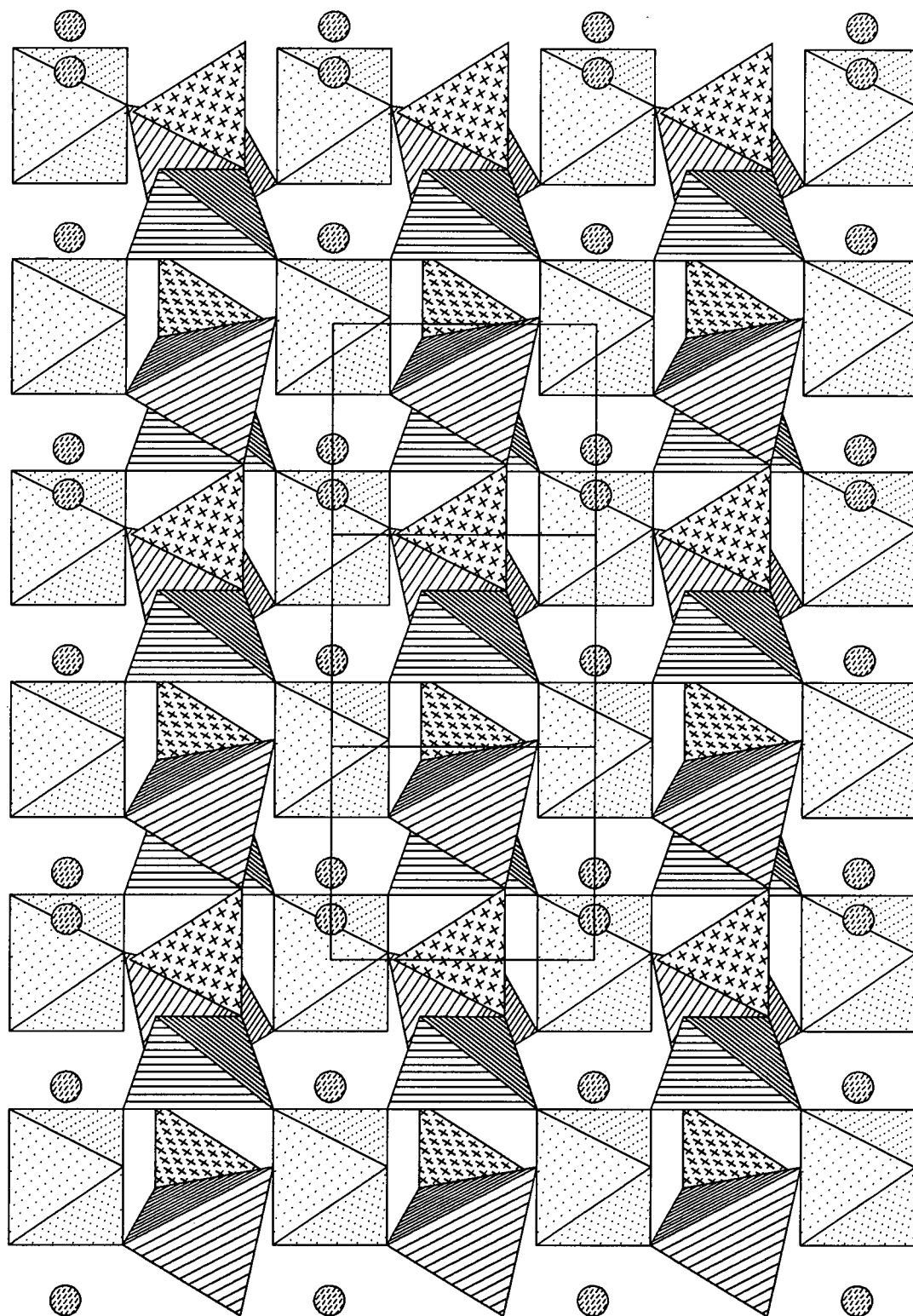


Figure 3.8. The dugganite structure projected onto (010). The shading is the same as in fig. 3.7.

3.5 Discussion

The ideal formula of dugganite is $\text{Pb}_3\text{Zn}_3\text{TeAs}_2\text{O}_{14}$. The electron microprobe and bond-valence analyses imply that there is little to no OH or H_2O in the dugganite structure. The empirical formula, based on the average results of the microprobe analyses, and calculated on the basis of nine cations per formula unit, is

$(\text{Pb}_{3.04}\text{Ca}_{0.06})_{\Sigma 3.10}(\text{Zn}_{2.71}\text{Cu}_{0.17})_{\Sigma 2.88}\text{Te}_{0.98}(\text{As}_{0.92}\text{P}_{0.88}\text{Si}_{0.23}\text{Al}_{0.02})_{\Sigma 2.05}\text{O}_{13.90}$. This is similar to the formula based on the structure analysis, which is $\text{Pb}_3\text{Zn}_3\text{Te}(\text{As}_{1.08}\text{P}_{0.92})_{\Sigma 2.00}\text{O}_{14}$. The empirical formulae calculated from the analyses in Williams (1978) and Kim *et al.* (1988) (on the basis of nine cations per formula unit) are $\text{Pb}_{3.44}(\text{Zn}_{3.00}\text{Cu}_{0.21})_{\Sigma 3.21}\text{Te}_{1.11}\text{As}_{1.25}\text{O}_{11.94}\text{OH}_{2.31}$ and $\text{Pb}_{2.94}\text{Zn}_{2.95}\text{Te}_{0.92}(\text{As}_{1.35}\text{V}_{0.51}\text{Si}_{0.20}\text{P}_{0.13}\text{Sb}_{0.01})_{\Sigma 2.20}\text{O}_{14.02}$, respectively. Note that in each study, As is the dominant cation in the *As* position. As noted above, minerals with V (cheremnykhite) and P (kuksite) dominant at the *As* site have been described by Kim *et al.* (1990), and are presumed to be isostructural with dugganite.

For comparison purposes, the indexed X-ray powder patterns are listed in Table 3.6 and are indexed according to *P321* for UBC data, *P6/mmm* for Williams (1978), and a *C*-centered cell for Kim *et al.* (1988).

Kim *et al.* (1988, 1990) chose an orthorhombic unit cell ($a \sim 8.6$, $b \sim 14.8$, $c \sim 5.2$ Å) for all three minerals, and suggested *Cmmm*, *C222*, *C2mm*, *Cm2m*, or *Cmm2* as possible space groups. The orthorhombic cell can be derived from a hexagonal unit cell by using the formula $b_{\text{orth}} \approx 2a_{\text{hex}} \cos 30^\circ$. However, it would only be necessary to use this cell if there were ordering e.g., of As between pseudo-equivalent As positions, and there is no evidence for this. In addition, the space groups proposed by Kim *et al.* (1988, 1990) are neither subgroups or supergroups of *P321*. Without studying the samples described by Kim *et al.* (1988, 1990), it is

suggested that dugganite, cheremnykhite and kuksite are isostructural, and crystallize in the hexagonal system with space group $P321$.

3.6 Conclusions

The formula of dugganite is revised to $\text{Pb}_3\text{Zn}_3\text{TeAs}_2\text{O}_{14}$ from $\text{Pb}_3(\text{Zn,Cu}^{2+})_3(\text{Te}^{6+}\text{O}_6)(\text{AsO}_4)(\text{OH})_3$. Dugganite crystallizes in the space group $P321$ and is probably isostructural with cheremnykhite and kuksite whose formulae are similar. The structure of dugganite is made up of heteropolyhedral sheets of lead and tellurium polyhedra, parallel to (001), alternating along c with layers of zinc and arsenic tetrahedra.

Table 3.6. Indexed* powder diffraction patterns for dugganite.

UBC			Williams			Kim <i>et al.</i>		
d _{meas}	Intensity	hkl	d _{meas}	I	hkl	d _{meas}	I	hkl
5.206	20.45	0 0 1	5.204	4	0 0 1	5.21	2	0 0 1
4.230	19.13	-1 2 0	4.233	4	1 1 0	4.27	2	2 0 0; 1 3 0; 0 2 1; 1 1 1
3.663	15.74	0 2 0	3.666	3	2 0 0	3.71	1	0 4 0; 2 2 0
3.283	100.00	-1 2 1	3.284	10	1 1 1	3.30	10	1 3 1; 2 0 1
2.996	40.76	-2 2 1	2.997	8	2 0 1	3.01	9	2 2 1; 0 4 1
2.996	44.58	0 2 1	2.773	5	1 2 0	2.80	3	1 5 0; 2 4 0; 3 1 0
2.769	26.69	-1 3 0	2.603	4	0 0 2	2.605	4	0 0 2
2.603	19.70	0 0 2	2.446	6	1 2 1	2.468	4	0 6 0; 3 3 0; 1 5 1; 2 4 1; 3 1 1
2.448	9.11; 4.67	-1 3 1 -2 3 1	2.215	4	1 1 2	2.442	1	1 1 2; 0 2 2; 0 6 1; 3 3 1
2.442	17.51	0 3 0	2.121	4	2 2 0	2.220	3 III	1 3 2; 2 0 2
2.217	8.15	-1 2 2	2.035	4	1 3 0	2.129	3 III	2 6 0; 4 0 0; 0 4 2; 2 2 2
2.122	6.41; 6.52	-2 2 2 0 2 2	1.963	0.5	2 2 1	2.056	2	1 2 0; 1 7 0; 3 5 0
2.032	17.45	-1 4 0	1.896	6	1 3 1	2.027	1	
1.960	2.90	-2 4 1	1.783	4	3 0 2	1.904	8	2 4 2; 1 5 2; 3 1 2
1.897	11.33; 9.07	-1 3 2 -2 3 2	1.734	0.5	0 0 3	1.867	1 III	0 8 0
1.893	11.63	-3 4 1	1.687	1		1.790	3	3 3 2; 0 6 2
1.893	11.02	-1 4 1	1.644	1		1.706	1	2 8 0; 5 1 0; 3 7 0
1.781	8.55; 7.70	-3 3 2 0 3 2	1.603	6		1.609	7	3 5 2; 4 2 2; 1 7 7; 2 0 3; 1 3 3
1.735	1.48	0 0 3	1.569	3		1.569	2	0 4 3; 2 2 3
1.681	4.35	-2 5 0	1.530	0.5		1.477	1 III	1 5 3; 2 4 3; 3 1 3

Table 3 continued.

UBC			Williams			Kim <i>et al.</i>		
d _{meas}	Intensity	hkl	d _{meas}	I	hkl	d _{meas}	I	hkl
1.642	2.81	-2 4 2	1.469	2		1.424	2 III	2 8 2; 5 1 2; 0 6 3; 3 3 3
1.606	8.87	-1 2 3	1.413	3		1.400	1	6 2 0; 4 8 0; 2 10 0; 2 6 3; 4 0 3
1.600	9.92; 9.48	-3 5 1 -2 5 1	1.387	1		1.356	1	6 2 1; 4 8 1; 2 10 1; 2 6 3; 4 0 3
1.568	4.14; 5.24	-2 2 3 0 2 3	1.364	1		1.324	1	1 7 3; 3 5 3; 4 2 3
			1.341	2		1.29	1 III	0 10 2; 5 5 2
			1.321	3		1.236	1 III	6 6 0; 0 12 0
			1.303	1		1.214	2	2 8 3; 3 7 3; 5 1 3
			1.279	3		1.181	1	2 4 4; 3 1 4; 1 5 4
			1.242	1		1.125	1	0 10 3; 5 5 3
			1.225	3		1.039	1	8 2 1; 0 14 1; 7 7 1
			1.209	4				
			1.117	5				

*UBC indexed based on *P*321, Williams based on *P*6/*mmm*; Kim *et al.* based on a C-centered cell.

4.0 CHOLOALITE: CRYSTAL STRUCTURE AND REVISED FORMULA

4.1 Introduction

According to Williams (1981), choloalite was first found in Arabia with a host of other unknown tellurium minerals. An X-ray powder pattern was taken and the material was then discarded. The type specimen of choloalite was described by Williams (1981) from waste rock in the tunnel at the Mina La Oriental, Moctezuma, Mexico. The type piece consists of a matrix of intensely sericitized rhyolite vitrophyre with veins of crystalline crusts and choloalite crystals. Soon after the discovery of the type material, samples with tiny crystals of choloalite were found between the dumps of the Joe and Grand Central shafts at Tombstone, Arizona. According to Williams (1981), the crystals occur with cerussite, emmonsite, and rodalquilarite within fragments of severely-brecciated shale replaced by opal and granular jarosite. The breccia matrix is vuggy quartz. A thin section showed large (1 mm) subhedra of choloalite corroded by fibrous crusts of emmonsite. From textural evidence, Williams (1981) obtained the paragenetic sequence, beginning with the first to crystallize: rodalquilarite, choloalite, emmonsite, cerussite.

According to Williams (1981), crystals of choloalite from both Mina La Oriental and Tombstone are invariably simple octahedra. Crystals viewed in thin section show sectoring into polygonal domains. Some are isotropic, others show birefringence up to 0.011, but with variable optical character.

Using powder X-ray diffraction data, Williams (1981) showed that choloalite is isometric. The refined cell dimensions were a 12.519 for the type specimen, 12.586 for the Arabian material, and 12.576 Å for the Tombstone sample. The larger cell edge of the

Tombstone specimen was attributed to the presence of minor amounts of antimony. Wet chemical analysis of the type material gave the empirical formula $\text{CuPb}(\text{Te}^{4+}\text{O}_3)_2 \cdot \text{H}_2\text{O}$.

Choloalite was also described by Roberts *et al.* (1994) from the McAlpine mine, Tuolumne County, California. Associated nonmetallic phases are annabergite, azurite, calcite, chlorargyrite, goethite, hematite, keystoneite, malachite, mcalpineite, mimetite, muscovite (mariposite), and a host of unidentified crusts, both crystalline and amorphous. Associated metallic minerals include acanthite, altaite, electrum, galena, hessite, owyheeite, pyrargyrite, pyrite, native silver, and sphalerite (Roberts *et al.* 1994).

The formula of choloalite was revised to $\text{CuPb}(\text{TeO}_3)_2$ by Powell *et al.* (1994). Crystals with this formula were synthesized by fusion of stoichiometric amounts of CuO, TeO_2 , and PbO. No weight loss was detected with heating to 400°C, and infrared spectroscopy was used to confirm the absence of water. Powder X-ray diffraction spectra of the synthetic material were similar to those obtained from type choloalite, with some additional weak reflections. Powell *et al.* (1994) concluded that choloalite is anhydrous, and that the water determined by Williams (1981), using only 156 µg of material, was adsorbed on the surface of the mineral particles. The cell dimension obtained from the synthetic phase was a 12.514 Å, and indexed reflections suggested possible space groups $P2_3$, $Pm\bar{3}$, $P4\bar{3}2$, $P4_3m$, or $Pm\bar{3}m$ (none of which would result in systematic absences).

Powell *et al.* (1994) also suggested an additional occurrence of choloalite. This was based on the original description of balyakinite (Spiridonov 1980), which occurs with teinite and two unnamed Cu, Pb tellurites with formulae $\text{CuPb}(\text{TeO}_3)\text{O}$ and $\text{CuPb}(\text{TeO}_3)_2$ (from microprobe analyses). The latter formula is the same as that obtained by Powell *et al.* (1994) for their synthetic material.

4.2 Experimental

Two data sets were collected because the absorption correction for the first set was not satisfactory. Structure refinement was attempted with the original, combined, and duplicate data sets; statistically, the results were always better using the duplicate data set with the better absorption correction. The final structure refinement was made with the second data set and unless otherwise specified, its experimental conditions are described.

The crystal used is from the Mina La Oriental locality (Canadian Museum of Nature sample MI58777). Data collection is as described in Chapter two with a few differences. In the original data collection, fifty reflections with 2θ 11.30 to 28.39° were centered using an automated search routine and from these results the unit cell was determined. In the second data set, one octant of reflections (3186 measurements, exclusive of standards) was collected from 3 to 60° 2θ ; 64 reflections were rejected because of asymmetric backgrounds, and one because of peak asymmetry. Fifteen strong reflections were used for ψ -scan and this data (920 measurements) was used to calculate an absorption correction. The merging R index for the ψ -scan data set decrease from 5.1% before the absorption correction to 2.1% after the absorption correction. This correction was then applied to the entire data set; minimum and maximum transmissions were 0.88 and 0.68 respectively. Of the 956 unique reflections, 455 were classed as observed [$I \geq 3\sigma(I)$].

Microprobe data for Ca, Cu, Sb, and Te were collected for twenty-five seconds; data for Cl, Zn, and Pb were collected for fifty seconds. The standards used were scapolite (ClK α), CaTa₄O₁₁ (CaK α), cuprite (CuK α), ZnWO₄ (ZnK α), stibiotantalite (SbL α), and Pb₂Te₃O₈ (TeL α and PbM α). The analysis is given in Table 4.1, together with that of Williams (1981).

The infrared spectrum of choloalite was obtained using a Spectra-Tech IR-Plan microscope connected to a Bomem Michelson MB100 Fourier-transform infrared spectrometer equipped with a mercury cadmium telluride (!) detector. A small amount of the mineral was mounted in a diamond anvil microsample cell, then pressure was applied to crush the sample and cause it to spread as a randomly-oriented powder. Two hundred scans were collected from 4000 to 400 cm^{-1} then coadded to generate the transmittance spectrum (Figure 4.1). The spectrum of an empty diamond cell collected with the same parameters was used as a reference. The spectrum shows a broad absorption band at approximately 3260 cm^{-1} (due to O–H stretching) and a weaker band at approximately 1590 cm^{-1} (due to H–O–H bending). These confirm the presence of H_2O in the crystal structure of choloalite.

Table 4.1. Chemical composition of choloalite.

		Williams (1981)*	This study [†]
CaO	wt. %	trace	0.50
PbO		33.0	31.22
CuO		11.0	11.81
ZnO		—	0.37
Sb ₂ O ₅		trace	1.10
TeO ₂		50.7	51.81
Cl		—	1.19
H ₂ O		3.4	0.34
O=Cl		—	-0.27
TOTAL		98.1	98.07
Ca ²⁺		trace	0.17
Pb ²⁺		2.53	2.65
Cu ²⁺		2.37	2.81
Zn ²⁺		—	0.09
Sb ⁵⁺		trace	0.13
Te ⁴⁺		5.44	6.14
Cl ⁻		—	0.64
H ⁺		6.46	0.72
O ²⁻		19.00	18.36

Note: Oxides are in weight percent; analyses are normalized on 19 anions per formula unit.

*Average of four wet chemical analyses for CuO, and three for PbO and TeO₂. Water by the Penfield method.

[†]H₂O is calculated to give one (Cl + H₂O) per formula unit.

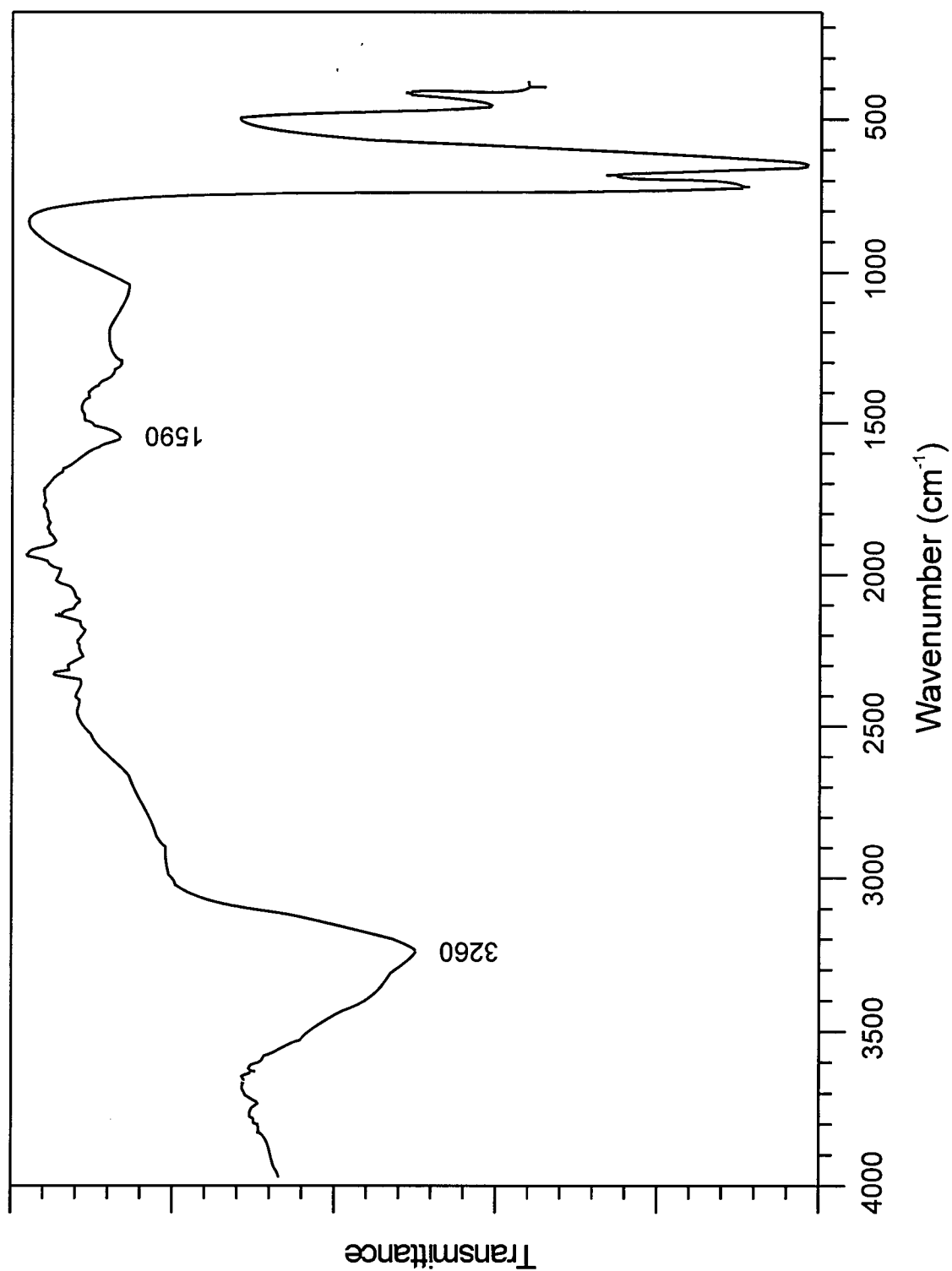


Figure 4.1 The infrared transmittance spectrum of choloalite. The absorption bands at 3260 cm^{-1} and 1590 cm^{-1} are indicative of water in the structure of choloalite.

4.3 Structure Solution and Refinement

The mean value of $|E^2 - 1|$ was 0.85, which is indicative of a non-centrosymmetric space group (Joel Grice pers. comm., 1998). Systematic absences in the original data set suggested space groups $P4_332$ and $P4_132$. In the second data collection, the reflections required to acknowledge these space groups were dismissed for having bad backgrounds and consequently gave the possible space groups as $P2_13$ and $P4_232$; structure solution and refinement using these space groups were attempted but there was no success. Upon closer scrutiny of the data, it was confirmed that the reflection conditions for a 4_1 or 4_3 screw axis $[(0,0,l)$ with $l = 4n$] were indeed met. The structure was solved by Patterson and direct methods and refined in $P4_332$ to an R index of 6.9 % for an isotropic displacement model. The refined atomic positions were used in the normalization program *STRUCTURE TIDY* (Gelato and Parthé 1987), which suggested space group $P4_132$, with an origin shift of $1/2, 1/2, 1/2$ and a redefined orientation matrix (by $-1\ 0\ 0, 0\ -1\ 0, 0\ 0\ -1$). Accordingly, the structure was refined in $P4_132$ to an R index of 6.9% for an isotropic displacement model. Conversion to anisotropic displacement factors for all cations and Cl resulted in convergence at R and wR indices of 5.2 and 5.9%, respectively (13.0 and 28.3% for all 956 data). Conversion to anisotropic displacement factors for the oxygen atoms resulted in convergence at an R index of 5.1% (due to “smearing” of the electron density), but did not improve the model. Addition of an isotropic extinction correction did not improve the results. The program *MISSYM* (Le Page 1987) was used to search for additional symmetry elements; none were indicated. Miscellaneous experimental information is found in Table 4.2. Positional coordinates and anisotropic and equivalent isotropic displacement factors are given in Table 4.3. Interatomic distance and angles are given in Table 4.4, and a bond-valence analysis in Table 4.5. Initially, bond-valence values were calculated using the curves of Brese and O’Keeffe (1991),

but the sums were poor. Bond-valence values calculated using the “correction” terms given by Wang and Liebau (1996) for Te^{4+} were consistently too high. The curves of Brown (1981) were found to give the best sums for bonds to oxygen atoms (when the correct R_0 value of 1.951 was used for Te^{4+} , as shown by Back 1990). Structure factors are listed in Appendix D.

Table 4.2. Miscellaneous information: choloalite.

a (Å)	12.520(4)	Rad/mono	MoK α /graphite
V (Å ³)	1963(2)	Total reflections	3186
Space group	$P4_132$	Unique reflections	956
Z	4	$[I \geq 3 \sigma(I)]$	455
Crystal size (mm)	$0.04 \times 0.04 \times 0.05$	R (observed) %	5.2
μ (MoK α ; mm ⁻¹)	35.6	Rw (observed) %	5.9
$R = \sum F_o - F_c / \sum F_o$			
$wR = \left[\sum (w \cdot F_o - F_c)^2 / \sum w \cdot F_o^2 \right]^{0.5}, w = 1$			

Table 4.3. Atomic parameters for choloalite

Site	x	y	z	U_{11}^*	U_{22}	U_{33}	U_{12}	U_{13}	U_{23}	U_{eq}
Te	0.0812(2)	0.4406(2)	0.3401(2)	204(11)	265(11)	201(10)	34(9)	47(8)	-5(9)	224(6)
Cu	1/8	0.2321(3)	-0.5179(3)	192(33)	198(27)	198(27)	-11(15)	11(15)	91(22)	196(17)
Pb(1)	0.1927(1)	0.1927(1)	0.1927(1)	378(7)	378(7)	378(7)	-73(7)	-73(7)	-73(7)	378(4)
Pb(2)	3/8	3/8	3/8	265(17)	265(17)	265(17)	-76(9)	-76(9)	-76(9)	265(10)
O(1)	0.0261(23)	0.1206(23)	0.2682(24)							414(65)
O(2)	0.1759(18)	0.3274(18)	0.3738(17)							233(48)
O(3)	0.1857(19)	0.5200(18)	0.2613(18)							248(50)
Cl	7/8	7/8	7/8	547(158)	547(158)	547(158)	26(92)	26(92)	26(92)	547(91)

* U_{ij} and U values are listed $\times 10^4$

Table 4.4. Selected interatomic distances (Å) and angles (°) for choloalite.

Te—O(1)a		1.87(3)	O(2)e—Cu—O(3)f	× 2	94.0(1.0)
—O(1)b		2.95(3)	O(2)e—Cu—O(3)h	× 2	85.7(1.0)
—O(2)		1.90(2)	O(2)e—Cu—Cl	× 2	93.4(7)
—O(3)		1.92(2)	O(3)f—Cu—Cl	× 2	<u>92.3(7)</u>
—O(3)c		2.71(2)	<O—Cu—O>		90
—O(3)d		<u>3.05(2)</u>	<O—Cu—O.Cl>		91.4
<Te—O>		2.40			
			O(1)—Pb(1)—O(1)i	× 3	98.9(9)
Cu—O(2)e	× 2	1.92(2)	O(1)—Pb(1)—O(1)j	× 3	65.1(1.0)
—O(3)f	× 2	1.86(2)	O(1)—Pb(1)—O(1)a	× 3	67.9(6)
—Cl		<u>2.53(6)</u>	O(1)—Pb(1)—O(2)	× 3	81.3(8)
<Cu—O>		1.89	O(1)—Pb(1)—O(2)i	× 3	115.0(8)
<Cu—O,Cl>		2.02	O(1)g—Pb(1)—O(1)j	× 3	119.4(0.1)
			O(1)g—Pb(1)—O(2)	× 3	122.3(7)
Pb(1)—O(1)	× 3	2.46(3)	O(1)g—Pb(1)—O(2)i	× 3	81.7(7)
—O(1)g	× 3	3.14(3)	O(1)g—Pb(1)—O(2)k	× 3	55.1(7)
—O(2)	× 3	<u>2.83(2)</u>	O(2)—Pb(1)—O(2)i	× 3	<u>68.1(7)</u>
<Pb(1)—O>		2.81	<O—Pb(1)—O>		87.5
Pb(2)—O(2)	× 6	2.56(2)	O(2)—Pb(2)—O(2)i	× 6	76.5(8)
—O(3)	× 6	<u>3.31(2)</u>	O(2)—Pb(2)—O(2)d	× 3	116.9(1.0)
<Pb(2)—O>		2.94	O(2)—Pb(2)—O(2)l	× 3	93.8(1.0)
			O(2)—Pb(2)—O(3)	× 6	55.1(6)
O(1)a—Te—O(1)b		79.0(6)	O(2)—Pb(2)—O(3)i	× 6	54.4(6)
O(1)a—Te—O(2)		94.9(1.1)	O(2)—Pb(2)—O(3)k	× 6	115.4(6)
O(1)a—Te—O(3)		97.5(1.1)	O(2)—Pb(2)—O(3)d	× 6	68.6(6)
O(1)a—Te—O(3)c		78.1(1.0)	O(2)—Pb(2)—O(3)m	× 6	142.5(6)
O(1)b—Te—O(3)		71.2(9)	O(2)—Pb(2)—O(3)l	× 6	107.2(6)
O(1)b—Te—O(3)c		127.6(7)	O(3)—Pb(2)—O(3)i	× 6	108.7(4)
O(1)b—Te—O(3)d		99.8(7)	O(3)—Pb(2)—O(3)d	× 3	53.0(8)

O(2)–Te–O(3)	94.3(1.0)	O(3)–Pb(2)–O(3)m	× 3	<u>92.3(8)</u>
O(2)–Te–O(3)c	65.1(8)	<O–Pb(2)–O>		90.6
O(2)–Te–O(3)d	82.1(8)			
O(3)–Te–O(3)d	68.6(9)			
O(3)c–Te–O(3)d	<u>113.0(9)</u>			
<O–Te–O>	89.3			

Note: <M– ϕ > denotes the mean metal-ligand distance (Å). Equivalent positions:
a = z + 3/4 - 1, y + 1/4, \bar{x} + 1/4; b = \bar{x} , y + 1/2, \bar{z} + 1/2; c = \bar{z} + 1/4, y + 3/4 - 1, x + 1/4; d = \bar{y} + 3/4, \bar{x} + 3/4, \bar{z} + 3/4; e = x, y, z - 1; f = z, x, y - 1; g = y + 1/4, \bar{x} + 1/4, z + 3/4 - 1; h = \bar{z} + 1/4, y + 3/4 - 1, x + 1/4 - 1; i = z, x, y; j = \bar{x} + 1/4, z + 3/4 - 1, y + 1/4; k = y, z, x; l = \bar{z} + 3/4, \bar{y} + 3/4, \bar{x} + 3/4; m = \bar{x} + 3/4, \bar{z} + 3/4, \bar{y} + 3/4.

Table 4.5. Bond-valence arrangement in choloalite.

	Te	Cu	Pb(1)	Pb(2)	Total
O(1)	1.21		$0.36 \times 3 \downarrow$		1.82
	0.16		$0.09 \times 3 \downarrow$		
O(2)	1.13	$0.55 \times 2 \downarrow$	$0.17 \times 3 \downarrow$	$0.26 \times 6 \downarrow$	2.11
O(3)	1.07	$0.66 \times 2 \downarrow$		$0.07 \times 6 \downarrow$	2.16
	0.23				
	0.13				
Cl		$0.26 \times 3 \rightarrow$			0.78
Total	3.93	2.68	1.86	1.98	

*Calculated from the curves of Brown (1981), as modified by Back (1990) for Te, and those of Brese and O'Keeffe (1991) for bonds to Cl.

4.4 Description of the Structure

The structure of choloalite is a difficult one to describe because of the intricate way in which the structure is connected together. The coordinations around each cation is discussed followed by a description of the complex structure connectivity. There are four distinct cation sites in the choloalite structure: Te, Cu, Pb(1), and Pb(2). The coordination polyhedra of these cations are shown in Figures 4.2 - 4.5.

4.4.1 *Te coordination*

The *Te* site is completely occupied by Te^{4+} , as shown by the electron microprobe analysis, refined site occupancy, and bond-valence analysis. The atom at the *Te* position is coordinated by at least four oxygen atoms at distances of 1.87, 1.90, 1.92, and 2.71 Å (Figure 4.2). In accordance with Zemmann (1968, 1971) and Lindqvist (1973), these atoms can be described as forming a trigonal dipyramid, with a lone-pair of electrons occupying one corner of the equatorial triangle. Brown (1974), however, assumed that the coordination environment of Te^{4+} (and Sn^{2+} , Sb^{3+} , I^{5+} , and Xe^{6+}) is an octahedron distorted by a lengthening of some of the bonds on one side. Rossell (1992) demonstrated that the coordination polyhedra of the four Te^{4+} atoms in the crystal structure of $\text{Bi}_2\text{Te}_4\text{O}_{11}$ can be described as distorted octahedra.

In the crystal structure of choloalite, two additional O atoms at distances of 2.95 and 3.05 Å can be considered to form bonds with the atom at the *Te* position contributing 0.16 and 0.13 *v.u.* respectively. The resulting polyhedron is a distorted octahedron, with three weak bonds occurring opposite three strong bonds. As suggested by Brown (1974), the bond-valence sum of each *trans* pair is approximately equal. The environment corresponds to type “c” of Brown

(1974) with three strong and three weak bonds. The mean Te–O distance is 2.40 Å, and the O–Te–O angles range from 65.1 to 127.6°, with a mean value of 89°. The octahedral angle variance is 354.12, the mean octahedral quadratic elongation (Robinson *et al.* 1971) is 1.2296, and the polyhedral volume is 14.47 Å³. The lone-pair of electrons is probably located on the side of the Te atom opposite the three closest O atoms, and within the volume defined by the Te atom and the three O atoms with the largest Te–O distances and O–Te–O angles. It is unlikely that the atom at the *Te* position forms a bond with the atom at the nearest *Cl* site, given the distance (3.701 Å), the possible bond-valence contribution (0.03 v.u.), and the presence of Cu sites at distances of 3.206 and 3.330 Å.

4.4.2 Copper coordination

The atom at the *Cu* site, special position $12d (1/8, x, 1/4+x)$, is coordinated by four oxygen atoms at distances of 1.86 and 1.92 Å (both $\times 2$), and by the atom (Cl) or molecule (H₂O) at the *Cl* site, at a distance of 2.53 Å. The resulting coordination sphere (Figure 4.3) is almost a square pyramid (actually a very distorted trigonal dipyramid; the oxygen atoms deviate from a common plane by ± 0.02 Å), with a mean Cu– ϕ (ϕ = unspecified anion) distance of 2.02 Å, a mean O–Cu– ϕ angle of 91.4°, and a polyhedral volume of 6.3 Å³. The structure refinement shows that the *Cu* site is predominately occupied by Cu²⁺. The electron microprobe analysis suggests 92.7% Cu, 4.3% Sb, and 3.0% Zn at the Cu site. The structure refinement shows 93(4)% Cu and 7(4)% Sb at the Cu position. According to Shannon (1976), the ionic radii of Cu²⁺ and Sb³⁺ in five-fold coordination, and of Sb⁵⁺ in six-fold coordination, are 0.65, 0.80, and 0.60 Å, respectively. This suggests that the Sb at the *Cu* position is pentavalent. In addition, the Cl in choloalite serves to balance the excess positive charge introduced by Sb, and the chemical formulae obtained from

both the electron microprobe and crystal-structure analyses are only charge-balanced with pentavalent Sb. The results of the crystal structure refinement (using 93% Cu and 7% Sb) suggest that the bond-valence sum of the *Cu* site should be 2.21 v.u.. In fact, the sum is 2.68 v.u. including a contribution from Cl plus H₂O at the *Cl* position of 0.26 v.u. This suggests that the bond-valence curves are not optimal for use with Cu in five-fold coordination. This is not surprising, since existing bond-valence curves are based primarily on Cu in six-fold coordination. It is interesting to note that of the ninety-four Cu-oxysalt minerals listed in the compendium by Eby and Hawthorne (1993), only eleven show Cu in five-fold coordination. Eight of the former and two of the latter also contain Cu in six-fold coordination. Of the eleven Cu-oxysalt minerals with Cu in five-fold coordination, ten contain Cu ϕ_5 square pyramids that share edges to form [Cu₂ ϕ_5] dimers. In fingerite the coordination polyhedron is a triangular dipyramid. Only in clinoclase are there "isolated" Cu ϕ_5 square pyramids, and these share edges with Cu ϕ_8 octahedra. Therefore the coordination of Cu in the crystal structure of choloalite is virtually unique.

The results of the crystal structure refinement show that the *Cl* site is occupied by 81(4)% Cl and 19(4)% H₂O, corresponding to 0.64 and 0.34 atoms (molecules) per formula unit, and 1.19 and 0.34 wt.%, respectively (Table 4.1). However, the infrared spectrum (Figure 4.1) suggests a higher H₂O content. This could be real (the spectrum was collected from different material, but from the same sample, as that used in the crystal structure analysis), or could be due to adsorbed H₂O. It is interesting to note that the maximum possible amount of H₂O in the choloalite structure is one molecule per formula unit (i.e., the *Cl* site completely filled with H₂O), corresponding to 0.97 wt.% H₂O, and a total of 97.78 wt.% for the analysis in Table 4.1.

4.4.3 *Lead(1) coordination*

The atom at the *Pb(1)* site, special position $8c$ (x,x,x), is coordinated by nine oxygen atoms (Figure 4.4) forming a triaugmented trigonal prism. The Pb(1)–O distances are 2.46, 2.83, and 3.14 Å (all $\times 3$; mean 2.81 Å), and the O–Pb(1)–O angles range from 55.1 to 122.3° (mean 87.4°). The lengths of the polyhedral edges are 2.78, 3.07, 3.17, 3.18, 3.46, 3.74, and 3.92 Å (all $\times 3$). The polyhedral volume is 40.6 Å³. The coordination polyhedron is somewhat distorted, suggesting the presence of a lone-pair of electrons. The results of the crystal structure refinement show that the *Pb(1)* site is completely occupied by Pb²⁺.

4.4.4 *Lead(2) coordination*

The atom at the *Pb(2)* site, special position $4a$ ($3/8,3/8,3/8$), is coordinated by twelve oxygen atoms forming a distorted icosahedron (Figure 4.5). The Pb(2)–O distances are 2.56 and 3.31 Å (both $\times 6$; mean 2.94 Å), and the O–Pb(2)–O angles range from 53.0 to 142.5° (mean 90.7°). The lengths of the polyhedral edges are 2.95 and 4.77 Å (both $\times 3$), and 2.76, 2.80, 3.17, and 3.37 Å (all $\times 6$). The polyhedral volume is 57.9 Å³. The electron microprobe analysis suggests that the *Pb(2)* site is occupied by 79% Pb and 21% Ca. The structure refinement shows 70(2)% Pb and 30(2)% Ca at the *Pb(2)* position. Other minerals with twelve-coordinated Pb²⁺ include osarizawaite (Giuseppetti and Tadini 1980), plumbojarosite (Szymanski 1985) and senaite (Grey and Lloyd 1976). All show six equal short and six equal longer Pb–O distances, with mean values of 2.82 to 2.92 Å (Table 4.6). Although the Pb(2)–O distances in choloalite show a larger range, the mean value is close to those for the other minerals.

Table 4.6. Bond lengths of twelve-coordinated lead icosahedra in different minerals.

Mineral	short Pb—O bonds (each × 6), (Å)	long Pb—O bonds (each × 6), (Å)	average Pb—O length (Å)
osarizawaite	2.784(4)	2.846(4)	2.815
plumbojarosite: Pb(1)	2.862(1)	2.965(1)	2.914
plumbojarosite: Pb(2)	2.690(1)	2.953(1)	2.822
senaite	2.786	2.849	2.817
choloalite	2.56(2)	3.31(2)	2.94

4.4.5 Structure connectivity

The intricately connected structure of choloalite makes its description a difficult job. To begin, the polymerization of coordination polyhedra by simple rotation around an atom (generally a central cation), at a special position, is considered. The *Cl* site, at special position *4b* ($1/8, 1/8, 7/8$), lies at the intersection of one two-fold and one three-fold rotational axes. The atom or molecule at this site forms bonds with three Cu atoms (each of which is on a two-fold rotational axis). Because of this, each $\text{Cu}\phi_5$ square pyramid is attached to two others by corner-sharing of the atom or molecule at the *Cl* site, forming a “pinwheel” (Figure 4.6a). In addition, each $\text{Cu}\phi_5$ polyhedron shares two *trans* O(2)–O(3) edges (length 2.57 Å) with two TeO_6 octahedra, and the other *trans* O(2)–O(3) edges (length 2.76 Å) with two $\text{Pb}(2)\text{O}_{12}$ polyhedra. The lengths of the unshared O(2)–Cl and O(3)–Cl edges are 3.26 and 3.20 Å, respectively. Each $\text{Cu}\phi_5$ polyhedron is also linked by corner-sharing to additional TeO_6 octahedra ($\times 4$) and $\text{Pb}(1)\text{O}_9$ polyhedra ($\times 2$).

The *Pb*(1) sites lie on three-fold rotational axes. Each $\text{Pb}(1)\text{O}_9$ polyhedron shares edges with three others, forming an additional “pinwheel” (Figure 4.6a). The “pinwheels” polymerize to form a three-dimensional network (Figure 4.7).

Like the Cl sites, the *Pb*(2) positions are at intersections of one two-fold and one three-fold rotational axes. Individual $\text{Pb}(2)\text{O}_{12}$ polyhedra are not joined; however, each is linked by the shared O(2)–O(3) edges to six $\text{Cu}\phi_5$ polyhedra. Each $\text{Cu}\phi_5$ polyhedron is then joined through the *trans* O(2)–O(3) edge to an additional $\text{Pb}(2)\text{O}_{12}$ polyhedron. The result is yet another “pinwheel” (Figure 4.6b). These polymerize to form an additional three-dimensional network (Figure 4.8).

The two three-dimensional networks are linked by the two *trans* O(2)–O(2)–O(2) faces (edge length 3.17 Å, $\times 3$) of each Pb(2)O₁₂ icosahedron, which are shared with adjacent Pb(1)O₉ polyhedra. The spaces are filled with TeO₆ octahedra (note that the Te atom, alone of the cations in the choloalite structure, is not on a rotational axis). The linkage of the TeO₆ polyhedra with neighbouring polyhedra is shown in Figure 4.9. Each TeO₆ octahedron shares one triangular O(2)–O(3)–O(3) face with a Pb(2)O₁₂ polyhedron; the lengths of the shared edges are 2.80, 2.95, and 3.37 Å. In addition, each TeO₆ polyhedron share one O(2)–O(3) edge (2.57 Å) with an adjacent Cu ϕ ₅ square pyramid, and one O(3)–O(3) edge (2.95 Å) and two O(1)–O(3) edges (2.96 Å $\times 2$) with three different TeO₆ octahedra. Furthermore, one O(1)–O(1) (3.18 Å) and one O(1)–O(2) (2.78 Å) edges are shared with adjacent Pb(1)O₉ polyhedra. This leaves only three unshared edges (lengths 4.60, 4.81, and 5.08 Å). Finally, each TeO₆ polyhedron is linked by corner-sharing to additional Cu ϕ ₅ ($\times 2$), TeO₆ ($\times 2$), Pb(1)O₉, and Pb(2)O₁₂ polyhedra.

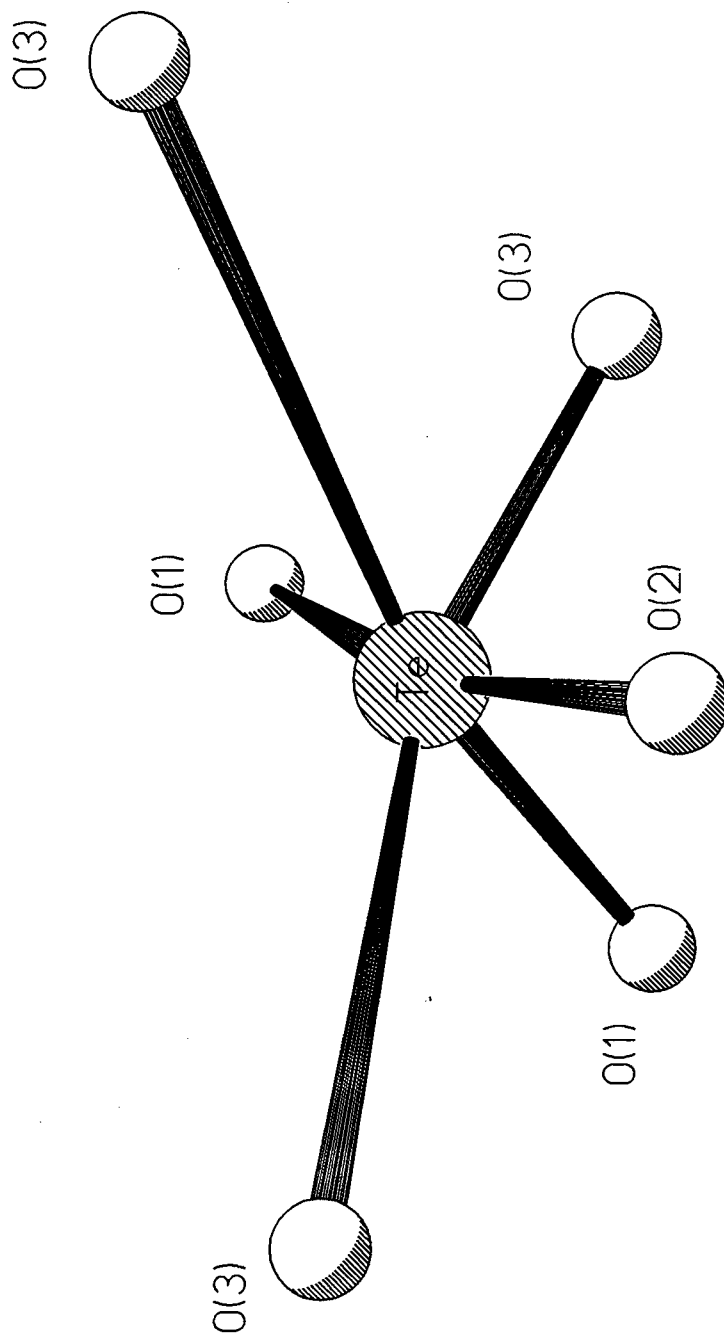


Figure 4.2. Coordination of the tellurium atom in choloalite.

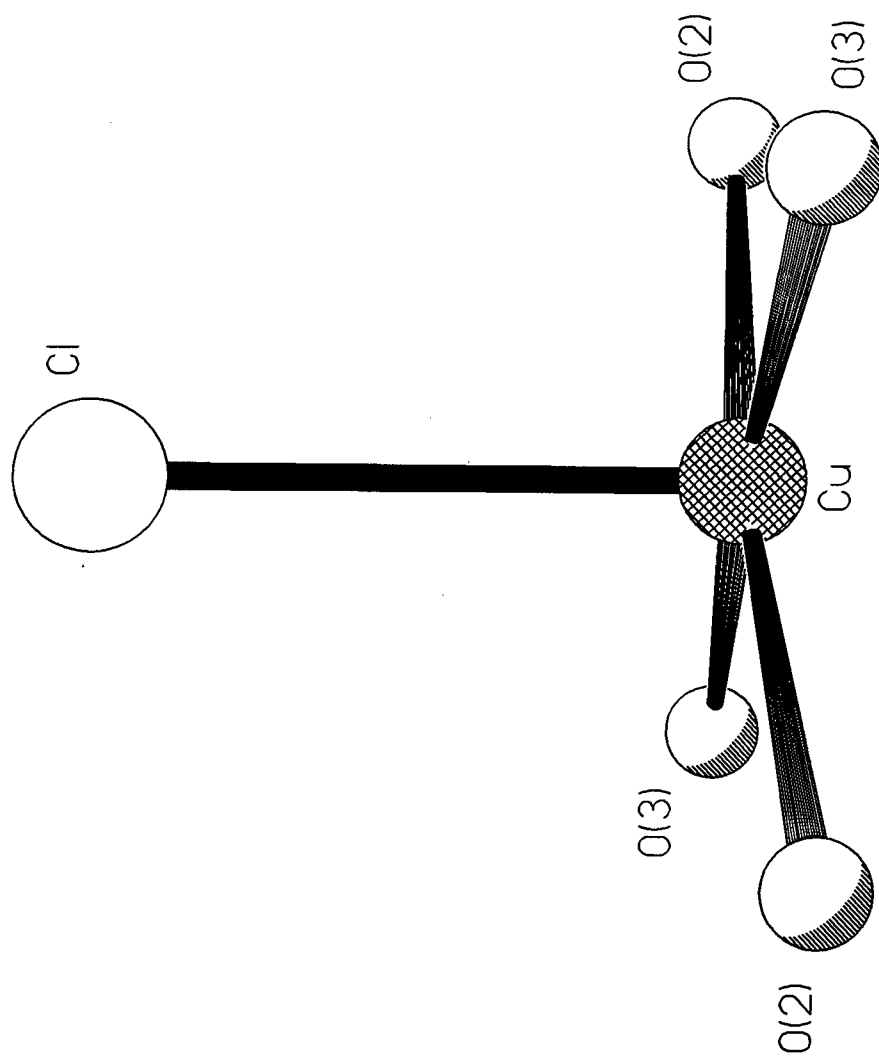


Figure 4.3. Coordination of the copper atom in chlodilite.

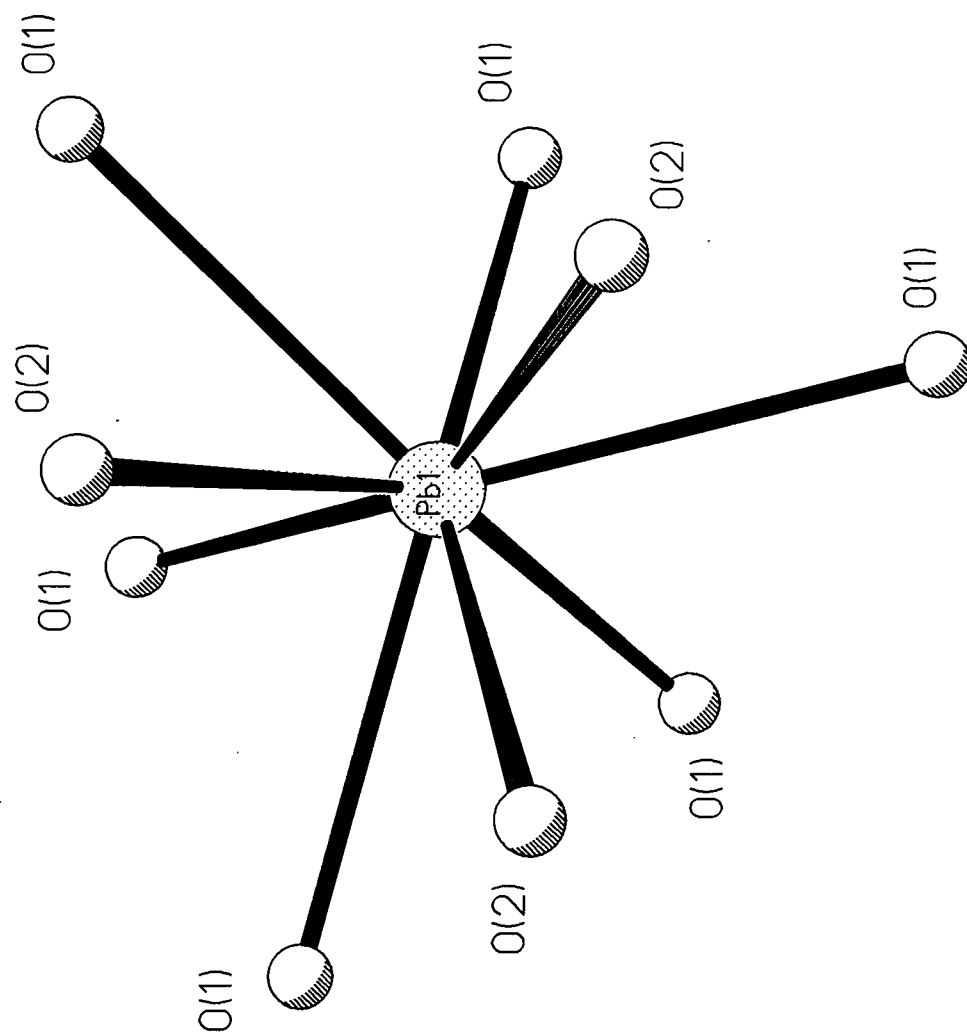


Figure 4.4. Coordination of the lead (1) atom in chlodolite.

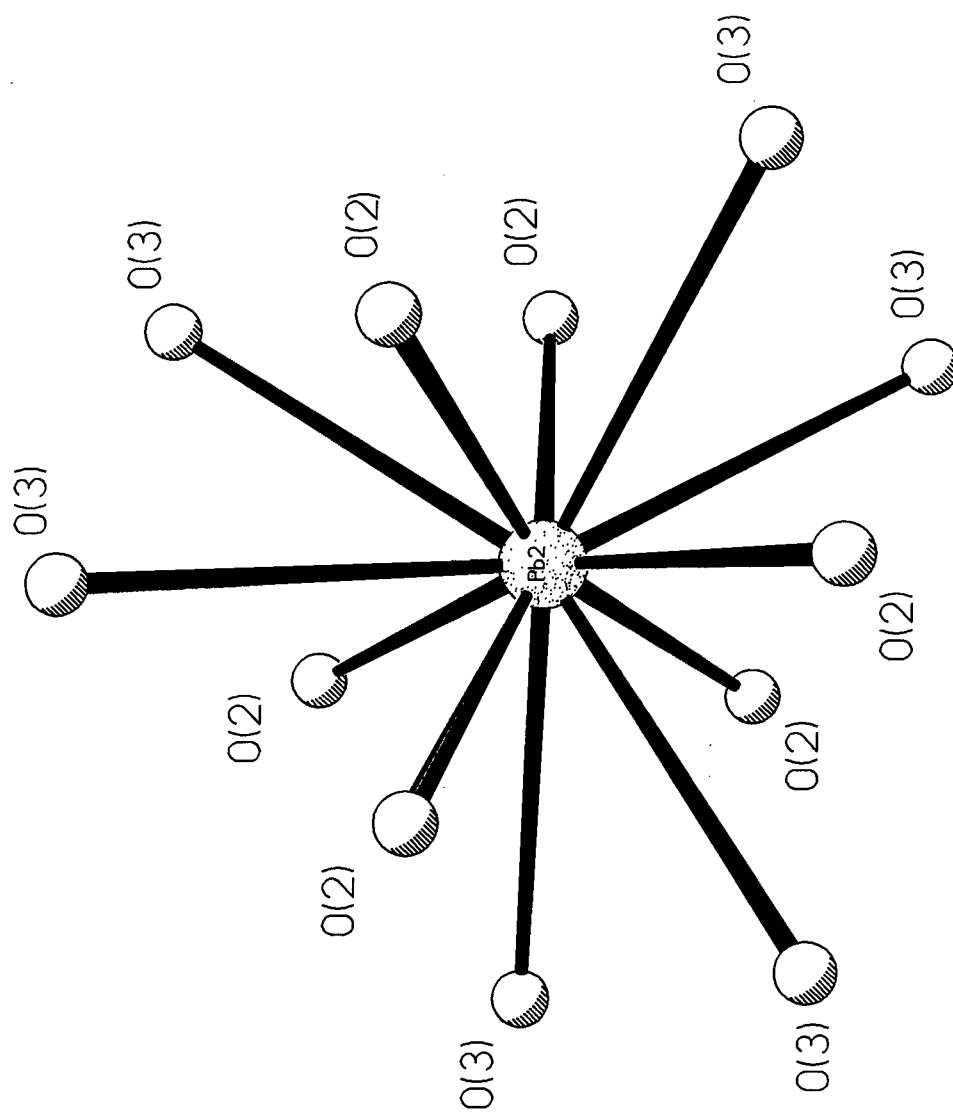


Figure 4.5. Coordination of the lead (2) atom in chalcocite.

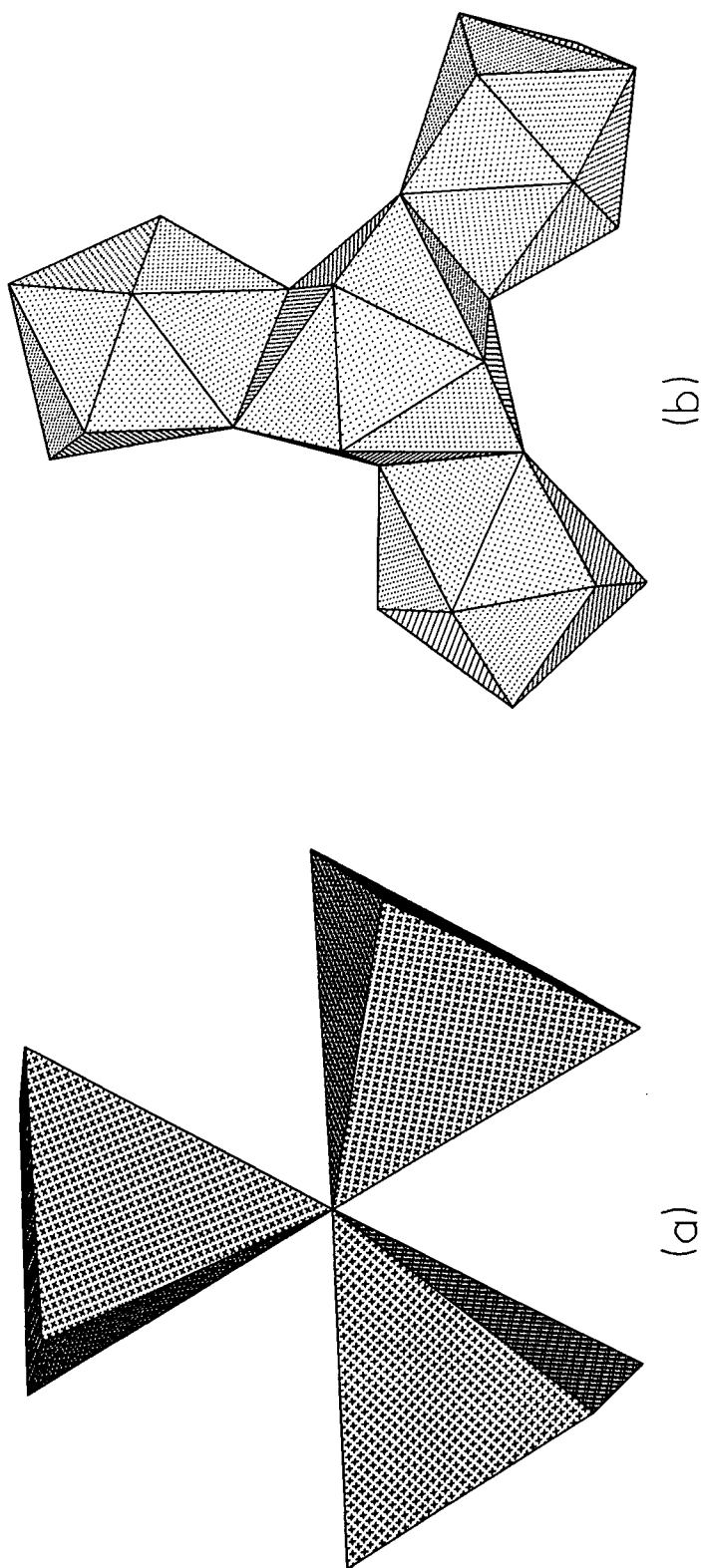


Figure 4.6a. "Pinwheels" in the chalcocite structure: (a) four Pb(1)O₉ polyhedra; (b) three Cu₄S polyhedra;

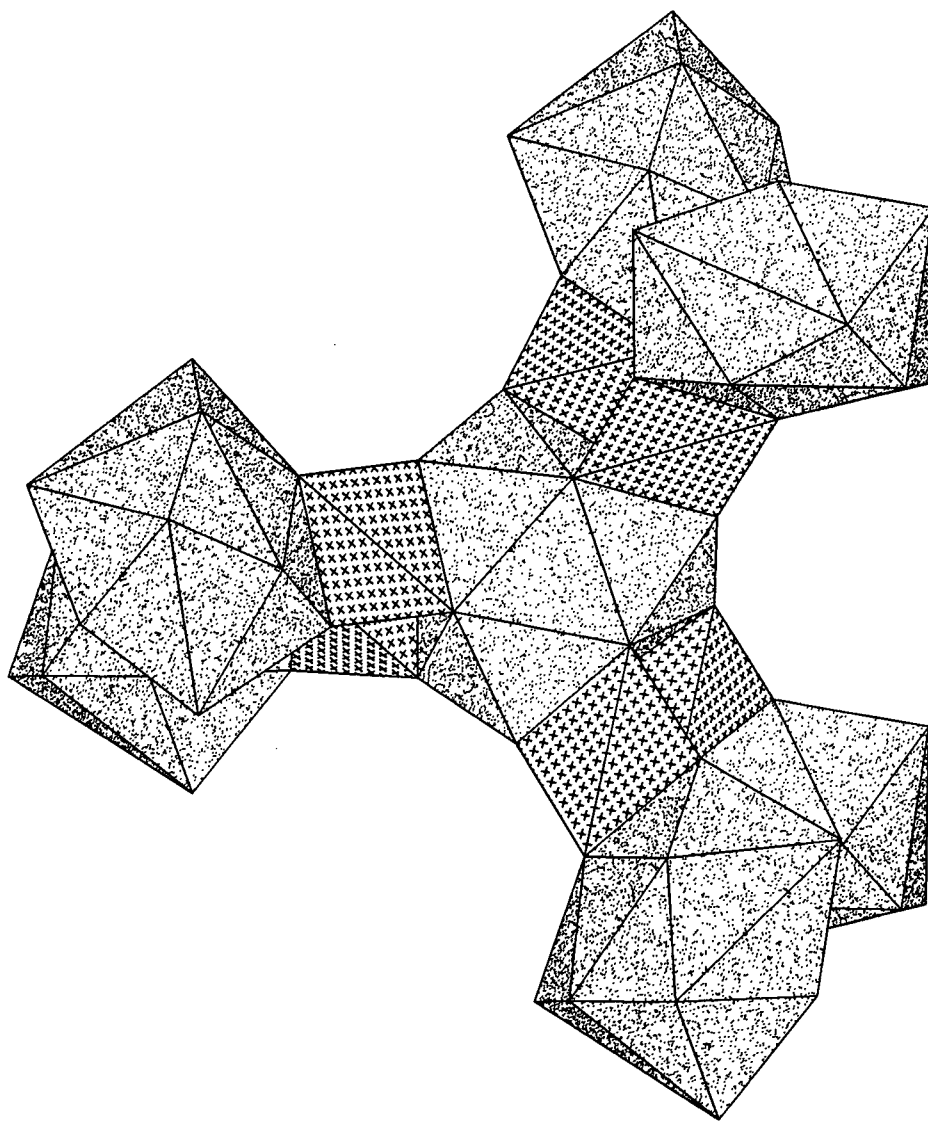


Figure 4.6b. "Pinwheel" in the chololite structure. Seven $\text{Pb}(2)\text{O}_{12}$ polyhedra linked by six Cuq_5 polyhedra.

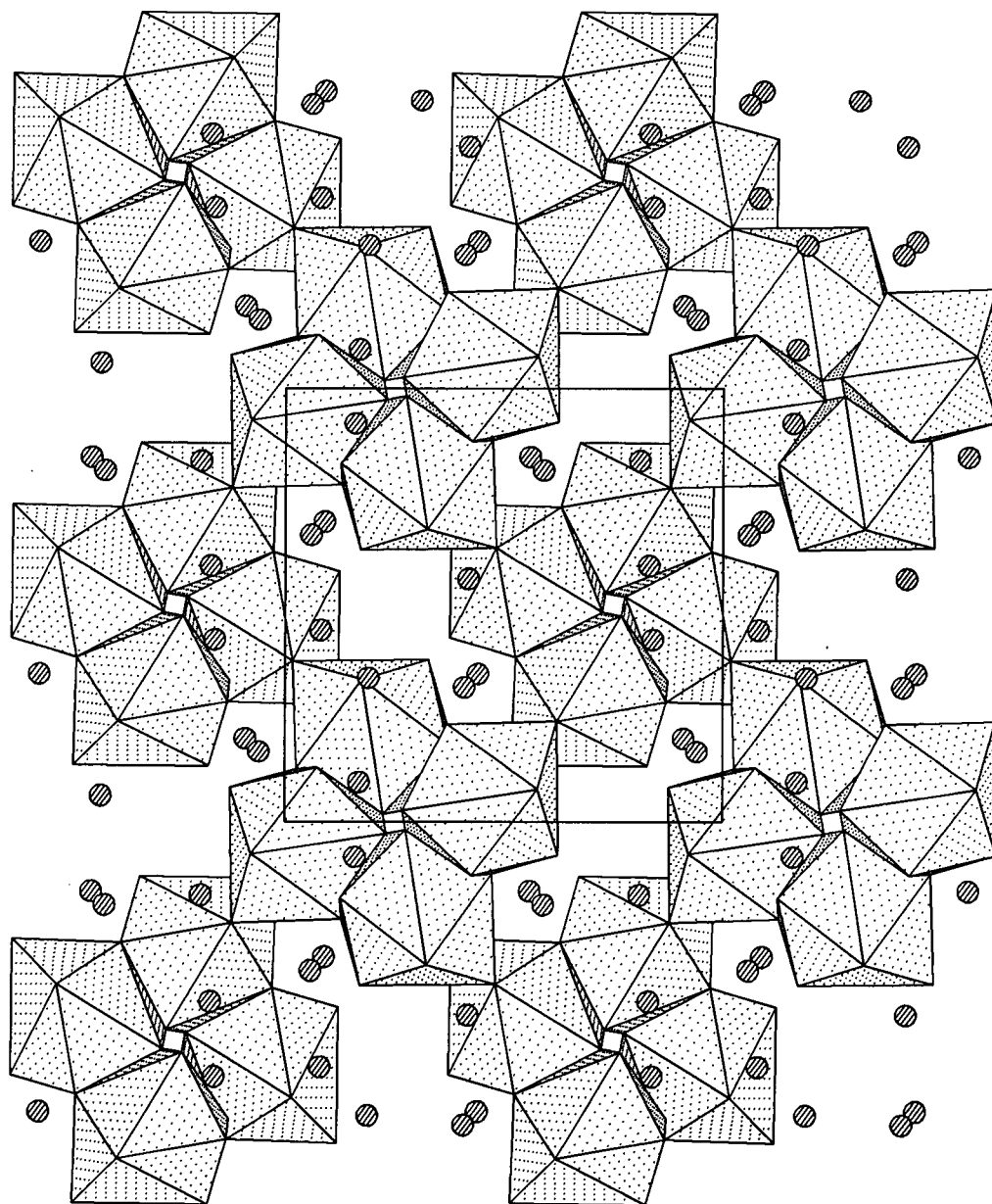


Figure 4.7. Three-dimensional network of $\text{Pb}(10g)$ polyhedra. The Te atoms are shown as spheres. The positions of the 4_1 axes are evident.

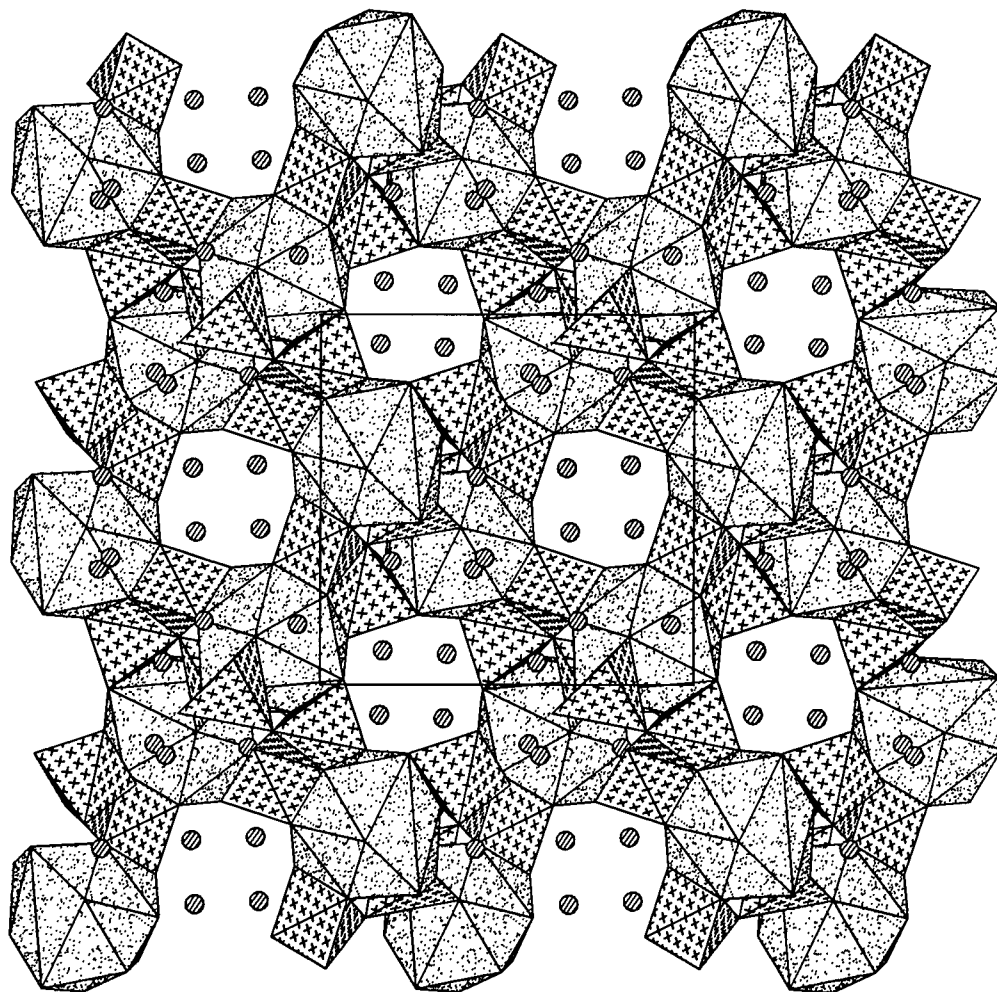


Figure 4.8. Three-dimensional network of Cuq_5 and Pb(2)O_{12} polyhedra. The Te atoms are shown as spheres.

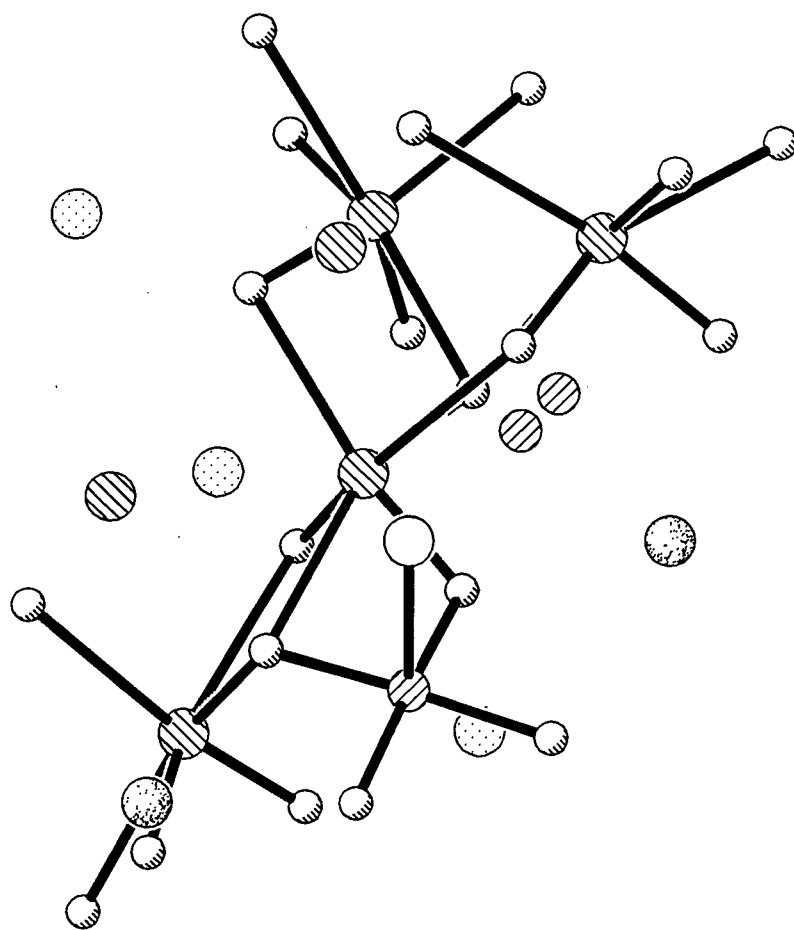


Figure 4.9. Linkage of adjacent polyhedra to the TeO_6 octahedron. Bonds are shown for the central TeO_6 octahedron and those adjacent polyhedra linked to it by shared edges. Only the central cation is shown for those polyhedra that link by shared corners. The Te atoms are shown as spheres with NE to SW ruling and the Cu atoms are shown as spheres with NW to SE ruling. The Pb(1) atoms are shown as spheres with a regular dot pattern, and the Pb(2) atoms as spheres with random dot pattern. The O atoms are shown as shadowed spheres, and the Cl atoms as open, larger spheres.

4.5 Discussion

The ideal formula of choloalite is $\text{Cu}_3\text{Pb}_3\text{Te}^{4+}_6\text{O}_{18}(\text{Cl},\text{H}_2\text{O})$. The empirical formula, based on the microprobe analysis, and calculated on the basis of nineteen anions per formula unit, is $(\text{Cu}_{2.81}\text{Sb}_{0.13}\text{Zn}_{0.09})_{\Sigma 3.03}(\text{Pb}_{2.65}\text{Ca}_{0.17})_{\Sigma 2.82}\text{Te}_{6.14}\text{O}_{18.00}(\text{Cl}_{0.64}\text{H}_2\text{O}_{0.36})_{\Sigma 1.00}$. This is similar to the formula based on the structure analysis, which is

$(\text{Cu}_{2.79}\text{Sb}_{0.21})_{\Sigma 3.00}(\text{Pb}_{2.70}\text{Ca}_{0.30})_{\Sigma 3.00}\text{Te}_{6.00}\text{O}_{18.00}(\text{Cl}_{0.81}\text{H}_2\text{O}_{0.19})_{\Sigma 1.00}$. The empirical formula calculated from the analysis in Williams (1981) (on the basis of 19 anions per formula unit) is $\text{Cu}_{2.37}\text{Pb}_{2.53}\text{Te}_{5.44}\text{O}_{15.77}(\text{H}_2\text{O})_{3.23}$. The results show a *Cl* position that is fully occupied by Cl plus H_2O , unlike the material synthesized by Powell *et al.* (1994), which presumably contains no Cl and is anhydrous.

Choloalite is one of five cubic Te-oxysalt minerals; the others are cliffordite, mcalpineite, winstanleyite, and yafsoanite. Only the crystal structures of cliffordite and yafsoanite (Jarosch and Zemmann 1989) are known. Brandstätter (1981) showed that there are three distinct cation sites in the crystal structure of cliffordite. The atom at the *Te* position, which is completely occupied by Te^{4+} , is coordinated by five (Brandstätter 1981) or more (Back 1990) O atoms. There are also two *U* positions in the crystal structure of cliffordite; each is coordinated by eight O atoms forming hexagonal bipyramids. The crystal structure of yafsoanite was most recently studied by Jarosch and Zemmann (1989), who showed that it is a garnet-type oxide with Ca, Te^{6+} , and Zn atoms coordinated by eight, six, and four O atoms, respectively.

4.6 Conclusions

The formula of choloalite is revised to $\text{Cu}_3\text{Pb}_3\text{Te}^{4+}_6\text{O}_{18}(\text{Cl},\text{H}_2\text{O})$ which is different from earlier formulas of $\text{CuPb}(\text{Te}^{4+}\text{O}_3)_2\cdot\text{H}_2\text{O}$ (Williams 1981), and $\text{CuPb}(\text{TeO}_3)_2$ (Powell *et al.* 1994). Microprobe and infrared analyses and structure refinement show that choloalite does contain water. The structure consists of two three-dimensional nets, one net contains only Pb(1) polyhedra and the other consists of Pb(2) and Cu polyhedra; these nets are joined together by TeO_6 octahedra.

5.0 RODALQUILARITE, A REFINEMENT OF THE STRUCTURE

5.1 Introduction

Rodalquilarite was first discovered by J. Sierra Lopez *et al.* in 1968 during a general study of the gold-bearing Rodalquilar deposit in the province of Almeria, Spain. Named after the deposit, it was determined to be an unknown chlorotellurite of iron. Associated with jarosite, emmonsite, and rarely with native gold, rodalquilarite was found in the oxidation zone of the gold-bearing field. Rodalquilarite occurs as tiny crystals often smaller than 0.1 mm forming crystalline crusts covering quartz geodes. The crystals are squat with a greasy lustre and the colour ranges from brass green to emerald green. Sierra Lopez *et al.* (1968) describes rodalquilarite as a possible alteration product of gold tellurides.

The cell parameters, determined with a precession camera, were: $a = 8.89 \text{ \AA}$ $b = 5.08 \text{ \AA}$ $c = 6.63 \text{ \AA}$ $\alpha = 103^\circ 10'$ $\beta = 107^\circ 5'$ $\gamma = 77^\circ 52'$ and $V = 275.9 \text{ \AA}^3$. The crystal system was found to be triclinic and the space group $P\bar{1}$. The original chemical, thermogravimetric, and microprobe analyses of rodalquilarite gave the formula $\text{Fe}_2^{3+}(\text{TeO}_3^{2-}/(\text{TeO}_3\text{H})_3/\text{Cl}^-) \cdot 0.5 \text{ H}_2\text{O}$. However, these analyses could not confidently define the Cl to H_2O ratio and Sierra Lopez *et al.* (1968) suggested that crystal structure analysis would resolve any questions about the formula.

The crystal structure of rodalquilarite was originally solved using film methods (Dusausoy and Protas 1969) to a final R index of 9.2%. Crystal structure analysis gave the revised formula as $\text{H}_3^+\text{Fe}_2^{3+}(\text{TeO}_3)_4^{2-}\text{Cl}^-$ allowing the conclusion be drawn that rodalquilarite is an anhydrous chlorotellurite of iron.

It was decided that a refinement of the crystal structure of rodalquilarite be done using a single crystal X-ray diffractometer. It was thought that with better data, the R index would be

reduced resulting in a better structural model which could allow the hydrogens and their bonds to be located with confidence.

5.2 Experimental

Forty reflections with 2θ 11.29-49.36° were centered using an automated search routine. One sphere of reflections (3342 measurements, exclusive of standards) was collected from 3 to 60° 2θ . No reflections were rejected. Eleven strong reflections were used for the ψ -scan and the data (395 measurements) was used to calculate an absorption correction. The merging R index for the ψ -scan data set decreased from 8.30% before the absorption correction to 3.39% after the absorption correction. This correction was then applied to the entire data set; maximum and minimum transmissions were 0.958 and 0.425 respectively. Of the 1672 unique reflections, 1555 were classed as observed [$I \geq 3\sigma(I)$].

5.3 Structure Solution and Refinement

The structure was solved by direct methods in the space group $P\bar{1}$ but the atomic positions were not the same as that published by Dusauroy and Protas (1969). The published atomic positions were put into the problem and the structure was refined to an R index of 5.3% for an isotropic displacement model and to $R = 4.1\%$ and $wR = 4.7\%$ using anisotropic displacement factors for the two tellurium atoms, iron, and chlorine. Using all 1672 data, R is 4.6% and wR is 6.4 %.

A hydrogen atom was tentatively located using the listing of possibly bonded atoms in the listing file. Previous results indicated that O(3), O(4), and O(1) may be bonded to hydrogens

and knowing that O(3) had the most deficient bond-valence sums, unassigned atoms that were joined to O(3) were the ones most likely to be hydrogen atoms. Luckily, only one unassigned atom appeared to be joined to both O(3) and O(4) and this atom was assigned as a hydrogen. The bond-valence sums improved for O(3), O(4), and O(1) with the addition of this atom although there was no improvement in the *R* index. Knowing that one of the hydrogens must lie on a special position, a hydrogen atom was located at a site proposed by Dusauroy and Protas (1969). The bond-valence sum for O(1) improved but again there was no improvement in the *R* index. No additional symmetry was detected when the program *MISSYM* was used on the redetermination (based on the 1969 atomic positions). The program *STRUCTURE TIDY* was used to standardize the atomic positions but, for comparison purposes, it was decided that the redetermination be described using the atomic positions based on Dusauroy and Protas (1969).

Miscellaneous experimental information is given in Table 5.1. Positional coordinates and anisotropic and equivalent isotropic displacement factors are given in Tables 5.2, 5.3, and 5.4 respectively for the refined, original (Dusauroy and Protas, 1969), and “*STRUCTURE TIDY*” refinements. Interatomic distances and bond angles are found in Table 5.5. A bond-valence table is given in Table 5.6. Structure factors are listed in Appendix E.

Table 5.1. Miscellaneous information: rodalquilarite

a (Å)	9.021(1)	Space group	$P\bar{1}$
b (Å)	5.1170(7)	μ (MoK α , mm ⁻¹)	13.00
c (Å)	6.6539(8)	Rad/mono	MoK α /graphite
α (°)	103.23(1)	Total reflections	3342
β (°)	106.66(1)	Unique reflections	1672
γ (°)	78.07(1)	[$I \geq 3 \sigma(I)$]	1555
V (Å ³)	283.15(6)	R (observed) %	4.1%
Z	1	Rw (observed) %	4.7%
Crystal size (mm)	0.19 × 0.13 × 0.05		
$R = \sum F_o - F_c / \sum F_o$			
$wR = \left[\sum (w \cdot F_o - F_c)^2 / \sum w \cdot F_o^2 \right]^{0.5}, w = 1$			

Table 5.2. Redetermined atomic parameters for rodalquilarite (based on the positions by Dusausoy & Protas, 1969).

Site	x	y	z	U_{11}^*	U_{22}	U_{33}	U_{12}	U_{13}	U_{23}	U_{eq}
Te(1)	0.16972(7)	0.3381(1)	0.33395(9)	94(3)	90(3)	108(3)	-20(2)	18(2)	44(2)	94(2)
Te(2)	0.31238(7)	0.8796(1)	0.83997(8)	98(3)	71(2)	48(2)	-21(2)	10(2)	10(2)	73(2)
Fe	0.4442(2)	0.7235(3)	0.3548(2)	100(5)	63(5)	58(5)	-31(4)	12(4)	17(4)	72(4)
Cl	0	0	$\frac{1}{2}$	208(15)	212(15)	204(15)	-60(13)	-10(12)	103(13)	206(11)
O(1)	0.1250(8)	0.100(1)	0.071(1)							148(12)
O(2)	0.3546(7)	0.114(1)	0.461(1)							88(11)
O(3)	0.1935(8)	0.594(1)	0.816(1)							135(12)
O(4)	0.2621(8)	0.544(1)	0.214(1)							118(12)
O(5)	0.5382(8)	0.192(1)	0.907(1)							98(11)
O(6)	0.4164(8)	0.637(1)	0.637(1)							103(11)
H(1)	0.172(6)	0.680(6)	-0.018(6)							500 [†]
H(2)	0	0	0							483(62)

* U_{ij} and U values are listed $\times 10^4$. [†]Fixed value to better refine the H(1) atomic position.

Table 5.3. Original atomic parameters from Dusaosoy & Protas (1969).

Site	x	y	z	$B^{\dagger} (\text{\AA}^2)$
Te(1)	0.1698(7)	0.3385(4)	0.3342(3)	1.204(30)
Te(2)	0.3129(6)	0.8802(4)	0.8409(3)	1.116(32)
Fe	0.4424(18)	0.7227(11)	0.3548(7)	1.028(72)
Cl	0	0	$\frac{1}{2}$	1.812(220)
O(1)	0.1176(106)	0.0941(64)	0.0683(41)	1.780(462)
O(2)	0.3476(83)	0.1143(52)	0.4667(37)	1.352(420)
O(3)	0.1968(104)	0.5986(65)	0.8145(41)	0.972(320)
O(4)	0.2607(112)	0.5458(64)	0.2061(47)	1.600(448)
O(5)	0.5271(104)	0.1937(62)	0.9059(42)	1.524(420)
O(6)	0.4110(106)	0.6526(64)	0.6352(46)	1.288(412)
H(1)*				
H(2)*	0	0	0	

*H(2) position located according to the written description. H(1) position was described but not located. [†]Thermal agitation factors.

Table 5.4. Atomic parameters for rodalquilarite (based on *STRUCTURE TIDY* standardized positions).

Site	x	y	z	U_{11}^*	U_{22}	U_{33}	U_{12}	U_{13}	U_{23}	U_{eq}
Te(1)	0.1204(1)	0.33994(8)	0.68762(6)	73(2)	50(2)	100(2)	-11(2)	-21(2)	-10(2)	75(2)
Te(2)	0.3381(1)	0.16604(9)	0.16971(7)	92(2)	110(3)	96(2)	-44(2)	-20(2)	-18(2)	96(2)
Fe	0.7235(2)	0.1452(2)	0.4444(1)	65(5)	61(5)	101(5)	-17(4)	-31(4)	-12(4)	74(3)
Cl	0	0	0	215(14)	204(14)	203(14)	-108(12)	-57(12)	12(11)	206(10)
O(1)	0.099(1)	0.428(1)	0.1257(8)							151(12)
O(2)	0.114(1)	0.0393(9)	0.3544(7)							90(10)
O(3)	0.192(1)	0.592(1)	0.5380(7)							102(11)
O(4)	0.362(1)	0.136(1)	0.5840(7)							106(11)
O(5)	0.544(1)	0.286(1)	0.2621(7)							119(11)
O(6)	0.594(1)	0.683(1)	0.194(8)							137(11)
H(1)	0.717(3)	0.529(3)	0.194(3)							550(35)
H(2)	0	1/2	0							580(35)

* U_{ij} and U values are listed x 10^4

Table 5.5. Selected interatomic distances (Å) and angles (°) for rodalquilarite.

Te(1)–O(1)	1.879(6)	Cl–Te(1)–O(1)	87.0(0.3)
–O(2)	1.912(6)	Cl–Te(1)–O(2)	84.2(0.2)
–O(4)	1.890(8)	Cl–Te(1)–O(3)	73.6(0.2)
–O(3)g	3.109(7)	Cl–Te(1)–O(4)	175.9(0.2)
–O(3)	3.139(7)	Cl–Te(1)–O(6)	119.7(0.2)
–O(6)	2.963(6)	Cl–Te(1)–Clb	102.2(0.0)
–Cl	3.082(1)	Cl–Te(1)–O(3)g	62.0(0.2)
–Clb	<u>3.486(1)</u>	O(1)–Te(1)–O(2)	95.7(0.3)
<Te(1)–O> _{3 closest}	1.894	O(1)–Te(1)–O(3)	160.5(0.3)
<Te(1)–O/Cl>	2.683	O(1)–Te(1)–O(4)	90.0(0.3)
		O(1)–Te(1)–O(6)	143.1(0.3)
Te(2)–O(3)	1.937(8)	O(1)–Te(1)–Clb	131.3(0.2)
–O(5)d	1.886(6)	O(1)–Te(1)–O(3)g	74.7(0.3)
–O(6)	1.931(7)	O(2)–Te(1)–O(3)	80.8(0.2)
–O(1)a	2.531(8)	O(2)–Te(1)–O(4)	98.9(0.3)
–O(2)b	3.174(8)	O(2)–Te(1)–O(6)	65.1(0.2)
–O(5)b	2.719(7)	O(2)–Te(1)–Clb	132.5(0.2)
–Clb	<u>3.115(1)</u>	O(2)–Te(1)–O(3)g	144.9(0.3)
<Te(2)–O> _{3 closest}	1.918	O(3)–Te(1)–O(4)	109.5(0.2)
<Te(2)–O/Cl>	2.470	O(3)–Te(1)–O(6)	52.1(0.2)
		O(3)–Te(1)–Clb	57.3(0.1)
Fe–O(2)b	2.037(6)	O(3)–Te(1)–O(3)g	97.1(0.1)
–O(2)e	2.092(6)	O(4)–Te(1)–O(6)	64.3(0.2)
–O(4)	1.941(7)	O(4)–Te(1)–Clb	77.7(0.2)
–O(5)e	1.946(8)	O(4)–Te(1)–O(3)g	114.4(0.2)
–O(6)e	2.010(6)	O(6)–Te(1)–Clb	71.3(0.1)
–O(6)	<u>2.114(8)</u>	O(6)–Te(1)–O(3)g	138.8(0.2)
<Fe–O>	2.023	Clb–Te(1)–O(3)g	<u>68.5(0.1)</u>
		<O–Te(1)–O>	99.0
H(1)–O(1)b	2.08(3)		
–O(3)f	1.15(4)	O(3)–Te(2)–O(6)	87.9(0.3)
–O(4)	1.75(4)	O(3)–Te(2)–Clb	74.2(0.2)
		O(3)–Te(2)–O(1)a	76.6(0.3)

H(2)–O(1),c	× 2	1.256(7)	O(3)–Te(2)–O(2)b	126.9(0.2)
			O(3)–Te(2)–O(5)b	166.4(0.2)
Cl–Te(1),i	× 2	3.082(1)	O(3)–Te(2)–O(5)d	96.0(0.3)
–Te(1)h,g	× 2	3.486(1)	O(6)–Te(2)–Clb	94.2(0.2)
–Te(2)h,g	× 2	<u>3.115(1)</u>	O(6)–Te(2)–O(1a)	164.0(0.3)
<Cl–Te>		3.228	O(6)–Te(2)–O(2)b	61.7(0.2)
			O(6)–Te(2)–O(5)b	85.6(0.3)
			O(6)–Te(2)–O(5)d	98.5(0.3)
O(1)–H(2)–O(1)c		180	Clb–Te(2)–O(1)a	78.2(0.1)
			Clb–Te(2)–O(2)b	66.7(0.1)
O(4)–H(1)–O(1)b		107.9(1.7)	Clb–Te(2)–O(5)b	118.1(0.1)
O(4)–H(1)–O(3)f		126.5(2.8)	Clb–Te(2)–O(5)d	163.7(0.2)
O(3)f–H(1)–O(1)b		117.8(2.8)	O(1)a–Te(2)–O(2)b	125.6(0.2)
			O(1)a–Te(2)–O(5)b	110.4(0.2)
Te(1)–Cl–Te(1)h		102.2	O(1)a–Te(2)–O(5)d	86.9(0.3)
Te(1)–Cl–Te(1)g		77.8	O(2)b–Te(2)–O(5)b	59.3(0.2)
Te(1)–Cl–Te(1)i		180	O(2)b–Te(2)–O(5)d	128.7(0.3)
Te(1)–Cl–Te(2)h		87.5	O(5)b–Te(2)–O(5)d	<u>73.3(0.3)</u>
Te(1)–Cl–Te(2)g		92.5	<O–Te(2)–O>	102.0
Te(1)h–Cl–Te(1)g		180		
Te(1)h–Cl–Te(1)i		77.8	O(4)–Fe–O(6)	84.8(0.3)
Te(1)h–Cl–Te(2)h		72.7	O(4)–Fe–O(2)b	104.6(0.3)
Te(1)g–Cl–Te(2)g		107.3	O(4)–Fe–O(2)e	172.2(0.3)
Te(1)g–Cl–Te(1)i		102.2	O(4)–Fe–O(5)e	93.9(0.3)
Te(1)g–Cl–Te(2)h		107.3	O(4)–Fe–O(6)e	90.8(0.3)
Te(1)i–Cl–Te(2)g		72.7	O(6)–Fe–O(2)b	85.8(0.3)
Te(1)i–Cl–Te(2)h		92.5	O(6)–Fe–O(2)e	88.0(0.3)
Te(1)h–Cl–Te(2)g		87.5	O(6)–Fe–O(5)e	177.9(0.3)
Te(2)–Cl–Te(2)g		<u>180</u>	O(6)–Fe–O(6)e	80.3(0.3)
<Te–Cl–Te>		108	O(2)b–Fe–O(2)e	77.9(0.3)
			O(2)b–Fe–O(5)e	93.0(0.3)
			O(2)b–Fe–O(6)e	158.3(0.2)

O(2)e-Fe-O(5)e	93.4(0.3)
O(2)e-Fe-O(6)e	84.9(0.2)
O(5)e-Fe-O(6)e	<u>101.3(0.3)</u>
<O-Fe-O>	105.8

Equivalent positions: $a = x, y + 1, z + 1$; $b = x, y + 1, z$; $c = \bar{x}, \bar{y}, \bar{z}$; $d = \bar{x} + 1, \bar{y} + 1, \bar{z} + 2$;
 $e = \bar{x} + 1, \bar{y} + 1, \bar{z} + 1$; $f = x, y, z - 1$; $g = \bar{x}, \bar{y} + 1, \bar{z} + 1$; $h = x, y - 1, z$; $i = \bar{x}, \bar{y}, \bar{z} + 1$.

Table 5.6. Bond-valence* arrangement[†] in rodalquilarite.

	Te(1)	Te(2)	Fe	H(1)	H(2)	Total
O(1)	1.30	0.22		0.07	0.44 × 2↓	2.03
O(2)	1.19	0.04	0.47			2.11
			0.41			
O(3)	0.04	1.11		0.76		1.96
	0.05					
O(4)	1.27		0.61	0.07		1.95
O(5)		0.13	0.60			2.01
		1.28				
O(6)	0.07	1.13	0.38			2.09
			0.51			
Cl	0.15 × 2→	0.13 × 2→				0.66
	0.05 × 2→					
Total	4.12	4.04	2.98	0.90	0.88	

*Based on the curves of Brese and O'Keeffe (1991). [†]Atomic positions refined based on those found in Dusauroy and Protas (1969).

5.4 Description of the Structure Based on Earlier Work

The structure of rodalquilarite was originally solved and described by Dusausoy and Protas in 1969. Further work using the original atomic positions was performed by Back (1990), mostly concentrating on bond valence and the coordination around tellurium.

5.4.1 Original structure description by Dusausoy and Protas (1969)

Rodalquilarite was described as consisting of chains of edge-sharing FeO_6 octahedra extending along the b -axis with triangular $\text{Te}(2)\text{O}_3$ pyramids linking these chains in the c -direction (Figures 5.1 and 5.2). Planes of FeO_6 octahedra and TeO_3 pyramids are therefore formed parallel to the bc -plane. Between these planes lie the chlorine and hydrogen atoms that connect the planes in the a -direction (Figure 5.3). The $\text{Te}(1)\text{O}_3$ pyramids do not serve to join chains or planes together as each $\text{Te}(1)\text{O}_3$ pyramid is only attached to a single chain of FeO_6 octahedra. Also described is hydrogen-bonding between $\text{O}(4)$ and $\text{O}(3)$ which are joined to the triangular pyramids of $\text{Te}(2)$ and $\text{Te}(1)$ respectively. Another hydrogen is located symmetrically between two $\text{O}(1)$'s, probably on a center of symmetry at $(0,0,0)$.

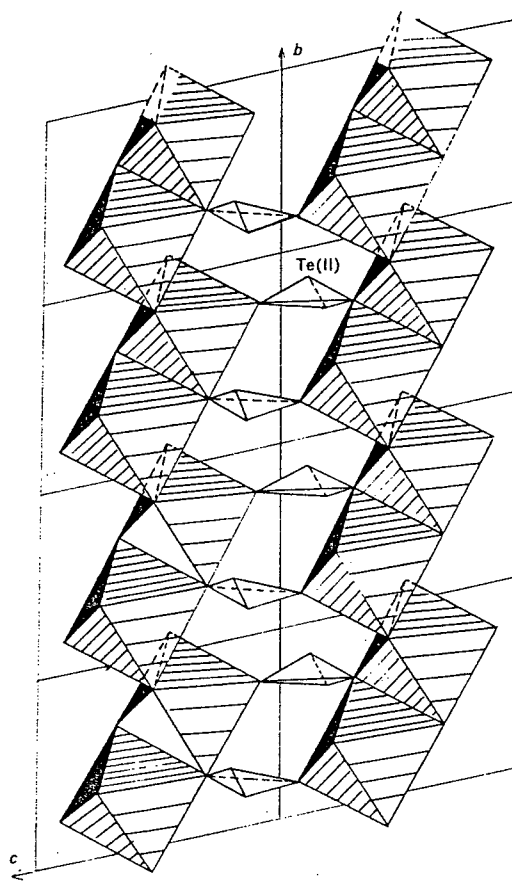


Figure 5.1. Chains of FeO_6 octahedra in rodalquilarite projected onto the bc -plane (after Dusauso and Protas, 1969).

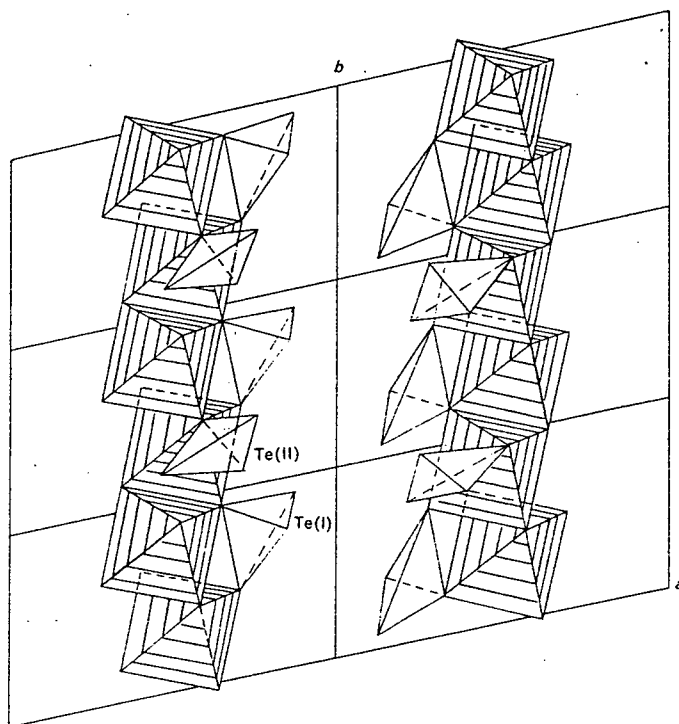


Figure 5.2. Chains of FeO_6 octahedra in rodalquilarite projected onto the ab -plane (after Dusauso and Protas, 1969).

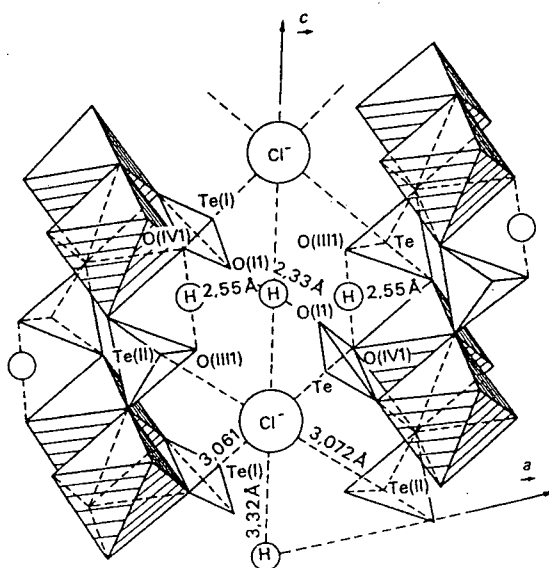


Figure 5.3. Projection of the rodalquilarite structure onto the ac -plane showing the diverse bond types in the structure (after Dusauso and Protas, 1969).

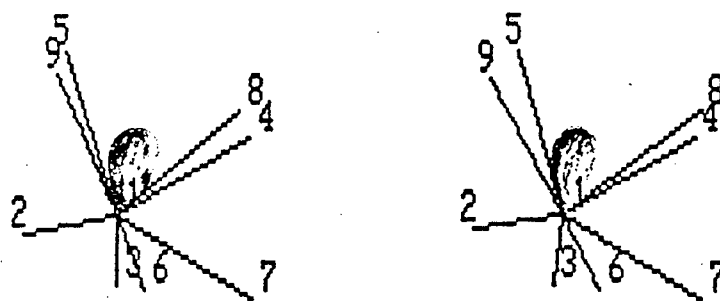
5.4.2 Previous work done by Back (1990)

Back (1990), in his general study of tellurites, performed some additional work on rodalquilarite using the results from Dusausoy and Protas (1969). The data was input into the NRCVAX structure program to determine bond lengths and angles so that bond-valence calculations could be done. Extra bonds were found for Te(1) [O(3), O(6), and Cl] and for Te(2) [O(1) and O(5)]. Bond-valence sums using the tables from Brown (1981) were found to be too high for Te(1), Te(2), O(1), O(2), O(4), and O(6). The bond-valence sums were too high for Te(1) and Te(2) even without Cl coordination. Similar problems were found with Te(2), O(1), O(2), and O(6) using the tables of Brown and Altermatt (1985). In calculating these sums, Back (1990) had to estimate the valence contributions of the hydrogens and that fact may explain the problem sums for O(1) and O(4).

Figure 5.4 shows the polyhedra drawn by Back (1990) assuming that Te(1) is eight-coordinated (with two Cl atoms) and Te(2) is seven-coordinated (with one Cl atom). He states that these Te^{4+} polyhedra have similar topologies to seven and eight-coordinated Te^{4+} in other tellurites. He also noticed that the chlorine atom takes up a normal oxygen position despite the 0.49Å difference in size between the ionic radii of the two ions.

According to Back (1990), the roles of chlorine and hydrogen-bonding in the structure are unclear. If these roles were defined, the difficulties with the bond-valence sums and the correct coordinations around Te(1) and Te(2) could be resolved. In his conclusions, Back (1990) recommended a redetermination of the structure using a diffractometer.

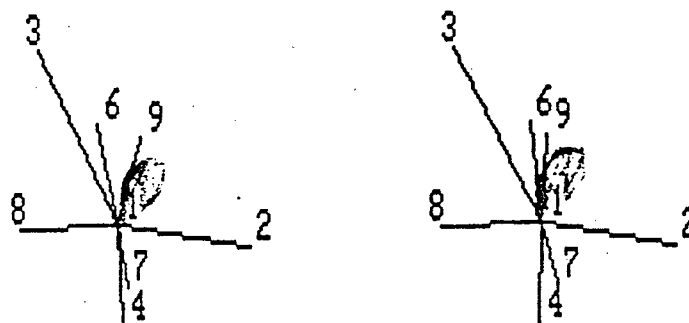
Te(1) Polyhedron



Atom Labels

1	Te(1)		
2	O(1)	1.91 Å	(Oc)
3	O(2)	1.86 Å	(Oa)
4	O(3)	3.12 Å	(Og)
5	O(3)'	3.08 Å	(Of)
6	O(4)	1.91 Å	(Ob)
7	O(6)	2.93 Å	(Od)
8	Cl	3.46 Å	(Oh position)
9	Cl'	3.06 Å	(Oe position)

Te(2) Polyhedron



Atom Labels

1	Te(2)		
2	O(1)	2.54 Å	(Od)
3	O(2)	3.10 Å	(Oe)
4	O(3)	1.88 Å	(Oa)
6	O(5)	2.61 Å	(Of)
7	O(5)'	1.91 Å	(Ob)
8	O(6)	1.87 Å	(Oc)
9	Cl	3.07 Å	(Og position)

Figure 5.4. Eight-coordinated Te(1) and seven-coordinated Te(2) in rodalquilarite (after Back, 1990). The proposed sites of the electron lone pair are shown as the shaded areas.

5.5 Description of the Refined Structure

In the redetermination of rodalquilarite, modifications are made to the coordination of the two Te^{4+} atoms, the hydrogen positions are confirmed and their bonds are detailed, and the role of chlorine is clarified.

5.5.1 Coordination of tellurium

The results of the redetermination were used to create a new bond-valence table (Table 5.6) using the values from Brese and O'Keeffe (1991). The values from Brown (1981) were comparable, however, it did not have constants for Te–Cl bonds which presented a problem.

With the evolution of the interpretation of the coordination around Te^{4+} , the description of the Te^{4+} in rodalquilarite should be brought up to date. Te(1) may be described as eight-coordinated with two Cl bonds; the eighth bond is to Cl at 3.486 Å away which is slightly more distant than an Fe atom that is 3.426 Å away. Te(2) is seven-coordinated with one chlorine bond. Both of these coordinations to Te agree with the results from Back (1990). The interatomic bond lengths and angles found in Table 5.5.

Both telluriums have the typical three close bonds of ~1.9 Å on one side of the coordination polyhedra while the remaining more distant bonds can be found on the other side of the polyhedra (Figures 5.5 and 5.6). As Back (1990) described, the lone electron pairs probably reside on the side opposite to the three close bonds.

5.5.2 Coordination of iron

The coordination around iron is unchanged with respect to its initial description in 1969. It remains coordinated with six oxygens to form octahedra (Figure 5.7). There is no evidence that iron is eight-coordinated (as suggested by Back in 1990). The bond lengths do not differ by much, ranging from 1.942 to 2.114 Å (average 2.024 Å). The polyhedral volume is 10.7573 Å³, the octahedral angle variance is 62.8457, and the mean octahedral quadratic elongation is 1.0190.

5.5.2 Coordination of chlorine

Chlorine is six-coordinated with bonds of 3.082 and 3.486 Å to Te(1) and 3.115 Å to Te(2) (all $\times 2$) (Figure 5.8). Bond-valence analysis shows the absence of some valence but this is not a new problem as there were also difficulties with bond valence with regards to chlorine in the structure of choloalite.

5.5.3 Hydrogen-bonding

Using Pauling's rules, Dusauroy and Protas (1969) rationalized which oxygen atoms the hydrogens would be bonded to. Bond-valence results support their choices of oxygen atoms by exposing which oxygen atoms were deficient in valence sums. It is also known that bond valences of oxygen, as the hydrogen donor, typically have sums of ~ 1.2 v.u. while H-acceptors are not as evident having sums of ~ 1.8 v.u. (Brown, 1981). Looking at the bond-valence table, it can then be proposed that O(3) is a H-donor and that O(4) and O(1) could be H-acceptors. The hydrogen, H(2), appears to be on special position a (0,0,0) exactly the same distance away, 1.256

Å, from two O(1)'s; however, hydrogen could be disordered about this site. The hydrogen, H(1), in the general position is closely bonded to O(3), (1.053 Å) and distantly bonded to O(1), (1.949 Å) and O(4), (1.954 Å). This would make O(3) a hydrogen donor and O(1) and O(4) hydrogen acceptors with respect to H(1). The hydrogen-bonding scheme is shown in Figure 5.9.

5.5.4 Structure connectivity

With the added coordination around the telluriums atoms the structure connectivity is harder to describe although the overall changes could be considered minor.

Edge-sharing iron octahedra (each sharing two edges) continue to form chains along the *b*-axis (Figure 5.10). The difficulty in description comes with the added coordinations around the tellurium atoms. Looking at the Te–O bonds less than 3 Å long (this results in four-coordinated Te(1) and five-coordinated Te(2) as compared to three-coordinated Te's described by Dusauroy and Protas, 1969), the chains of Fe-octahedra are connected in the *c*-direction by these Te–O bonds to form relatively strongly held planes of iron and tellurium polyhedra parallel to the *bc*-plane (Figure 5.11 and 5.12). The more distant Te–O and Te–Cl bonds (> 3 Å) help to connect the structure in the *a*-direction (Figure 5.13). Thus the original structure description of planes of iron octahedra and tellurium polyhedra parallel to *bc* held together by weak Te–Cl and H–O(1) bonds still basically holds true. The refinement served to locate additional weak Te–O bonds that help to hold these *bc*-planes together in the *a*-direction.

Te(1) shares faces with one Te(1) and one Te(2) atom, edges with two Te(2) and two Fe atoms, and is corner-sharing with four Te(1), two Te(2), and one Fe atom (Figure 5.14). Te(2) shares edges with three Te(1), one Te(2), and two Fe atoms and is also corner-sharing with two Te(1), one Te(2), and two Fe atoms (Figure 5.15).

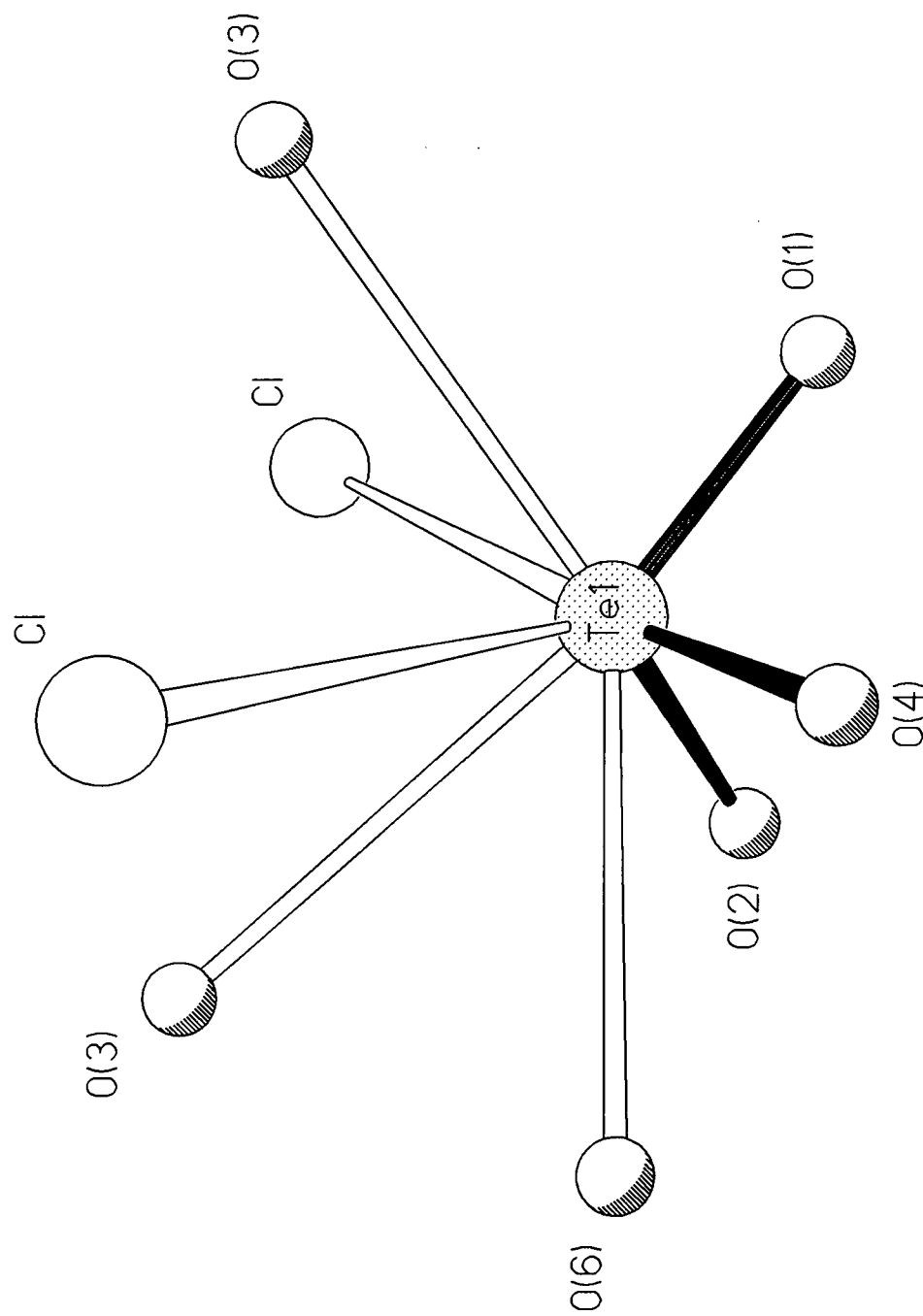


Figure 5.5. Coordination of tellurium (1) in rodalquilarite. Solid bonds show the three short bonds on one side of the coordination polyhedron as found by Dusauroy and Protas (1969). Hollow bonds show the longer bonds not found in 1969.

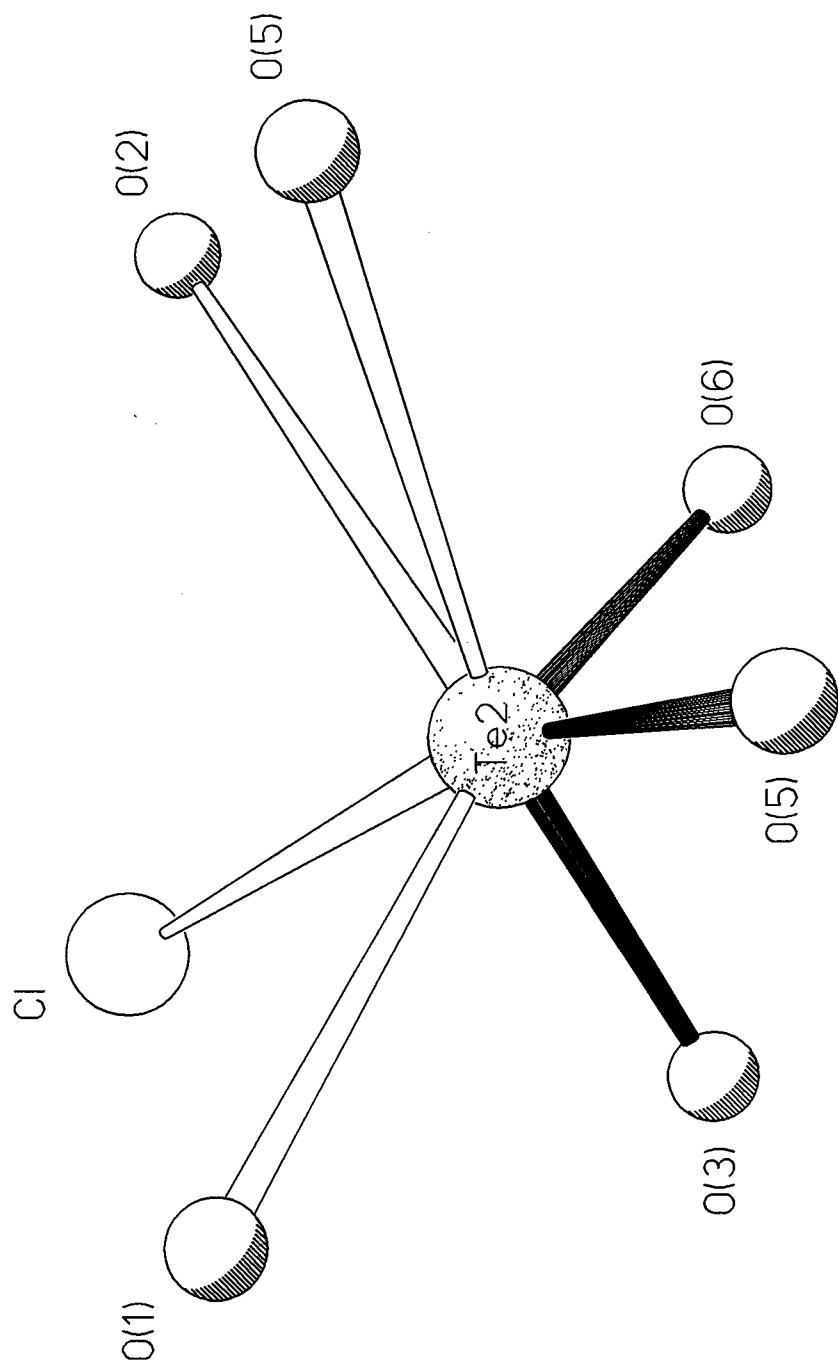


Figure 5.6. Coordination of tellurium (2) in rodalquilarite. Shading of the bonds is the same as that in figure 5.5.

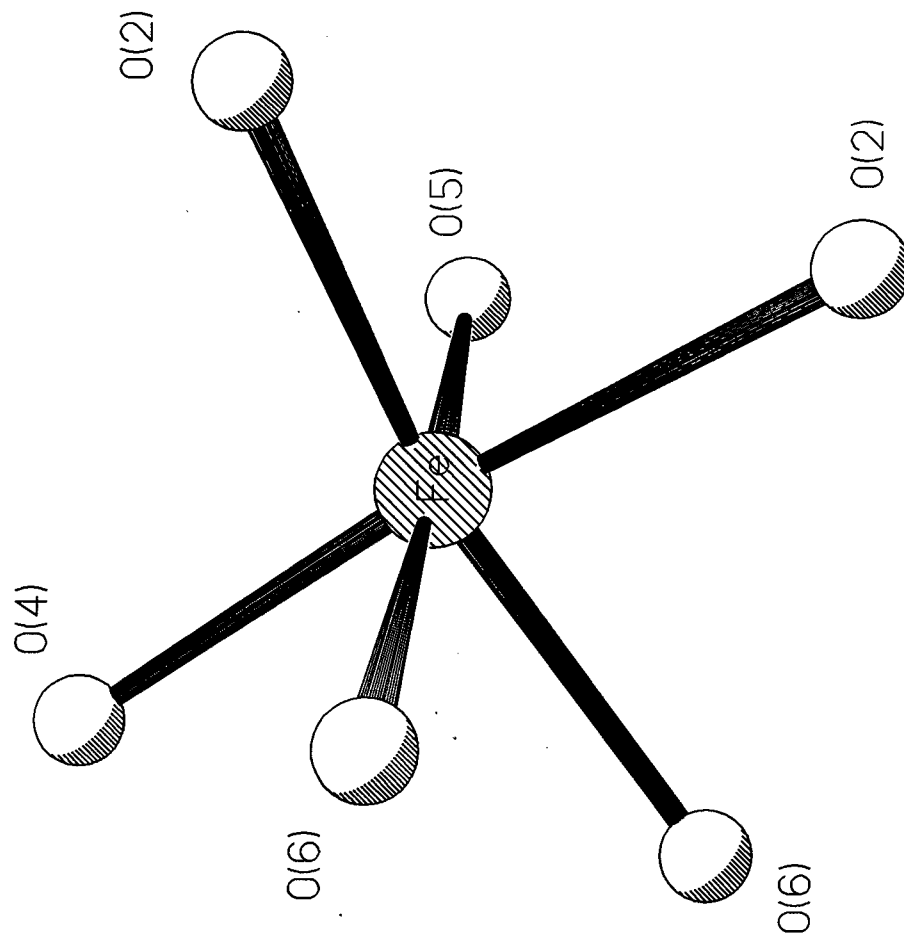


Figure 5.7. Coordination of the iron atom in rodalquilarite.

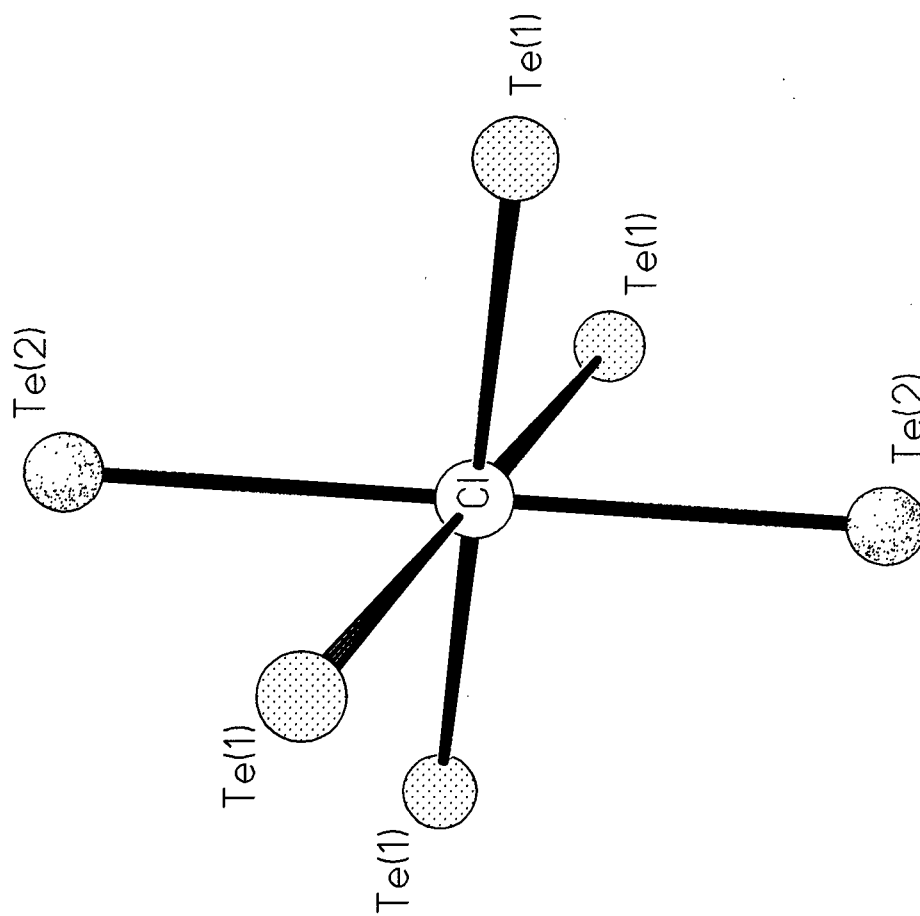


Figure 5.8. Coordination of the chlorine atom in roddalquilarite.

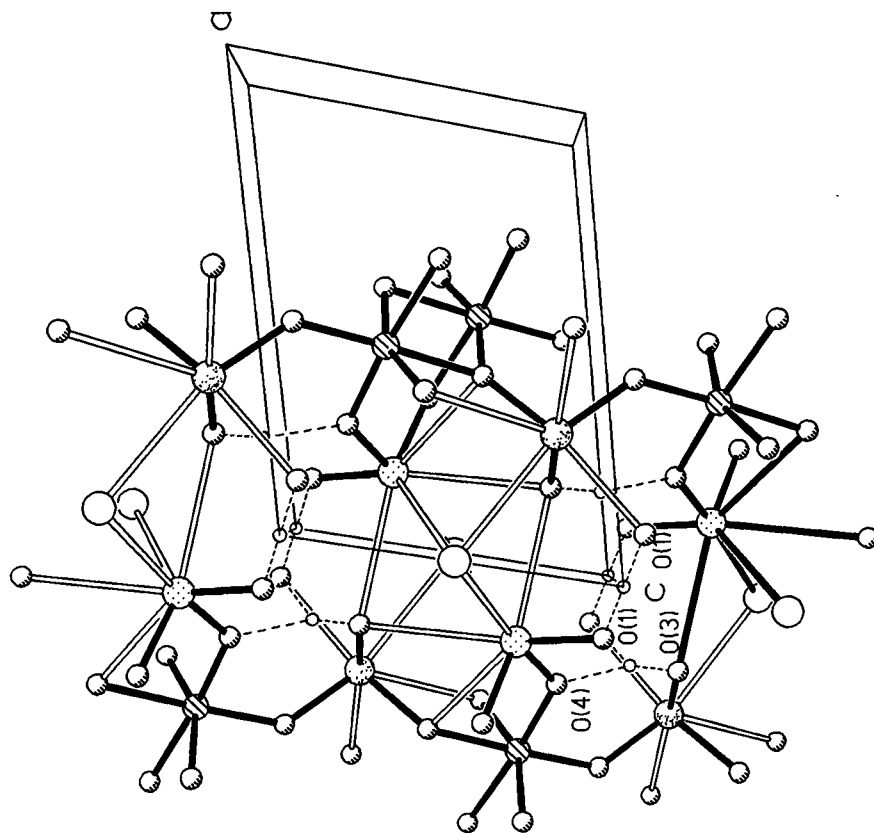


Figure 5.9. Hydrogen-bonding in roddalquarite viewed down the b-axis. The hydrogen bonds are shown as dashed lines. The bonds found by Dusauroy and Protas (1969) are shown as solid bonds. Fe atoms are shown ruled, Te(1) atoms have a regular array of dots, Te(2) atoms have a random array of dots, Cl atoms are shown as large open spheres, H atoms as small open spheres, and O atoms as shaded spheres.

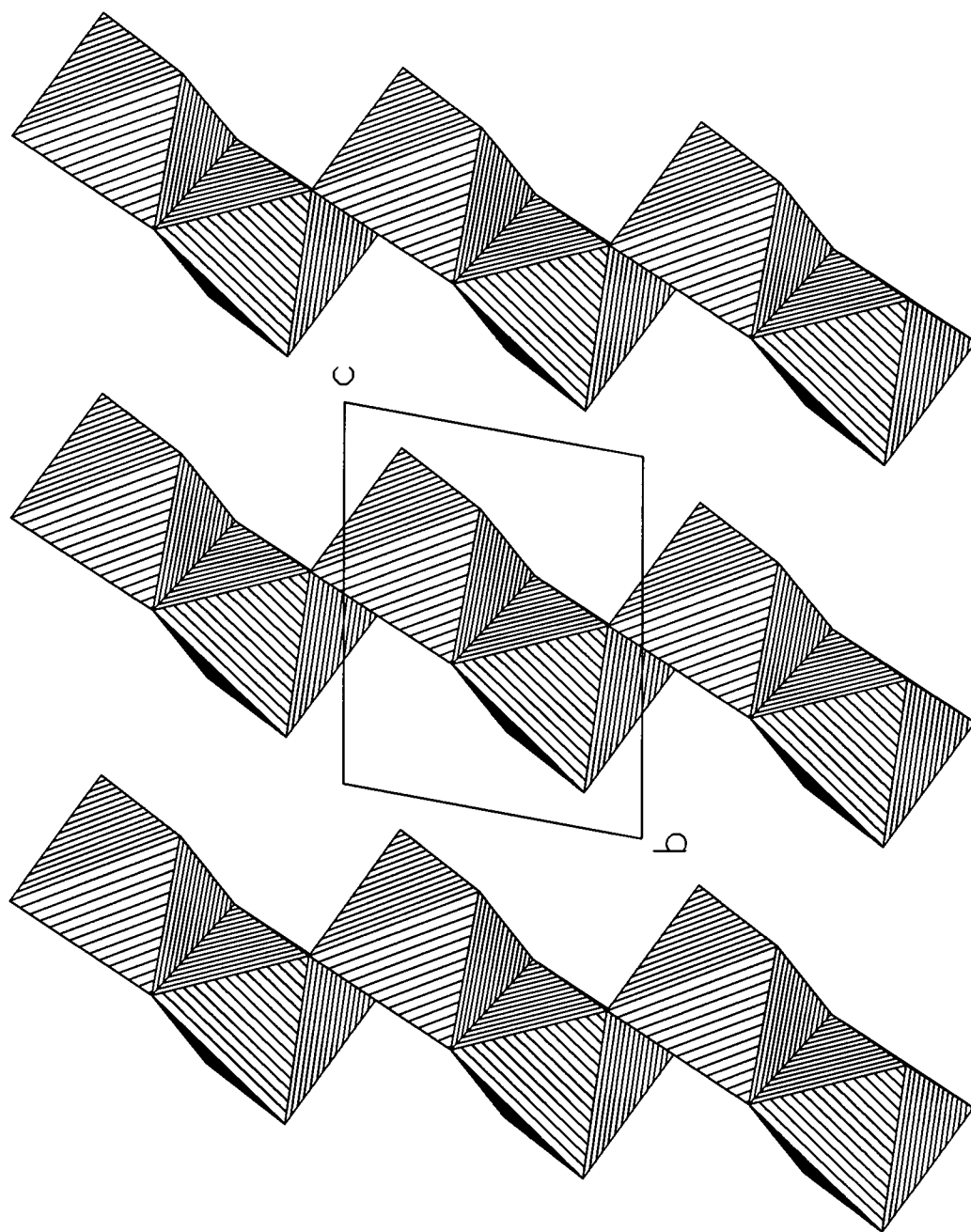


Figure 5.10. Chains of edge-sharing iron octahedra parallel to the b-axis.

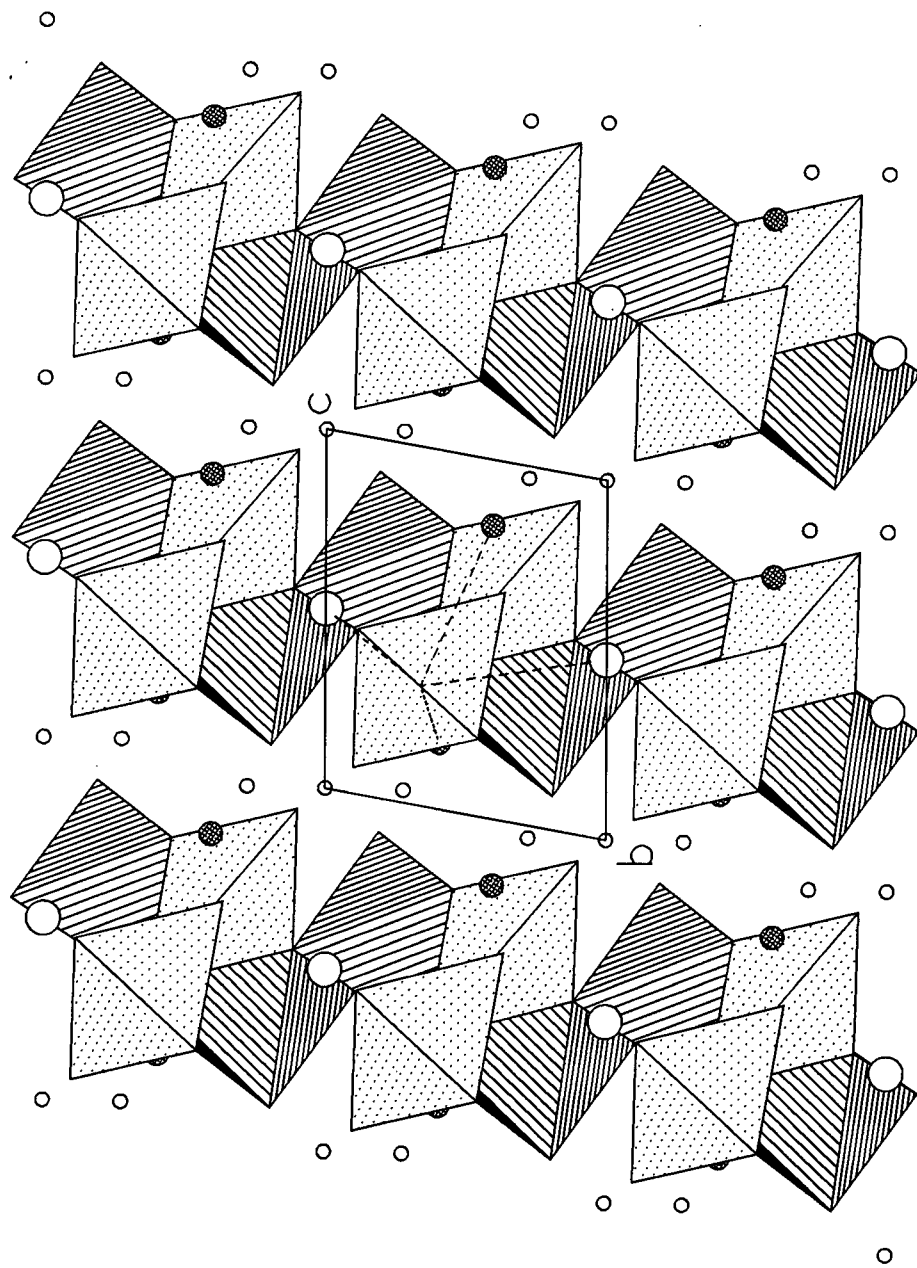


Figure 5.11. Te(1) and Fe polyhedra viewed down the *a*-axis. The Te polyhedra (regular dot pattern) are shown with bonds < 3.0 angstroms. The longer bonds of one tellurium atom are shown as dashed lines. Fe octahedra are shown ruled, O atoms as larger open spheres, H atoms as cross-hatched spheres, and H atoms as smaller open spheres. This figure shows Te(1) does not join the Fe octahedra in the *c*-direction. Notice the longer bonds to tellurium have a strong component in the *a*-direction.

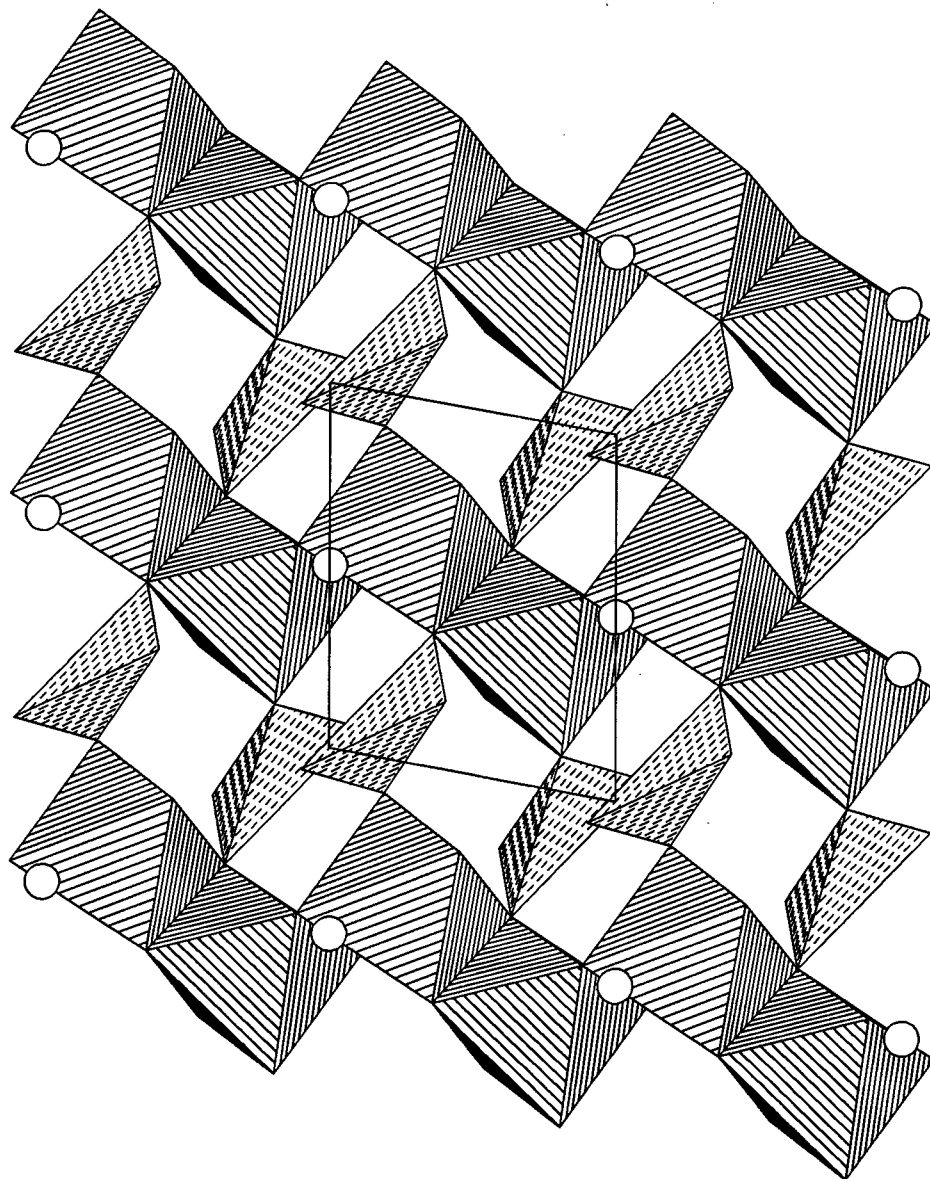


Figure 5.12. Te(2) and Fe polyhedral sheet parallel to the bc-plane. The Te polyhedra (shown with dashes) are shown with bonds < 3.0 angstroms. The Fe octahedra are shown ruled and the Cl atoms are shown as open spheres. The axes are in the same orientation as figure 5.11.

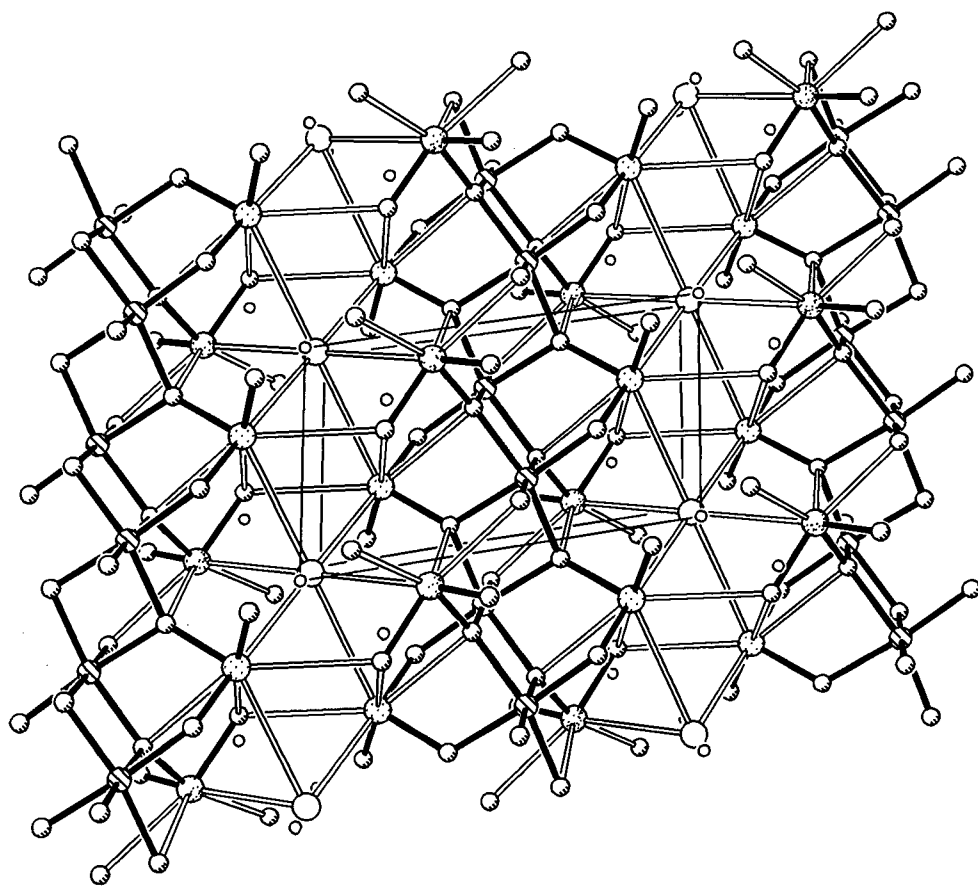


Figure 5.13. Connectivity of rodalquilarite as viewed down the c -axis. The unit cell is shown with the a -axis roughly top to bottom and the b -axis left to right. The longer (hollow) bonds connect planes of Te/Fe polyhedra in the a -direction. The shading of bonds and atoms is the same as in figure 5.9.

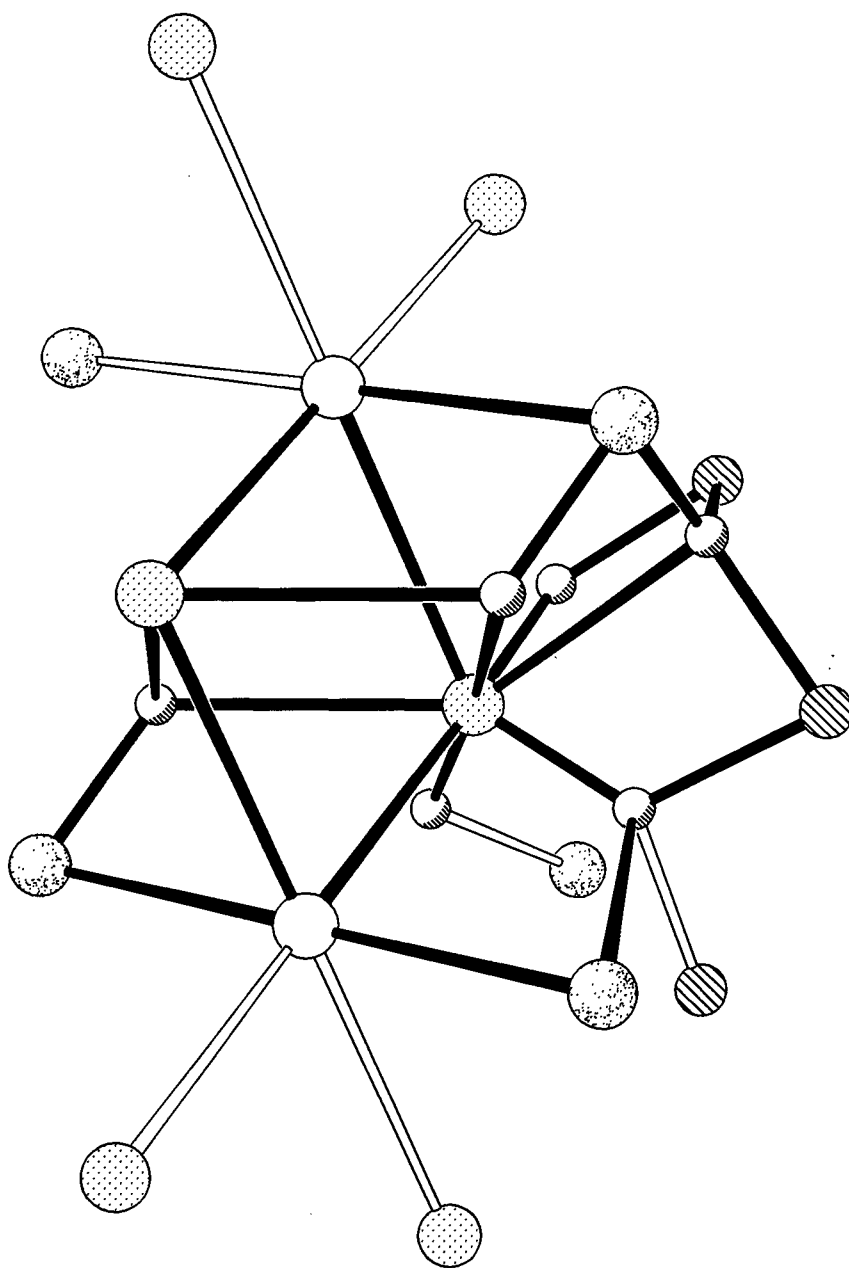


Figure 5.14. Linkage of adjacent cations to Te(1) in rodalquilarite. The shading of atoms is the same as in figure 5.13. Hollow bonds indicate linking by corners while the solid bonds indicate linking by edges or faces.

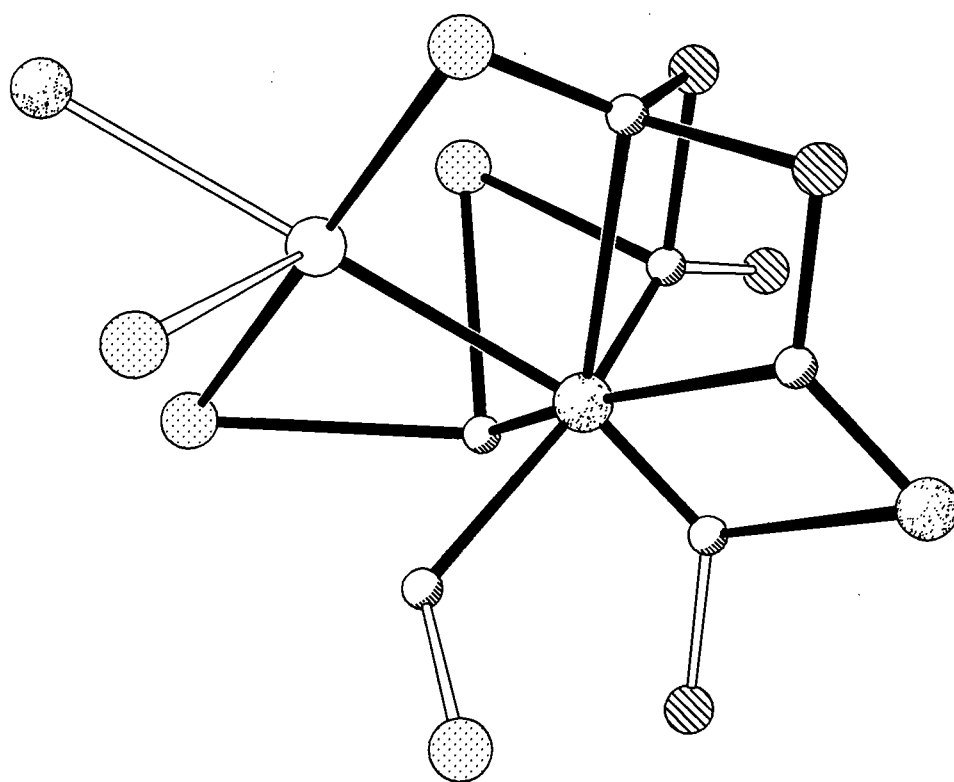


Figure 5.15. Linkage of adjacent cations to Te(2) in rodalquilarite. The shading of atoms and bonds is the same as in figure 5.14.

5.6 Conclusions About the Refinement of Rodalquilarite

The original structure description of planes of iron and tellurium octahedra parallel to bc held together by weak Te–Cl and H–O(1) bonds still basically holds true. The refinement served to locate more weak Te–O bonds that help to hold these planes together in the a -direction. Te(1) and Te(2) are described as eight- and seven-coordinated respectively and both have three short Te–O bonds on one side of the coordination polyhedra. Chlorine is bonded to six tellurium atoms and help to bond the Fe/Te polyhedral planes in the a -direction. A hydrogen-bonding scheme is proposed; the hydrogen that appears to be on special position a (0,0,0) may be disordered about the site but there is no way of knowing for sure as there is not enough material for neutron diffraction.

6.0 GRAEMITE

6.1 Introduction

The type specimen of graemite ($\text{CuTeO}_3 \cdot \text{H}_2\text{O}$), originally described by Williams (1975), was found in 1959 by Richard Graeme in an ore car at the Cole shaft at Bisbee, Arizona. The rock sample, which bears about 500 mg of graemite, measures $2.5 \times 2.5 \times 2$ inches and "is a loose spongy aggregate of cuprite crystals embedded in a dense matted matrix of tiny malachite needles." Embedded within the malachite are several large (8 mm) teinite prisms with corroded and pitted surfaces. Cuprite and graemite are found on these surfaces and in two cases graemite totally replaces two large teinite crystal (one was 20 mm long and the other had an 8 mm cross section). The graemite replaces the teinite as "divergent platy, bladed crystals arranged in a random fashion. In the stoutest teinite relic they show a radial divergence but on the surface of both pseudomorphs they tend to lie with their long axes [100] near parallel to the prism axis of the teinite." Bisbee is known for its copper oxide ores and it is uncertain where the tellurium, required to form teinite and graemite, is found. Rickardite, Cu_7Te_5 , could be the source as traces of it was detected in the ores.

A second locality for graemite was found at a small prospect in the Dome Rock Mountains, Yuma County, Arizona. Samples consist of massive chalcocite in a quartz-tourmaline gangue with small corroded blebs of bornite and traces of weissite embedded within the chalcocite. Brochantite and malachite film the fractures that are lined with crystalline goethite and gold. Small cavities housing goethite, gypsum, teinite, and graemite are found by breaking the chalcocite where it is fresh, not at the brochantite-filled fractures. At both the Bisbee and Yuma County localities, teinite is corroded and graemite appears to be replacing it,

probably through a partial dehydration of teinite. The species description by Williams (1975) was based on the Bisbee material only.

Chemically, Williams (1975) found graemite to be $\text{Cu}_{9.77}(\text{TeO}_3)_{9.62} \cdot 11.42\text{H}_2\text{O}$ or $\text{CuTeO}_3 \cdot \text{H}_2\text{O}$. Cu was analyzed by atomic absorption, Te colorimetrically, and water was determined by the Penfield method. The initial result of 9.5% H_2O was considered incorrectly high because a small particle was ejected from the tube during decrepitation. Emission spectrographic analysis showed a trace amount of silver. The test specific for tellurite was positive and the test for tellurate was negative. Tests for halogens and sulfate were also negative.

Williams (1975) describes the X-ray powder data of graemite as that of a typically layered mineral. Weissenberg level photographs taken with $\text{CuK}\alpha$ radiation showed strong sets of $0kl$ reflections and very weak $h0l$ reflections. *Pcmm*, the proposed space group, is far from being a certainty because of the problem of recording many $h0l$ reflections. A good cleavage was found on $\{010\}$ and a pronounced parting on $\{100\}$. There was no evidence either morphologically or optically that graemite is not orthorhombic *2mm*. Cell edges, refined from powder data, are $a = 6.805 \text{ \AA} \pm 0.006$, $b = 25.613 \pm 0.015$, $c = 5.780 \pm 0.006$. The calculated density is 4.24 g/cm^3 , measured specific gravity is 4.13, and $Z=10$.

6.2 Experimental

The crystal used in this study was provided by Andy Roberts, of the Geological Survey of Canada, who stated that this was the “best graemite crystal in the world”. The crystal was mounted on a Siemens *P3* automated four-circle diffractometer equipped with a molybdenum-target X-ray tube (operating at 55 kV, 35mA) and a precisely oriented graphite crystal

monochromator mounted with equatorial geometry. Two sets of data were collected but, due to power fluctuations, parts of both sets of data were lost. The second data set was interrupted six times and all confidence was lost that this was a consistent set of data. Problems with structure solution also lead to suspicions that the data sets were at fault. Initial precession photos showed that the crystal did not diffract well at all. A third data set was collected using synchrotron light in hopes that the poor diffracting qualities of the crystal could be overcome as well as achieving one consistent set of data.

In the first graemite data collection at UBC, fourteen reflections with 2θ 6.34 to 17.41° were centered using an automated search routine, and the correct unit cell was selected from an array of real space vectors corresponding to potential unit cell axes. One octant of reflections (1558 measurements, exclusive of standards) was collected from 3 to $60^\circ 2\theta$.

Details of the synchrotron collection are given in Chapter 2.

6.3 Structure Solution and Refinement

Initial attempts at solving the structure of graemite with the suggested space group *Pcmm* (William 1975) led to poor results and it was decided that precession work be carried out on the crystal to see which space groups are likely. These photographs also provided information on the crystallinity of the crystal, apparently there is some disorder present.

6.3.1 Determination of possible space groups

Precession photographs of *hk0*, *0kl*, *1kl*, and *hk1* were taken (Figures 6.1 to 6.4), however, the planned photographs of *h0l* and of the second levels could not be obtained because

the X-ray generator was destroyed by a power surge. This difficulty was somewhat overcome by using the program XPREP to look at the reflections in reciprocal space. It was determined from the three data sets that the reflection conditions for $h0l$ was $l = 2n$ and this would be the limiting factor in determining possible space groups for graemite. These space groups are: non-centrosymmetric $Pmc2_1$ (#26 in the International Tables of X-ray Crystallography), $P2cm$ (#28, $Pma2$ is the standard setting), and centrosymmetric $Pmcm$ (#51, $Pmma$ is the standard setting). Of course if the condition $h0l \ l = 2n$ is not real, then the space group choices would increase and involve the ones with less symmetry such as $P222$ (#16), $P222_1$ (#17), $P2_12_12$ (#18), $P2_12_12_1$ (#19), $Pmm2$ (#25), and $Pmmm$ (#47).

The $hk0$ precession photograph showed that the reflections of the odd h levels were smeared along k . This indicates a disordering of atoms (Joel Grice, personal communication 1997) along the b -axis. There was no smearing on the $0kl$ photograph but everything on the $1kl$ photograph was smeared along k . It should be pointed out that the smearing was only detected on film and that the XPREP program showed the smears in reciprocal space as spots. This was very misleading and kept in mind when XPREP was used as the sole method for looking at systematic absences. It was also noticed that the spots on the $hk0$ photograph were present when $h+k = 2n+1$. This is not a reflection condition useful for the determination of space groups; however, if the a -axis is reduced by half, this now becomes $h + k = 2n$ which is a valid reflection condition and leads to possible space groups for a reduced unit cell.

Attempts at solving the structure with the space group $Pcmm$ as suggested by Williams (1975) never gave satisfactory results. It should also be noted that no acceptable space groups could be determined on any of the data sets by the computer program using its default parameters; the intensity/sigma gap had to be reduced to <0.2 to generate possible space groups.

Several other space groups were tried without success and it was decided that the problem should be approached from a new direction.

The prominence of the reflection condition $h + k = 2n$ for $hk0$ when a is reduced by half gave some hope that this structure could be solved by using a space group for a smaller cell. It was also encouraging because a appears to be the axis that is most affected by the disorder and reducing its length could possibly make it easier to model a sub-structure which could then be extrapolated to the full structure in the proper unit cell. In reducing a by half, additional reflection conditions for the reduced cell were met with $h0l$ $l = 2n$, $h00$ $h = 2n$ (only 2 spots were found), $0k0$ $k = 2n$, and $00l$ $l = 2n$. These lead to possible space groups of non-centrosymmetric $P2_1cn$ (#33, $Pna2_1$ is the standard setting) and centrosymmetric $Pmcn$ (#62, $Pnma$ is the standard setting).

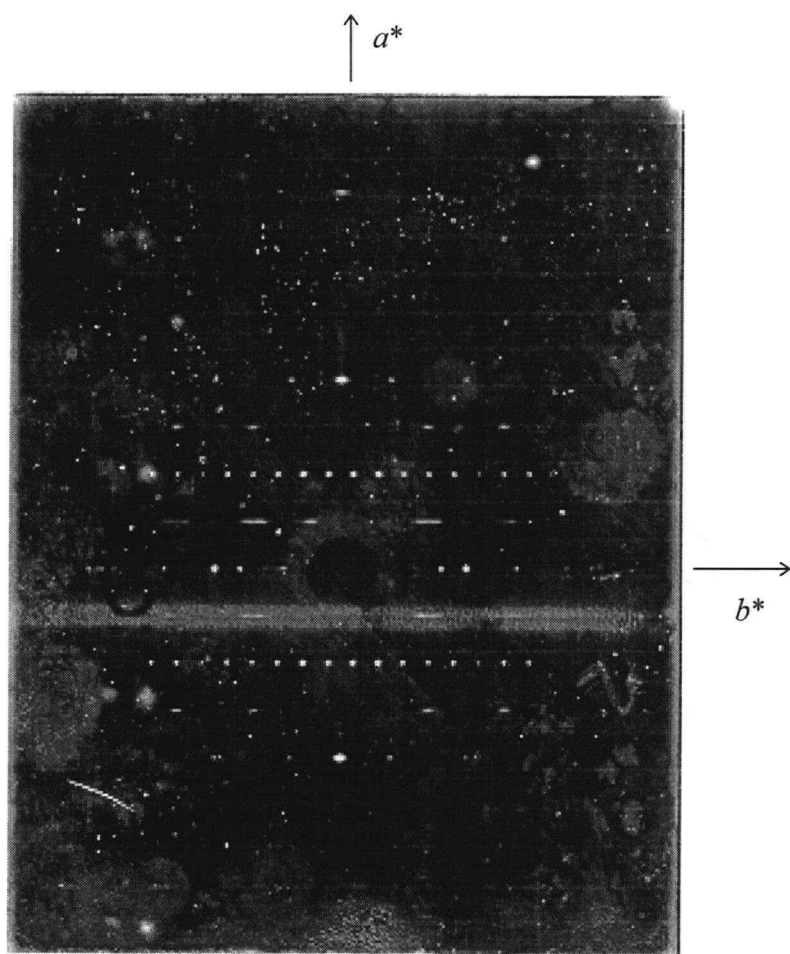


Figure 6.1. Precession photograph of graemite showing $hk0$. Notice the streaking of reflections, along the b -axis, on odd h -levels.

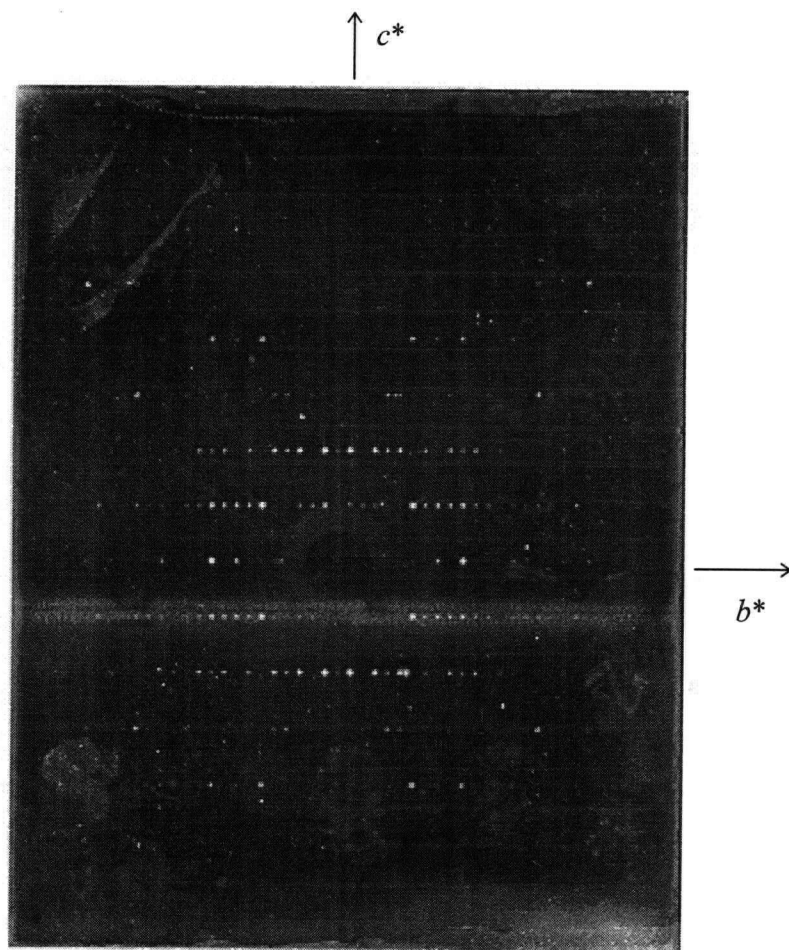


Figure 6.2. Precession photograph of graemite showing $0kl$. All reflections are sharp.

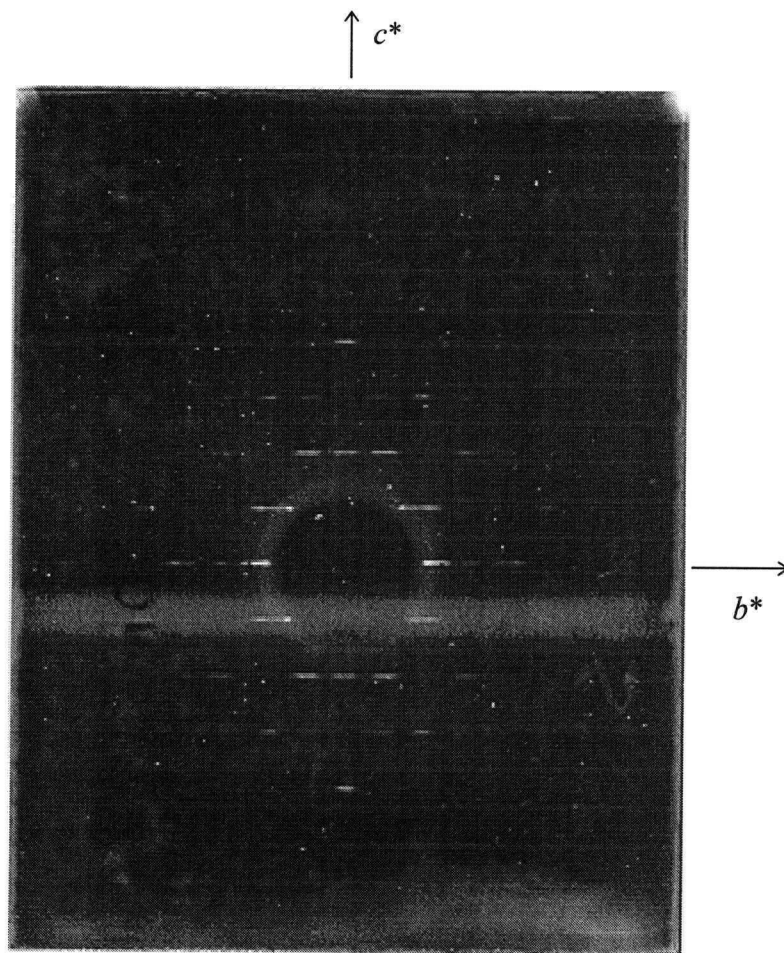


Figure 6.3. Precession photograph of graemite showing $1kl$. All reflections are smeared along the b -axis.

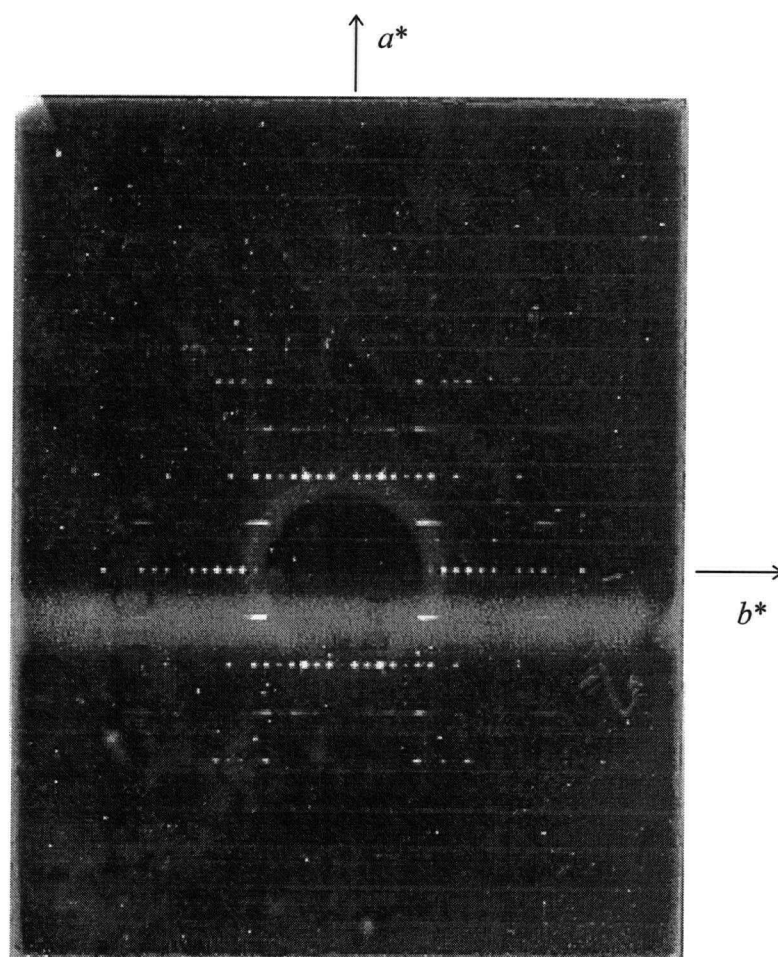


Figure 6.4. Precession photograph of graemite showing $hk1$. Reflections are smeared on odd h -levels along the b -axis.

6.3.2 Structure solution

Using the reduced cell, structure solution was attempted with both space groups and both gave similar results. To convert the synchrotron data to the standard space group settings, the orientation matrix (0 0 1, 0 -1 0, 0.5 0 0) was used for *Pna*2₁ and the orientation matrix (0 0 1, -0.5 0 0, 0 -1 0) was used for *Pnma*. A final *R* index of ~9.3 % was achieved with *Pnma* and 7.7 % for *Pna*2₁. Refinement of anisotropic temperature factors was attempted and actually reduced the *R* value for both space groups but many of the cations and oxygen atoms became “non-positive definite” indicating that the anisotropic temperature factors could not be satisfactorily refined. The two space group models both have a Te-Te distance of approximately 1 Å, which is probably where the disorder is located. The $|E^2-1|$ statistic of 0.812 shows that the structure is most likely non-centrosymmetric and upon closer scrutiny of the actual bond lengths, the non-centrosymmetric structure appears to be a better model. Other factors such as the better *R* value for *Pna*2₁ and the chemistry of the models also point to the structure as being non-centrosymmetric.

Using the proper unit cell, the structure of graemite was refined in non-centrosymmetric *Pmc*2₁ to an *R* value of 6.9 %. Refinement of anisotropic temperature factors lead to a lower *R* value but once again the atoms showed that this refinement could not be performed satisfactorily. Like the reduced cell models, there is a Te-Te distance of ~1 Å which is probably due to disorder. The results here are not final as some of the occupancies were allowed to refine freely, many of the temperature factors had to be fixed at reasonable values because they were unstable, and there are still questions regarding the chemistry of the crystal; it is however the best model to date using the full unit cell and it is expected that many questions will be answered with chemical analyses from the electron microprobe.

Knowing that the synchrotron data collection is probably the best data set that could be achieved with this crystal, the R_{int} is 2.7% which is very good, and the fact that precession photographs show smearing of spots on selected levels, it is likely that the atomic disorder is the reason the R values are so high. The model using the full unit cell still has many problems associated with it and at this time the sub-structure appears to be the most definitive model, albeit of only part of the structure, of graemite that is possible with this crystal.

Structure factors are listed in Appendix F.

6.4 Description of the Proposed Structure of Graemite

Two structural models are proposed, one in the reduced cell (a 5.78, b 25.63, c 3.41 Å, $\alpha = \beta = \gamma = 90^\circ$) with space group $Pna2_1$ and one with the proper unit cell (a 6.82, b 25.62, and c 5.78, $\alpha = \beta = \gamma = 90^\circ$) with the space group $Pmc2_1$. Until further work is completed with regards to upper level precession photographs and electron microprobe analysis, questions about the correct space group and chemistry of graemite still remain.

6.4.1 Description of the proposed substructure in $Pna2_1$

The atomic positions used to refine the space group $Pna2_1$ to an R value of 7.7% is listed in Table 6.1. Te(2) is about 1 Å away from Te(3) and O(7) is very close to O(1) at 1.4 Å and to O(3) at 1.9 Å away. The disorder appears to be related to these atoms. Figure 6.5 shows how these atoms may be presented as smeared reflections along the b -axis on the bc -plane (remembering that a 6.82 Å has been transformed so that it is c 3.41 Å). The clustering of these atoms is not as prominent in the ab -plane (Figure 6.6) which is consistent with the fact that no

reflections are smeared on the precession photograph of this plane. Figure 6.7 shows how Te(2) and Te(3) may be bonded to six common oxygen atoms and it can be imagined that only one of the sites may be occupied at any one time. No figure of the *ac*-plane is depicted but, because of the 25.63 Å long *b*-axis, one can see why Williams (1975) had trouble recording *h0l* reflections. Figures 6.8 and 6.9 show the connectivity of the proposed structure looking down the *c*- and *a*-axes respectively.

There are still many problems with the substructure even if the disorder of Te(2) and Te(3) as well as that of O(1), O(3), and O(7) is accepted. The Te(2) and Te(3) sites have been fixed at half occupancy but the Te(1) and Cu(2) sites also appear to be half-occupied. The O(1), O(3), and O(7) sites seem to be half-occupied, O(7) being present when O(1) is not, but it is unclear how O(3) is related although logically it should be present when O(7) is not. The O(5) site is partially occupied and it has been tentatively assigned as a hydroxyl group. The chemistry of this substructure does not match the accepted formula as no water molecule has been located and both copper and tellurium each sum up to six in the half unit cell when there should be only five of each. With all these problems, one can see that there is still more work to be done in determining the roles of all the atoms. It was hoped that solving the substructure would lead to the solution of the full structure but it was too difficult a task to project the full structure from the substructure.

6.4.2 *The proposed structure in Pmc2₁*

The atomic positions used to obtain an *R* value of 6.9% in *Pmc2₁* are listed in Table 6.2. There are many unanswered questions with regards to the chemistry and occupancy of sites. With the large *b*-axis dimension and *Z* = 10, there are many atomic positions to work out.

Without knowing if there are elements substituting for copper and/or tellurium and with the effect of disorder causing some sites to be partially occupied, no definite conclusion of the model can yet be made. No figures will be shown using the space group $Pmc2_1$ because, to this date, much of it is speculation based on chemical assumptions and experimentation with various elements in the cation sites.

Table 6.1. Atomic positions for the proposed graemite substructure solved in $Pna2_1$.

Atom	x	y	z	K	[†] U _{eq}
Cu(1)	0.1505(9)	0.6651(2)	0.02260*	1	87(15)
Cu(2)	0.522(2)	0.2562(4)	-0.028(7)	*0.5	31(27)
Te(1)	0.888(1)	0.4489(2)	-0.025(6)	*0.5	154(17)
Te(2)	0.377(1)	0.3617(2)	-0.027(5)	*0.5	72(15)
Te(3)	1.253(1)	0.3904(2)	0.026(5)	*0.5	89(14)
O(1)	0.200(8)	0.301(2)	0.03(3)	*0.5	39(103)
O(2)	0.782(6)	0.261(1)	0.399(8)	1	88(96)
O(3)	0.686(8)	0.334(2)	0.05(2)	0.59(6)	*100
O(4)	0.985(6)	0.404(1)	-0.41(1)	1	148(101)
O(5)	-0.16(1)	0.511(2)	-0.45(3)	0.50(7)	*100
O(6)	0.436(6)	0.356(1)	0.62(1)	1	185(101)
O(7)	0.500(9)	0.169(2)	-0.04(3)	*0.5	39(103)

[†]U_{eq} are listed $\times 10^4$. *Fixed value.

Table 6.2. Atomic positions for the proposed graemite structure solved in $Pmc2_1$.

Atom	x	y	z	K	$^{\dagger}U_{eq}$
Te(1)	0	0.1989(4)	0	0.5	62(19)
Te(2)	0	0.1130(4)	-0.479(3)	0.5	78(24)
Te(3)	0.25000	0.0836(8)	0.041(4)	*0.5	132(44)
Te(4)	0.227(2)	0.3898(6)	0.277(3)	*0.5	82(35)
Te(5)	0.275(1)	0.3598(6)	0.143(3)	*0.5	*400
‡ Ru	$\frac{1}{2}$	0.8594(6)	0.139(3)	0.5	*400
Cu(2)	0	0.5856(7)	0.237(4)	0.5	15(42)
Cu(3)	$\frac{1}{2}$	0.587(1)	0.241(5)	0.5	228(60)
‡ Rb	$\frac{1}{2}$	-0.0073(4)	0.870(3)	0.5	*400
Cu(5)	0.218(2)	0.301(1)	-0.231(4)	0.52(2)	*400
O(1)	0.22(1)	0.419(4)	0.60(1)	0.66(3)	*800
O(2)	0.17328	0.152(2)	0.90(1)	1	*800
O(3)	0.326(8)	0.107(2)	0.458(9)	1	*800
O(4)	$\frac{1}{2}$	0.086(3)	-0.11(1)	0.5	*1000
O(5)	$\frac{1}{2}$	0.492(3)	-0.34(1)	0.5	*1000
O(6)	0.232(7)	0.445(2)	0.087(8)	1	*800
O(7)	0	0.239(3)	-0.27(1)	0.5	*1000
O(8)	0.331(7)	0.012(2)	0.11(1)	1	*800
O(9)	0	0.351(3)	-0.13(2)	0.5	*800
O(10)	0	0.082(4)	0.24(1)	0.5	*800
O(11)	$\frac{1}{2}$	0.396(4)	0.32(1)	0.5	*800
O(12)	$\frac{1}{2}$	0.347(3)	-0.09(1)	0.5	*1000
O(13)	0	0.479(3)	-0.34(1)	0.45(3)	*800
H ₂ O	0.288(5)	0.499(2)	0.423(7)	1	*800
H ₂ Oa	0	0.015(2)	0.37(1)	0.5	*800
H ₂ Ob	$\frac{1}{2}$	0.199(2)	1.01(1)	0.5	*1000

$^{\dagger}U_{eq}$ are listed $\times 10^4$. *Fixed value. ‡ Ru and Rb were used to emulate scattering powers between that of copper and tellurium in an attempt to see if silver, tellurium, or other elements were substituting in this site.

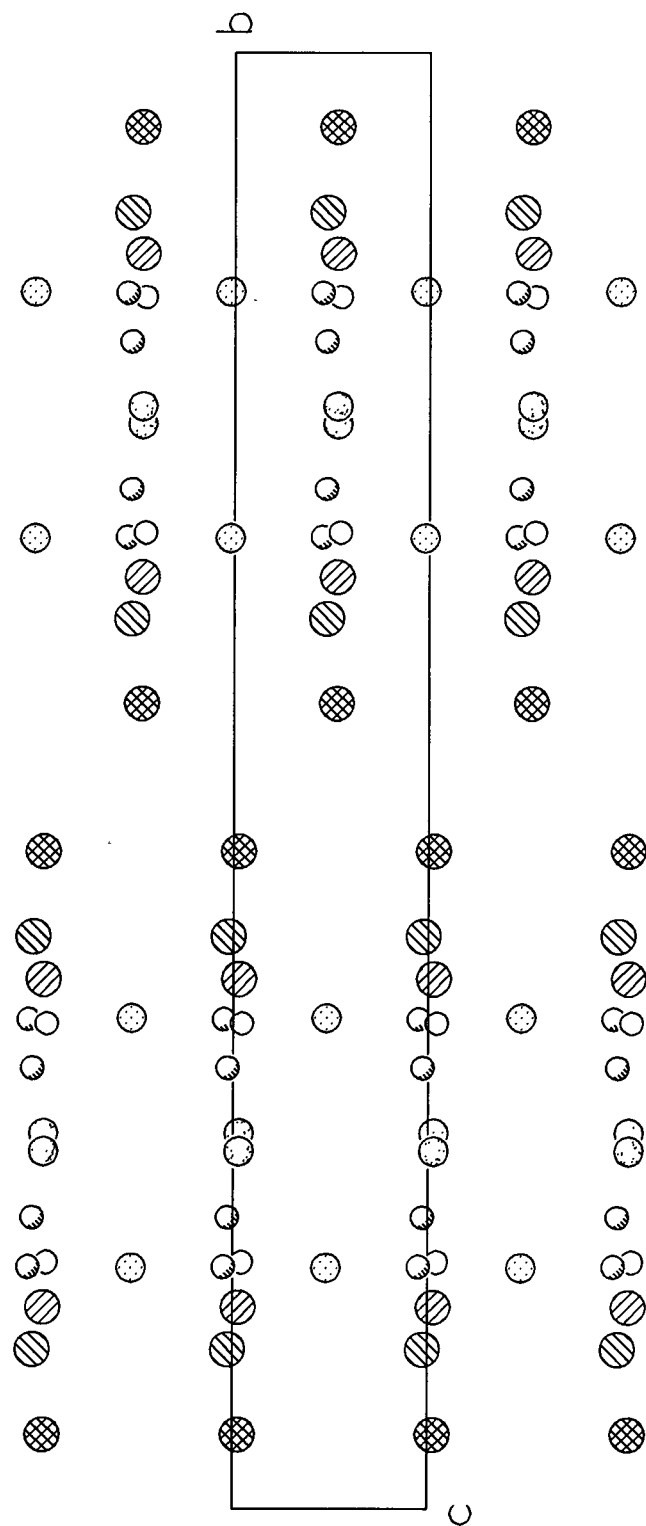


Figure 6.5. The bc-plane showing disorder in the proposed substructure of graemite in $Pna2_1$. Cu(1) atoms are shown as spheres with a regular pattern of dots, Cu(2) atoms as spheres with a random array of dots, Te(1) atoms as cross-hatched spheres, Te(2) atoms as spheres with NW to SE ruling, and Te(3) atoms with NE to SW ruling. Selected oxygen atoms are shown. O(1) and O(3) atoms are shown as shaded spheres and O(7) atoms are shown as open spheres. The proposed disorder is between the Te(2) and Te(3) atoms and between the O(1), O(3), and O(7) atoms.

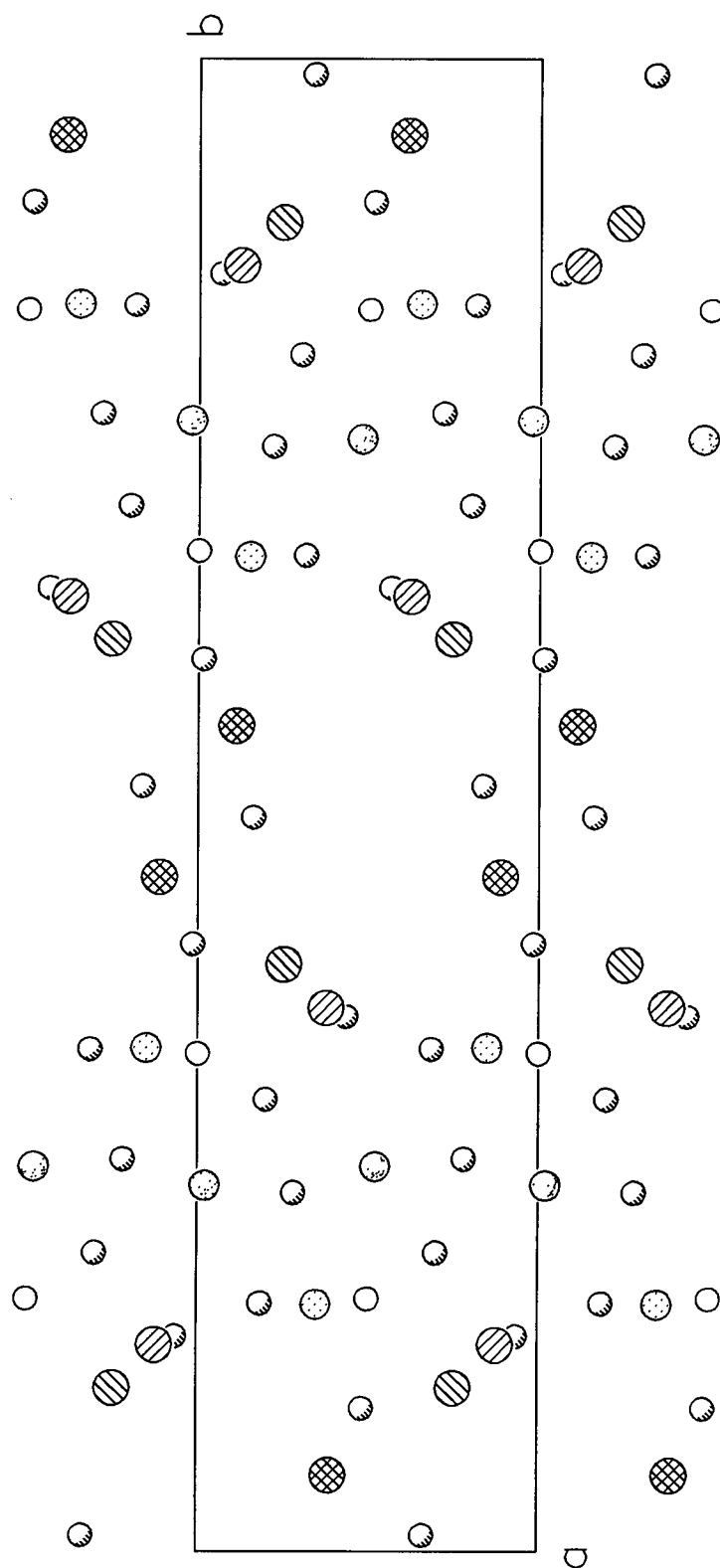


Figure 6.6. The ab -plane of the proposed substructure of graemite in $Pna2_1$. Disorder is not apparent in this orientation. The shading of cations is the same as that in figure 6.5. All oxygen atoms are shown. O(7) atoms are shown as open spheres while the rest of the oxygen atoms are shown as shaded spheres.

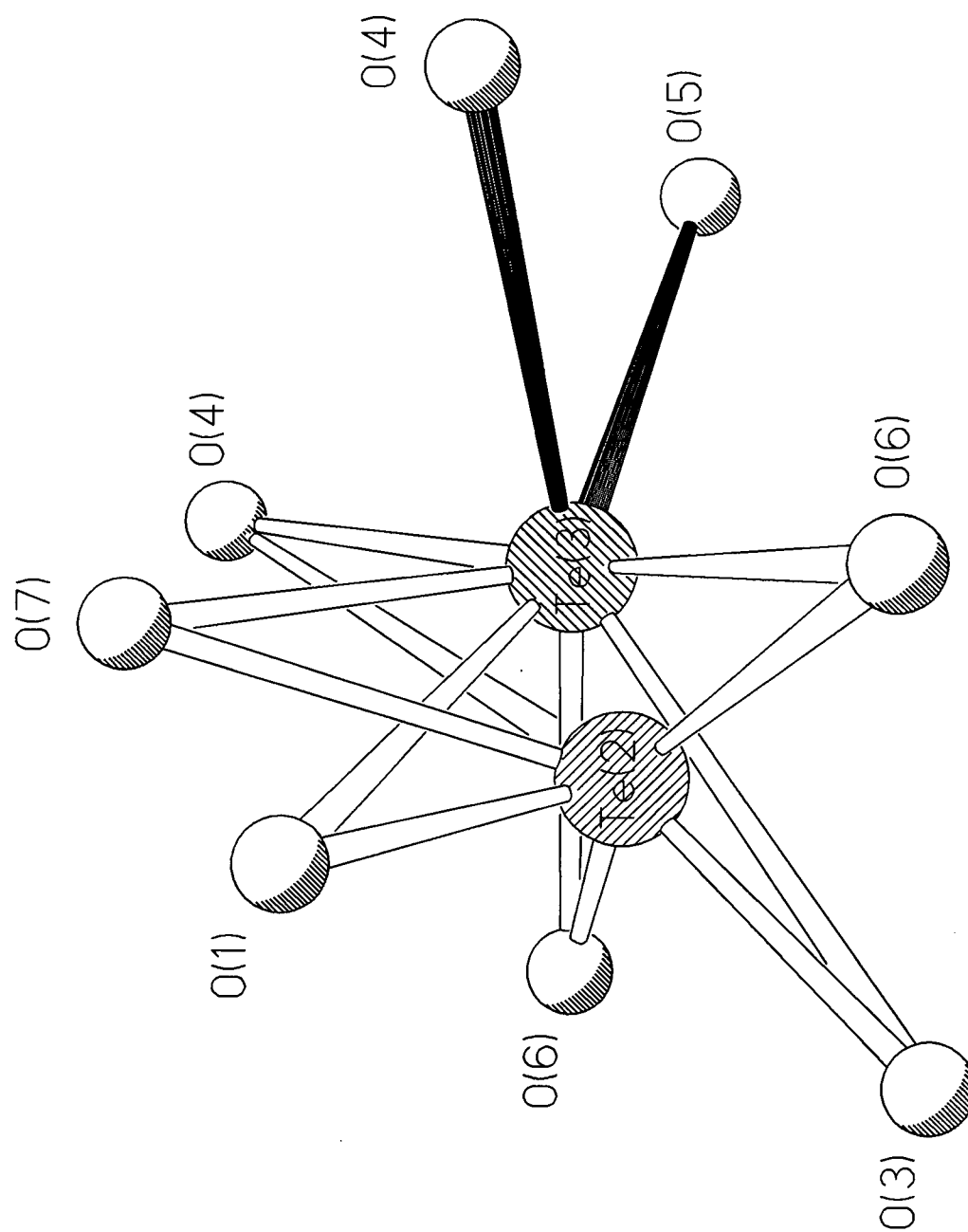


Figure 6.7. Disorder of Te(2) and Te(3) in the proposed graemite substructure in Pna2₁. Oxygen atoms bonded to either Te(2) or Te(3) are shown with hollow bonds.

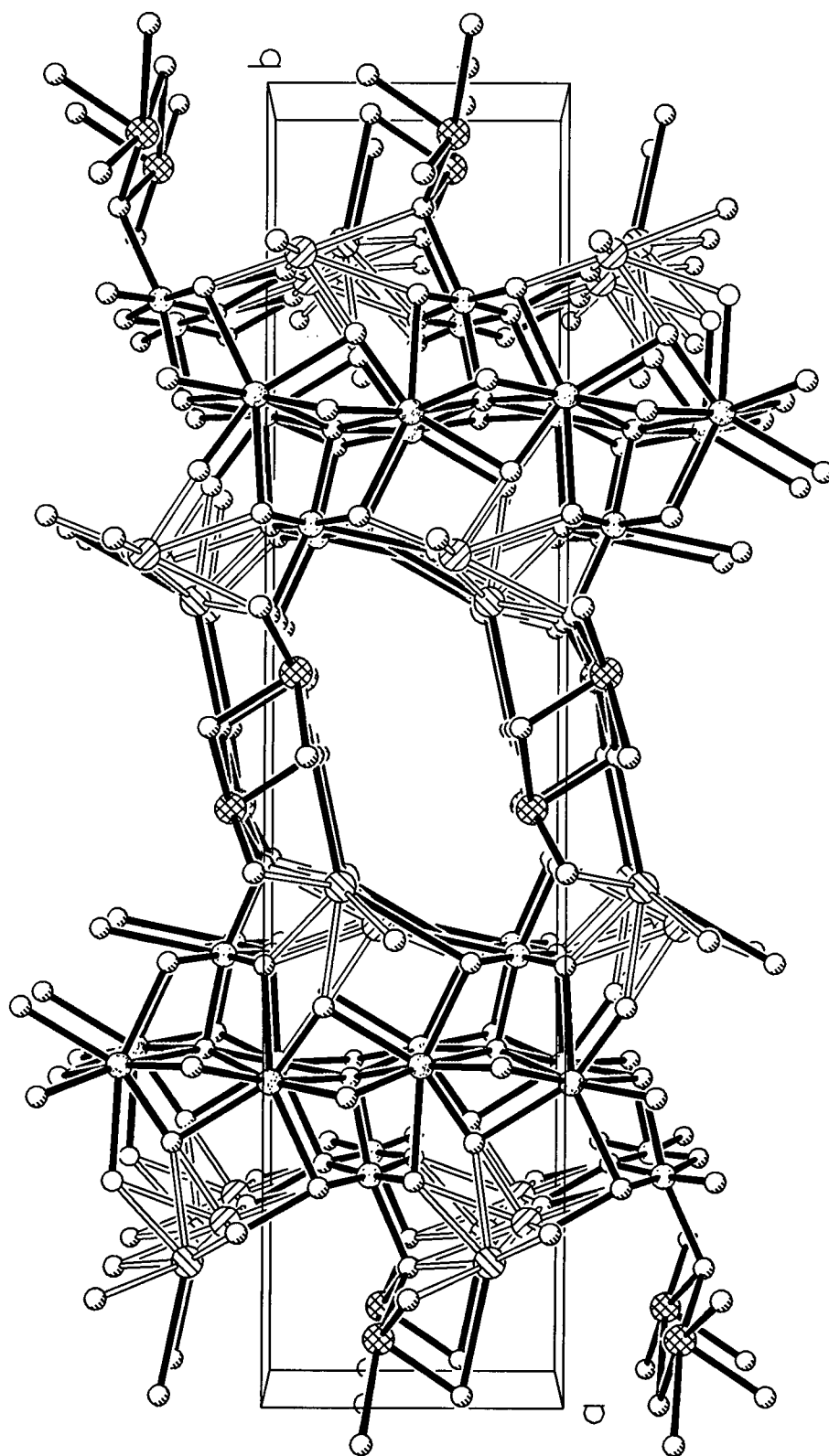


Figure 6.8. Connectivity of the proposed graemite substructure in $Pna2_1$ as viewed down the c -axis. Hollow bonds show disorder between $Te(2)$ and $Te(3)$. The shading of the atoms is consistent with figure 6.5.

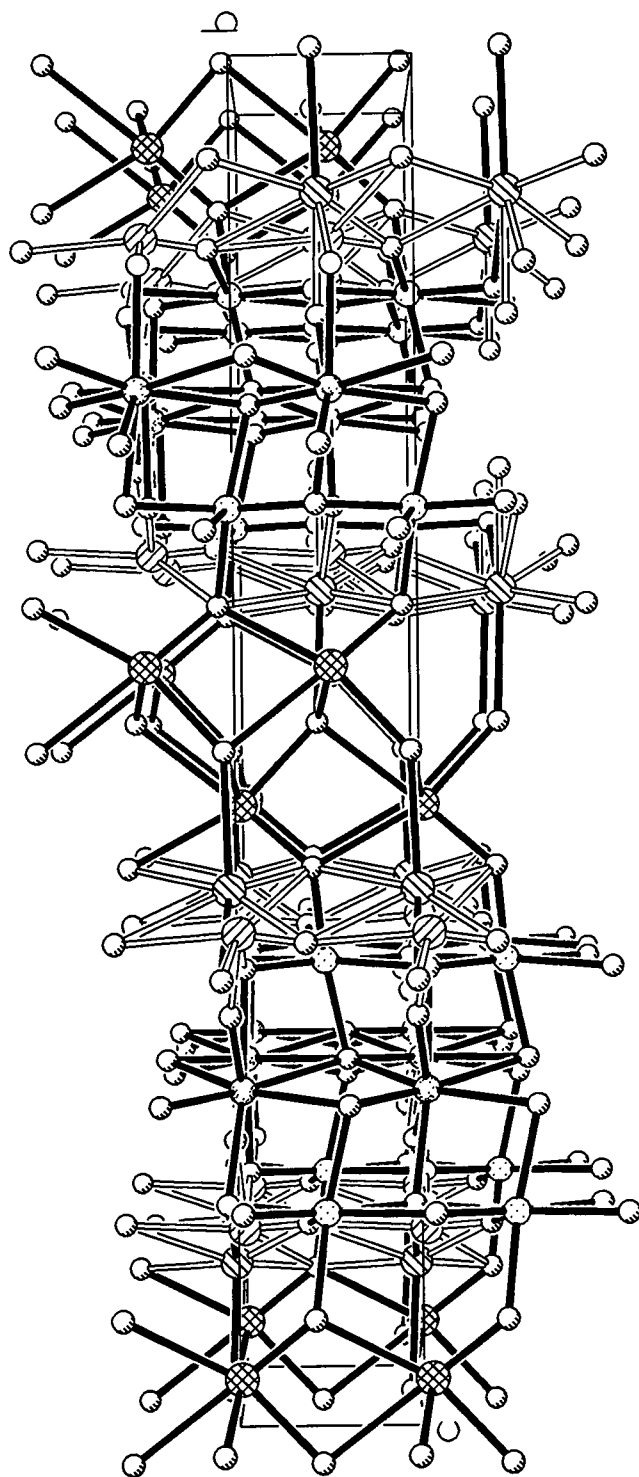


Figure 6.9. Connectivity of the proposed graemite substructure in $Pna2_1$ as viewed down the a -axis. The shading of bonds and atoms is the same as in figure 6.8.

6.5 Discussion

The magnitude of the task of solving the graemite structure becomes clear when one thinks of it as attempting to model disorder; add to that a relatively large unit cell, not knowing the correct space group, and unconfirmed chemistry of the crystal, and the problem can be seen to be immensely difficult. It is already incredible that the disorder can be modeled to the point that it is logical and consistent with the precession photographs. As stated earlier, every space group that gave a somewhat acceptable model had two cations (usually Te-Te) 1 Å apart.

It is hoped that with future work in obtaining upper level precession photographs and chemical analysis with the electron microprobe, some of the questions will be cleared up enabling some conclusions to be drawn about the structure. As this is the "best graemite crystal in the world" there is a reluctance to possibly ruin it in the procedure of electron microprobe analysis. It would certainly be unwise to do so before all precession photographs are satisfactorily obtained and that cannot be done until the new X-ray generator arrives and is up and running (September 1998). Thus the crystal structure of graemite remains unsolved although inroads have been made in solving this mystery.

6.6 Conclusions

The crystal structure of graemite remains unsolved although a substructure using a 5.78, b 25.63, c 3.41 Å, $\alpha = \beta = \gamma = 90^\circ$, and the space group $Pna2_1$ has been proposed. The full structure is probably non-centrosymmetric and probably crystallizes in the orthorhombic space group $Pmc2_1$ with a 6.82, b 25.62, c 5.78, $\alpha = \beta = \gamma = 90^\circ$. This is different from the originally proposed centrosymmetric space group of $Pmma$. There is disorder in the mineral that shows up

in precession photographs of the $hk0$, $1kl$, and hkl planes but not in the $0kl$ plane. The smearing of reflections is always along the b -axis. This disorder appears to be caused by two cations approximately 1 Å apart from one another and possibly by some disordered oxygen as well. Upper level precession work and a complete chemical analysis by the electron microprobe remain to be completed.

7.0 CONCLUSIONS

The intent of this thesis was to study, by single crystal X-ray crystallography, the structures of a number of tellurium oxysalt minerals. It was fortunate that there was an opportunity to work intimately with both tellurate and tellurite minerals because it afforded the chance to learn about the coordination of both Te^{6+} and Te^{4+} by way of contrast and comparison.

The main reason behind the structural difference between these two valence states is the presence of a lone electron pair that distorts the coordination polyhedra of Te^{4+} and the absence of it in Te^{6+} . The coordination of Te^{6+} is straightforward as it is six-coordinated to form a regular octahedron. As discussed in the introduction, the interpretation of the coordination around Te^{4+} has progressed from what was originally thought to be three- or four-coordination to recent descriptions of eight-coordinated Te^{4+} . The earlier descriptions, using the three and four closest coordinations, are still valid but the added coordination brings a better understanding of how the structures are connected by the addition of weaker bonds that previously have been neglected.

7.1 Dugganite, Choloalite, Rodalquilarite, and Graemite

The formula of dugganite is revised to $\text{Pb}_3\text{Zn}_3\text{TeAs}_2\text{O}_{14}$ from $\text{Pb}_3(\text{Zn,Cu}^{2+})_3(\text{Te}^{6+}\text{O}_6)(\text{AsO}_4)(\text{OH})_3$. Dugganite was solved to an R value of 2.7% in the hexagonal (trigonal) space group $P321$ which differs from the space group suggested by Williams (1978) of $P6/mmm$. The parameters are a 8.460(2), c 5.206(2) Å, V 322.6(2) Å³, Z 1. The structure of dugganite consists of heteropolyhedral sheets of lead and tellurium polyhedra parallel to (001) joined together in the c -direction by AsO_4 and ZnO_4 tetrahedra. The revised

formula of dugganite is similar to that of cheremnykhite, $\text{Pb}_3\text{Zn}_3\text{TeV}_2\text{O}_{14}$, and kuksite, $\text{Pb}_3\text{Zn}_3\text{TeP}_2\text{O}_{14}$, and it is proposed that these minerals are isostructural.

The formula of choloalite has been revised as well to $\text{Cu}_3\text{Pb}_3\text{Te}_6^{4+}\text{O}_{18}(\text{Cl},\text{H}_2\text{O})$ from the original formula of $\text{CuPb}(\text{Te}^{4+}\text{O}_3)_2\cdot\text{H}_2\text{O}$ (Williams, 1981) and the recently revised formula of $\text{CuPb}(\text{TeO}_3)_2$ (Powell *et al.* 1994). Electron microprobe and infrared analyses and structure refinement show that choloalite contains water. Choloalite crystallizes in the cubic space group $P4_132$ with a 12.520(4) Å, V 1963(2) Å³ and Z 4. The structure consists of two three-dimensional nets, one net contains only Pb(1) polyhedra and the other consists of Pb(2) and Cu polyhedra; these nets are joined together by distorted TeO_6 octahedra. Choloalite was solved to a final R value of 5.2%.

The original structure description of rodalquilarite by Dusauso and Protas (1969) still basically holds true. It consists of planes of iron and tellurium octahedra parallel to bc held together by weak $\text{Te}-\text{Cl}$ and $\text{H}-\text{O}(1)$ bonds. The refinement served to locate more weak $\text{Te}-\text{O}$ bonds that help to hold these planes together in the a -direction. Rodalquilarite crystallizes in the triclinic space group $P\bar{1}$, a 9.021(1) Å, b 5.1170(7), c 6.6539(8) Å, α 103.23(1)°, β 106.66(1)°, γ 78.07(1)°, V 283.15(6) Å³, Z 1. Eight-coordinated Te(1) and seven-coordinated Te(2) both have three short $\text{Te}-\text{O}$ bonds on one side of the coordination polyhedra. Chlorine is bonded to six tellurium atoms and help to bond the Fe/Te polyhedral planes together in the a -direction. Finally, a hydrogen-bonding scheme has been proposed. The redetermination of rodalquilarite gave a final R index of 4.1% which is improved from the original value of R 9.2% obtained by Protas and Dusauso (1969).

Although excellent data was collected using synchrotron light, graemite has not been structurally refined to satisfaction. The problem appears to be disordering along the b -axis which shows up in the $hk0$, $1kl$, and $hk1$ precession photographs. In all attempts at structure

solution, two atoms (usually tellurium) were found approximately one angstrom away from each other. The cell obtained from the synchrotron data is a 6.816, b 25.627, c 5.784, and with all angles 90° . The structure has been refined in $Pna2_1$ using a reduced cell ($\frac{1}{2} a$) to an R index of 7.7%. This is probably a substructure of the full structure. Using the full cell, the structure has been refined in $Pmc2_1$ to an R value of 6.9% but the atoms are not as "well-behaved" as that for the substructure. Further study of graemite is required to rationalize the problem with disorder before any final structure model can be accepted.

7.2 A Comment on Experimental Procedures

As mentioned in Chapter one, crystals of tellurium oxysalt minerals suitable for single crystal X-ray diffractometry are difficult to obtain. This fact along with original descriptions that are often incorrect means that future structure solution and refinement of these minerals will probably continue to be quite difficult. Simply put, the easy crystals have been solved and the ones that remain unsolved are usually associated with some sort of difficulty such as: poor crystal quality, misleading original description of the chemistry and/or space group, and other unforeseen problems. Structure solution and refinement becomes even more difficult when these problems are compounded.

In this thesis, crystal quality was a problem for dugganite and graemite, the published chemistry was wrong for dugganite and choloalite, and published space groups that were incorrect were misleading for dugganite, choloalite, and graemite. Unforeseen problems were also encountered with graemite.

As discussed earlier, these tellurium-bearing minerals absorb more X-rays than light element-bearing crystals and thus lead to long data collection times. The crystals could not be

shaped into spheres because of their brittleness so, to combat absorption problems, more data was collected than needed. The absorption scan became very important with regards to the success of the final refinement and so extra reflections were collected for the ψ -scan which added to the total collection time. Also, because the crystals usually diffracted poorly, longer than normal peak scan times were used. These factors combined to result in data collection times (including the absorption collection) of six to eight weeks.

In the case of graemite, these long collection times were detrimental to the success of the final result because power fluctuations over the six week period lead to a loss of a significant amount of data in the first collection. In the second collection, six power interruptions lead to loss of data and cohesion as six individual parts of the collection had to be combined together to form a complete data set. With these power fluctuations, the confidence in the data set was undermined. With the inability to solve the structure of graemite using these two data sets, it was not known whether the problem lay with the crystal or with the data itself, although it was suspected that the data was at fault. After data collection with synchrotron light, it was determined that the crystal was probably at fault.

Precession work was initially attempted with the graemite crystal but it diffracted very poorly and no helpful information was gleaned from the work. Finally, after the synchrotron collection, (with much appreciated help from Joel Grice) useful precession photos were taken (24 to 36 hour exposure times) which showed disorder in the crystal; this disorder is probably the cause of the problems with structure solution.

From the experience of these difficulties, it is recommended that precession work be one of the first procedures carried out in crystal structure analysis. It will provide information on the quality of the crystal, its cell dimensions, and help to confirm or disprove possible space groups. It will also determine if the crystal is twinned and whether or not disorder is present. This is

definitely a more scientific route than that of trial and error with suggested space groups from a computer program based on reflections that may be in error.

This recommendation is certainly not a new one and has been personally communicated by Joel Grice and Scott Ercit of the Canadian Museum of Nature and by Mark Cooper, a crystallographer at the University of Manitoba. The importance of this kind of work has also been emphasized by Stout and Jensen (1989) who, in comparing photographic film methods to automated diffractometers, say:

“nothing can supplant photographic methods for the purpose of obtaining a general view of the geometry and symmetry of the reciprocal lattice. A disturbing number of errors have arisen recently in space group and lattice assignments. Many of these could have been avoided if photographs of the crystal lattice had been taken rather than depending solely on individual reflections found by an automated diffractometer.”

An increasing number of incidents of erroneous space groups and lattice assignment, probably resulting from the blind confidence in the automated diffractometer, have been documented (Marsh and Herbstein, 1983; Baur and Tillmans, 1986) which subsequently prompted Yvon Le Page to develop the program *MISSYM* in an attempt to counteract this problem.

It is also recommended that additional chemical analysis be performed to confirm the chemistry of the crystal in question. Methods include the use of the electron microprobe for exact microchemical analysis, infrared analysis (commonly used to detect water and hydroxyl groups), and the scanning electron microscope for a quick scan of the elements that may be present in the crystal.

7.3 Crystal Structure Analysis as a Means For Chemical Analysis of Crystals

In the course of this work, it has come to attention and confirmed by Joel Grice (personal communication 1997) that crystal structure analysis can be a powerful tool with regards to determining the chemistry of minerals. Crystal structure analysis as a chemical analytical method has been documented for light elements by Hawthorne and Grice (1990).

In the case of dugganite, structure refinement revealed that arsenic occupied a special position that would give two times the amount of arsenic that should be present. The problem became more perplexing when bond-valence analysis of arsenic at this site yielded extremely poor sums. By reviewing the literature, it was determined that there could be significant substitution at this site. Upon further bond-valence analysis and structure refinement, it was predicted that the site (and therefore the extra cation) was real and fully occupied and that the site had approximately fifty percent substitution by phosphorus. Chemical analysis by the electron microprobe confirmed the prediction almost exactly.

With choloalite, the site that is occupied by water and chlorine was either supposed to contain nothing (using the formula of Powell, 1994) or only water (using the formula of Williams, 1981). Structure refinement showed that the site definitely had something scattering X-rays but that it was heavier than water. The site refinement indicated that chlorine was probably present however, if it were so, then the crystal would not be charge-balanced. The original description suggested that antimony may be present which would require an anion, like chlorine, to balance its charge. Another prediction of the chemistry was made based on structure refinement with antimony refining versus copper in the copper site and chlorine versus water in the water site. Once again the chemical analysis obtained from the electron microprobe was very close to that predicted by structure analysis.

With regards to rodalquilarite, Dusauroy and Protas (1969) used crystal structure analysis to redefine the chemistry of the mineral as being anhydrous. The work in this thesis found no reason to disagree with their conclusions. Earlier work by Sierra Lopez *et al.* (1968) had shown rodalquilarite to be hydrous.

It is therefore a conclusion that a good structure refinement of a crystal can be chemically definitive. One problem is that only two elements can be refined versus one another and if a site contains more than two elements, these elements cannot be refined for. However, when crystal structure analysis is used in cooperation with other chemical analysis techniques that scan and analyze for the whole range of elements, many difficulties with the chemistry of minerals can be alleviated.

8.0 CONSIDERATIONS FOR FUTURE RESEARCH

In the process of completing this thesis, future research in this and related topics were considered and are now proposed.

1. Solve the structure of graemite. A complete chemical analysis and a full set of precession photographs should be obtained.
2. Determine the crystal structures of cheremnykhite and kuksite to learn if they truly are isostructural with dugganite. Compare the three structures and note the different effects, if any, that arsenic, vanadium, phosphorus, and silicon have on the structures. Research the genesis of these three minerals to gather information on the similarities of the geochemical environment.
3. Solve the structures of the rest of the Te-oxysalt minerals. This is a logical continuation of this thesis which will help determine the behaviour of tellurium in minerals.
4. A complete study of tellurium structurally with oxidation states from -2 to +6. This could lead to a structural classification scheme for tellurium-bearing minerals.
5. The formal coordination of Te^{4+} should be standardized with the known tellurite structures redrawn with these coordinations for comparison purposes. Back (1990) surveyed the then known structures of the tellurite minerals with substantial work done on calculating bond valences and determining coordinations around Te^{4+} . However, the work was never published outside of his thesis and tellurites continue to be described with various coordinations because there are no set rules.
6. The lone electron pair of Te^{4+} in tellurite minerals needs to be studied in detail. Back (1990) stated that all the tellurites in his study involved stereochemically active lone

electron pairs and he attempted to define the locations of the electron lone pairs based on differences in Te–O bond lengths and O–Te–O bond angles. Work by Wang and Liebau (1996) may help in decisively locating these electron lone pairs.

7. A study of the geochemical conditions for formation of Te-oxysalts. To learn which conditions lead to the formation of tellurites, tellurates, and mixed valence Te-oxysalt minerals.
8. The determinations of the crystal structures of selenates and selenites. This would be a logical progression in future studies as selenium is similar to tellurium in its electronic configuration and in its place on the periodic table. It would be of great interest to compare the structures of selenium-bearing and tellurium-bearing minerals to see if there are any isostructural minerals and to determine whether the elements have similar roles in the crystal structures. As discussed in the introduction, there are some differences in the primary occurrences of selenium and tellurium-bearing minerals; the difference in the atomic radii allows selenium to substitute isotypically with sulfur whereas tellurium forms its own discrete minerals. A look at the electronic lone pairs and ligand coordinations around Se and comparing it to Te would provide more information on these complex subjects.
9. In a larger scheme of research, it would be of interest to compare the structures of Group VIB oxysalt minerals to see what conclusions can be drawn with regards to the location of the elements in the family.
10. A standardization of previous minerals with the program *STRUCTURE TIDY* for comparison purposes.

11. The use of crystal structure analysis as a chemical analytical method should be further investigated. The work should complement that done by Hawthorne and Grice (1990).

As one can see, there is much more work to be done on tellurium oxysalt minerals and related topics. As this author has discovered, research into a specific topic leads to questions in a myriad of other subjects and quite often there are unanswered questions in these other topics. Research itself seems to be a self-propagating venture.

9.0 REFERENCES

- BACK, M.E. (1990): A Study of Tellurite Minerals: Their Physical and Chemical Data Compatibility, and Structural Crystallography. Master's thesis. University of Toronto, Canada.
- BAUR, W.H., and TILLMANN, E. (1986): How to avoid unnecessarily low symmetry in crystal structure determinations. *Acta Cryst.* **B42**, 95-111.
- BEYER, H. (1967): Verfeinerung der kristallstruktur von tellurit, dem rhombischen TeO_2 . *Zeitschrift für Kristallographie* **124**, 228-237.
- BRANDSTÄTTER, F. (1981): Non-stoichiometric, hydrothermally synthesized cliffordite. *Tschermaks Min. Petr. Mitt.* **29**, 1-8.
- BRESE, N.E. and O'KEEFE, M. (1991): Bond-valence parameters for solids. *Acta Cryst.* **B47**, 192-197.
- BROWN, I.D. (1974): Bond valence as an aid to understanding the stereochemistry of O and F complexes of Sn(II), Sb(III), Te(IV), I(V) and Xe(VI). *Journal of Solid State Chemistry* **11**, 214-233.
- BROWN, I.D. (1981): The bond-valence method: An empirical approach to chemical structure and bonding. In *Structure and Bonding in Crystals II* (M. O'Keeffe and A. Navrotsky, eds.). Academic Press, New York (1-30).
- BROWN, I.D. and ALTERMATT, D. (1985): Bond-valence parameters obtained from a systematic analysis of the inorganic crystal structure database. *Acta Cryst.* **B41**, 244-247.
- BURNS, P.C., COOPER, M.A., and HAWTHORNE, F.C. (1995): Parakhinite, $\text{Cu}^{2+}_3\text{PbTe}^{6+}\text{O}_6(\text{OH})_2$: crystal structure and revision of chemical formula. *Canadian Mineralogist* **33**, 33-40.
- COOPER, M.A. and HAWTHORNE, F.C. (1996): The crystal structure of spiroffite. *Canadian Mineralogist* **34**, 821-826.
- COOPER, W.C. editor (1971): Tellurium. Van Nostrand Reinhold Company, Toronto.
- CROMER, D.T. and MANN, J.B. (1968): X-ray scattering factors computed from numerical Hartree-Fock wave functions. *Acta Cryst.* **A24**, 321-324.
- CROMER, D.T. and LIBERMANN, D. (1970): Relativistic calculation of anomalous scattering factors for X-rays. *J. Chem. Phys.* **53**, 1891-1898.

- DONNAY, G., STEWART, J.M., and PRESTON, H. (1970): The crystal structure of sonoraite, $\text{Fe}^{3+}\text{Te}^{4+}\text{O}_3(\text{OH})\cdot\text{H}_2\text{O}$. *Tschermaks Min. Petr. Mitt.* **14**, 27-44.
- DUSAUSOY, P.Y. and PROTAS, J. (1969): Determination et Etude de la structure cristalline de la rodalquilarite, chlorotellurite acide de fer. *Acta Cryst.* **B25**, 1551-1558.
- EBY, R.K. and HAWTHORNE, F.C. (1993): Structural relations in copper oxysalt minerals. I. Structural hierarchy. *Acta Cryst.* **B49**, 28-56.
- EFFENBERGER, H. (1977): Verfeinerung der kristallstruktur von synthetischem teineit, $\text{CuTeO}_3\cdot 2\text{H}_2\text{O}$. *Tschermaks Min. Petr. Mitt.* **24**, 287-298.
- EFFENBERGER, H., ZEMANN, J., and MAYER, H. (1978): Carlfriesite: crystal structure, revision of chemical formula, and synthesis. *American Mineralogist* **63**, 847-852.
- FISCHER, R., PERTLIK, F., and ZEMANN, J. (1975): The crystal structure of mroseite, $\text{CaTeO}_2(\text{CO}_3)$. *Canadian Mineralogist* **13**, 383-387.
- GALY, J., MEUNIER, G., ANDERSSON, S., and ÅSTRÖM, A. (1975): Stéréochimie des Eléments Comportant des Paires Non Liées: Ge (II), As (III), Se (IV), Br (V), Sn (II), Sb (III), Te (IV), I (V), Xe (VI), Tl (I), Pb (II), et Bi (III) (Oxydes, Fluorures et Oxyfluorures). *Journal of Solid State Chemistry* **13**, 142-159.
- GELATO, L.M., and PARTHÉ, E. (1987): STRUCTURE TIDY - a computer program to standardize crystal structure data. *J. Appl. Cryst.* **20**, 139-143.
- GILLESPIE, R.J. (1972): Molecular Geometry. Van Nostrand Reinhold Company, Toronto.
- GIUSEPPE, G. and TADINI, C. (1980): The crystal structure of osarizawaite. *N. Jahrbuch f. Mineralogie, Monatshefte* **9**, 401-407.
- GREENWOOD, N.N. and EARNSHAW, A. (1984): Chemistry of the Elements. Pergamon Press, Toronto.
- GREY, I.E. and LLOYD, D.J. (1976): The crystal structure of senaite. *Acta Cryst.* **B32**, 1509-1513.
- GRICE, J. (1989): The crystal structure of magnolite, $\text{Hg}_2^{1+}\text{Te}^{4+}\text{O}_3$. *Canadian Mineralogist* **27**, 133-136.
- GRICE, J., and ROBERTS, A.C. (1995): Frankhawthorneite, a unique HCP framework structure of a cupric tellurate. *Canadian Mineralogist*. **33**, 649-653.
- GRICE, J.D., GROAT, L.A., and ROBERTS, A.C., (1996): Jensenite, a cupric tellurate framework structure with two coordinations of copper. *Canadian Mineralogist* **34**, 55-59.

- HAHN, T. editor (1996): International Tables For Crystallography. Volume A Space-Group Symmetry. Fourth edition. Kluwer Academic Publishers, Boston.
- HANKE, K., KUPCIK, V., and LINDQVIST, O. (1973): The crystal structure of CuTe_2O_5 . *Acta Cryst.* **B29**, 963-970.
- HAWTHORNE, F.C. and GRICE, J. (1990): Crystal-structure analysis as a chemical analytical method: application to light elements. *Canadian Mineralogist* **28**, 693-702.
- HEISERMAN, D.L. (1992): Exploring Chemical Elements and Their Components. McGraw-Hill, Blue Ridge Summit, PA.
- JAROSCH, D. and ZEMANN, J. (1989): Yafsoanite: a garnet type calcium-tellurium (VI)-zinc oxide. *Mineralogy and Petrology* **40**, 111-116.
- JOHNSON, N.W. (1965): Convex polyhedra with regular faces. *Can. J. Math.* **18**, 169-200.
- KIM, A.A., ZAYAKINA, N.V., and MAKHOTKO, V.F. (1990): Kuksite $\text{Pb}_3\text{Zn}_3\text{TeO}_6(\text{PO}_4)_2$ and chermnykhite $\text{Pb}_3\text{Zn}_3\text{TeO}_6(\text{VO}_4)_2$ – New tellurates from the Kuranakh gold deposit (Central Aldan, southern Yakutia). *Zapiski Vses. Mineral. Obshch.* **119**, 50-57 (in Russian).
- KIM, A.A., ZAYAKINA, N.V., LAVRENT'EV, Yu.G., and MAKHOTKO, V.F. (1988): Vanadian silician variety of dugganite – the first find in the USSR. *Mineralog. Zhurnal* **10**, 85-89 (in Russian).
- KIRFEL, A. and EICHHORN, K. (1990): Accurate structure analysis with synchrotron radiation: The electron density in Al_2O_3 and Cu_2O . *Acta Cryst.*, **A46**, 271-284.
- KROSCWITZ, J.I. and HOWE-GRANT, M. editors (1997): Kirk-Othmer Encyclopedia of Chemical Technology. Fourth edition. Volume 23. John Wiley & Sons, Toronto.
- KUDRYAVTSEV, A.A. (1974): The Chemistry and Technology of Selenium and Tellurium (translated from the second Russian edition and revised by E.M. Elkin). Collet's Ltd., London.
- LAM, A.E., GROAT, L.A., and ERCIT, T.S. (1998): The crystal structure of dugganite, $\text{Pb}_3\text{Zn}_3\text{Te}^{6+}\text{As}_2\text{O}_{14}$. *Canadian Mineralogist*. In press.
- LAM, A.E., GROAT, L.A., GRICE, J., ERCIT, T.S., and MOFFATT, E. (1998): The crystal structure and revised formula of choloalite, $\text{Cu}_3\text{Pb}_3\text{Te}^{4+}_6\text{O}_{18}(\text{Cl}, \text{H}_2\text{O})$. *Canadian Mineralogist*. In Press.
- LE PAGE, Y. (1987): Computer derivation of the symmetry elements implied in a structure description. *J. Appl. Cryst.* **20**, 264-269.
- LINDQVIST, O. (1973): The Oxygen Coordination Of Tellurium (IV) And Tellurium (VI). Dissertation, University of Göteborg, Sweden.

- LINDQVIST, O. (1972): The crystal structure of CuTeO_3 . *Acta Chemica Scandinavica* **26**, 1423-1430.
- LOOPSTRA, B.O. and BRANDENBURG, N.P. (1978): Uranyl selenite and uranyl tellurite. *Acta Cryst.*, **B29**, 1251-1255.
- MARGISON, S.M., GRICE, J.D., and GROAT, L.A. (1997): The crystal structure of leisingite, $(\text{Cu}^{2+}, \text{Mg}, \text{Zn})_2(\text{Mg}, \text{Fe})\text{Te}^{6+}\text{O}_6 \cdot 6\text{H}_2\text{O}$. *Canadian Mineralogist* **35**, 759-763.
- MARIOLACOS, K. (1969): Die kristallstruktur von PbTeO_3 . *Anz. Oesterr. Akad. Wiss. Math. - Naturwiss.*, **K1**, Nd. 06, 129.
- MARSH, R. and HERBSTEIN, F.H. (1983): Some additional changes in space groups of published crystal structures. *Acta Cryst.* **B39**, 280-287.
- MARTY, J., JENSEN, M.C., and ROBERTS, A.C. (1993): Minerals of the Centennial Eureka Mine, Tintic District, Eureka, Utah. *Rock and Minerals* **68**, 406-416.
- MATZAT, E., (1967): Die kristallstruktur eines unbenannten zeolithartigen telluritminerals, $\{(\text{Zn}, \text{Fe})_2[\text{TeO}_3]_3\}\text{Na}_x\text{H}_{2-x}\cdot y\text{H}_2\text{O}$. *Tschermaks Min. Petr. Mitt.* **12**, 108-117.
- MEUNIER, G. and GALY, J. (1971): Sur une déformation inédite du réseau de type fluorine. Structure cristalline des phases MTe_3O_8 ($\text{M}=\text{Ti}, \text{Sn}, \text{Hf}, \text{Zr}$). *Acta Cryst.*, **B27**, 602-608.
- MEUNIER, G. and GALY, J. (1973): Structure cristalline de la schmitterite synthétique UTeO_5 . *Acta Cryst.* **B29**, 1251.
- MILETICH, R. (1995): Crystal chemistry of the microporous tellurite minerals zemannite and kinichilite, $\text{Mg}_{0.5}[\text{Me}^{2+}\text{Fe}^{3+}(\text{TeO}_3)_3] \cdot 4.5\text{H}_2\text{O}$, ($\text{Me}^{2+} = \text{Zn}; \text{Mn}$). *Eur. J. Mineral.* **7**, 509-523.
- NORTH, A.C.T., PHILLIPS, D.C., and MATHEWS, F.S. (1968): A semi-empirical method of absorption correction. *Acta Cryst.* **A24**, 351-359.
- O'KEEFFE, M.O. and HYDE, B.G. (1980): Plane nets in crystal chemistry. *Phil. Trans. R. Soc. London* **295A**, 553-618.
- PARTHÉ, E. and GELATO, L.M. (1984): The standardization of inorganic crystal-structure data. *Acta Cryst.* **A40**, 169-183.
- PERTLIK, F. (1971): Die kristallstruktur von poughit, $\text{Fe}_2[\text{TeO}_3]_2[\text{SO}_4] \cdot 3\text{H}_2\text{O}$. *Tschermaks Min. Petr. Mitt.* **15**, 279-290.
- PERTLIK, F. (1972): Der strukturtyp von emmosit, $\{\text{Fe}_2[\text{TeO}_3]_3 \cdot \text{H}_2\text{O}\} \cdot x\text{H}_2\text{O}$ ($x = 0-1$). *Tschermaks Min. Petr. Mitt.* **18**, 157-168.

- PERTLIK, F. and GIEREN, A. (1977): Verfeinerung der kristallstruktur von makayit, $\text{Fe}(\text{OH})[\text{Te}_2\text{O}_5]$. *N. Jahrbuch f. Mineralogie, Monatshefte* 145-154.
- PERTLIK, F. and ZEMANN, J. (1988): The crystal structure of nabokoite, $\text{Cu}_7\text{TeO}_4(\text{SO}_4)_5 \cdot \text{KCl}$: The first example of a $\text{Te}(\text{IV})\text{O}_4$ pyramid with exactly tetragonal symmetry. *Mineralogy and Petrology* **38**, 291-298.
- POWELL, D.W., THOMAS, R.G., WILLIAMS, P.A., BIRCH, W.D., and PLIMER, I.R. (1994): Choloalite: synthesis and revised chemical formula. *Mineralogical Magazine* **58**, 505-508.
- ROBERTS, A.C., ERCIT, T.S., CRIDDLE, A.J., JONES, G.C., WILLIAMS, R.S., CURETON II, F.F., and JENSEN, M.C. (1994): Mcalpineite, $\text{Cu}_3\text{TeO}_6 \cdot \text{H}_2\text{O}$, a new mineral from the McAlpine mine, Tuolumne County, California, and from the Centennial Eureka mine, Juab County, Utah. *Mineralogical Magazine* **58**, 417-424.
- ROBINSON, K., GIBBS, G.V., and RIBBE, P.H. (1971): Quadratic elongation: A quantitative measure of distortion in coordination polyhedra. *Science* **172**, 567-570.
- ROSSELL, H.J., LEBLANC, M., FÉREY, G., BEVAN, D.J.M., SIMPSON, D.J., and TAYLOR, M.R. (1992): On the crystal structure of $\text{Bi}_2\text{Te}_4\text{O}_{11}$. *Aust. J. Chem.* **45**, 1415-1425.
- SHANNON, R.D. (1976): Revised effective ionic radii and systematic studies of interatomic distances in halides and chalcogenides. *Acta Cryst.* **A32**, 751-767.
- SIERRA LOPEZ, J., LEAL, G., PIERROT, R., LAURENT, Y., PROTAS, J., and DUSAUSOY, Y. (1968): La rodalquilarite, chlorotellurite de fer, une nouvelle espèce minérale. *Bull. Soc. fr. Minéral. Cristallogr.* **91**, 28-33.
- SPIRIDONOV, E.M. (1980): Balyakinite, CuTeO_3 , a new mineral from the zone of oxidation. *Doklady Akademii Nauk SSSR* **253**, 1448-1450.
- STOUT, G.H., and JENSEN, L.H. (1989): X-ray Structure Determination. A Practical Guide. Second edition. John Wiley & Sons, Toronto.
- SWIHART, G.H., GUPTA, P. K. S., SCHLEMPER, E. O., BACK, M. E., and GAINES, R.V., (1993): The crystal structure of moctezumite $[\text{PbUO}_2](\text{TeO}_3)_2$. *American Mineralogist* **78**, 835-839.
- SZYMANSKI, J.T. (1985): The crystal structure of plumbojarosite $\text{Pb}[\text{Fe}_3(\text{SO}_4)_2(\text{OH})_6]_2$. *Canadian Mineralogist* **23**, 659-668.
- THOMAS, P.A. (1988): The crystal structure and absolute optical chirality of paratellurite, $\alpha\text{-TeO}_2$. *J. Phys. C: Solid State Phys.* **21**, 4611-4627.
- VLASOV, K.A. editor (1966): Geochemistry and Mineralogy of Rare Elements and Genetic Types of Their Deposits. Volume 1. Daniel Davey & Co., Inc. New York.

- WALITZI, E.M. (1964): Die kristallstruktur von denningit, $(\text{Mn,Ca,Zn})\text{Te}_2\text{O}_5$. Ein biespiel für koordination um vier wertiges tellur. *Tschermaks Min. Petr. Mitt.* **10**, 241-255.
- WANG, X. and LIEBAU, F. (1996): Influence of lone-pair electrons of cations on bond-valence parameters. *Zeitschrift für Kristallographie* **211**, 437-439.
- WILLIAMS, S.A. and MATTER III, P. (1975): Graemite, a new Bisbee mineral. *Mineralogical Record* **6**, 32-34.
- WILLIAMS, S.A. (1978): Khinite, parakhinite, and dugganite, three new tellurates from Tombstone, Arizona. *American Mineralogist* **63**, 1016-1019.
- WILLIAMS, S.A. (1981): Choloalite, $\text{CuPb}(\text{TeO}_3)_2 \cdot \text{H}_2\text{O}$, a new mineral. *Mineralogical Magazine* **44**, 55-57.
- ZEMANN J. (1971): Zur stereochemie des Te(IV) gegenüber sauerstoff. Monatshefte für Chemie **102**, 1209-1216.
- ZEMANN, J. (1968): The crystal chemistry of the tellurium oxide and tellurium oxosalt minerals. *Zeitschrift für Kristallographie* **127**, 319-326.
- ZEMANN, V.A. and ZEMANN, J. (1962): Die kristallstruktur von teineit. Ein beispiel für die korrektur einer chemischen formel auf grund der strukturbestimmung. *Acta Cryst.* **15**, 698-702.

APPENDIX A. COMMONLY USED SYMBOLS AND TERMS

A.1 Commonly used symbols and terms.

tellurite	Tellurium oxysalt mineral containing Te^{4+} .
tellurate	Tellurium oxysalt mineral containing Te^{6+} .
a, b, c	Unit cell axes.
α, β, γ	Unit cell angles.
x, y, z	Used to indicate atomic positions on cartesian axes.
hkl	Miller index.
V	Volume.
Z	Number of empirical formula units in the unit cell.
μ	Linear absorption coefficient.
R	$R = \sum F_o - F_c / \sum F_o$; indicates how closely your model matches the true model.
R_w	Weighted R .
R_{int}	Integrated R .
Rad/mono	Type of radiation and monochromator used.
$ E^2 - 1 $	Value of 0.968 indicates centrosymmetric, 0.736 indicates non-centrosymmetric.
I	Intensity.
U	Displacement factor.
$\langle \rangle$	Indicates average values on the tables of bond lengths and interatomic angles.
d_{meas}	Measured distance between planes.
d_{calc}	Calculated distance between planes.
F_o	Observed structure factor.
F_c	Calculated structure factor.

APPENDIX B. CATEGORIZED TELLURIUM OXYSALT MINERALS

B.1 Tellurite Minerals

Name	Formula
balyakinite	CuTeO_3
blakeite	$\text{Fe}_2\text{TeO}_3(?)$
burckhardtite	$\text{Pb}_2(\text{Fe},\text{Mn})\text{Te}(\text{Si}_3\text{Al})\text{O}_{12}(\text{OH})_2\cdot\text{H}_2\text{O}$
cesbronite	$\text{Cu}_5(\text{TeO}_3)_2(\text{OH})_6\cdot 2\text{H}_2\text{O}$
chekhovite	$\text{Bi}_2\text{Te}_4\text{O}_{11}$
choloalite	$\text{Pb}_3\text{Cu}_3\text{Te}^{4+}\text{O}_{18}\cdot(\text{Cl},\text{H}_2\text{O})$
cliffordite	UTe_3O_9
denningite	$(\text{Ca},\text{Mn})(\text{Mn},\text{Zn})\text{Te}_4\text{O}_{10}$
dunhamite	$\text{PbTeO}_3(?)$
emmonsite	$\text{Fe}_2(\text{TeO}_3)_3\cdot 2\text{H}_2\text{O}$
fairbankite	PbTeO_3
graemite	$\text{CuTeO}_3\cdot\text{H}_2\text{O}$
keystoneite	$\text{H}_{0.8}\text{Mg}_{0.8}(\text{Ni},\text{Fe},\text{Mn})_2(\text{TeO}_3)_3\cdot 5\text{H}_2\text{O}$
kinichilite	$\text{Mg}_{0.5}(\text{Mn}^{2+},\text{Zn})\text{Fe}^{3+}(\text{TeO}_3)_3\cdot 4.5\text{H}_2\text{O}$
mackayite	$\text{FeTe}_2\text{O}_5(\text{OH})$
magnolite	Hg_2TeO_3
moctezumite	$\text{Pb}(\text{UO}_2)(\text{TeO}_3)_2$
mroseite	$\text{CaTeO}_2(\text{CO}_3)$
nabokoite	$\text{Cu}_7\text{TeO}_4(\text{SO}_4)_5\cdot\text{KCl}$
paratellurite	$\alpha\text{-TeO}_2$
pingguite	$\text{Bi}_6\text{Te}_2\text{O}_{13}$
plumbotellurite	$\alpha\text{-PbTeO}_3$
poughite	$\text{Fe}_2(\text{TeO}_3)_2(\text{SO}_4)\cdot 3\text{H}_2\text{O}$
quetzalcoatlite	$\text{Cu}_4\text{Zn}_8(\text{TeO}_3)_3(\text{OH})_{18}$
rajite	CuTe_2O_5
rodalquilarite	$\text{H}_3\text{Fe}_2(\text{TeO}_3)_4\text{Cl}$
schmitterite	$(\text{UO}_2)\text{TeO}_3$

Tellurites continued

smirnite	Bi_2TeO_5
sonoraite	$\text{Fe}^{3+}\text{Te}^{4+}\text{O}_3(\text{OH})\cdot\text{H}_2\text{O}$
spiroffite	$(\text{Mn,Zn})_2\text{Te}_3\text{O}_8$
teineite	$\text{CuTeO}_3\cdot 2\text{H}_2\text{O}$
tellurite	TeO_2
unnamed 624	Au_2TeO_3
unnamed 626	$\text{Au}_2(\text{Bi,Te})\text{O}_3$
winstanleyite	TiTe_3O_8
zemannite	$(\text{H,Na})_2(\text{Zn,Fe})_2(\text{TeO}_3)_3\cdot n\text{H}_2\text{O}$

B.2 Tellurate Minerals

Name	Formula
cheremnykhite	$\text{Pb}_3\text{Zn}_3\text{TeO}_6(\text{VO}_4)_2$
chiluite	$\text{Bi}_6\text{Te}_2\text{Mo}_2\text{O}_{21}$
cuzticite	$\text{Fe}_2\text{TeO}_6 \cdot 3\text{H}_2\text{O}$
dugganite	$\text{Pb}_3\text{Zn}_3\text{Te}^{6+}\text{As}_2\text{O}_{14}$
ferrotellurite	$\text{FeTeO}_4(?)$
frankhawthorneite	$(\text{Cu}^{2+})_4\text{Te}^{6+}\text{O}_4(\text{OH})_2$
jensenite	$(\text{Cu}^{2+})_3\text{Te}^{6+}\text{O}_6 \cdot 2\text{H}_2\text{O}$
juabite	$\text{Cu}_5(\text{TeO}_4)_2(\text{AsO}_4)_2 \cdot 3\text{H}_2\text{O}$
khinite	$\text{Cu}_3\text{PbTeO}_4(\text{OH})_6$
kuksite	$\text{Pb}_3\text{Zn}_3\text{TeO}_6(\text{PO}_4)_2$
kuranakhite	PbMnTeO_6
leisingite	$\text{Cu}(\text{Mg}, \text{Cu}, \text{Fe}, \text{Zn})_2\text{Te}^{6+}\text{O}_6 \cdot 6\text{H}_2\text{O}$
mcalpineite	$\text{Cu}_3\text{TeO}_6 \cdot \text{H}_2\text{O}$
montanite	$(\text{BiO})_2\text{TeO}_4 \cdot 2\text{H}_2\text{O}$
parakhinite	$(\text{Cu}^{2+})_3\text{PbTe}^{6+}\text{O}_6(\text{OH})_2$
schieffelinite	$\text{Pb}(\text{Te}, \text{S})\text{O}_4 \cdot \text{H}_2\text{O}$
utahite	$\text{Cu}_5\text{Zn}_3(\text{TeO}_4)_4(\text{OH})_8 \cdot 7\text{H}_2\text{O}$
unnamed 604	$\text{Au}_4\text{Pb}_3\text{Te}_2\text{O}_{11}$
unnamed 625	$\text{Au}_2\text{TeO}_6 \cdot 2\text{H}_2\text{O}$
unnamed 627	$(\text{Zn}, \text{Pb}, \text{Cu})_3\text{TeO}_6 \cdot 2\text{H}_2\text{O}$
unnamed 628	$\text{Au}_6(\text{PbO}_3)_2\text{TeO}_4$
unnamed 629	$\text{Au}_6\text{Pb}_2(\text{PbO}_3)_2(\text{TeO}_4)_3 \cdot 6\text{H}_2\text{O}$
xocomecatlite	$\text{Cu}_3\text{TeO}_4(\text{OH})_4$
yafsoanite	$(\text{Ca}, \text{Pb})_3\text{Zn}_3\text{Te}_2\text{O}_{12}$

B.3 Tellurium Oxyalt Minerals With Mixed Te^{4+} and Te^{6+} valences

Name	Formula
carlfriesite	CaTe_3O_8
eztlite	$\text{Pb}_2\text{Fe}_6\text{Te}_4\text{O}_{15}(\text{OH})_{10}\cdot 8\text{H}_2\text{O}$
girdite	$\text{H}_2\text{Pb}_3(\text{TeO}_3)(\text{TeO}_6)$
oboyerite	$\text{H}_6\text{Pb}_6(\text{TeO}_3)_3(\text{TeO}_6)_2\cdot 2\text{H}_2\text{O}$
tlalocite	$\text{Cu}_{10}\text{Zn}_6\text{Te}_3\text{O}_{11}\text{Cl}(\text{OH})_{25}\cdot 27\text{H}_2\text{O}$
tlapallite	$\text{H}_6(\text{Ca,Pb})_2(\text{Cu,Zn})_3\text{SO}_4(\text{TeO}_3)_4\text{TeO}_6$
yecoraite	$\text{Fe}_3\text{Bi}_5\text{O}_9(\text{TeO}_3)(\text{TeO}_4)_2\cdot 9\text{H}_2\text{O}$

APPENDIX C. STRUCTURE FACTOR TABLES FOR DUGGANITE

Observed and calculated structure factors for dugganite in P 321

1

h	k	l	Fo	Fc	s	h	k	l	Fo	Fc	s	h	k	l	Fo	Fc	s
0	1	0	22	15	1	-4	4	1	47	47	1	-6	10	1	15	14	1
1	1	0	102	98	1	-3	4	1	119	116	3	-5	10	1	49	49	1
-1	2	0	84	81	1	-2	4	1	62	60	1	-4	10	1	19	17	2
0	2	0	104	94	-1	-1	4	1	118	112	2	-3	10	1	46	46	1
1	2	0	132	122	-2	0	4	1	26	27	1	-2	10	1	23	23	1
2	2	0	85	80	1	1	4	1	38	37	0	-1	10	1	13	13	1
-1	3	0	130	123	-1	2	4	1	62	64	1	0	10	1	41	40	1
0	3	0	159	157	2	3	4	1	41	42	1	-9	11	1	15	14	1
1	3	0	141	135	3	4	4	1	80	84	2	-8	11	1	12	15	2
2	3	0	79	78	1	-9	5	1	5	6	-2	-7	11	1	26	27	1
3	3	0	104	102	0	-8	5	1	42	42	1	-6	11	1	13	10	2
-2	4	0	89	87	2	-7	5	1	70	70	1	-5	11	1	11	11	-2
-1	4	0	135	132	2	-6	5	1	44	43	1	-4	11	1	26	25	1
0	4	0	50	48	1	-5	5	1	135	134	5	-3	11	1	11	13	2
1	4	0	57	55	1	-4	5	1	44	44	1	-2	11	1	16	16	1
2	4	0	84	84	1	-3	5	1	128	131	4	0	0	2	271	272	9
3	4	0	44	43	1	-2	5	1	131	129	2	0	1	2	25	26	1
4	4	0	55	55	1	-1	5	1	36	36	1	1	1	2	80	83	1
-2	5	0	84	84	1	0	5	1	133	129	1	-3	2	2	103	106	3
-1	5	0	61	59	1	1	5	1	43	44	1	-2	2	2	106	107	3
0	5	0	147	143	3	2	5	1	64	64	1	-1	2	2	80	81	2
1	5	0	33	35	1	3	5	1	44	46	1	0	2	2	106	107	2
2	5	0	91	92	2	4	5	1	12	11	1	1	2	2	116	116	4
3	5	0	43	45	1	5	5	1	44	46	1	2	3	2	62	64	1
4	5	0	9	12	-2	-11	6	1	16	14	2	-5	3	2	48	51	1
5	5	0	61	63	1	-10	6	1	9	10	-2	-4	3	2	94	96	2
-3	6	0	88	89	3	-9	6	1	34	35	1	-3	3	2	142	153	-5
-2	6	0	85	85	1	-8	6	1	31	32	1	-2	3	2	103	108	3
-1	6	0	40	41	1	-7	6	1	70	70	2	-1	3	2	122	121	4
0	6	0	9	5	-2	-6	6	1	6	7	-2	0	3	2	147	146	4
1	6	0	42	44	1	-5	6	1	36	36	1	1	3	2	106	105	3
2	6	0	43	45	1	-4	6	1	87	89	2	2	3	2	68	70	1
3	6	0	55	56	1	-3	6	1	26	25	1	3	3	2	76	76	1
4	6	0	11	13	-2	-2	6	1	76	77	2	-7	4	2	34	35	1
5	6	0	4	11	-2	-1	6	1	35	37	1	-6	4	2	69	70	2
-3	7	0	38	38	1	0	6	1	29	29	1	-5	4	2	39	37	2
-2	7	0	89	89	1	1	6	1	76	75	1	-4	4	2	36	35	1
-1	7	0	48	48	1	2	6	1	32	32	1	-3	4	2	87	88	2
0	7	0	59	59	1	3	6	1	32	33	1	-2	4	2	68	70	2
1	7	0	38	40	1	4	6	1	10	13	2	-1	4	2	93	91	2
2	7	0	9	8	-2	5	6	1	14	15	1	0	4	2	59	58	2

Observed and calculated structure factors for dugganite in *P*321

h	k	l	Fo	Fc	s	h	k	l	Fo	Fc	s	h	k	l	Fo	Fc	s
3	7	0	22	22	1	-11	7	1	26	27	1	1	4	2	34	33	1
4	7	0	19	17	1	-10	7	1	42	44	1	2	4	2	85	86	2
-4	8	0	70	71	3	-9	7	1	34	35	1	3	4	2	45	43	1
-3	8	0	43	45	1	-8	7	1	27	27	1	4	4	2	48	50	1
-2	8	0	44	45	1	-7	7	1	67	68	1	-9	5	2	4	8	-2
-1	8	0	45	46	1	-6	7	1	59	59	1	-8	5	2	44	46	1
0	8	0	45	44	1	-5	7	1	73	72	2	-7	5	2	70	71	2
1	8	0	40	39	1	-4	7	1	39	39	1	-6	5	2	21	22	1
2	8	0	34	33	1	-3	7	1	36	37	1	-5	5	2	140	142	5
3	8	0	18	19	1	-2	7	1	69	67	1	-4	5	2	42	41	1
-4	9	0	11	9	-2	-1	7	1	68	67	1	-3	5	2	56	58	1
-3	9	0	50	51	1	0	7	1	63	61	1	-2	5	2	72	73	2
-2	9	0	12	8	-2	1	7	1	29	29	1	-1	5	2	38	37	1
-1	9	0	36	35	1	2	7	1	37	39	1	0	5	2	128	123	2
0	9	0	25	27	1	3	7	1	45	47	1	1	5	2	8	12	-2
1	9	0	15	15	1	4	7	1	25	25	1	2	5	2	70	71	2
2	9	0	27	27	1	-11	8	1	17	18	1	3	5	2	38	40	1
-5	10	0	59	61	2	-10	8	1	20	20	1	4	5	2	17	16	1
-4	10	0	11	12	-2	-9	8	1	42	41	1	5	5	2	55	57	1
-3	10	0	26	25	1	-8	8	1	19	20	1	-11	6	2	14	12	1
-2	10	0	35	34	1	-7	8	1	27	27	1	-10	6	2	12	10	-2
-1	10	0	16	16	1	-6	8	1	38	39	1	-9	6	2	49	50	2
0	10	0	30	30	1	-5	8	1	40	41	1	-8	6	2	33	34	1
-5	11	0	14	13	2	-4	8	1	78	80	2	-7	6	2	36	36	1
-4	11	0	25	24	1	-3	8	1	46	47	1	-6	6	2	6	6	-2
-3	11	0	17	17	1	-2	8	1	41	41	1	-5	6	2	25	26	1
-2	11	0	29	28	1	-1	8	1	29	28	1	-4	6	2	73	72	1
0	0	1	121	127	2	0	8	1	19	19	1	-3	6	2	73	74	2
-1	1	1	13	15	1	1	8	1	37	38	1	-2	6	2	83	84	2
0	1	1	11	11	1	2	8	1	22	23	1	-1	6	2	16	17	1
1	1	1	204	200	2	3	8	1	17	16	1	0	6	2	5	4	-2
-3	2	1	54	50	2	-11	9	1	5	9	-2	1	6	2	41	41	2
-2	2	1	192	192	6	-10	9	1	12	9	1	2	6	2	28	29	1
-1	2	1	195	192	3	-9	9	1	11	11	2	3	6	2	49	50	1
0	2	1	214	201	-6	-8	9	1	38	38	1	4	6	2	10	9	-2
1	2	1	54	53	1	-7	9	1	38	38	1	5	6	2	7	8	-2
2	2	1	136	135	2	-6	9	1	36	37	1	-11	7	2	17	14	1
-5	3	1	125	123	3	-5	9	1	5	4	-2	-10	7	2	16	19	1
-4	3	1	33	32	1	-4	9	1	6	7	-2	-9	7	2	4	6	-2
-3	3	1	33	32	1	-3	9	1	31	31	1	-8	7	2	31	31	1
-2	3	1	61	60	1	-2	9	1	41	42	1	-7	7	2	59	58	1

Observed and calculated structure factors for dugganite in P321

h	k	l	Fo	Fc	s	h	k	l	Fo	Fc	s	h	k	l	Fo	Fc	s
-1	3	1	89	87	1	-1	9	1	33	35	1	-6	7	2	35	35	1
0	3	1	106	103	2	0	9	1	11	9	2	-5	7	2	67	66	2
1	3	1	125	119	2	1	9	1	11	11	2	-4	7	2	32	33	1
2	3	1	134	130	2	2	9	1	12	12	2	-3	7	2	39	38	1
3	3	1	30	29	1	-10	10	1	43	42	1	-2	7	2	70	69	1
-7	4	1	45	45	1	-9	10	1	11	11	-2	-1	7	2	46	45	1
-6	4	1	74	77	1	-8	10	1	19	20	1	0	7	2	61	62	2
-5	4	1	46	45	1	-7	10	1	42	43	1	1	7	2	35	33	1
4	4	4	32	33	1	0	7	4	48	48	2	-1	3	5	24	25	1
-9	5	4	6	5	-2	1	7	4	26	25	2	0	3	5	32	33	1
-8	5	4	36	36	2	2	7	4	10	5	-2	1	6	5	55	55	2
-7	5	4	50	50	2	-9	8	4	25	25	2	2	3	5	53	54	2
-6	5	4	21	20	1	-8	8	4	36	35	1	3	3	5	20	19	1
-5	5	4	92	93	4	-7	8	4	27	26	1	-7	4	5	24	25	2
-4	5	4	25	26	1	-6	8	4	24	25	1	-6	4	5	32	31	2
-3	5	4	42	44	2	-5	8	4	37	36	1	-5	4	5	12	11	2
-2	5	4	54	54	2	-4	8	4	43	43	1	-4	4	5	8	10	-2
-1	5	4	28	29	1	-3	8	4	26	24	1	-3	4	5	53	54	3
0	5	4	84	84	3	-2	8	4	25	24	1	-2	4	5	33	31	1
1	5	4	5	6	-2	-1	8	4	31	30	1	-1	4	5	47	47	2
2	5	4	50	51	2	0	8	4	25	25	1	0	4	5	22	20	1
3	5	4	26	24	1	1	8	4	26	25	1	1	4	5	9	10	-2
4	5	4	15	14	2	-8	9	4	21	22	1	2	4	5	32	30	1
5	5	4	38	38	1	-7	9	4	8	12	-2	3	4	5	18	18	1
-9	6	4	36	35	2	-6	9	4	31	31	1	4	4	5	36	35	2
-8	6	4	25	25	1	-5	9	4	6	3	-2	-8	5	5	18	17	1
-7	6	4	23	22	1	-4	9	4	12	12	1	-7	5	5	38	37	2
-6	6	4	7	2	-2	-3	9	4	34	32	1	-6	5	5	22	21	1
-5	6	4	24	23	1	-2	9	4	5	3	-2	-5	5	5	53	53	3
-4	6	4	48	48	2	-1	9	4	22	21	2	-4	5	5	13	13	2
-3	6	4	48	48	2	-5	10	4	40	38	2	-3	5	5	63	64	3
-2	6	4	50	53	2	0	0	5	72	71	7	-2	5	5	53	53	2
-1	6	4	10	11	2	-1	1	5	8	6	-2	-1	5	5	8	9	-2
0	6	4	7	3	-2	0	1	5	4	5	-2	0	5	5	62	62	2
1	6	4	26	26	1	1	1	5	74	76	3	1	5	5	17	17	1
2	6	4	22	22	1	-3	2	5	25	25	1	2	5	5	41	40	3
3	6	4	37	35	2	-2	2	5	64	65	3	3	5	5	25	26	2
-9	7	4	8	10	-2	-1	2	5	68	68	4	-8	6	5	21	19	1
-8	7	4	23	22	2	0	2	5	82	85	4	-7	6	5	35	34	2
-7	7	4	34	33	2	1	2	5	17	18	2	-6	6	5	6	2	-2

APPENDIX D. STRUCTURE FACTOR TABLES FOR CHOLOALITE

Observed and calculated structure factors for choleolite in P4₁32

1

h	k	l	Fo	Fc	s	h	k	l	Fo	Fc	s	h	k	l	Fo	Fc	s	h	k	l	Fo	Fc	s
1	1	1	298	280	4	-2	3	7	363	365	5	-3	7	8	49	53	-19	7	8	9	51	95	-17
0	1	2	16	6	-6	-1	3	7	265	279	5	-2	7	8	119	128	7	8	8	9	75	50	-15
1	1	2	81	112	5	0	3	7	24	27	-9	-1	7	8	99	110	8	0	9	9	134	148	6
0	2	2	79	77	5	1	3	7	276	275	2	0	7	8	25	28	-10	1	9	9	102	110	9
2	2	2	506	506	5	2	3	7	355	349	5	1	7	8	113	111	6	2	9	9	183	191	9
1	1	3	19	58	-19	3	3	7	34	28	-16	2	7	8	114	124	7	3	9	9	37	56	-16
2	2	3	667	621	-6	-3	4	7	157	157	9	3	7	8	35	50	-16	4	9	9	210	209	11
0	3	3	509	493	12	-2	4	7	194	190	4	4	7	8	172	195	7	5	9	9	26	24	-15
3	3	3	299	297	3	-1	4	7	84	79	10	5	7	8	64	91	-14	6	9	9	29	33	-17
0	1	4	666	657	11	0	4	7	428	427	4	6	7	8	25	21	-14	7	9	9	26	61	-15
-2	3	4	137	143	4	1	4	7	84	82	9	7	7	8	275	289	7	8	9	9	49	13	-20
-1	3	4	415	418	9	2	4	7	215	210	4	0	8	8	524	516	12	9	9	9	28	19	-28
0	3	4	62	82	-24	3	4	7	136	131	18	1	8	8	24	7	-14	0	1	10	99	101	8
1	3	4	443	441	2	4	4	7	202	189	4	2	8	8	24	31	-14	1	1	10	116	109	10
2	3	4	198	194	11	-4	5	7	287	278	3	3	8	8	53	49	-18	-1	2	10	262	265	11
3	3	4	151	151	8	-3	5	7	220	226	4	4	8	8	95	108	12	0	2	10	286	287	7
0	4	4	183	200	6	-2	5	7	220	225	6	5	8	8	28	36	-16	1	2	10	261	263	6
1	4	4	166	166	5	-1	5	7	148	156	4	6	8	8	143	141	7	2	2	10	454	447	13
2	4	4	258	255	3	0	5	7	192	186	4	7	8	8	26	23	-15	-2	3	10	135	135	7
3	4	4	151	159	3	1	5	7	145	158	6	8	8	8	62	48	-30	-1	3	10	24	32	-14
4	4	4	430	426	3	2	5	7	226	225	6	0	1	9	112	104	6	0	3	10	191	190	4
0	1	5	31	61	-10	3	5	7	212	222	4	1	1	9	44	83	-15	1	3	10	71	50	-12
1	1	5	34	38	-17	5	5	7	296	294	3	-1	2	9	25	28	-15	2	3	10	140	141	5
-1	2	5	111	127	7	5	5	7	60	69	-16	0	2	9	74	73	8	3	3	10	113	97	9
0	2	5	153	157	3	-5	6	7	150	152	5	1	2	9	32	35	-14	-3	4	10	27	44	-16
1	2	5	132	142	3	-4	6	7	181	183	6	2	2	9	273	276	7	-2	4	10	30	60	-18
2	2	5	259	248	5	-3	6	7	207	218	4	-2	3	9	131	138	7	-1	4	10	208	213	12
-2	3	5	89	93	10	-2	6	7	120	122	7	-1	3	9	156	165	8	0	4	10	37	43	-12
-1	3	5	172	187	4	-1	6	7	162	176	9	0	3	9	97	79	7	1	4	10	199	205	5
0	3	5	59	70	7	0	6	7	74	76	8	1	3	9	153	155	4	2	4	10	32	62	-15
1	3	5	149	156	4	1	6	7	189	201	4	2	3	9	136	127	15	3	4	10	73	89	-15
2	3	5	46	60	-15	2	6	7	162	155	4	3	3	9	24	20	-14	4	4	10	24	32	-14
3	3	5	513	501	10	3	6	7	191	195	5	-3	4	9	122	118	6	-4	5	10	92	79	15
-3	4	5	149	138	4	4	6	7	150	158	7	-2	4	9	238	242	5	-3	5	10	92	114	8
-2	4	5	155	157	8	5	6	7	165	154	4	-1	4	9	31	36	-18	-2	5	10	109	124	10
-1	4	5	357	350	9	6	6	7	155	152	8	0	4	9	147	153	4	-1	5	10	179	180	5
0	4	5	283	276	4	0	7	7	262	269	8	1	4	9	30	49	-15	0	5	10	102	114	7
1	4	5	375	366	11	1	7	7	146	131	7	2	4	9	254	254	4	1	5	10	169	167	11
2	4	5	182	178	6	2	7	7	41	36	-16	3	4	9	131	129	7	2	5	10	83	113	11
3	4	5	134	128	6	3	7	7	150	141	5	4	4	9	53	66	-16	3	5	10	99	107	10
4	4	5	237	240	3	4	7	7	49	15	-19	-4	5	9	243	241	5	4	5	10	71	99	11

Observed and calculated structure factors for choleolite in P4₁32

h	k	l	Fo	Fc	s	h	k	l	Fo	Fc	s	h	k	l	Fo	Fc	s	h	k	l	Fo	Fc	s
0	5	5	69	91	7	5	7	7	174	181	5	-3	5	9	83	91	-19	5	5	10	72	75	-21
1	5	5	20	37	-12	6	7	7	24	19	-14	-2	5	9	274	280	4	-5	6	10	99	104	8
2	5	5	247	249	4	7	7	7	221	228	6	-1	5	9	130	143	9	-4	6	10	24	17	-14
3	5	5	357	351	10	0	0	8	380	369	14	0	5	9	28	20	-11	-3	6	10	167	169	8
4	5	5	87	89	7	0	1	8	56	49	9	1	5	9	127	143	6	-2	6	10	42	45	-17
5	5	5	611	607	3	1	1	8	339	359	9	2	5	9	291	289	9	-1	6	10	79	83	11
0	1	6	191	188	4	-1	2	8	119	120	6	3	5	9	101	106	11	0	6	10	204	207	8
1	1	6	19	5	-11	0	2	8	52	53	-10	4	5	9	244	238	7	1	6	10	93	93	10
-1	2	6	293	295	6	1	2	8	95	79	12	5	5	9	136	146	6	2	6	10	26	44	-15
0	2	6	175	186	2	2	2	8	171	159	5	-5	6	9	81	89	10	3	6	10	173	180	6
1	2	6	294	288	10	-2	3	8	83	76	14	-4	6	9	225	219	6	4	6	10	27	18	-16
2	2	6	430	424	9	-1	3	8	57	79	-13	-3	6	9	250	256	8	5	6	10	96	95	9
-2	3	6	261	259	6	0	3	8	243	235	2	-2	6	9	52	63	-15	6	6	10	116	112	7
-1	3	6	317	319	5	1	3	8	99	100	7	-1	6	9	214	209	7	-6	7	10	116	112	7
0	3	6	20	27	-8	2	3	8	126	83	-20	0	6	9	123	124	6	-5	7	10	52	33	-20
1	3	6	320	311	4	3	3	8	97	92	8	1	6	9	233	217	4	-4	7	10	110	85	17
2	3	6	274	271	6	-3	4	8	86	99	9	2	6	9	70	57	-13	-3	7	10	24	14	-14
3	3	6	21	24	-12	-2	4	8	256	251	3	3	6	9	247	253	7	-2	7	10	24	63	-14
-3	4	6	169	161	4	-1	4	8	272	277	7	4	6	9	189	206	5	-1	7	10	134	138	9
-2	4	6	197	178	3	0	4	8	27	43	-11	5	6	9	96	105	12	0	7	10	94	91	9
-1	4	6	248	243	8	1	4	8	273	276	9	6	6	9	71	62	-20	1	7	10	114	119	7
0	4	6	284	264	5	2	4	8	247	241	9	-6	7	9	115	105	14	2	7	10	25	40	-14
1	4	6	231	222	4	3	4	8	82	85	13	-5	7	9	27	69	-16	3	7	10	25	18	-14
2	4	6	205	186	4	4	4	8	24	41	-14	-4	7	9	118	115	11	4	7	10	98	91	-19
3	4	6	175	170	6	-4	5	8	123	115	6	-3	7	9	111	115	8	5	7	10	55	31	-16
4	4	6	53	52	-20	-3	5	8	249	249	5	-2	7	9	40	61	-16	6	7	10	105	110	8
-4	5	6	23	27	-13	-2	5	8	175	183	7	-1	7	9	107	133	7	7	7	10	99	83	12
-3	5	6	51	65	-17	-1	5	8	181	199	4	0	7	9	73	88	9	-7	8	10	29	56	-18
-2	5	6	331	322	5	0	5	8	132	130	5	1	7	9	106	125	7	-6	8	10	197	188	6
-1	5	6	306	307	6	1	5	8	191	211	9	2	7	9	78	86	12	-5	8	10	135	155	13
0	5	6	253	254	2	3	5	8	171	177	4	3	7	9	111	106	8	-4	8	10	114	139	8
1	5	6	297	299	6	2	5	8	259	255	15	4	7	9	80	100	12	-3	8	10	166	158	10
2	5	6	314	307	7	4	5	8	88	91	11	5	7	9	49	51	-16	-2	8	10	138	146	6
3	5	6	86	76	11	5	5	8	151	142	6	6	7	9	101	101	11	-1	8	10	75	53	-14
4	5	6	61	47	-16	-5	6	8	24	44	-14	7	7	9	53	47	-19	0	8	10	31	58	-11
5	5	6	132	143	5	-4	6	8	156	158	13	-7	8	9	91	79	10	1	8	10	31	45	-18
0	6	6	178	182	5	-3	6	8	124	205	4	-6	8	9	155	154	6	2	8	10	143	144	6
1	6	6	129	132	8	-2	6	8	212	109	6	-5	8	9	75	64	12	3	8	10	197	186	4
2	6	6	54	62	-15	-1	6	8	162	164	5	-4	8	9	153	153	6	4	8	10	140	147	6
3	6	6	104	90	7	0	6	8	126	119	4	-3	8	9	25	36	-14	5	8	10	140	158	6
4	6	6	23	13	-14	1	6	8	162	162	8	-2	8	9	113	127	10	6	8	10	180	174	8

Observed and calculated structure factors for choleolite in $P4_32$

h	k	l	Fo	Fc	s	h	k	l	Fo	Fc	s	h	k	l	Fo	Fc	s	h	k	l	Fo	Fc	s
5	6	6	24	18	-14	2	6	8	57	87	-17	-1	8	9	99	97	12	7	8	10	58	70	-21
6	6	6	367	338	4	3	6	8	222	207	10	0	8	9	66	58	-15	8	8	10	27	64	-16
0	1	7	474	477	9	4	6	8	160	159	6	1	8	9	1199	100	-254	-8	9	10	76	83	-14
1	1	7	134	152	4	5	6	8	24	57	-14	2	8	9	112	124	7	-7	9	10	91	88	13
-1	2	7	239	236	5	6	6	8	107	123	11	3	8	9	25	23	-14	-6	9	10	32	65	-17
0	2	7	23	20	-8	-6	7	8	24	38	-14	4	8	9	154	146	6	-5	9	10	54	66	-21
1	2	7	241	237	6	-5	7	8	27	63	-16	5	8	9	85	85	13	-4	9	10	92	118	11
2	2	7	79	93	8	-4	7	8	175	188	4	6	8	9	179	176	5	-3	9	10	140	138	12
4	8	11	67	27	-25	3	6	12	40	60	-19	0	2	13	93	108	6	0	10	13	58	54	-18
5	8	11	129	122	14	4	6	12	143	136	9	1	2	13	70	81	12	1	10	13	41	77	-19
6	8	11	64	11	-19	5	6	12	113	65	-17	2	2	13	59	34	-19	2	10	13	69	83	-21
7	8	11	125	121	13	6	6	12	26	13	-15	-2	3	13	27	35	-16	3	10	13	29	43	-17
8	8	11	121	129	16	-6	7	12	83	99	12	-1	3	13	69	74	-17	4	10	13	108	104	-20
-8	9	11	122	54	-30	-5	7	12	26	35	-15	0	3	13	99	99	8	5	10	13	48	71	-21
-7	9	11	68	66	-19	-4	7	12	26	45	-15	1	3	13	77	70	11	6	10	13	29	28	-17
-6	9	11	117	65	-30	-3	7	12	85	95	-16	2	3	13	25	39	-14	-4	11	13	29	37	-17
-5	9	11	61	93	-17	-2	7	12	78	92	-14	3	3	13	97	98	11	-3	11	13	108	104	12
-4	9	11	97	80	-17	-1	7	12	81	95	10	-3	4	13	25	22	-15	-2	11	13	46	51	-21
-3	9	11	88	88	-17	0	7	12	120	118	7	-2	4	13	50	64	-18	-1	11	13	31	21	-18
-2	9	11	105	87	14	1	7	12	106	97	11	-1	4	13	173	172	7	0	11	13	34	19	-13
-1	9	11	26	61	-15	2	7	12	105	104	8	0	4	13	113	109	8	1	11	13	31	18	-18
0	9	11	26	5	-10	3	7	12	92	104	11	1	4	13	149	161	5	2	11	13	90	48	-12
1	9	11	87	65	-15	4	7	12	45	60	-19	2	4	13	84	69	-15	3	11	13	133	113	10
2	9	11	96	77	11	5	7	12	26	42	-15	3	4	13	25	33	-15	4	11	13	29	53	-17
3	9	11	61	73	-20	6	7	12	122	107	10	4	4	13	154	150	6	0	1	14	94	85	6
4	9	11	97	89	-25	7	7	12	76	83	-23	-4	5	13	32	48	-17	1	1	14	241	247	12
5	9	11	95	89	-26	-7	8	12	62	80	-17	-3	5	13	202	201	5	-1	2	14	52	28	-20
6	9	11	88	63	12	-6	8	12	115	110	8	-2	5	13	53	70	-17	0	2	14	39	63	-12
7	9	11	41	52	-20	-5	8	12	35	34	-17	-1	5	13	101	99	12	2	2	14	27	40	-16
8	9	11	94	68	15	-4	8	12	80	86	-14	0	5	13	189	188	6	2	2	14	35	52	-16
9	9	11	142	125	18	-3	8	12	81	77	13	1	5	13	113	104	7	-2	3	14	81	57	11
-9	10	11	62	48	-22	-2	8	12	32	5	-16	2	5	13	55	86	-18	-1	3	14	158	159	10
-8	10	11	93	57	-26	-1	8	12	97	117	9	3	5	13	205	208	10	0	3	14	186	201	8
-7	10	11	88	90	-22	0	8	12	150	151	8	4	5	13	35	38	-16	1	3	14	152	155	7
-6	10	11	104	58	-29	1	8	12	109	122	8	5	5	13	28	46	-17	2	3	14	69	66	-15
-5	10	11	94	55	-13	2	8	12	26	10	-15	-5	6	13	76	71	-14	3	3	14	26	17	-15
-4	10	11	64	68	-18	3	8	12	102	83	15	-4	6	13	35	45	-19	-3	4	14	56	70	-18
-3	10	11	27	66	-15	4	8	12	91	90	10	-3	6	13	176	177	6	-2	4	14	69	89	-19
-2	10	11	56	36	-19	5	8	12	45	31	-18	-2	6	13	54	61	-19	-1	4	15	79	91	13
-1	10	11	26	34	-15	6	8	12	95	105	13	-1	6	13	31	44	-16	0	4	15	60	48	-12
																		1	4	15	112	100	8

Observed and calculated structure factors for choleolite in $P4_132$

h	k	l	Fo	Fc	s	h	k	l	Fo	Fc	s	h	k	l	Fo	Fc	s	h	k	l	Fo	Fc	s
0	10	11	77	38	-14	7	8	12	80	72	-16	0	6	13	86	81	14	1	4	14	87	80	10
1	10	11	52	53	-19	8	8	12	36	47	-18	1	6	13	26	40	-15	2	4	14	93	93	12
2	10	11	65	37	-24	-8	9	12	61	38	-24	2	4	14	67	65	-19	3	4	15	102	94	14
3	10	11	77	71	13	-7	9	12	68	56	-18	3	6	13	165	173	10	4	4	14	40	81	-20
4	10	11	64	81	-18	-6	9	12	84	96	-14	4	4	14	29	37	-18	-4	5	15	108	82	16
5	10	11	59	53	-18	-5	9	12	94	65	11	5	6	13	35	32	-15	-3	5	15	110	91	11
6	10	11	53	66	-21	-4	9	12	27	31	-16	6	6	13	43	68	-20	-2	5	15	28	53	-16
7	10	11	89	83	14	-3	9	12	124	125	12	-6	7	13	124	127	13	-1	5	15	92	100	11
8	10	11	31	52	-18	-2	9	12	69	82	-16	-5	7	13	27	18	-16	0	5	14	33	8	-17
9	10	11	78	56	-23	-1	9	12	158	143	6	-4	7	13	104	105	9	1	5	14	67	67	-14
0	11	11	33	38	-17	0	9	12	97	110	9	-3	7	13	61	61	-23	2	5	14	88	80	-30
1	11	11	156	155	6	1	9	12	151	146	9	-2	7	13	26	55	-15	3	5	14	26	42	-15
2	11	11	27	15	-16	2	9	12	30	75	-18	-1	7	13	28	42	-17	4	5	14	29	21	-17
3	11	11	61	71	-18	3	9	12	132	120	11	0	7	13	104	92	8	5	5	14	48	71	-19
4	11	11	28	63	-16	4	9	12	29	21	-18	1	7	13	26	50	-15	-5	6	15	41	34	-18
5	11	11	28	15	-16	5	9	12	35	79	-21	2	7	13	50	60	-19	-4	6	15	54	51	-20
6	11	11	81	67	-15	6	9	12	91	84	13	3	7	13	35	72	-17	-3	6	15	108	112	14
7	11	11	72	15	-22	7	9	12	30	53	-18	4	7	13	110	104	13	-2	6	14	117	108	14
8	11	11	98	38	-18	8	9	12	37	29	-18	5	7	13	28	11	-16	-1	6	14	93	81	15
0	0	12	37	71	-16	9	9	12	56	55	-23	6	7	13	118	122	8	0	6	14	28	21	-11
0	1	12	190	187	5	-8	10	12	76	53	-19	7	8	13	32	52	-19	1	6	14	65	76	-16
1	1	12	24	59	-14	-7	10	12	65	70	-18	-7	8	13	86	65	-16	2	6	15	77	79	-16
-1	2	12	53	80	-15	-6	10	12	37	29	-23	-6	8	13	43	23	-18	3	6	15	110	111	10
0	2	12	128	139	5	-5	10	12	136	144	8	-4	8	13	27	24	-16	3	6	14	88	110	12
1	2	12	32	67	-15	-4	10	12	64	68	-19	-4	8	13	27	54	-16	5	6	14	28	25	-16
2	2	12	32	20	-18	-3	10	12	77	79	-14	-3	8	13	63	64	-18	-6	7	15	104	101	14
-2	3	12	183	190	8	-2	10	12	39	19	-17	-2	8	13	71	69	-15	-5	7	15	65	84	-22
-1	3	12	94	93	14	-1	10	12	123	116	13	-1	8	13	34	44	-11	-4	7	14	67	49	-18
0	3	12	60	44	-11	0	10	12	53	84	-14	0	8	13	47	40	-18	-3	7	14	86	54	-21
1	3	12	122	117	13	1	10	12	117	108	15	1	8	13	31	11	-18	-4	7	14	30	40	-18
2	3	12	185	189	13	2	10	12	31	18	-18	2	8	13	46	69	-19	-2	7	14	98	102	11
3	3	12	71	32	-16	3	10	12	68	66	-20	3	8	13	66	54	-19	-1	7	14	30	47	-17
-3	4	12	48	93	-17	4	10	12	80	66	-23	4	8	13	27	9	-16	0	7	14	27	35	-11
-2	4	12	121	134	11	5	10	12	137	146	16	5	8	13	31	11	-18	1	7	14	27	43	-16
-1	4	12	54	89	-17	6	10	12	45	37	-21	6	8	13	64	86	-21	2	7	14	106	95	-26
0	4	12	26	14	-10	7	10	12	32	61	-19	7	8	13	29	50	-17	3	7	14	52	44	-19
1	4	12	87	88	-17	8	10	12	72	58	-26	8	8	13	58	68	-20	4	7	14	28	51	-16
2	4	12	134	131	11	-6	11	12	85	90	13	-7	9	13	29	60	-17	5	7	14	71	39	-22
3	4	12	74	94	12	-5	11	12	45	102	-19	-6	9	13	29	16	-17	6	7	14	108	86	13
4	4	12	150	147	6	-4	11	12	57	39	-22	-5	9	13	49	74	-20	7	7	14	190	185	6
-4	5	12	192	194	6	-3	11	12	52	43	-20	-4	9	13	116	97	13	-7	8	14	29	37	-17
-3	5	12	106	99	15	-2	11	12	28	59	-16	-3	9	13	93	98	14	-6	8	14	32	54	-19

Observed and calculated structure factors for choleolite in $P4_132$

h	k	l	Fo	Fc	s	h	k	l	Fo	Fc	s	h	k	l	Fo	Fc	s	h	k	l	Fo	Fc	s
-2	5	12	79	67	10	-1	11	12	113	94	13	-2	9	13	55	55	-21	-5	8	14	87	58	-20
-1	5	12	116	120	11	0	11	12	128	127	7	-1	9	13	71	81	-17	-4	8	14	73	71	-21
0	5	12	64	17	-10	1	11	12	98	98	12	0	9	13	94	88	13	-3	8	14	31	38	-19
1	5	12	117	116	12	2	11	12	44	69	-19	1	9	13	82	83	-14	-2	8	14	145	122	7
2	5	12	39	48	-18	3	11	12	28	43	-16	2	9	13	33	48	-18	-1	8	14	86	68	-16
3	5	12	151	95	-23	4	11	12	30	36	-18	3	9	13	80	104	-14	0	8	14	38	5	-12
4	5	12	191	193	16	5	11	12	80	103	-16	4	9	13	100	95	-26	1	8	14	65	52	-27
5	5	12	34	39	-16	6	11	12	146	101	-20	5	9	13	65	72	-19	2	8	14	134	130	8
-5	6	12	75	89	-14	0	12	12	46	73	-20	6	9	13	32	41	-19	3	8	14	28	34	-16
-4	6	12	116	124	10	1	12	12	32	13	-19	7	9	13	54	63	-20	4	8	14	82	71	-22
-3	6	12	86	63	12	2	12	12	115	120	11	-6	10	13	72	34	-22	5	8	14	84	65	-17
-2	6	12	65	87	-15	3	12	12	31	8	-18	-5	10	13	90	73	13	6	8	14	29	55	-17
-1	6	12	102	110	8	4	12	12	43	44	-20	-4	10	13	79	98	-24	7	8	14	29	33	-17
0	6	12	129	105	15	0	1	13	36	39	-11	-3	10	13	70	47	-18	-5	9	14	46	63	-19
1	6	12	102	90	14	1	1	13	118	120	10	-2	10	13	80	73	-17	-4	9	14	86	117	-20
2	6	12	75	95	12	-1	2	13	92	83	10	-1	10	13	80	76	-15	-3	9	14	32	78	-19
2	2	16	27	30	-16	2	4	16	28	28	-16	4	5	16	99	99	15	-2	7	16	29	23	-17
-2	3	16	118	108	12	3	4	16	35	52	-21	5	5	16	32	7	-19	-1	7	16	108	98	10
-1	3	16	74	60	-19	4	4	16	126	110	13	-4	6	16	87	82	-24	0	7	16	74	71	-13
0	3	16	34	22	-12	-4	5	16	108	101	10	-3	6	16	44	8	-19	1	7	16	97	99	11
1	3	16	53	54	-21	-3	5	16	28	13	-16	-2	6	16	48	61	-20	2	7	16	49	34	-20
2	3	16	99	115	10	-2	5	16	49	22	-20	-1	6	16	28	40	-16	0	1	17	97	93	8
3	3	16	70	93	-18	-1	5	16	31	16	-19	0	6	16	92	80	10	1	1	17	72	96	-17
-3	4	16	65	56	-22	0	5	16	28	28	-11	1	6	16	62	46	-18	-1	2	17	71	55	-22
-2	4	16	38	28	-18	1	5	16	28	10	-16	2	6	16	68	52	-19	0	2	17	44	58	-13
-1	4	16	31	23	-19	2	5	16	31	28	-18	3	6	16	29	12	-17	1	2	17	61	54	-19
0	4	16	45	21	-14	3	5	16	29	15	-17	4	6	16	82	81	-15	2	2	17	28	15	-16
1	4	16	28	39	-16	3	5	16	29	15	-17	4	6	16	82	81	-15	2	2	17	28	15	-16
2	4	16	28	39	-16	3	5	16	29	15	-17	4	6	16	82	81	-15	2	2	17	28	15	-16
3	4	16	28	39	-16	3	5	16	29	15	-17	4	6	16	82	81	-15	2	2	17	28	15	-16
4	4	16	28	39	-16	3	5	16	29	15	-17	4	6	16	82	81	-15	2	2	17	28	15	-16
5	4	16	28	39	-16	3	5	16	29	15	-17	4	6	16	82	81	-15	2	2	17	28	15	-16
6	4	16	28	39	-16	3	5	16	29	15	-17	4	6	16	82	81	-15	2	2	17	28	15	-16
7	4	16	28	39	-16	3	5	16	29	15	-17	4	6	16	82	81	-15	2	2	17	28	15	-16
8	4	16	28	39	-16	3	5	16	29	15	-17	4	6	16	82	81	-15	2	2	17	28	15	-16
9	4	16	28	39	-16	3	5	16	29	15	-17	4	6	16	82	81	-15	2	2	17	28	15	-16
10	4	16	28	39	-16	3	5	16	29	15	-17	4	6	16	82	81	-15	2	2	17	28	15	-16
11	4	16	28	39	-16	3	5	16	29	15	-17	4	6	16	82	81	-15	2	2	17	28	15	-16
12	4	16	28	39	-16	3	5	16	29	15	-17	4	6	16	82	81	-15	2	2	17	28	15	-16
13	4	16	28	39	-16	3	5	16	29	15	-17	4	6	16	82	81	-15	2	2	17	28	15	-16
14	4	16	28	39	-16	3	5	16	29	15	-17	4	6	16	82	81	-15	2	2	17	28	15	-16
15	4	16	28	39	-16	3	5	16	29	15	-17	4	6	16	82	81	-15	2	2	17	28	15	-16
16	4	16	28	39	-16	3	5	16	29	15	-17	4	6	16	82	81	-15	2	2	17	28	15	-16
17	4	16	28	39	-16	3	5	16	29	15	-17	4	6	16	82	81	-15	2	2	17	28	15	-16
18	4	16	28	39	-16	3	5	16	29	15	-17	4	6	16	82	81	-15	2	2	17	28	15	-16
19	4	16	28	39	-16	3	5	16	29	15	-17	4	6	16	82	81	-15	2	2	17	28	15	-16
20	4	16	28	39	-16	3	5	16	29	15	-17	4	6	16	82	81	-15	2	2	17	28	15	-16
21	4	16	28	39	-16	3	5	16	29	15	-17	4	6	16	82	81	-15	2	2	17	28	15	-16
22	4	16	28	39	-16	3	5	16	29	15	-17	4	6	16	82	81	-15	2	2	17	28	15	-16
23	4	16	28	39	-16	3	5	16	29	15	-17	4	6	16	82	81	-15	2	2	17	28	15	-16
24	4	16	28	39	-16	3	5	16	29	15	-17	4	6	16	82	81	-15	2	2	17	28	15	-16
25	4	16	28	39	-16	3	5	16	29	15	-17	4	6	16	82	81	-15	2	2	17	28	15	-16
26	4	16	28	39	-16	3	5	16	29	15	-17	4	6	16	82	81	-15	2	2	17	28	15	-16
27	4	16	28	39	-16	3	5	16	29	15	-17	4	6	16	82	81	-15	2	2	17	28	15	-16
28	4	16	28	39	-16	3	5	16	29	15	-17	4	6	16	82	81	-15	2	2	17	28	15	-16
29	4	16	28	39	-16	3	5	16	29	15	-17	4	6	16	82	81	-15	2	2	17	28	15	-16
30	4	16	28	39	-16	3	5	16	29	15	-17	4	6	16	82	81	-15	2	2	17	28	15	-16
31	4	16	28	39	-16	3	5	16	29	15	-17	4	6	16	82	81	-15	2	2	17	28	15	-16
32	4	16	28	39	-16	3	5	16	29	15	-17	4	6	16	82	81	-15	2	2	17	28	15	-16
33	4	16	28	39	-16	3	5	16	29	15	-17	4	6	16	82	81	-15	2	2	17	28	15	-16
34	4	16	28	39	-16	3	5	16	29	15	-17	4	6	16	82	81	-15	2	2	17	28	15	-16
35	4	16	28	39	-16	3	5	16	29	15	-17	4	6	16	82	81	-15	2	2	17	28	15	-16
36	4	16	28	39	-16	3	5	16	29	15	-17	4	6	16	82	81	-15	2	2	17	28	15	-16
37	4	16	28	39	-16	3	5	16	29	15	-17	4	6	16	82	81	-15	2	2	17	28	15	-16
38	4	16	28	39	-16	3	5	16	29	15	-17	4	6	16	82	81	-15	2	2	17	28	15	-16
39	4	16	28	39	-16	3	5	16	29	15	-17	4	6	16	82	81	-15	2	2	17	28	15	-16
40	4	16	28	39	-16	3	5	16	29	15	-17	4	6	16	82	81	-15	2	2	17	28	15	-16
41	4	16	28	39	-16	3	5	16	29	15	-17	4	6	16	82	81	-15	2	2	17	28	15	-16
42	4	16	28	39	-16	3	5	16	29	15	-17	4	6	16	82	81	-15	2	2	17	28	15	-16
43	4	16	28	39	-16	3	5	16	29	15	-17	4	6	16	82	81	-15	2	2	17	28	15	-16
44	4	16	28	39	-16	3	5	16	29	15	-17	4	6	16	82	81	-15	2	2	17	28	15	-16
45	4	16	28	39	-16	3	5	16	29	15	-17	4	6	16	82	81	-15	2	2	17	28	15	-16
46	4	16	28	39	-16	3	5	16	29	15	-17	4	6	16	82	81	-15	2	2	17	28	15	-16

APPENDIX E. STRUCTURE FACTOR TABLES FOR RODALQUILARITE

Observed and calculated structure factors for rodalquilarite in P-1

1

h	k	l	Fo	Fc	s	h	k	l	Fo	Fc	s	h	k	l	Fo	Fc	s
1	0	0	42	-42	0	0	4	0	79	-75	1	1	4	1	6	-4	1
2	0	0	71	-73	1	1	4	0	46	-43	0	2	4	1	14	13	0
3	0	0	28	-29	0	2	4	0	26	25	0	3	4	1	41	-39	0
4	0	0	22	-22	0	3	4	0	7	-5	1	4	4	1	67	-67	1
5	0	0	5	-3	1	4	4	0	70	66	0	5	4	1	37	37	1
6	0	0	91	92	1	5	4	0	76	72	0	6	4	1	46	48	1
7	0	0	67	69	0	6	4	0	84	-80	0	7	4	1	30	-32	1
8	0	0	90	-89	1	7	4	0	30	-29	0	8	4	1	7	6	1
9	0	0	1	0	-1	8	4	0	23	22	0	9	4	1	29	-29	0
10	0	0	3	0	-1	9	4	0	19	17	0	10	4	1	37	-37	0
11	0	0	11	10	1	10	4	0	8	8	0	11	4	1	2	1	-1
12	0	0	26	23	0	7	5	0	28	-30	1	8	5	1	18	-17	0
13	0	0	57	-51	1	6	5	0	31	-33	1	9	5	1	6	5	1
14	0	0	25	-22	0	5	5	0	32	33	1	10	5	1	96	94	1
15	0	0	65	62	0	4	5	0	72	73	1	11	5	1	52	-51	1
16	0	0	32	30	0	3	5	0	24	-22	0	12	5	1	81	-78	1
17	0	0	19	-8	-1	2	5	0	15	-15	0	13	5	1	15	-13	0
18	0	0	76	75	0	1	5	0	5	2	1	14	5	1	18	17	0
19	0	0	132	-139	3	0	5	0	66	-62	1	15	5	1	18	17	0
20	0	0	43	-41	1	1	5	0	43	41	1	16	5	1	83	77	1
21	0	0	90	93	2	2	5	0	81	78	2	17	5	1	2	-1	-1
22	0	0	141	141	2	3	5	0	1	1	1	18	5	1	152	-145	1
23	0	0	41	-38	0	4	5	0	57	-55	1	19	5	1	13	11	0
24	0	0	21	19	0	5	5	0	22	20	0	20	5	1	42	39	0
25	0	0	14	-11	0	6	5	0	16	-15	0	21	5	1	6	4	1
26	0	0	142	-136	1	7	5	0	6	-5	1	22	5	1	16	18	0
27	0	0	141	136	1	8	5	0	65	63	1	23	5	1	19	20	0
28	0	0	60	58	0	9	5	0	11	10	0	24	5	1	83	-87	3
29	0	0	9	9	0	10	5	0	9	10	1	25	5	1	30	-31	1
30	0	0	43	-43	1	11	5	0	39	-39	0	26	5	1	56	54	1
31	0	0	18	17	0	12	5	0	37	-36	0	27	5	1	49	-48	0
32	0	0	42	-41	0	13	5	0	69	66	1	28	5	1	9	-9	0
33	0	0	16	16	0	14	5	0	21	20	0	29	5	1	48	50	1
34	0	0	82	80	0	15	5	0	15	-14	0	30	5	1	38	38	0
35	0	0	12	-11	0	16	5	0	14	14	0	31	5	1	61	-64	0
36	0	0	34	-32	0	17	5	0	22	-21	0	32	5	1	11	-12	0
37	0	0	13	-11	0	18	5	0	34	-32	1	33	5	1	30	-28	0
38	0	0	34	30	0	19	5	0	30	29	0	34	5	1	71	-67	0
39	0	0	46	41	0	20	5	0	71	68	1	35	5	1	126	121	1
40	0	0	4	4	-1	21	5	0	32	-32	0	36	5	1	69	64	1
41	0	0	99	-97	3	22	5	0	67	-65	1	37	5	1	135	-126	2

Observed and calculated structure factors for rodalquilarite in P-1

h	k	l	Fo	Fc	s	h	k	l	Fo	Fc	s	h	k	l	Fo	Fc	s
-6	2	0	24	24	0	2	7	0	9	8	1	-1	-2	1	100	-95	1
-5	2	0	46	47	1	-4	-7	1	60	-57	1	0	-2	1	42	38	0
-4	2	0	106	-10	1	-3	-7	1	18	-15	0	1	-2	1	51	-48	0
-3	2	0	102	105	1	-2	-7	1	5	-4	1	2	-2	1	70	67	1
-2	2	0	34	-30	0	-1	-7	1	7	-7	1	3	-2	1	97	98	1
-1	2	0	61	-57	0	0	-7	1	6	4	-	4	-2	1	83	-86	0
0	2	0	50	-49	0	-8	-6	1	39	39	0	5	-2	1	85	-91	2
1	2	0	139	136	1	-7	-6	1	17	15	0	6	-2	1	3	-4	-1
2	2	0	12	-8	0	-6	-6	1	42	-40	0	7	-2	1	39	39	1
3	2	0	21	20	0	-5	-6	1	8	7	0	8	-2	1	11	-8	0
4	2	0	50	47	0	-4	-6	1	77	-46	5	9	-2	1	49	45	1
5	2	0	90	-86	1	-3	-6	1	29	-27	0	10	-2	1	25	-21	1
6	2	0	40	-39	0	-2	-6	1	91	86	2	-12	-1	1	33	32	0
7	2	0	75	74	0	-1	-6	1	2	1	-	-11	-1	1	18	-17	0
8	2	0	71	71	0	0	-6	1	35	-33	0	-10	-1	1	17	13	0
9	2	0	40	-39	0	1	-6	1	32	-31	0	-9	-1	1	34	-33	0
10	2	0	15	15	0	2	-6	1	6	-6	1	-8	-1	1	78	-78	0
11	2	0	23	-22	0	3	-6	1	29	-28	0	-7	-1	1	20	20	0
12	2	0	36	-35	0	4	-6	1	49	50	1	-6	-1	1	133	136	1
-10	3	0	38	-33	1	-10	-5	1	7	8	1	-5	-1	1	54	-53	0
-9	3	0	5	-2	-1	-9	-5	1	2	-1	-	-4	-1	1	74	-68	0
-8	3	0	18	-14	0	-8	-5	1	27	27	0	-3	-1	1	27	-26	1
-7	3	0	8	2	-1	-7	-5	1	67	-65	0	-2	-1	1	114	-107	2
-6	3	0	25	27	1	-6	-5	1	51	-49	0	-1	-1	1	149	148	0
-5	3	0	90	93	1	-5	-5	1	28	26	0	0	-1	1	53	53	0
-4	3	0	78	-79	1	-4	-5	1	78	76	0	1	-1	1	130	-147	1
-3	3	0	43	-42	1	-3	-5	1	40	-38	0	2	-1	1	13	-13	0
-2	3	0	38	36	0	-2	-5	1	12	11	0	3	-1	1	44	-48	1
-1	3	0	10	9	0	-1	-5	1	34	-33	0	5	-1	1	9	-8	0
0	3	0	39	37	1	0	-5	1	84	-80	2	6	-1	1	55	58	1
1	3	0	86	81	0	1	-5	1	25	23	0	7	-1	1	37	38	0
2	3	0	5	-4	0	2	-5	1	70	68	0	8	-1	1	58	-57	1
3	3	0	161	-155	1	3	-5	1	4	4	-	9	-1	1	50	-46	0
4	3	0	51	48	0	4	-5	1	50	-49	0	10	-1	1	35	33	0
5	3	0	62	59	0	5	-5	1	9	8	1	11	-1	1	30	-27	0
6	3	0	22	20	0	6	-5	1	33	-34	1	12	0	1	22	20	0
7	3	0	40	39	0	7	-5	1	7	-8	1	-11	0	1	85	-77	1
8	3	0	2	1	-1	-11	-4	1	31	31	0	-10	0	1	27	-25	0
9	3	0	72	-72	1	-10	-4	1	9	8	0	-9	0	1	57	55	0
10	3	0	10	-9	1	-9	-4	1	98	-100	1	-8	0	1	22	21	0
11	3	0	62	61	1	-8	-4	1	8	7	0	-8	0	1	22	21	0

Observed and calculated structure factors for rodalquilarite in P-1

h	k	l	Fo	Fc	s	h	k	l	Fo	Fc	s	h	k	l	Fo	Fc	s
-8	4	0	55	55	2	-7	4	1	26	25	0	-7	0	1	4	-2	-1
-7	4	0	8	9	1	-6	4	1	4	4	2	-6	0	1	6	5	1
-6	4	0	37	-42	1	-5	4	1	35	33	0	-5	0	1	72	-71	1
-5	4	0	7	-7	1	-4	4	1	22	15	0	-4	0	1	122	-123	1
-4	4	0	5	0	-2	-3	4	1	84	-81	1	-3	0	1	99	99	1
-3	4	0	34	-31	0	-2	4	1	91	-87	2	-2	0	1	52	51	0
-2	4	0	126	121	1	-1	4	1	89	84	2	-1	0	1	2	3	-1
-1	4	0	34	32	0	0	4	1	11	10	0	0	0	1	29	-29	0
7	4	2	33	-36	1	9	0	2	24	-23	0	-3	5	2	61	64	2
8	4	2	35	-36	0	10	0	2	5	-5	1	-2	5	2	20	-20	0
-12	-3	2	31	-31	0	11	0	2	15	-14	1	-1	5	2	37	37	1
-11	-3	2	26	-26	0	-11	1	2	44	41	0	0	5	2	4	0	-1
-10	-3	2	89	94	1	-10	1	2	35	-32	0	1	5	2	62	-62	2
-9	-3	2	12	12	0	-9	1	2	54	-49	1	2	5	2	15	-11	1
-8	-3	2	24	-24	0	-8	1	2	35	32	0	3	5	2	61	60	1
-7	-3	2	35	-35	0	-7	1	2	18	-16	0	4	5	2	43	42	1
-6	-3	2	22	22	0	-6	1	2	39	38	0	5	5	2	39	-38	0
-5	-3	2	50	-48	1	-5	1	2	94	100	2	6	5	2	32	32	0
-4	-3	2	101	98	1	-4	1	2	65	-67	1	7	5	2	44	-42	0
-3	-3	2	105	102	1	-3	1	2	87	-83	0	-3	6	2	37	38	0
-2	-3	2	113	-107	1	-2	1	2	30	26	0	-2	6	2	21	-21	1
-1	-3	2	50	-46	0	-1	1	2	83	81	0	-1	6	2	61	-64	0
0	-3	2	6	4	1	0	1	2	23	22	0	0	6	2	42	42	1
1	-3	2	57	55	1	1	1	2	89	90	2	1	6	2	5	4	-1
2	-3	2	12	13	0	2	1	2	37	-34	0	2	6	2	21	21	1
3	-3	2	97	96	2	3	1	2	123	-122	1	3	6	2	24	22	0
4	-3	2	39	-39	1	4	1	2	19	18	0	4	6	2	6	4	1
5	-3	2	76	-78	0	5	1	2	79	79	0	5	6	2	61	-59	1
6	-3	2	23	23	1	6	1	2	25	24	0	-5	7	3	13	14	0
7	-3	2	23	24	0	7	1	2	4	-1	1	-4	-7	3	59	58	0
8	-3	2	11	12	0	8	1	2	41	41	0	-3	-7	3	16	-16	1
9	-3	2	28	28	1	9	1	2	73	-73	0	-2	-7	3	5	4	-2
-12	-2	2	63	63	1	10	1	2	16	-15	0	-1	-7	3	16	-15	0
-11	-2	2	27	-27	0	11	1	2	51	49	0	-9	-6	3	60	-66	0
-10	-2	2	14	14	0	-11	2	2	3	3	1	-8	-6	3	24	-24	0
-9	-2	2	9	-9	1	-10	2	2	33	-30	0	-7	-6	3	20	23	0
-8	-2	2	62	-65	0	-9	2	2	8	8	0	-6	-6	3	18	18	0
-7	-2	2	39	40	0	-8	2	2	68	64	0	-5	-6	3	6	4	1
-6	-2	2	94	91	1	-7	2	2	31	30	1	-4	-6	3	37	37	0
-5	-2	2	49	47	1	-6	2	2	68	-73	2	-3	-6	3	72	-70	0

h	k	l	Fo	Fc	s	h	k	l	Fo	Fc	s	h	k	l	Fo	Fc	s
-4	-2	2	108	-105	1	-5	2	2	4	4	1	-2	-6	3	55	-53	0
-3	-2	2	31	30	0	-4	2	2	8	-8	0	-1	-6	3	40	38	0
-2	-2	2	65	-62	1	-3	2	2	9	-7	0	0	-6	3	31	29	0
-1	-2	2	13	7	1	-2	2	2	99	100	1	1	-6	3	6	-5	-1
0	-2	2	141	141	1	-1	2	2	82	79	2	2	-6	3	5	-3	-1
1	-2	2	54	51	1	0	2	2	87	-84	0	3	-6	3	8	-7	1
2	-2	2	69	-69	1	1	2	2	85	-84	1	-10	-5	3	7	9	0
3	-2	2	24	-24	0	2	2	2	78	76	0	0	-9	3	25	-26	0
4	-2	2	20	22	0	3	2	2	36	-33	0	0	-8	3	19	20	0
5	-2	2	45	-49	1	4	2	2	55	53	0	0	-7	3	58	61	0
6	-2	2	74	79	1	5	2	2	79	75	1	0	-6	3	16	-16	0
7	-2	2	49	53	1	6	2	2	26	-25	0	3	-5	3	85	-85	0
8	-2	2	46	-46	1	7	2	2	76	-74	1	-4	-5	3	15	-15	0
9	-2	2	32	-30	0	8	2	2	22	23	0	-3	-5	3	48	46	0
10	-2	2	21	21	0	9	2	2	36	35	1	-2	-5	3	26	-25	0
-12	-1	2	15	11	0	10	2	2	13	-12	0	-1	-5	3	54	51	0
-11	-1	2	36	-33	0	-10	3	2	34	30	1	0	-5	3	10	-9	1
-10	-1	2	57	-57	0	-9	3	2	8	-7	0	1	-5	3	71	-68	0
-9	-1	2	81	81	1	-8	3	2	6	-1	1	2	-5	3	44	-41	0
-8	-1	2	20	21	0	-7	3	2	6	-7	1	3	-5	3	61	58	0
-7	-1	2	23	24	0	-6	3	2	48	-56	2	4	-5	3	13	13	0
-6	-1	2	24	23	1	-5	3	2	13	14	0	5	-5	3	13	-13	1
-5	-1	2	50	-50	1	-4	3	2	115	122	3	6	-5	3	23	22	0
-4	-1	2	111	-106	1	-3	3	2	22	-21	1	-11	-4	3	24	-25	0
-3	-1	2	73	70	0	-2	3	2	25	-26	0	-10	-4	3	47	51	0
-2	-1	2	158	159	1	-1	3	2	7	-6	1	-9	-4	3	42	46	0
-1	-1	2	59	-56	1	0	3	2	31	-29	0	-8	-4	3	67	-72	1
0	-1	2	61	60	0	1	3	2	30	-28	0	-7	-4	3	17	-18	0
2	-1	2	101	-108	1	2	3	2	122	120	1	-6	-4	3	14	-14	0
3	-1	2	22	22	0	3	3	2	39	37	0	-5	-4	3	6	-6	0
4	-1	2	122	135	1	4	3	2	86	-83	0	-4	-4	3	15	15	0
5	-1	2	1	-2	-1	5	3	2	20	19	0	-3	-4	3	87	85	0
6	-1	2	48	-51	0	6	3	2	25	-24	0	-2	-4	3	74	-73	0
7	-1	2	16	14	1	7	3	2	16	15	0	0	-4	3	87	-86	0
8	-1	2	31	-32	0	8	3	2	43	40	1	0	-4	3	35	34	0
9	-1	2	16	14	0	9	3	2	44	44	0	1	-4	3	25	-24	0
10	-1	2	54	52	0	10	3	2	60	-57	0	2	-4	3	36	35	0
-12	0	2	6	-6	1	-8	4	2	20	-22	0	3	-4	3	38	38	0
-11	0	2	23	21	0	-7	4	2	41	42	1	4	-4	3	7	-6	1
-10	0	2	6	4	1	-6	4	2	33	38	1	5	-4	3	94	-96	0
-9	0	2	69	65	0	-5	4	2	14	-13	0	6	-4	3	17	18	1

Observed and calculated structure factors for rodalquilarite in *P*-1

<i>h</i>	<i>k</i>	<i>l</i>	<i>F</i> _o	<i>F</i> _c	<i>s</i>	<i>h</i>	<i>k</i>	<i>l</i>	<i>F</i> _o	<i>F</i> _c	<i>s</i>	<i>h</i>	<i>k</i>	<i>l</i>	<i>F</i> _o	<i>F</i> _c	<i>s</i>
-8	0	2	29	27	0	-4	4	2	33	34	0	7	-4	3	18	16	0
-7	0	2	133	-130	2	-3	4	2	45	-45	1	-12	-3	3	35	35	0
-6	0	2	11	10	1	-2	4	2	63	-64	1	-11	-3	3	3	2	-1
-5	0	2	61	61	1	-1	4	2	82	82	2	-10	-3	3	31	-33	0
-4	0	2	19	21	0	0	4	2	42	41	1	-9	-3	3	9	9	0
-3	0	2	51	47	1	1	4	2	5	-1	1	-8	-3	3	67	-71	1
-2	0	2	84	79	2	2	4	2	25	-25	0	-7	-3	3	2	-2	-1
-1	0	2	131	-133	2	3	4	2	11	11	0	-6	-3	3	96	101	1
0	0	2	74	-72	1	4	4	2	71	-69	1	-5	-3	3	12	-12	0
1	0	2	138	148	2	5	4	2	59	56	0	-4	-3	3	44	44	0
2	0	2	49	51	1	6	4	2	77	75	1	-3	-3	3	39	-39	0
3	0	2	7	9	0	7	4	2	28	-26	0	-2	-3	3	24	-23	0
4	0	2	8	-8	0	8	4	2	27	-24	0	-1	-3	3	87	-87	0
5	0	2	35	-38	0	9	4	2	10	-10	0	0	-3	3	147	147	2
6	0	2	57	-61	0	-6	5	2	14	-15	0	1	-3	3	27	28	0
7	0	2	75	77	0	-5	5	2	47	-49	1	2	-3	3	78	-78	0
8	0	2	61	63	1	-4	5	2	4	-2	1	3	-3	3	29	-29	0
-1	-6	4	19	19	0	-3	-1	4	149	-144	1	5	3	4	8	-9	0
0	-6	4	33	32	0	-2	-1	4	46	42	0	6	3	4	9	8	0
1	-6	4	68	-67	0	-1	-1	4	77	73	0	7	3	4	25	-23	0
2	-6	4	10	-9	0	0	-1	4	11	-9	0	8	3	4	35	-33	0
3	-6	4	41	40	0	1	-1	4	80	80	1	-7	4	4	33	-32	1
-10	-5	4	31	36	0	2	-1	4	8	-8	0	-6	4	4	12	11	1
-9	-5	4	46	54	0	3	-1	4	60	-62	0	-5	4	4	18	17	0
-8	-5	4	34	-39	0	4	-1	4	55	-59	1	-4	4	4	4	0	-1
-7	-5	4	27	-30	0	5	-1	4	88	94	1	-3	4	4	72	76	0
-6	-5	4	24	26	0	6	-1	4	12	12	0	-2	4	4	41	-44	0
-5	-5	4	32	-33	0	7	-1	4	14	15	0	-1	4	4	57	-60	1
-4	-5	4	52	55	1	8	-1	4	14	15	0	0	4	4	12	12	0
-3	-5	4	59	60	1	9	-1	4	40	-42	1	1	4	4	40	42	0
-2	-5	4	28	-29	0	-12	0	4	22	-20	0	2	4	4	10	8	1
-1	-5	4	63	-64	1	-11	0	4	4	-3	1	3	4	4	25	24	1
0	-5	4	24	24	0	-10	0	4	2	-3	1	4	4	4	20	20	0
1	-5	4	12	12	0	-9	0	4	42	-41	0	5	4	4	74	-75	0
2	-5	4	8	66	0	-8	0	4	96	91	1	6	4	4	45	46	1
3	-5	4	12	-11	0	-7	0	4	50	50	0	7	4	4	46	-49	1
4	-5	4	51	-51	0	-6	0	4	77	-71	1	-4	5	4	20	-19	1
5	-5	4	11	-11	1	-5	0	4	30	-28	0	-3	5	4	20	-19	1
-11	-4	4	11	-11	1	-4	0	4	6	-6	0	-2	5	4	22	23	0
-10	-4	4	5	5	1	-3	0	4	23	21	0	-1	5	4	20	-21	0

h	k	l	Fo	Fc	s	h	k	l	Fo	Fc	s	h	k	l	Fo	Fc	s
-9	-4	4	8	-8	0	-2	0	4	40	39	1	0	5	4	41	43	1
-8	-4	4	34	-39	0	-1	0	4	143	144	1	1	5	4	34	35	1
-7	-4	4	14	-13	0	0	0	4	101	-99	2	2	5	4	27	-29	1
-6	-4	4	99	109	1	1	0	4	57	-58	0	3	5	4	44	46	1
-5	-4	4	24	25	0	2	0	4	4	7	1	4	5	4	32	33	0
-4	-4	4	53	-56	0	3	0	4	24	24	0	-8	-6	5	19	-21	0
-3	-4	4	4	2	-1	4	0	4	33	34	1	-7	-6	5	39	-44	0
-2	-4	4	33	-34	0	5	0	4	50	51	0	-6	-6	5	5	7	1
-1	-4	4	10	-10	0	6	0	4	7	7	1	-5	-6	5	18	-16	0
0	-4	4	67	68	1	7	0	4	90	-96	2	-4	-6	5	6	5	1
1	-4	4	85	85	1	8	0	4	34	36	0	-3	-6	5	70	73	0
2	-4	4	66	-65	1	9	0	4	26	27	0	-2	-6	5	43	-44	1
3	-4	4	31	-31	0	-11	1	4	4	27	24	-1	-6	5	51	-52	0
4	-4	4	12	11	0	-10	1	4	62	58	1	0	-6	5	15	-16	0
5	-4	4	6	-5	-1	-9	1	4	6	7	0	1	-6	5	30	30	0
6	-4	4	31	32	0	-8	1	4	35	-33	1	-10	-5	5	23	-24	0
-12	-3	4	35	34	0	-7	1	4	13	12	0	-9	-5	5	4	3	-1
-11	-3	4	49	-49	0	-6	1	4	75	-82	1	-8	-5	5	50	-55	1
-10	-3	4	50	-54	1	-5	1	4	41	44	0	-7	-5	5	5	5	-1
-9	-3	4	50	56	0	-4	1	4	90	92	1	-6	-5	5	45	50	0
-8	-3	4	48	55	0	-3	1	4	39	39	0	-5	-5	5	53	56	1
-7	-3	4	9	10	0	-2	1	4	70	-71	0	-4	-5	5	77	-82	1
-6	-3	4	4	-5	-1	-1	1	4	10	-10	0	-3	-5	5	17	-17	0
-5	-3	4	5	-5	1	0	1	4	8	8	0	-2	-5	5	14	-15	0
-4	-3	4	94	-100	0	1	1	4	58	-57	0	-1	-5	5	32	-33	0
-3	-3	4	43	46	0	2	1	4	129	134	1	0	-5	5	59	60	1
-2	-3	4	105	108	1	3	1	4	21	21	0	1	-5	5	35	35	0
-1	-3	4	8	7	0	4	1	4	53	-54	1	2	-5	5	39	-39	0
0	-3	4	31	-30	0	5	1	4	36	-37	0	3	-5	5	53	-52	1
1	-3	4	13	-2	0	6	1	4	43	43	0	4	-5	5	21	21	0
2	-3	4	31	-32	1	7	1	4	10	-10	0	-11	-4	5	15	-14	1
3	-3	4	14	-14	0	8	1	4	23	22	0	-10	-4	5	76	-80	0
4	-3	4	108	111	1	9	1	4	50	50	1	-9	-4	5	42	47	0
5	-3	4	10	-11	0	-10	2	4	2	2	-	-8	-4	5	42	47	1
6	-3	4	32	-34	0	-9	2	4	31	-30	1	-7	-4	5	10	-11	0
7	-3	4	5	-4	-1	-8	2	4	52	-52	1	-6	-4	5	5	4	1
8	-3	4	2	3	-1	-7	2	4	59	61	1	-5	-4	5	29	-30	0
-12	-2	4	15	-14	0	-6	2	4	48	52	0	-4	-4	5	59	-63	1
-11	-2	4	45	43	0	-5	2	4	36	-38	0	-3	-4	5	9	-9	0
-10	-2	4	2	0	-1	-4	2	4	42	44	1	-2	-4	5	104	106	2
-9	-2	4	48	50	0	-3	2	4	39	-39	0	-1	-4	5	36	-37	1

h	k	l	Fo	Fc	s	h	k	l	Fo	Fc	s	h	k	l	Fo	Fc	s
-8	-2	4	14	15	0	-2	2	4	41	-42	0	0	-4	5	23	-23	0
-7	-2	4	64	-72	0	-1	2	4	14	15	0	1	-4	5	5	-3	-1
-6	-2	4	36	-41	0	0	2	4	118	123	1	2	-4	5	45	-44	1
-5	-2	4	71	79	1	1	2	4	46	-47	1	3	-4	5	12	-12	0
-4	-2	4	34	36	0	2	2	4	24	-25	1	4	-4	5	56	55	1
-3	-2	4	13	-13	0	3	2	4	24	24	0	5	-4	5	19	19	0
-2	-2	4	77	76	1	4	2	4	53	-54	0	-12	-3	5	20	-19	0
-1	-2	4	95	-94	2	5	2	4	31	32	0	-11	-3	5	27	27	0
0	-2	4	42	-41	0	6	2	4	60	60	0	-10	-3	5	5	4	1
1	-2	4	74	74	1	7	2	4	17	15	0	-9	-3	5	11	12	0
2	-2	4	78	79	2	8	2	4	52	-51	0	-8	-3	5	41	45	1
3	-2	4	41	-42	1	9	2	4	10	11	1	-7	-3	5	95	-105	0
4	-2	4	15	15	1	-9	3	4	17	15	1	-6	-3	5	26	-29	0
5	-2	4	2	-4	-1	-8	3	4	11	9	0	-5	-3	5	43	45	0
6	-2	4	61	-67	1	-7	3	4	10	9	0	-4	-3	5	18	18	0
7	-2	4	48	51	1	-6	3	4	38	43	1	-3	-3	5	15	-15	0
8	-2	4	40	43	1	-5	3	4	81	-87	2	-2	-3	5	26	25	0
-12	-1	4	24	21	0	-4	3	4	4	-4	1	-1	-3	5	40	-40	1
-11	-1	4	61	57	0	-3	3	4	63	66	1	0	-3	5	95	-94	2
-10	-1	4	28	-26	0	-2	3	4	3	3	1	1	-3	5	60	61	1
-9	-1	4	59	-59	0	-1	3	4	20	21	1	2	-3	5	44	43	1
-8	-1	4	40	42	1	0	3	4	6	5	0	3	-3	5	13	-13	0
-7	-1	4	14	-15	0	1	3	4	36	-38	1	4	-3	5	22	-22	0
-6	-1	4	21	24	0	2	3	4	60	-62	0	5	-3	5	12	-11	1
-5	-1	4	71	74	0	3	3	4	86	91	0	6	-3	5	46	-48	0
-4	-1	4	15	14	0	4	3	4	28	28	0	7	-3	5	9	8	1
5	-3	6	66	65	1	-1	1	6	36	-35	0	3	-4	7	28	-27	0
-11	-2	6	6	-5	1	0	1	6	27	28	0	-10	-3	7	8	8	0
-10	-2	6	6	0	-1	1	1	6	32	-32	0	-9	-3	7	27	-28	0
-9	-2	6	22	-23	0	2	1	6	60	-60	0	-8	-3	7	30	30	0
-8	-2	6	69	67	1	3	1	6	64	65	1	-7	-3	7	60	60	1
-7	-2	6	44	44	0	4	1	6	53	53	1	-6	-3	7	59	-58	0
-6	-2	6	37	-37	0	5	1	6	12	-13	0	-5	-3	7	48	-47	0
-5	-2	6	82	-78	1	6	1	6	19	-17	0	-4	-3	7	6	-6	0
-4	-2	6	65	60	1	-9	2	6	38	37	1	-3	-3	7	22	20	0
-3	-2	6	26	-24	0	-8	2	6	13	-12	0	-2	-3	7	18	-15	0
-2	-2	6	40	38	0	-7	2	6	72	-71	1	-1	-3	7	71	68	0
-1	-2	6	91	87	1	-6	2	6	35	34	0	0	-3	7	22	-21	0
0	-2	6	40	-38	0	-5	2	6	27	26	0	1	-3	7	77	-74	1
1	-2	6	67	-63	0	-4	2	6	5	-3	1	2	-3	7	2	0	-1

h	k	l	Fo	Fc	s	h	k	l	Fo	Fc	s	h	k	l	Fo	Fc	s
2	-2	6	5	3	-1	3	-3	7	15	14	0	-6	2	7	29	29	0
3	-2	6	51	49	0	4	-3	7	10	8	1	-5	2	7	44	44	0
4	-2	6	12	-12	1	-10	-2	7	48	47	1	-4	2	7	36	-35	0
5	-2	6	47	47	0	0	-2	7	26	25	0	-3	2	7	64	-63	1
6	-2	6	3	1	-2	0	-2	7	58	-55	1	-2	2	7	34	35	0
-11	-1	6	8	-5	1	2	-2	7	6	5	0	-1	2	7	21	-21	0
-10	-1	6	92	90	1	3	-2	7	44	-42	0	0	2	7	14	13	1
-9	-1	6	21	-21	0	4	-2	7	23	-21	0	1	2	7	41	41	0
-8	-1	6	20	-18	0	5	-2	7	62	60	0	2	2	7	14	-14	0
-7	-1	6	3	2	-1	6	-2	7	42	40	1	3	2	7	65	-67	0
-6	-1	6	36	-34	0	-7	-2	7	51	-49	0	-5	3	7	9	-8	0
-5	-1	6	12	-12	0	-6	-2	7	52	-49	1	-4	3	7	7	-6	1
-4	-1	6	80	76	1	1	-2	7	27	26	0	4	3	7	26	-26	0
-3	-1	6	71	67	0	0	-2	7	58	-54	0	-3	3	7	52	52	0
-2	-1	6	84	-79	0	4	-3	7	57	53	0	-2	3	7	22	23	0
-1	-1	6	13	9	0	3	-2	7	38	36	0	0	3	7	62	-63	0
0	-1	6	14	-14	0	-1	-2	7	43	-41	0	1	3	7	1	-1	-1
1	-1	6	10	-9	0	-10	-1	7	2	3	-2	-5	-5	8	35	35	0
2	-1	6	50	48	0	-9	-1	7	22	-20	0	-4	-5	8	13	11	0
3	-1	6	57	55	0	0	-8	1	63	-61	0	-3	-5	8	8	41	0
4	-1	6	38	-37	0	3	-1	7	15	13	0	-8	-4	8	9	9	0
5	-1	6	44	-44	1	4	-1	7	84	82	1	-7	-4	8	63	63	0
6	-1	6	33	34	1	-4	-1	7	46	-45	0	-6	-4	8	19	-19	0
-11	0	6	1	-3	-1	-3	-1	7	7	5	0	-5	-4	8	61	-60	1
-10	0	6	18	-18	0	-3	-1	7	25	-23	0	-4	-4	8	21	21	0
-9	0	6	16	-14	0	-2	-1	7	46	-44	0	-3	-4	8	9	2	-1
-8	0	6	75	-72	0	-1	-1	7	23	-14	0	-2	-4	8	20	19	0
-7	0	6	57	54	0	0	0	7	95	90	1	-1	-4	8	48	45	1
-6	0	6	45	43	0	1	-1	7	6	-4	0	0	-4	8	10	10	1
-5	0	6	11	11	0	2	-1	7	73	-70	0	-9	-3	8	17	16	0
-4	0	6	11	-11	0	3	-1	7	16	15	0	-8	-3	8	26	-25	0
-3	0	6	3	1	-1	4	-1	7	74	-32	-30	-7	-3	8	16	-15	0
-2	0	6	60	-58	1	5	-1	7	6	5	1	-6	-3	8	5	-35	0
-1	0	6	11	10	0	-10	0	7	4	-4	-1	-5	-3	8	34	-35	0
0	0	6	116	112	1	-9	0	7	27	27	0	-4	-3	8	75	73	1
1	0	6	20	-20	0	-8	0	7	18	15	0	-3	-3	8	50	48	0
2	0	6	32	-32	0	-1	-5	7	36	-35	0	-2	-3	8	55	-52	1
3	0	6	3	0	-1	0	-5	7	49	-49	1	-1	-3	8	19	-18	0
4	0	6	12	-11	0	1	-5	7	23	22	0	0	-3	8	11	10	0
5	0	6	14	-13	0	-9	-4	7	76	-76	1	1	-3	8	2	-1	-1
6	0	6	74	73	0	-8	-4	7	14	13	0	2	-3	8	16	14	0

h	k	l	Fo	Fc	s	h	k	l	Fo	Fc	s	h	k	l	Fo	Fc	s
7	0	6	21	21	1	-7	-4	7	11	11	0	-2	0	7	13	13	0
-10	1	6	21	-20	1	-6	-4	7	4	3	-1	-1	0	7	6	-5	0
-9	1	6	47	43	1	-5	-4	7	28	26	0	0	0	7	23	-22	0
-8	1	6	5	2	1	-4	-4	7	14	10	0	1	0	7	6	-7	0
-7	1	6	17	18	0	-3	-4	7	84	-82	1	2	0	7	70	-68	1
-6	1	6	33	33	0	-2	-4	7	30	-29	0	3	0	7	40	39	0
-5	1	6	77	-76	0	-1	-4	7	63	62	2	4	0	7	48	47	0
-4	1	6	25	-25	0	0	-4	7	10	-7	1	5	0	7	23	-24	0
-3	1	6	67	67	0	1	-4	7	13	12	0	-9	1	7	43	41	1
-2	1	6	50	51	0	2	-4	7	3	-3	-2						

APPENDIX F. STRUCTURE FACTOR TABLES FOR GRAEMITE

Observed and calculated structure factors for graemite in Pna2(1)

1

h	k	l	Fo	Fc	s	h	k	l	Fo	Fc	s	h	k	l	Fo	Fc	s	h	k	l	Fo	Fc	s
2	0	-3	35	73	-11	3	8	-2	34	34	-7	3	6	-1	94	85	4	0	27	-1	25	44	-18
0	1	-3	81	86	4	4	8	-2	65	62	5	4	6	-1	55	55	3	1	27	-1	37	15	-12
1	1	-3	54	60	5	1	9	-2	99	91	7	5	6	-1	67	65	5	2	0	0	49	47	4
2	1	-3	15	48	-11	2	9	-2	67	68	3	0	7	-1	94	94	2	4	0	0	54	55	4
3	1	-3	15	32	-11	3	9	-2	59	59	3	1	7	-1	123	113	1	6	0	0	13	2	-13
1	2	-3	53	43	4	4	9	-2	14	18	-10	2	7	-1	63	64	2	1	1	0	65	75	2
2	2	-3	52	50	5	0	10	-2	111	129	3	3	7	-1	92	89	2	2	1	0	162	166	2
3	2	-3	39	53	-9	1	10	-2	116	108	3	4	7	-1	58	49	-10	3	1	0	11	34	-8
0	3	-3	58	69	5	2	10	-2	75	67	3	5	7	-1	76	69	3	4	1	0	37	33	5
1	3	-3	89	101	3	3	10	-2	29	18	-9	1	8	-1	9	10	-7	5	1	0	17	7	-9
2	3	-3	50	48	5	4	10	-2	105	107	4	2	8	-1	23	15	-10	6	1	0	84	76	3
3	3	-3	46	47	6	1	11	-2	42	42	-7	3	8	-1	113	100	4	0	2	0	64	72	4
1	4	-3	65	68	8	2	11	-2	74	69	3	4	8	-1	52	47	4	1	2	0	43	44	3
2	4	-3	31	39	-13	3	11	-2	22	16	-12	5	8	-1	35	16	-14	2	2	0	10	12	-7
3	4	-3	59	57	5	4	11	-2	20	33	-11	0	9	-1	115	104	1	3	2	0	60	63	3
0	5	-3	43	47	5	0	12	-2	12	25	-9	1	9	-1	87	77	2	4	2	0	47	39	3
1	5	-3	34	32	-7	1	12	-2	55	56	4	2	9	-1	68	65	3	5	2	0	86	78	2
2	5	-3	33	25	-10	2	12	-2	30	25	-8	3	9	-1	45	43	4	6	2	0	40	52	-7
3	5	-3	33	41	-12	3	12	-2	53	49	6	4	9	-1	52	45	5	1	3	0	43	54	-3
1	6	-3	70	61	3	4	12	-2	15	47	-11	5	9	-1	77	74	3	2	3	0	122	129	1
2	6	-3	45	49	-9	1	13	-2	11	25	-8	1	10	-1	17	29	-8	3	3	0	16	2	-8
3	6	-3	54	54	5	2	13	-2	56	64	4	2	10	-1	55	60	3	4	3	0	53	45	3
0	7	-3	76	85	3	3	13	-2	38	21	-9	3	10	-1	39	41	5	5	3	0	72	64	3
1	7	-3	71	73	3	4	13	-2	43	42	-10	4	10	-1	24	22	-10	6	3	0	37	28	-10
2	7	-3	33	55	-9	0	14	-2	55	68	4	5	10	-1	20	13	-11	0	4	0	167	176	12
3	7	-3	59	63	6	1	14	-2	52	51	4	0	11	-1	84	85	3	1	4	0	17	35	-8
1	8	-3	13	24	-9	2	14	-2	34	36	-7	1	11	-1	46	43	3	2	4	0	73	80	5
2	8	-3	15	21	-11	3	14	-2	43	18	-16	2	11	-1	149	137	1	3	4	0	93	87	2
3	8	-3	58	52	7	4	14	-2	79	80	4	3	11	-1	28	12	-6	4	4	0	49	41	3
0	9	-3	71	80	3	1	15	-2	48	50	6	4	11	-1	24	6	-11	5	4	0	13	4	-10
1	9	-3	16	30	-11	2	15	-2	24	15	-12	5	11	-1	18	18	-10	6	4	0	47	33	-9
2	9	-3	13	33	-9	3	15	-2	68	69	4	1	12	-1	12	29	-9	1	5	0	33	36	4
1	10	-3	12	38	-9	4	15	-2	14	4	-14	2	12	-1	175	165	3	2	5	0	106	91	3
2	10	-3	49	54	6	0	16	-2	13	45	-10	3	12	-1	21	27	-9	3	5	0	88	85	3
0	11	-3	40	69	-8	1	16	-2	61	66	5	4	12	-1	11	17	-8	4	5	0	12	10	-9
1	11	-3	27	32	-12	2	16	-2	35	29	-7	5	12	-1	13	7	-9	5	5	0	25	11	-10
2	11	-3	68	74	4	3	16	-2	126	114	4	0	13	-1	120	113	2	6	5	0	28	17	-14
1	12	-3	26	32	-15	1	17	-2	39	36	5	0	13	-1	12	24	-9	0	6	0	35	32	4
2	12	-3	92	91	4	2	17	-2	50	46	5	2	13	-1	21	22	-9	1	6	0	197	176	-14
0	13	-3	53	65	5	3	17	-2	54	57	5	3	13	-1	96	82	3	2	6	0	27	29	-6
1	13	-3	13	28	-9	0	18	-2	72	78	3	4	13	-1	170	153	7	3	6	0	55	50	3

Observed and calculated structure factors for graemite in Pna2(1)

h	k	l	Fo	Fc	s	h	k	l	Fo	Fc	s	h	k	l	Fo	Fc	s
2	13	-3	39	26	-9	1	18	-2	20	11	-11	5	13	-1	101	89	3
1	14	-3	45	45	-8	2	18	-2	74	71	9	1	14	-1	90	91	2
0	15	-3	62	65	5	3	18	-2	13	25	-9	2	14	-1	77	70	3
1	15	-3	17	36	-11	1	19	-2	89	90	5	3	14	-1	55	55	3
1	16	-3	18	41	-11	2	19	-2	17	13	-11	4	14	-1	12	6	-8
0	17	-3	19	33	-11	3	19	-2	46	43	-9	5	14	-1	25	4	-12
0	0	-2	325	340	1	0	20	-2	68	65	4	0	15	-1	134	123	2
2	0	-2	39	46	6	1	20	-2	28	26	-11	1	15	-1	56	53	4
4	0	-2	61	55	5	2	20	-2	13	9	-9	2	15	-1	11	10	-8
1	1	-2	44	44	6	1	21	-2	40	41	6	3	15	-1	56	51	4
2	1	-2	105	104	2	2	21	-2	19	9	-11	4	15	-1	37	35	6
3	1	-2	34	26	-6	0	22	-2	19	35	-11	1	16	-1	10	30	-7
4	1	-2	29	34	-12	1	22	-2	36	51	-9	2	16	-1	75	65	3
5	1	-2	14	12	-10	1	23	-2	21	26	-21	3	16	-1	13	19	-10
0	2	-2	39	36	4	0	24	-2	25	21	-12	4	16	-1	25	18	-10
1	2	-2	37	27	-6	2	0	-1	9	50	-9	0	17	-1	58	51	4
2	2	-2	22	20	-10	4	0	-1	44	49	6	1	17	-1	12	16	-9
3	2	-2	52	59	4	6	0	-1	83	81	5	2	17	-1	50	45	5
4	2	-2	30	41	-12	0	1	-1	100	104	2	3	17	-1	85	82	3
5	2	-2	63	66	5	1	1	-1	96	97	2	4	17	-1	59	63	6
1	3	-2	12	29	-9	2	1	-1	11	47	-8	1	18	-1	42	32	5
2	3	-2	91	89	3	3	1	-1	71	63	2	2	18	-1	61	55	7
3	3	-2	14	26	-9	4	1	-1	47	47	5	3	18	-1	18	5	-10
4	3	-2	31	26	-7	5	1	-1	25	2	-10	4	18	-1	52	46	6
5	3	-2	45	49	7	6	1	-1	44	39	-17	0	19	-1	71	70	3
0	4	-2	108	118	2	1	2	-1	77	71	2	1	19	-1	28	30	-8
1	4	-2	27	41	-6	2	2	-1	107	105	1	2	19	-1	42	25	-8
2	4	-2	92	85	2	3	2	-1	106	91	2	3	19	-1	85	75	3
3	4	-2	60	56	4	4	2	-1	12	3	-9	4	19	-1	76	75	4
4	4	-2	40	51	-7	5	2	-1	14	10	-10	1	20	-1	39	41	-7
5	4	-2	16	19	-11	0	3	-1	129	126	2	2	20	-1	60	53	4
1	5	-2	34	30	5	1	3	-1	198	180	1	3	20	-1	32	32	-11
2	5	-2	66	64	3	2	3	-1	137	126	2	0	21	-1	62	54	4
3	5	-2	54	54	6	3	3	-1	53	55	3	1	21	-1	50	46	4
4	5	-2	16	21	-10	4	4	-1	61	53	3	2	21	-1	22	31	-11
5	5	-2	32	6	-11	5	5	-1	76	66	7	3	21	-1	28	19	-14
0	6	-2	34	41	5	1	4	-1	105	106	2	2	22	-1	14	16	-11
1	6	-2	117	114	3	2	4	-1	30	35	5	2	22	-1	111	110	2
2	6	-2	31	25	-12	3	4	-1	124	119	1	3	22	-1	67	64	6
3	6	-2	39	43	-7	4	4	-1	11	15	-8	0	23	-1	99	91	4
4	6	-2	106	98	8	5	4	-1	65	54	3	1	23	-1	50	41	5

Observed and calculated structure factors for graemite in Pna2(1)

h	k	l	Fo	Fc	s	h	k	l	Fo	Fc	s	h	k	l	Fo	Fc	s
5	6	-2	14	25	-10	0	5	-1	97	93	2	2	23	-1	13	26	-9
1	7	-2	42	39	6	1	5	-1	50	42	3	3	23	-1	58	60	5
2	7	-2	76	75	3	2	5	-1	66	65	2	1	24	-1	12	27	-9
3	7	-2	40	49	6	3	5	-1	53	48	3	2	24	-1	63	59	8
4	7	-2	12	18	-8	4	5	-1	47	44	4	0	25	-1	14	21	-10
0	8	-2	45	44	4	5	5	-1	69	65	4	1	25	-1	31	5	-13
1	8	-2	90	92	2	1	6	-1	98	101	2	2	25	-1	72	68	4
2	8	-2	14	10	-10	2	6	-1	83	77	2	1	26	-1	25	9	-12
2	7	1	58	64	5	2	16	1	73	65	3	5	1	2	14	11	-10
3	7	1	82	88	3	3	16	1	32	19	-7	0	2	2	35	34	-6
4	7	1	57	50	4	4	16	1	17	17	-11	1	2	2	29	28	-7
5	7	1	69	69	4	0	17	1	54	52	3	2	2	2	29	21	-12
1	8	1	17	6	-8	1	17	1	15	16	-9	3	2	2	53	59	3
2	8	1	21	15	-8	2	17	1	48	45	6	4	2	2	25	41	-11
3	8	1	102	100	3	3	17	1	81	81	3	5	2	2	51	67	7
4	8	1	51	48	5	4	17	1	64	62	5	1	3	2	30	31	-5
5	8	1	12	15	-8	1	18	1	40	31	5	2	3	2	77	90	2
0	9	1	103	104	5	2	18	1	55	55	5	3	3	2	23	30	-10
1	9	1	75	78	2	3	18	1	22	6	-11	4	3	2	35	26	-8
2	9	1	67	65	4	4	18	1	50	47	5	5	3	2	36	49	-9
3	9	1	43	43	4	0	19	1	64	67	3	0	4	2	101	120	3
4	9	1	47	45	5	1	19	1	11	32	-8	1	4	2	16	41	-8
5	9	1	74	74	3	2	19	1	17	23	-10	2	4	2	83	85	5
1	10	1	9	29	-7	3	19	1	84	76	3	3	4	2	54	57	4
2	10	1	48	61	3	4	19	1	74	75	4	4	4	2	18	49	-10
3	10	1	42	42	4	1	20	1	34	41	-7	5	4	2	14	21	-10
4	10	1	31	21	-8	2	20	1	45	52	5	1	5	2	40	28	4
5	10	1	12	14	-9	3	20	1	28	33	-13	2	5	2	59	66	4
0	11	1	76	85	2	0	21	1	46	54	4	3	5	2	53	55	3
1	11	1	40	45	6	1	21	1	52	48	4	4	5	2	36	20	-8
2	11	1	137	136	3	2	21	1	15	31	-11	5	5	2	21	7	-11
3	11	1	29	12	-6	3	21	1	13	19	-9	0	6	2	12	42	-9
4	11	1	11	6	-8	1	22	1	44	17	-8	1	6	2	107	113	4
5	11	1	12	19	-9	2	22	1	105	110	3	2	6	2	28	28	-12
1	12	1	10	26	-7	3	22	1	67	64	4	3	6	2	29	44	-8
2	12	1	164	165	7	0	23	1	88	89	3	4	6	2	93	98	3
3	12	1	22	27	-11	1	23	1	44	40	-8	5	6	2	14	26	-10
4	12	1	14	17	-10	2	23	1	30	27	-12	1	7	2	33	41	-6
5	12	1	13	7	-9	3	23	1	47	60	7	2	7	2	70	74	3
0	13	1	112	112	11	1	24	1	12	27	-9	3	7	2	29	49	-7
2	7	2	72	89	4	0	1	3	99	107	3	4	10	2	99	107	3
3	7	2	43	60	5	1	1	3	36	44	5	1	11	2	36	44	5
4	7	2	13	45	-9	2	1	3	66	69	4	2	11	2	66	69	4
5	7	2	21	32	-11	3	1	3	13	15	-10	3	11	2	13	15	-10
1	8	3	43	43	5	1	2	3	19	32	-11	4	11	2	19	32	-11
2	8	3	51	50	5	2	2	3	27	27	-7	0	12	2	11	27	-7
3	8	3	48	52	6	3	2	3	58	55	3	1	12	2	58	55	3
4	8	3	59	66	4	0	3	3	18	26	-13	2	12	2	18	26	-13
5	8	3	82	99	3	1	3	3	50	49	-8	3	12	2	50	49	-8
0	9	3	38	50	-7	2	3	3	16	49	-12	4	12	2	16	49	-12
1	9	3	35	47	-9	3	3	3	14	27	-10	1	13	2	14	27	-10
2	9	3	60	67	6	4	3	3	51	66	4	2	13	2	51	66	4
3	9	3	13	41	-9	2	4	3	32	22	-9	3	13	2	32	22	-9
4	9	3	50	56	6	3	4	3	41	41	7	4	13	2	41	41	7
5	9	3	37	50	6	0	5	3	57	67	3	0	14	2	57	67	3
1	10	3	30	32	-9	1	5	3	27	51	-10	1	14	2	27	51	-10
2	10	3	16	25	-11	2	5	3	29	35	-12	2	14	2	29	35	-12
3	10	3	33	41	-10	3	5	3	31	18	-8	3	14	2	31	18	-8
4	10	3	53	62	4	1	6	3	71	80	4	4	14	2	71	80	4
5	10	3	15	51	-11	2	6	3	47	50	4	1	15	2	47	50	4
0	11	3	46	54	6	3	6	3	60	66	4	2	15	2	60	66	4
1	11	3	72	86	4	0	7	3	72	86	4	3	15	2	72	86	4
2	11	3	73	73	3	1	7	3	45	45	-10	0	16	2	13	45	-10
3	11	3	54	54	-11	2	7	3	54	65	8	1	16	2	54	65	8
4	11	3	20	20	4	3	7	3	28	28	-8	2	16	2	37	28	-8
5	11	3	43	62	7	1	8	3	115	115	5	3	16	2	115	115	5
1	12	3	18	22	-10	2	8	3	30	36	-12	2	17	2	30	36	-12
2	12	3	32	21	-10	3	8	3	45	46	-11	1	17	2	45	46	-11
3	12	3	54	53	6	0	9	3	62	81	5	2	17	2	62	81	5
4	12	3	62	81	5	1	9	3	77	77	3	3	17	2	77	77	3
5	12	3	31	31	-12	2	9	3	15	12	-11	0	18	2	15	12	-11
0	13	3	29	33	-13	3	10	3	69	69	4	1	18	2	69	69	4
1	13	3	15	39	-11	4	10	3	84	82	4	2	18	2	84	82	4

[illegible]